

Development of Homogeneous Molybdenum Catalysts for the Activation of Small
Molecules

by

Raja Pal

A Dissertation Presented in Partial Fulfillment
of the Requirements for the Degree of
Doctor of Philosophy

Approved October 2016 by the
Graduate Supervisory Committee:

Ryan J. Trovitch, Chair
Daniel Buttry
Don Seo

ARIZONA STATE UNIVERSITY

December 2016

ABSTRACT

Over the last few decades, homogeneous molybdenum catalysis has been a center of interest to inorganic, organic, and organometallic chemists. Interestingly, most of the important advancements in molybdenum chemistry such as non-classical dihydrogen coordination, dinitrogen reduction, olefin metathesis, and water reduction utilize diverse oxidation states of the metal. However, employment of redox non-innocent ligands to tune the stability and reactivity of such catalysts have been overlooked. With this in mind, the Trovitch group has developed a series of novel bis(imino)pyridine (or pyridine diimine, PDI) and diimine (DI) ligands that have coordinating phosphine or amine arms to exert coordination flexibility to the designed complexes. The research described in this dissertation is focused on the development of molybdenum catalysts that are supported by PDI and DI chelates and their application in small molecule activation.

Using the phosphine containing PDI chelate, $^{\text{Ph}_2\text{PPr}}\text{PDI}$, several low-valent molybdenum complexes have been synthesized and characterized. While the zerovalent monocarbonyl complex, $(^{\text{Ph}_2\text{PPr}}\text{PDI})\text{MoCO}$, catalyzes the reduction of aldehyde C=O bonds, the C-H activated Mo(II) complex, $(\kappa^6\text{-}P,N,N,N,C,P\text{-}^{\text{Ph}_2\text{PPr}}\text{PDI})\text{MoH}$ was found to be the first well-defined molybdenum catalyst for reducing carbon dioxide to methanol. Along with low-oxidation state compounds, a Mo(IV) complex, $[(^{\text{Ph}_2\text{PPr}}\text{PDI})\text{MoO}][\text{PF}_6]_2$ was also synthesized and utilized in electrocatalytic hydrogen production from neutral water. Moreover, with the proper choice of reductant, an uncommon Mo(I) oxidation state was stabilized and characterized by electron paramagnetic resonance spectroscopy and single crystal X-ray diffraction.

While the synthesized (PDI)Mo complexes unveiled versatile reduction chemistry, varying the ligand backbone to DI uncovered completely different reactivity when bound to molybdenum. Unlike PDI, no chelate-arm C-H activation was observed with the propyl phosphine DI, $^{\text{Ph}_2\text{PPr}}\text{DI}$; instead, a bis(dinitrogen) Mo(0) complex, $(^{\text{Ph}_2\text{PPr}}\text{DI})\text{Mo}(\text{N}_2)_2$ was isolated. Surprisingly, this complex was found to convert carbon dioxide into dioxygen and carbon monoxide under ambient conditions through a novel tail-to-tail CO_2 reductive coupling pathway. Detailed experimental and theoretical studies are underway to gain further information about the possible mechanism of Mo mediated direct conversion of CO_2 to O_2 .

ACKNOWLEDGMENTS

During my doctoral program at Arizona State University (ASU), many individuals have contributed to the success of my dissertation. First and foremost, I would like to express my strong acknowledgement to my advisor, Prof. Ryan J. Trovitch. I was fortunate to join ASU at the time when Prof. Trovitch started his independent career as a faculty at the School of Molecular Sciences (formerly Department of Chemistry & Biochemistry). As one of his first graduate students, I have enjoyed working with him since the very first day when we started setting up the laboratory. His endless courage, intellectual thinking, and dedication to science have inspired me in many ways to explore and learn new avenues in the field. His supervision, advisement, and guidance have helped me mature my scientific thinking and grow as an independent researcher. I personally thank him for listening to my countless ideas and letting me explore my own interests, at the same time, directing me to the right path to accelerate my success (without letting me get carried away too far by excitement). I shall always be grateful to him for correcting my writing and helping me improve my professional skills with his valuable inputs. Finally, I thank him for being open and approachable whenever I was in need for his suggestions and I shall always be appreciative to him for supporting me throughout my graduate school and helping me to make this dissertation a reality.

There are faculty members and collaborators who have helped me during my doctoral tenure for which I would like to acknowledge them. I thank Prof. Anne K. Jones for her valuable thoughts and guidance during my water reduction project. I appreciate her trust while letting me work in her lab which has helped me to complete the project on time. I

thank Prof. Amanda C. Bowman for her time to perform theoretical calculations on the bis(ligand) compound during my first paper. A special thanks to Prof. Andrew Chizmeshya for his willingness to run DFT calculations for my last project despite being super busy at that time, I appreciate all the effort he has put in to help me complete my manuscript on CO₂ disproportionation. I would also take this opportunity to thank my committee members, Prof. Daniel Buttry and Prof. Don Seo for their priceless discussion and suggestions on my projects throughout graduate school. I am also fortunate to participate in the classes they offered during my time at ASU, it helped me learn a lot of the technical and theoretical details about inorganic chemistry.

There are number of amazing people I have met at ASU without whom this thesis would be impossible. First, one of the main instruments that my projects relied on is the single crystal X-ray diffractometer and I am lucky enough to have the most patient and experienced crystallographer here at ASU, Dr. Thomas L. Groy (Tom). He has never stopped amazing me with his excitement of mounting crystals and solving structures, no matter how many times I have come with samples. I thank him for teaching me the technical details behind data collection and I will remember all the interesting stories he has shared with me. I am also thankful to Dr. Sue Roberts from University of Arizona for her time to solve few of my crystal structures when our diffractometer was down. I also thank Dr. Marco Flores for helping me with the EPR data collection and his insightful discussion on EPR interpretation. I thank Dr. Brian Cherry for helping me with different NMR experiments which were all very useful for my projects. I personally thank my friend and colleague, Joseph Laureanti (Joe) from Prof. Jones lab for his endless enthusiasm and

interest to work with me and to help me finish the electrochemical project. And I must be thankful to all the amazing past and present staff members at the chemistry department office, specially our graduate advisors, Mrs. Martha McDowell and Mr. David Nutt for helping me with all the official paperwork throughout my graduate program.

A list of friends and colleagues at ASU are worth mentioning who have helped me in many ways to make my Ph.D. journey a memorable period of my life. I thank all my present and previous lab mates for being so cooperative and friendly, it helped a lot to balance my stress level at work. I am grateful to be surrounded by so many of my friends right from the beginning of my arrival at Tempe. Sena da, Sriloy da, Suratna di, Ashok, Subarna da, Shibom, Tufan, and Chandrani, all of them are truly amazing and I will remember all the time and fun we have shared together.

Last but not the least, I would like to express my heartfelt gratitude to those who have provided me with an endless amount of emotional support throughout my educational career and graduate study. To my parents, Mr. Bimal Pal and Mrs. Arati Pal, I can never express myself in words how much your support, courage, and sacrifice mean to me. My mother and sister have been my stabilizing factors, especially whenever I have felt homesick or worried, calling them and listening to their voices without even discussing my actual worry would made me feel focused. And most importantly, I would like to express my special appreciation and dedicate this dissertation to my elder brother, Mr. Ratan Pal, without whom I could never pursued a career in science. I am fortunate and indebted to have him in my life who has sacrificed his own dreams to see me succeed. Thank you for all the support and being there for me all the time.

TABLE OF CONTENTS

| | Page |
|--|-------|
| LIST OF TABLES | xiv |
| LIST OF FIGURES..... | xv |
| SUMMARY | xxiii |
| CHAPTER | |
| 1. PREPARATION AND HYDROSILYLATION ACTIVITY OF A MOLYBDENUM CARBONYL COMPLEX FEATURING A PENTADENTATE BIS(IMINO)PYRIDINE LIGAND | 1 |
| 1.1. Abstract | 1 |
| 1.2. Introduction | 2 |
| 1.3. Results and Discussion | 3 |
| 1.4. Conclusion..... | 19 |
| 1.5. Experimental Procedures | 20 |
| 1.5.1. General Considerations | 20 |
| 1.5.2. X-ray Crystallography..... | 21 |
| 1.5.3. Calculations | 22 |
| 1.5.4. Improved Preparation of 2,6-((2-NC ₅ H ₄)CH ₂ CH ₂ N=C(CH ₃)) ₂ C ₅ H ₃ N (^{PyEt} PDI) | 22 |
| 1.5.5. Preparation of (^{PyEt} PDI) ₂ Mo (1)..... | 23 |

| CHAPTER | Page |
|--|------|
| 1.5.6. Preparation of (Ph_2PPtPDI)Mo(CO) (2) | 25 |
| 1.5.7. General Procedure for Silane Screening | 28 |
| 1.6. Catalytic Experiments | 29 |
| 1.6.1. General Procedure for Aldehyde Hydrosilylation | 29 |
| 1.6.2. Hydrosilylation of Benzaldehyde Using PhSiH_3 at 90 °C (1.0 mol%) | 29 |
| 1.6.3. Hydrosilylation of Benzaldehyde Using Ph_2SiH_2 at 90 °C (1.0 mol%) | 30 |
| 1.6.4. Hydrosilylation of Benzaldehyde Using Ph_3SiH at 90 °C (1.0 mol%) | 30 |
| 1.6.5. Hydrosilylation of Benzaldehyde Using $(\text{EtO})_3\text{SiH}$ at 90 °C (1.0 mol%) | 30 |
| 1.6.6. Hydrosilylation of Benzaldehyde Using $(\text{EtO})_2\text{MeSiH}$ at 90 °C (1.0 mol%) | 31 |
| 1.6.7. Hydrosilylation of Benzaldehyde Using $(\text{EtO})\text{Me}_2\text{SiH}$ at 90 °C (1.0 mol%) | 31 |
| 1.6.8. Hydrosilylation of Benzaldehyde Using Et_3SiH at 90 °C (1.0 mol%) | 32 |
| 1.6.9. Hydrosilylation of Benzaldehyde at 120 °C (1.0 mol%) | 32 |
| 1.6.10. Hydrosilylation of Benzaldehyde at 90 °C (0.1 mol%) | 32 |
| 1.6.11. Hydrosilylation of Benzaldehyde at 60 °C (0.1 mol%) | 33 |
| 1.6.12. Hydrosilylation of 4-Cyanobenzaldehyde (0.1 mol%) | 33 |
| 1.6.13. Hydrosilylation of 4-Chlorobenzaldehyde (0.1 mol%) | 34 |
| 1.6.14. Hydrosilylation of 4-Fluorobenzaldehyde (0.1 mol%) | 35 |
| 1.6.15. Hydrosilylation of <i>p</i> -Tolualdehyde (0.1 mol%) | 35 |
| 1.6.16. Hydrosilylation of <i>p</i> -Anisaldehyde (0.1 mol%) | 36 |
| 1.6.17. Hydrosilylation of <i>trans</i> -Cinnamaldehyde (0.1 mol%) | 37 |
| 1.6.18. Hydrosilylation of Furfural (0.1 mol%) | 37 |

| CHAPTER | Page |
|--|-----------|
| 1.6.19. Hydrosilylation of 3-Cyclohexene-1-carboxaldehyde (0.1 mol%)..... | 38 |
| 1.6.20. Hydrosilylation of Cyclohexanecarboxaldehyde (0.1 mol%) | 39 |
| 1.6.21. Hydrosilylation of Decanal (0.1 mol%) | 39 |
| 1.7. Addition of 5 eq Benzaldehyde to 2 | 40 |
| 1.8. Hydrosilylation of Benzaldehyde Using PhSiH ₃ at 90 °C (10 mol%)..... | 40 |
| 1.9. Test for Catalyst Homogeneity..... | 41 |
| 1.10. References | 42 |
| 2. CONVERSION OF CARBON DIOXIDE TO METHANOL USING A C-H ACTIVATED BIS(IMINO)PYRIDINE MOLYBDENUM HYDROBORATION CATALYST..... | 47 |
| 2.1. Abstract | 47 |
| 2.2. Introduction | 49 |
| 2.3. Results and Discussion | 51 |
| 2.3.1. Synthesis and Characterization..... | 51 |
| 2.3.2. CO ₂ Functionalization..... | 58 |
| 2.4. Mechanism of Hydroboration | 65 |
| 2.5. Catalyst Comparison and Intricacies | 67 |
| 2.6. Conclusion..... | 68 |
| 2.7. Experimental Details..... | 69 |

| CHAPTER | Page |
|--|-----------|
| 2.7.1. General Considerations | 69 |
| 2.7.2. X-ray Crystallography..... | 70 |
| 2.7.3. Synthesis of [$(\text{Ph}^2\text{PPrPDI})\text{MoI}(\text{CO})$][I] (3)..... | 71 |
| 2.7.4. Synthesis of [$(\text{Ph}^2\text{PPrPDI})\text{MoI}$][I] (4)..... | 72 |
| 2.7.5. Synthesis of ($\kappa^6\text{-P,N,N,N,C,P-Ph}^2\text{PPrPDI}$)MoH (5)..... | 73 |
| 2.7.6. Synthesis of ($\kappa^6\text{-P,N,N,N,C,P-Ph}^2\text{PPrPDI}$)Mo(OCOH) (6) | 76 |
| 2.7.7. Hydroboration of CO ₂ Using 5 mol% 5 | 79 |
| 2.7.8. Hydroboration of CO ₂ Using 1 mol% 5 | 79 |
| 2.7.9. Hydroboration of CO ₂ Using 0.1 mol% 5 | 79 |
| 2.7.10. Control Reaction Between Pinacolborane and CO ₂ | 80 |
| 2.7.11. Control Reaction Employing Ph^2PPrPDI as a Catalyst..... | 80 |
| 2.8. References | 81 |
| 3. ISOLATION OF A BIS(IMINO)PYRIDINE MOLYBDENUM(I) IODIDE COMPLEX THROUGH CONTROLLED REDUCTION AND INTERCONVERSION OF ITS REACTION PRODUCTS | 86 |
| 3.1. Abstract | 86 |
| 3.2. Introduction | 88 |
| 3.3. Results and Discussion | 90 |
| 3.4. Conclusion..... | 102 |
| 3.5. Experimental Details..... | 103 |

| CHAPTER | Page |
|---|---------|
| 3.5.1. General Considerations | 103 |
| 3.5.2. Electrochemistry | 104 |
| 3.5.3. X-ray Crystallography..... | 104 |
| 3.5.4. Electron Paramagnetic Resonance Spectroscopy | 105 |
| 3.5.4.1. Instrumentation | 105 |
| 3.5.4.2. Spin Hamiltonian | 105 |
| 3.5.4.3. Fitting of EPR Spectra..... | 106 |
| 3.5.5. Alternative Synthesis of [$(\text{Ph}^2\text{PPrPDI})\text{MoI}[\text{I}]$] (4) | 106 |
| 3.5.6. Preparation of $(\kappa^6\text{-P,N,N,N,C,P-Ph}^2\text{PPrPDI})\text{MoI}$ (7) | 107 |
| 3.5.7. Preparation of $(\text{Ph}^2\text{PPrPDI})\text{MoI}$ (8) | 111 |
| 3.5.8. Preparation of $(\text{Ph}^2\text{PPrPDI})\text{MoH}_2$ (9) | 112 |
| 3.5.9. Observation of $(\text{Ph}^2\text{PPrPDI})\text{MoD}_2$ (9-d₂) | 115 |
| 3.5.10. Alternative Synthesis of $(\kappa^6\text{-P,N,N,N,C,P-Ph}^2\text{PPrPDI})\text{MoH}$ (5) | 116 |
| 3.6. References | 117 |
| 4. HYDROGEN PRODUCTION FROM WATER USING A BIS(IMINO)PYRIDINE MOLYBDENUM ELECTROCATALYST | 120 |
| 4.1. Abstract | 120 |
| 4.2. Introduction | 121 |
| 4.3. Results and Discussion | 122 |
| 4.3.1. Cyclic Voltammetry..... | 126 |
| 4.3.2. Catalysis in the Presence of Water..... | 127 |

| CHAPTER | Page |
|---|----------|
| 4.4. Mechanism | 131 |
| 4.5. Conclusion..... | 138 |
| 4.6. Experimental Details..... | 139 |
| 4.6.1. General Considerations | 139 |
| 4.6.2. Electrochemistry | 140 |
| 4.6.3. Open Circuit Potential Determination..... | 141 |
| 4.6.4. X-ray Crystallography..... | 141 |
| 4.6.5. Synthesis of [^{Ph₂PPr} PDI)MoO][PF ₆] ₂ (10)..... | 142 |
| 4.6.6. Synthesis of (^{Ph₂PPr} PDI)MoO (11) | 144 |
| 4.7. References | 147 |
| 5. DIRECT CONVERSION OF CARBON DIOXIDE TO DIOXYGEN USING A SINGLE MOLYBDENUM CATALYST | 146 |
| CHAPTER | Page |
| 5.1. Abstract | 147 |
| 5.2. Introduction | 148 |
| 5.3. Results and Discussion | 150 |
| 5.4. Attempts Toward Catalytic O ₂ Generation from CO ₂ | 156 |
| 5.5. Conclusion..... | 159 |
| 5.6. Experimental Details..... | 160 |

| | |
|---|-----|
| 5.6.1. General Considerations | 160 |
| 5.6.2. X-ray Crystallography..... | 161 |
| 5.6.3. Synthesis of (^{Ph2PPr} DI)MoI ₂ (13)..... | 161 |
| 5.6.4. Synthesis of (^{Ph2PPr} DI)Mo(N ₂) ₂ (14)..... | 163 |
| 5.6.5. Synthesis of (^{Ph2PPr} DI)Mo(CO) ₂ (15) | 163 |
| 5.7. References | 166 |
| BIBLIOGRAPHY | 169 |
| APPENDIX | 184 |
| A. UNPUBLISHED BIS(IMINO)PYRIDINE MOLYBDENUM CHEMISTRY | 184 |
| A.1. Preparation of (^{PyEt} PDI)MoOCl ₂ | 184 |
| A.2. Preparation of [(^{Ph2PPr} PDI)MoCl ₂][Cl] using Mo(THF) ₃ Cl ₃ | 185 |
| A.3. Isolation of (□ ⁶ -N,N,N,P,P,C- ^{Ph2PPr} PDI)MoCl | 186 |
| A.4. Isolation of [(^{Ph2PPr} PDI)Mo(H ₂ O)][CO ₃]..... | 186 |
| A.5. Preparation of (^{Ph2PPr} PDI)Mo(C ₂ H ₄) | 187 |
| A.6. Preparation of (^{Ph2PEt} PDI)MoCO | 189 |
| A.7. Synthesis of ^{iPrAr,Ph2PPr} PDI | 190 |
| B. UNPUBLISHED BIS(IMINO)PYRIDINE COBALT CHEMISTRY | 192 |
| B.1. Preparation of (^{PyEt} PDI)CoCl ₂ | 192 |
| B.2. Preparation of (^{PyEt} PDIH)Co..... | 192 |
| C. UNPUBLISHED BIS(IMINO)PYRIDINE AND DIIMINE IRON CHEMISTRY... | 194 |

| APPENDIX | Page |
|---|------|
| C.1. Preparation of (^{PyEt} PDI)FeBr ₂ | 194 |
| C.2. Preparation of (^{PyEt} PDI)Fe | 194 |
| C.3. Preparation of ^{PhPPr2} PDI..... | 195 |
| C.4. Preparation of (^{PhPPr2} PDI)FeBr ₂ | 196 |
| C.5. Reduction of (^{PhPPr2} PDI)FeBr ₂ | 196 |
| C.6. Preparation of (^{Ph2PPr} DI)Fe(OTf) ₂ | 197 |
| REFERENCES..... | 199 |
| COPYRIGHT AND PERMISSIONS | 200 |
| BIOGRAPHICAL SKETCH | 204 |

LIST OF TABLES

| Table | Page |
|---|------|
| 1.1 Experimental and Calculated (RKS and RKS/COSMO) Bond Lengths (Å) and Angles (°) for 1 | 6 |
| 1.2 Relative orbital energies calculated for (Py ^{Et} PDI) ₂ Mo | 7 |
| 1.3 Experimental Bond Lengths (Å) and Angles (°) Determined for 2 | 11 |
| 1.4 The Hydrosilylation of Benzaldehyde Using 2 as a Catalyst..... | 13 |
| 1.5 The Preparation of Alcohols from Aldehydes via 2 -Mediated Hydrosilylation . | 15 |
| 2.1 Wavelengths of Maximum Absorption (λ_{\max}) and Extinction Coefficients (ϵ) for Each Complex Analyzed by UV-vis Spectroscopy..... | 54 |
| 2.2 Notable Bond Lengths (Å) and Angles (°) Determined for 4 | 55 |
| 2.3 Notable Bond Lengths (Å) and Angles (°) Determined for 5 | 58 |
| 3.1 Notable Bond Lengths (Å) and Angles (°) Determined for 7 , Along with Values Previously Reported for 5 | 91 |
| 3.2 Parameters Used to fit the EPR Spectra of 8 at 108 K and 296 K..... | 95 |
| 3.3 Notable Bond Lengths (Å) and Angles (°) Determined for 8 and 9 , Compared with Those Reported for 4 | 96 |
| 4.1 Notable Bond Lengths (Å) and Angles (°) Determined for 10 , Compared with Those Reported for 11 | 125 |
| 4.2 Overpotential Calculated from the Open Circuit Potential (OCP) vs Fc ⁺⁰ . | 129 |
| 5.1 Notable Bond Lengths (Å) and Angles (°) Determined for 13 , 14 , and 15 | 154 |

LIST OF FIGURES

| Figure | Page |
|--|------|
| 1.1 Synthetic Scheme of (PyEtPDI) ₂ Mo (1)..... | 4 |
| 1.2 The Solid State Structure of 1 | 5 |
| 1.3 Orbital Representations for 1 | 8 |
| 1.4 Synthesis of (Ph ² PPrPDI)Mo(CO) (2) From Mo(CO) ₆ | 9 |
| 1.5 The Solid State Structure of 2 | 11 |
| 1.6 ³¹ P NMR Spectrum of 5 eq Benzaldehyde Addition to 2 | 17 |
| 1.7 Proposed Mechanism for 2 -Catalyzed Aldehyde Hydrosilylation | 18 |
| 1.8 ¹ H NMR Spectrum of 1 in Benzene- <i>d</i> ₆ | 25 |
| 1.9 ¹³ C NMR Spectrum of 1 in Benzene- <i>d</i> ₆ | 25 |
| 1.10 ¹ H NMR Spectrum of (Ph ² PPrPDI)Mo(CO) in Benzene- <i>d</i> ₆ | 27 |
| 1.11 ¹³ C NMR Spectrum of (Ph ² PPrPDI)Mo(CO) in Benzene- <i>d</i> ₆ | 27 |
| 1.12 ³¹ P NMR Spectrum of (Ph ² PPrPDI)Mo(CO) in Benzene- <i>d</i> ₆ | 27 |
| 1.13 IR Spectrum of (Ph ² PPrPDI)Mo(CO) in KBr..... | 28 |
| 1.14 Cyclic Voltammogram of (Ph ² PPrPDI)Mo(CO) | 28 |
| 2.1 Previously Described Transition Metal Catalysts for the Hydroboration of CO ₂ to Methoxyborane..... | 50 |
| 2.2 Synthetic Scheme for [Ph ² PPrPDIMoI][I] (4) From Ph ² PPrPDIMo(CO) (2)..... | 52 |
| 2.3 Absorption Spectra Comparison of 2 , 3 , and 4 | 53 |
| 2.4 The Solid State Structure of 4 | 55 |
| 2.5 Synthesis of (κ ⁶ - <i>P,N,N,N,C,P</i> -Ph ² PPrPDI)MoH (5) From 4 | 56 |

| Figure | Page |
|--|------|
| 2.6 The Solid State Structure of 5 | 57 |
| 2.7 Synthesis of (κ^6 - <i>P,N,N,N,C,P</i> -Ph ₂ PPrPDI)Mo(OCOH) (6) From 5 | 58 |
| 2.8 ¹ H NMR Spectra Illustrating the Slow Conversion of CO ₂ to H ₃ COBPin and O(BPin) ₂ Over 3 d at 25 °C Using 5 | 60 |
| 2.9 ¹ H NMR Spectra Illustrating the Slow Conversion of 6 to 5 Over 3 d at 25 °C. | 60 |
| 2.10 ¹ H NMR Spectra Illustrating the Stoichiometric Conversion of CO ₂ to H ₃ COBPin and O(BPin) ₂ Over 2 d at 60 °C Using 5 | 61 |
| 2.11 ³¹ P NMR Spectra Illustrating the Conversion of 6 to 5 Over 2 d at 60 °C | 61 |
| 2.12 ¹ H NMR Spectra of 5 -Mediated CO ₂ Hydroboration Over the Course of 5 h at 90 °C | 62 |
| 2.13 Overall Reaction of 5 -Mediated CO ₂ Hydroboration Over the Course of 8 h at 90 °C | 63 |
| 2.14 ¹¹ B NMR Spectrum of CO ₂ Hydroboration Using 0.1 mol% 5 After 8 h at 90 °C | 63 |
| 2.15 ¹ H NMR Spectrum of Attempted CO ₂ Hydroboration Using 1.0 mol% Ph ₂ PPrPDI as a Catalyst in Benzene- <i>d</i> ₆ | 64 |
| 2.16 ¹¹ B NMR Spectrum of Attempted CO ₂ Hydroboration Using 1.0 mol% Ph ₂ PPrPDI as a Catalyst in Benzene- <i>d</i> ₆ | 64 |
| 2.17 ¹ H NMR Spectrum of CO ₂ Hydroboration Using 0.1 mol% 5 After 8 h at 90 °C in Benzene- <i>d</i> ₆ | 64 |

| Figure | Page |
|--|------|
| 2.18 ¹ H NMR Spectrum of Distilled Methanol from the Hydrolysis of CO ₂ Hydroboration Products Using 0.1 mol% 5 in Benzene- <i>d</i> ₆ | 65 |
| 2.19 ¹³ C NMR Spectrum of Distilled Methanol from the Hydrolysis of CO ₂ Hydroboration Products Using 0.1 mol% 5 in Benzene- <i>d</i> ₆ | 65 |
| 2.20 Proposed Mechanism of 5 -Mediated CO ₂ Hydroboration | 66 |
| 2.21 ³¹ P NMR Spectrum of [(^{Ph} 2PPrPDI)MoI(CO)][I] (3) in Acetone- <i>d</i> ₆ | 72 |
| 2.22 ³¹ P NMR Spectrum of [(^{Ph} 2PPrPDI)MoI][I] (4) in Acetonitrile- <i>d</i> ₃ | 73 |
| 2.23 ¹ H NMR Spectrum of (κ ⁶ - <i>P,N,N,N,C,P</i> - ^{Ph} 2PPrPDI)MoH (5) in Benzene- <i>d</i> ₆ | 74 |
| 2.24 ¹³ C NMR Spectrum of (κ ⁶ - <i>P,N,N,N,C,P</i> - ^{Ph} 2PPrPDI)MoH (5) in benzene- <i>d</i> ₆ | 75 |
| 2.25 gHSQCAD NMR Spectrum of (κ ⁶ - <i>P,N,N,N,C,P</i> - ^{Ph} 2PPrPDI)MoH (5) in Benzene- <i>d</i> ₆ | 75 |
| 2.26 ¹ H-Coupled ¹³ C NMR Spectrum of (κ ⁶ - <i>P,N,N,N,C,P</i> - ^{Ph} 2PPrPDI)MoH (5) in Benzene- <i>d</i> ₆ | 76 |
| 2.27 ³¹ P NMR Spectrum of (κ ⁶ - <i>P,N,N,N,C,P</i> - ^{Ph} 2PPrPDI)MoH (5) in Benzene- <i>d</i> ₆ | 76 |
| 2.28 ¹ H NMR Spectrum of (κ ⁶ - <i>P,N,N,N,C,P</i> - ^{Ph} 2PPrPDI)Mo(OCOH) (6) in Benzene- <i>d</i> ₆ | 77 |
| 2.29 ¹³ C NMR Spectrum of (κ ⁶ - <i>P,N,N,N,C,P</i> - ^{Ph} 2PPrPDI)Mo(OCOH) (6) in Benzene- <i>d</i> ₆ | 78 |
| 2.30 gHSQCAD NMR Spectrum of (κ ⁶ - <i>P,N,N,N,C,P</i> - ^{Ph} 2PPrPDI)Mo(OCOH) (6) in Benzene- <i>d</i> ₆ | 78 |

| Figure | Page |
|--|------|
| 2.31 ^{31}P NMR Spectrum of (κ^6 - <i>P,N,N,N,C,P</i> - Ph_2PPr PDI)Mo(OCOH) (6) in Benzene- d_6 | 78 |
| 3.1 Previously Described Synthesis of (Ph_2PPr PDI)Mo Complexes 3-5 from 2 | 92 |
| 3.2 Synthesis of [Ph_2PPr PDI)MoI][I] (4) from $(\text{CO})_3\text{MoI}_2(\text{NCCH}_3)_2$ | 92 |
| 3.3 Cyclic Voltammogram of 3.0 mM 4 in Dry Acetonitrile..... | 93 |
| 3.4 Synthesis of (κ^6 - <i>P,N,N,N,C,P</i> - Ph_2PPr PDI)MoI (7) from [Ph_2PPr PDI)MoI][I] | 95 |
| 3.5 The Solid State Structure of 7 | 95 |
| 3.6 Synthesis of (Ph_2PPr PDI)MoI (8) from [Ph_2PPr PDI)MoI][I] | 96 |
| 3.7 Experimental (black) and Simulated (red) X-band EPR Spectra of 8 | 98 |
| 3.8 The Solid State Structure of 8 | 100 |
| 3.9 Attempt to Isolate (Ph_2PPr PDI)MoH from [Ph_2PPr PDI)MoI | 101 |
| 3.10 Interconversion of (Ph_2PPr PDI)Mo Complexes 4, 5, 7, and 9 | 102 |
| 3.11 The Molecular Structure of 9 | 102 |
| 3.12 Synthesis of (Ph_2PPr PDI)MoD ₂ (9-d₂) from 5 | 103 |
| 3.13 ^1H NMR Spectrum of (κ^6 - <i>P,N,N,N,C,P</i> - Ph_2PPr PDI)MoI (7) in Benzene- d_6 | 111 |
| 3.14 ^{13}C NMR Spectrum of (κ^6 - <i>P,N,N,N,C,P</i> - Ph_2PPr PDI)MoI (7) in Benzene- d_6 | 112 |
| 3.15 ^{31}P NMR Spectrum of (κ^6 - <i>P,N,N,N,C,P</i> - Ph_2PPr PDI)MoI (7) in Benzene- d_6 | 112 |
| 3.16 gHSQCAD NMR Spectrum of 7 in Benzene- d_6 | 113 |
| 3.17 ^1H NMR Spectrum of (Ph_2PPr PDI)MoH ₂ (9) in Benzene- d_6 | 115 |
| 3.18 ^{13}C NMR Spectrum of (Ph_2PPr PDI)MoH ₂ (9) in Benzene- d_6 | 116 |
| 3.19 ^{31}P NMR Spectrum of (Ph_2PPr PDI)MoH ₂ (9) in Benzene- d_6 | 116 |

| Figure | Page |
|---|------|
| 3.20 gHSQCAD NMR Spectrum of (^{Ph2PPr} PDI)MoH ₂ (9) in Benzene- <i>d</i> ₆ | 117 |
| 3.21 ² H NMR Spectrum of 7-d ₂ in Benzene- <i>d</i> ₆ | 117 |
| 3.22 ³¹ P NMR Spectrum of 9-d ₂ in Benzene- <i>d</i> ₆ | 118 |
| 4.1 Synthesis of [(^{Ph2PPr} PDI)MoO][PF ₆] ₂ (10) | 123 |
| 4.2 ¹ H NMR Spectrum of [(^{Ph2PPr} PDI)MoO][PF ₆] ₂ (10) in Acetonitrile- <i>d</i> ₃ | 123 |
| 4.3 ³¹ P NMR Spectrum of [(^{Ph2PPr} PDI)MoO][PF ₆] ₂ (10) in Acetonitrile- <i>d</i> ₃ | 124 |
| 4.4 Infrared Spectrum of [(^{Ph2PPr} PDI)MoO][PF ₆] ₂ (10) in KBr..... | 124 |
| 4.5 The Solid State Structure of 10 | 125 |
| 4.6 Cyclic Voltammogram of 2.1 mM 10 | 126 |
| 4.7 A. Cyclic Voltammograms of 1.25 mM 10 in Acetonitrile with Variable Water B. Cyclic Voltammogram from 2.0 mM 10 in 3.5 M Water in Acetonitrile | 127 |
| 4.8 A. Dependence of Catalytic Current (<i>i_{cat}/i_p</i>) on Concentration of Water. B. Anodic Peak that Develops at Increasing Water Concentrations | 128 |
| 4.9 A. Catalytic Current Depends Linearly on the Concentration of 10 . B. Dependence of Normalized Catalytic Current on Water Concentration | 131 |
| 4.10 Synthesis of (^{Ph2PPr} PDI)MoO (11) | 132 |
| 4.11 ¹ H NMR Spectrum of (^{Ph2PPr} PDI)MoO (11) in Benzene- <i>d</i> ₆ | 133 |
| 4.12 ³¹ P NMR Spectrum of (^{Ph2PPr} PDI)MoO (11) in Benzene- <i>d</i> ₆ | 133 |
| 4.13 The Solid State Structure of 11 | 133 |
| 4.14 Synthesis of 11 from [(κ ⁶ - <i>P,P,N,N,N,C</i> - ^{Ph2PPr} PDI)MoH] (5)..... | 135 |

| Figure | Page |
|---|------|
| 4.15 ¹ H NMR Spectrum of 11 in Benzene- <i>d</i> ₆ Obtained from Stoichiometric H ₂ O Addition to [(κ ⁶ - <i>P,P,N,N,N,C</i> - ^{Ph₂PPr} PDI)MoH] (5) | 135 |
| 4.16 ³¹ P NMR Spectrum of 10 in Acetonitrile After Bulk Electrolysis with D ₂ O.. | 136 |
| 4.17 ² H NMR Spectrum of 10 in Acetonitrile After Bulk Electrolysis with D ₂ O .. | 136 |
| 4.18 Proposed Electrocatalytic Cycle for Hydrogen Evolution from Water | 137 |
| 4.19 Alternative Ligand-assisted Electrocatalytic Cycle for Generation of H ₂ and Hydroxide Ions from Water | 138 |
| 4.20 ¹³ C NMR Spectrum of [(^{Ph₂PPr} PDI)MoO][PF ₆] ₂ (10) in Acetonitrile- <i>d</i> ₃ | 143 |
| 4.21 gHSQCAD NMR Spectrum of [(^{Ph₂PPr} PDI)MoO][PF ₆] ₂ (10) in Acetonitrile- <i>d</i> ₃ | 143 |
| 4.22 ¹³ C NMR Spectrum of (^{Ph₂PPr} PDI)MoO (11) in Benzene- <i>d</i> ₆ | 145 |
| 4.23 Infrared Spectrum of (^{Ph₂PPr} PDI)MoO (11) in KBr..... | 145 |
| 4.24 gHSQCAD NMR Spectrum of 11 in Benzene- <i>d</i> ₆ | 146 |
| 5.1 Reductive Coupling Modes of CO ₂ | 151 |
| 5.2 Synthesis of (^{Ph₂PPr} DI)MoI ₂ (13) and (^{Ph₂PPr} DI)Mo(N ₂) ₂ (14) | 153 |
| 5.3 ¹ H NMR of (^{Ph₂PPr} DI)MoI ₂ (13) in Benzene- <i>d</i> ₆ | 153 |
| 5.4 Single Crystal Structures of 13 (Left), 14 (Middle), and 15 (Right) | 154 |
| 5.5 ¹ H NMR of (^{Ph₂PPr} DI)Mo(N ₂) ₂ (14) in Benzene- <i>d</i> ₆ | 155 |
| 5.6 ³¹ P NMR of (^{Ph₂PPr} DI)Mo(N ₂) ₂ (14) in Benzene- <i>d</i> ₆ | 155 |
| 5.7 Formation of (^{Ph₂PPr} DI)Mo(CO) ₂ (15) from (^{Ph₂PPr} DI)Mo(N ₂) ₂ (14) and CO ₂ (Forward) and from Mo(CO) ₆ (Reverse) | 156 |

| Figure | Page |
|--|------|
| 5.8 ^1H NMR of $(^{\text{Ph}_2\text{PPrDI}}\text{Mo}(\text{CO})_2)$ (15) in Benzene- d_6 | 157 |
| 5.9 ^{31}P NMR of $(^{\text{Ph}_2\text{PPrDI}}\text{Mo}(\text{CO})_2)$ (15) in Benzene- d_6 | 157 |
| 5.10 Infrared Spectrum of $(^{\text{Ph}_2\text{PPrDI}}\text{Mo}(\text{CO})_2)$ (15) in KBr Pellet..... | 157 |
| 5.11 Time-dependent ^{31}P NMR Spectroscopy After Addition of 1 atm CO_2 to 14 | 159 |
| 5.12 Proposed Mechanistic Pathway for the Formation of $(^{\text{Ph}_2\text{PPrDI}}\text{Mo}(\text{CO})_2)$ (15) and O_2 from $(^{\text{Ph}_2\text{PPrDI}}\text{Mo}(\text{N}_2)_2)$ (14) and CO_2 | 160 |
| 5.13 PDI and Modified DI Supported Mo Dicarbonyl Complexes..... | 161 |
| A.1 ^1H NMR of $^{\text{PyEt}}\text{PDIMoOCl}_2$ in Benzene- d_6 | 184 |
| A.2 ^{31}P NMR Spectrum of $[(^{\text{Ph}_2\text{PPr}}\text{PDI})\text{MoCl}_2][\text{Cl}]$ in Chloroform- d | 185 |
| A.3 Single Crystal Structure of $[(^{\text{Ph}_2\text{PPr}}\text{PDI})\text{MoCl}_2][\text{Cl}]$ | 185 |
| A.4 Single Crystal Structure of $(\kappa^6\text{-}N,N,N,P,P,C\text{-}^{\text{Ph}_2\text{PPr}}\text{PDI})\text{MoCl}$ | 186 |
| A.5 Single Crystal Structure of $[(^{\text{Ph}_2\text{PPr}}\text{PDI})\text{Mo}(\text{H}_2\text{O})][\text{CO}_3]$ | 186 |
| A.6 ^1H NMR Spectrum of $(^{\text{Ph}_2\text{PPr}}\text{PDI})\text{Mo}(\text{CH}_2=\text{CH}_2)$ in Benzene- d_6 | 188 |
| A.7 ^{31}P NMR Spectrum of $(^{\text{Ph}_2\text{PPr}}\text{PDI})\text{Mo}(\text{CH}_2=\text{CH}_2)$ in Benzene- d_6 | 188 |
| A.8 Single Crystal Structure of $(^{\text{Ph}_2\text{PPr}}\text{PDI})\text{Mo}(\text{CH}_2=\text{CH}_2)$ | 188 |
| A.9 ^1H NMR Spectrum of $(^{\text{Ph}_2\text{PEt}}\text{PDI})\text{Mo}(\text{CO})$ in Benzene- d_6 | 190 |
| A.10 ^{31}P NMR Spectrum of $(^{\text{Ph}_2\text{PEt}}\text{PDI})\text{Mo}(\text{CO})$ in Benzene- d_6 | 190 |
| A.11 ^1H NMR Spectrum of $^{\text{iPrAr,Ph}_2\text{PPr}}\text{PDI}$ in Benzene- d_6 | 191 |
| A.12 ^{31}P NMR Spectrum of $^{\text{iPrAr,Ph}_2\text{PPr}}\text{PDI}$ in Benzene- d_6 | 191 |
| B.1 ^1H NMR Spectrum of $(^{\text{PyEt}}\text{PDI})\text{CoCl}_2$ in Chloroform- d | 192 |

| Figure | Page |
|---|------|
| B.2 ^1H NMR Spectrum of $(^{\text{PyEt}}\text{PDIH})\text{Co}$ in Benzene- d_6 | 193 |
| B.3 Single Crystal Structure of $(^{\text{PyEt}}\text{PDIH})\text{Co}$ | 193 |
| C.1 ^1H NMR Spectrum of $(^{\text{PyEt}}\text{PDI})\text{Fe}$ in Benzene- d_6 | 195 |
| C.2 ^1H NMR Spectrum of $^{\text{PhPPr2}}\text{PDI}$ in Benzene- d_6 | 195 |
| C.3 ^{13}C NMR Spectrum of $^{\text{PhPPr2}}\text{PDI}$ in Benzene- d_6 | 196 |
| C.4 ^{31}P NMR Spectrum of $^{\text{PhPPr2}}\text{PDI}$ in Benzene- d_6 | 196 |
| C.5 ^1H NMR Spectrum of $^{\text{PhPPr2}}\text{PDI}$ in Benzene- d_6 | 197 |
| C.6 ^{31}P NMR Spectrum of $^{\text{PhPPr2}}\text{PDI}$ in Benzene- d_6 | 197 |
| C.7 ^1H NMR Spectrum of $(^{\text{Ph2PPr}}\text{DI})\text{Fe}(\text{OTf})_2$ in Acetonitrile- d_3 | 198 |
| C.8 ^{31}P NMR Spectrum of $(^{\text{Ph2PPr}}\text{DI})\text{Fe}(\text{OTf})_2$ in Acetonitrile- d_3 | 198 |

SUMMARY

Selective and efficient utilization of small molecules has been a center of interest in the fields of catalysis, renewable energy production, pharmaceuticals, and the polymer industry. While precious metals have shown superior efficacy in terms of activity, selectivity, and longevity, their high cost and toxicity have opened up a new search for inexpensive and less-toxic homogeneous metal catalysts.¹ Although many researchers are focused on developing earth-abundant, first-row metal catalysts, due to complex one-electron processes and air-sensitivity, efficient and robust homogeneous catalysts have yet to be introduced in the industrial market.² Molybdenum, despite being a second row transition metal, is non-toxic, relatively abundant in the earth's crust (1.2 mg/kg),³ and the only second-row metal that is widely utilized in biological systems.⁴ Hence, for my graduate research, I hypothesized that properly tuned molybdenum catalysts could serve as sustainable alternatives to precious metals for small molecule activation. Although, homogeneous molybdenum catalysis has developed over the last few decades, extensive success has been limited to R. R. Schrock's metathesis catalysts (*Nobel Prize*, 2005).⁵ Efforts have been made to activate dinitrogen (N_2) to generate ammonia using various low-valent molybdenum catalysts,⁶ however, utilization of molybdenum to activate carbon dioxide (CO_2)⁷ and water (H_2O)⁸ to produce renewable fuels, such as formate, methanol, carbon monoxide or hydrogen has been scarce. To help meet these goals, my colleagues and I have developed a series of pendant amine- and phosphine-substituted bis(imino)pyridine or pyridine diimine (PDI)⁹ and diimine (DI)¹⁰ ligands which are capable of stabilizing a wide-number of transition metals, mainly low-electron count, early transition

metals beyond their traditional κ^3 -coordination motifs in different oxidation states relevant to catalysis. With a set of novel ligands in hand, I have devoted my Ph.D. work to the design, synthesis, characterization, and application of homogeneous molybdenum catalysts for organic transformations and the utilization of earth-abundant small molecules, such as CO_2 , N_2 , and H_2O to make useful chemical commodities and renewable fuels as shown in Fig. 1.

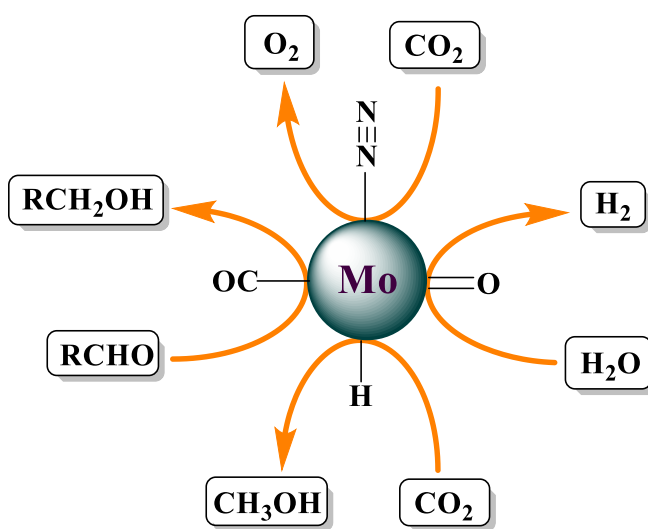


Figure 1. Summary of Mo-mediated transformations discovered in this dissertation.

C=O Bond Reduction

Reduction of C=O and C=C bonds by silanes is an interesting approach to produce a range of silicone polymers useful for the adhesive and coating industries.¹¹ Most of the industrial-scale hydrosilylation processes are dependent on platinum based catalysts, such as Karstedt's catalyst and Speier's catalysts. In the hope of developing inexpensive and sustainable alternatives, Berke and coworkers have recently showed that $[(\text{DPEphos})\text{Mo}(\text{NO})(\text{NCMe})_3][\text{BArF}^4]$ can catalyze the hydrosilylation of aldehydes and

ketones at 120 °C with turn over frequencies (TOF) of up to 4864 and 32000 h⁻¹, respectively.¹² Inspired by this, we decided to design a set of low-valent molybdenum catalysts supported by penta-coordinated PDI ligands which can hydrosilylate unsaturated organics at milder conditions. Refluxing a pyridine substituted PDI, ^{PyEt}PDI, and Mo(CO)₆ resulted in formation of the bis(ligand) complex, (^{PyEt}PDI)₂Mo (**1**). Using a three-carbon chain phosphine PDI, ^{Ph₂PPt}PDI, allowed for the isolation of (^{Ph₂PPt}PDI)Mo(CO) (**2**). Both compounds were characterized by multinuclear NMR, IR, UV-Vis, and single crystal X-ray diffraction. Although the imine bond distances obtained from solid-state structures of **1** and **2** support PDI ligand reduction, a density functional theory (DFT) calculation on **1** revealed that the complex possesses a zero-valent metal center, Mo(0) that engages in significant backbonding with each ^{PyEt}PDI ligand. Interestingly, both **1** and **2** act as active precatalysts for the hydrosilylation of aldehydes with comparable activity. Varying the silane reductant was found to dramatically impact the rate of aldehyde hydrosilylation. Using **2** as the precatalyst, a range of silanes have been screened and it was found that phenylsilane is the most effective in reducing a wide number of aromatic and aliphatic aldehydes with turnover frequencies (TOF) ranging from 173-330 h⁻¹ at 90 °C (61-93% isolated yield of the corresponding alcohols). While controlled addition of phenylsilane did not result in modification of the catalyst, addition of benzaldehyde to **2** showed C=O coordination with concomitant phosphine arm dissociation. Then catalytic Si-H oxidative addition followed by substrate insertion and reductive elimination produced the corresponding silyl ethers.¹³

C-H Activation & CO₂ Functionalization

A growing awareness of global climate change and increasing atmospheric CO₂ concentrations has propelled the search for alternative CO₂ utilization technologies.¹⁴ Since **2** catalyzes C=O bond hydrosilylation, we sought to extend the utility of ^{Ph₂PPr}PDI supported Mo chemistry to the reduction of CO₂ into methanol, which is an important commodity chemical and fuel. Although **2** catalyzes hydrosilylation of aldehydes, due to the presence of the strong π-accepting carbonyl ligand at the primary coordination sphere, it is reluctant towards the reduction of CO₂. Attempts to remove the CO ligand thermally were unsuccessful because of strong metal-to-ligand π-backbonding. However, oxidation of the Mo(0) center by adding stoichiometric I₂, resulted a seven coordinate Mo(II) complex, [^{Ph₂PPr}PDI)Mo(CO)I][I] (**3**) with a diminished degree of backdonation. When heated at 100 °C, CO dissociation results in a six coordinate molybdenum diiodide complex, [^{Ph₂PPr}PDI)MoI][I] (**4**) which was characterized by multinuclear NMR, UV-Vis, cyclic voltammetry, and single crystal X-ray diffraction.

Interestingly, reduction of **4** in the presence of excess K-Hg allowed for the isolation of a seven-coordinate Mo(II) hydride complex, (κ⁶-*P,N,N,N,C,P*-^{Ph₂PPr}PDI)MoH (**5**) following C-H activation of one α-methylene PDI imine substituent. The unusual coordination arrangement of **5** was confirmed by multinuclear NMR and single crystal X-ray diffraction. The geometry about molybdenum can best be described as distorted pentagonal bipyramidal with a three-membered metallacycle having an exceptionally short N(1)-Mo(1)-C(10) angle of 38°. Interestingly, instantaneous insertion into the Mo-H bond was observed when **5** was exposed to CO₂ yielding the corresponding formate complex,

(κ^6 -*P,N,N,N,C,P*-Ph²PPrPDI)Mo(OCHO) (**6**). Inspired by the ability of **5** to reduce CO₂ into formate, we sought to further reduce the bound formate moiety by using a sacrificial hydrogen source, pinacolborane (HBpin). When CO₂ was limiting, its quantitative conversion to CH₃OBpin and (Bpin)₂O was observed along with regeneration of **5** by ¹H and ³¹P NMR over the course of 2 d at 60 °C. After addition of 1 atm of CO₂ to a J Young NMR tube containing a C₆D₆ solution of 100 equivalents HBpin relative to **5** at -70 °C, the reaction was heated to 90 °C and monitored by ¹H NMR. Within 2 h, near complete consumption of HBpin was observed with the formation of CH₃OBpin, CH₂(OBpin)₂, and (Bpin)₂O in a 1:2:2 ratio. After 5 h of heating, a 1:1 mixture of CH₃OBpin and (Bin)₂O was observed, indicating complete conversion of CO₂ to a methanol equivalent via the methylene intermediate, CH₂(OBpin)₂. This reaction was optimized such that 0.1 mol% of **5** was used in the absence of solvent at 90 °C, allowing a methoxide formation TOF of 40.4 h⁻¹ (B-H utilization TOF = 121.2 h⁻¹). Hydrolyzing the reaction mixture with water followed by short-path distillation allowed for the isolation of methanol. Finally, the mechanism of **5**-mediated CO₂ hydroboration has been proposed to proceed through a series of insertion and σ -bond metathesis. This advance is noteworthy because **5** is the first well-defined molybdenum hydroboration catalyst that is capable of converting CO₂ to methanol.¹⁵

Uncommon Mo(I) Oxidation State

Along with stabilizing unusual geometries, the Ph²PPrPDI chelate was also found to stabilize an uncommon oxidation state of molybdenum. While the common oxidation states of molybdenum are 0, +2, +3, +4, +5, and +6, there are only few examples of well-defined

Mo(+1) complexes in the literature.³ One thoroughly characterized example is the dimeric [(Cp)Mo(CO)₃]₂ reported by Wilson.¹⁶ Wieghardt and co-workers reported the synthesis and solid state structure of [(Bn₃tacn)Mo(CO)₃][PF₆] (Bn₃tacn = 1,4,7-tribenzyl-1,4,7-triazacyclononane) with persistent monovalent molybdenum center.¹⁷ Recently, Chirik and coworkers have reported a terpyridine ligand supported Mo(I) complex, (Ph^hTpy)(PPh₂Me)₂MoCl with distorted ligand distances due to π-backbonding rather than chelate reduction.¹⁸ Interestingly, when an acetonitrile solution of **4** was analyzed by cyclic voltammetry, a reversible wave at -1.20 V vs. Fc⁺⁰, corresponding to the Mo^{III/I} redox couple was observed. Attempts to isolate the one-electron reduced product of **4** using stoichiometric K/naphthalene resulted in ligand deprotonation rather than reduction to yield a Mo(II) monoiodide complex, (κ⁶-*P,N,N,N,C,P*-Ph²PPrPDI)MoI (**7**) which is isostructural to **5**. However, successful isolation of the inner-sphere Mo(I) monoiodide complex, (Ph²PPrPDI)MoI (**8**) was achieved via reduction of **4** with equimolar Na/naphthalene. This complex was found to be NMR silent and have a near octahedral geometry by single crystal X-ray diffraction. Electron paramagnetic resonance (EPR) spectroscopy of **8** revealed an unpaired Mo-based electron which is delocalized onto two adjacent imine bonds. Efforts to prepare a Mo(I) monohydride complex upon adding NaEt₃BH to **8** resulted in disproportionation to yield a 1:1 mixture of **5** and newly identified (Ph²PPrPDI)MoH₂ (**9**) which showed a minimum hydride resonance *T*₁ value of 176 ms at -20 °C, suggesting that the Mo-bound H atoms are best described as classical hydrides. Along with the independent synthesis of **9**, facile interconversion of **4**, **5**, **7**, **8**, and **9** has been demonstrated.¹⁹

Water-splitting

Along with methanol, hydrogen gas is also a fuel of interest because it is a zero-emission, carbon-neutral, and high-energy density molecule. Although hydrogen evolution is a well-established field of research, most of the Ni/C electrodes are operable only in basic conditions, while traditional Pt catalysts are not cost-effective.²⁰ Recently, Long and Chang group have shown that a high-valent molybdenum oxo electrocatalyst, [(Py₅Me₂)MoO][PF₆]₂ can produce hydrogen from neutral water with TOF = 2.3 s⁻¹, albeit at an overpotential of 1.0 V.⁸ Inspired by this, I have designed a homogeneous Mo(IV) oxo electrocatalyst, [(^{Ph}2PPrPDI)MoO][PF₆]₂ (**10**) which is capable of generating hydrogen from water with TOF as high as 55 s⁻¹. Heating an acetonitrile solution of **4** and styrene oxide at 60 °C in the presence of two equivalents AgPF₆ allowed for the isolation of **10**, which was characterized by multi-nuclear NMR, UV-Vis, IR, electrochemistry, and single crystal X-ray diffraction. Analysis of **10** by cyclic voltammetry displayed two reversible transitions at -0.70 V and -1.26 V vs Fc⁺⁰, corresponding to the Mo^{IV/III} and Mo^{III/II} redox couples, respectively. Two irreversible redox events corresponding to Mo^{II/I} and Mo^{I/0} were also observed at -1.53 and -1.95 V vs Fc⁺⁰, respectively. This complex acts as an efficient electrocatalyst for the production of H₂ from neutral water with 96% faradaic efficiency at an overpotential of 1.65-1.70 V and a rate constant of as high as 55 s⁻¹. While two electron reduction of **10** afforded the key intermediate (^{Ph}2PPrPDI)MoO (**11**), adding a stoichiometric amount of water to the C-H activated compound, **5** resulted in H₂ elimination along with the formation of **11**. A distorted octahedral geometry of **11** was confirmed by single-crystal X-ray diffraction. The possibility of ligand C-H activation during the electrocatalytic cycle

has been eliminated by controlled potential electrolysis using D₂O. Analysis of the post-electrolysis catalyst by ³¹P and ²H NMR spectroscopy showed the presence of **10** without incorporation of deuterium into the ligand arm. Furthermore, adding 4 atm of H₂ to a C₆D₆ solution of **11** allowed for the observation of a new symmetric compound, (Ph²PPrPDI)Mo(H₂O) (**12**), which under vacuum, regenerates **11** followed by H₂ elimination. Based on the experimental evidences, a possible mechanism for **11** catalyzed electrochemical reduction of the H₂O to H₂ has been proposed to undergo by two consecutive proton-coupled single electron transfer (PCET) processes to yield **12**, which followed by O-H oxidative addition and 1,2-elimination of H₂, regenerates the active catalyst, **11**.²¹

Direct Conversion of CO₂ to O₂

While the donor substituted PDI ligands exhibited a number of unique and interesting features when bound to molybdenum as discussed above, changing the ligand-backbone from PDI to DI produced completely different reactivity. Unlike the PDI chelates, these DI ligands are tetradentate and have two open coordination sites, instead of one, when bound to molybdenum which allow for performing reductive coupling of substrates. Heating an equimolar solution of (CO)₃MoI₂(NCMe)₂ and Ph²PPrDI to 110 °C allowed for the isolation of a green paramagnetic compound, (Ph²PPrDI)MoI₂ (**13**). Interestingly, unlike PDI, no arm C-H activation has been observed when **13** was reduced by excess K/Hg; instead, a red, diamagnetic bis(dinitrogen) complex, (Ph²PPrDI)Mo(N₂)₂ (**14**) was isolated that exhibits two IR stretches at 1895 and 1980 cm⁻¹ corresponding to the symmetric and asymmetric vibrations of two weakly activated *cis*-dinitrogen ligands. Surprisingly, when 1 atm of CO₂

was added to a C_6D_6 solution of **14**, clean conversion to a new compound, $(^{Ph_2PPt}DI)Mo(CO)_2$ (**15**) was observed by multinuclear NMR and IR spectroscopy. Head-space analysis of the NMR tube by GC revealed formation of dioxygen (O_2). Detail experimental and theoretical investigations are underway to elucidate the possible mechanistic pathway for this transformation.

References

- (1) (a) Gaillard, S.; Renaud, J.-L. *Chem. Sus. Chem.* **2008**, *1*, 505–509. (b) Troegel, D.; Stohrer, J. *Coord. Chem. Rev.* **2011**, *255*, 1440–1459.
- (2) (a) Morris, R. H. *Chem. Soc. Rev.* **2009**, *38*, 2282–2291. (b) Bullock, R. M. *Catalysis without Precious Metals*; Wiley-VCH: Weinheim, Germany, 2010. (c) Junge, K.; Schroeder, K.; Beller, M. *Chem. Commun.* **2011**, *47*, 4849–4859.
- (3) Haynes, W. M. *CRC Handbook of Chemistry and Physics: A Ready-Reference Book of Chemical and Physical Data*, 94th ed.; Taylor & Francis: Boca Raton, FL, 2013–2014.
- (4) Hille, R.; Hall, J.; Basu, P. *Chem. Rev.* **2014**, *114*, 3963–4038.
- (5) Schrock, R. R.; Murdzek, J. S.; Bazan, G. C.; Robbins, J.; DiMare, M.; O'Regan, M. J. *Am. Chem. Soc.* **1990**, *112*, 3875–3886.
- (6) (a) Chatt, J.; Dilworth, J. R.; Richards, R. L.; *Chem. Rev.* **1978**, *78*, 589–625. (b) Arashiba, K.; Miyake, Y.; Nishibayashi, Y. *Nat. Chem.* **2011**, *3*, 120–125. (c) Kinoshita, E.; Arashiba, K.; Kuriyama, S.; Miyake, Y.; Shimazaki, R.; Nakanishi, H.; Nishibayashi, Y. *Organometallics* **2012**, *31*, 8437–8443. (d) C. Laplaza, C.; Cummins, C. C. *Science* **1995**, *268*, 861–863. (e) Yandulov, D. V.; Schrock, R. R. *Science* **2003**, *301*, 76–78.
- (7) (a) Maia, L. B.; Fonseca, L.; Moura, I.; Moura, J. J. G. *J. Am. Chem. Soc.* **2016**, *138*, 8834–8846. (b) Sieh, D.; Lacy, D. C.; Peters, J. C.; Kubiak, C. P. *Chem. Eur. J.* **2015**, *21*, 8497–8503. (c) Grice, K. A.; Saucedo, C. *Inorg. Chem.* **2016**, *55*, 6240–6246. (d) Bagherzadeh, S.; Mankad, N. P. *J. Am. Chem. Soc.* **2015**, *137*, 10898–10901. (e) Bernskoetter, W. H.; Tyler, B. T. *Organometallics* **2011**, *30*, 520–527.
- (8) (a) Karunadasa, H. I.; Chang, C. J.; Long, J. R. *Nature* **2010**, *464*, 1329–1333. (b) Karunadasa, H. I.; Montalvo, E.; Sun, Y.; Majda, M.; Long, J. R.; Chang, C. J. *Science* **2012**, *335*, 698–702.
- (9) Ben-Daat, H.; Hall, G. B.; Groy, T. L.; Trovitch, R. J. *Eur. J. Inorg. Chem.* **2013**, 4430–4442.
- (10) Porter, T. M.; Hall, G. B.; Groy, T. L.; Trovitch, R. J. *Dalton Trans.* **2013**, *42*, 14689–14692.
- (11) Parshall, G. W.; Ittel, S. D. in *Homogeneous Catalysis: The Applications and Chemistry of Catalysis by Soluble Transition Metal Complexes*, 2nd ed.; John Wiley & Sons, Inc.: New York, 1992; pp 39–41.
- (12) Chakraborty, S.; Blacque, O.; Fox, T.; Berke, H. *ACS Catal.* **2013**, *3*, 2208–2217.
- (13) Pal, R.; Groy, T. L.; Bowman, A. C.; Trovitch, R. J. *Inorg. Chem.* **2014**, *53*, 9357–9365.

- (14) (a) Sakakura, T.; Choi, J.-C.; Yasuda, H. *Chem. Rev.* **2007**, *107*, 2365–2387. (b) Boogaerts, I. I. F.; Nolan, S. P. *Chem. Commun.* **2011**, *47*, 3021–3024. (c) Boogaerts, I. I. F.; Nolan, S. P. *J. Am. Chem. Soc.* **2010**, *132*, 8858–8859. (d) Boogaerts, I. I. F.; Fortman, G. C.; Furst, M. R. L.; Cazin, C. S. J.; Nolan, S. P. *Angew. Chem., Int. Ed.* **2010**, *49*, 8674–8677. (e) Zhang, L.; Cheng, J.; Ohishi, Z.; Hou, Z. *Angew. Chem., Int. Ed.* **2010**, *49*, 8670–8673. (f) Vechorkin, O.; Hirt, N.; Hu, X. *Org. Lett.* **2010**, *12*, 3567–3569. (g) Darensbourg, D. J. *Chem. Rev.* **2007**, *107*, 2388–2410.
- (15) Pal, R.; Groy, T. L.; Trovitch, R. J. *Inorg. Chem.* **2015**, *54*, 7506–7515.
- (16) Wilson, F. C.; Shoemaker, D. P. *J. Chem. Phys.* **1957**, *27*, 809.
- (17) Beissel, T.; Della Vedova, B. S. P. C.; Wieghardt, K.; Boese, R. *Inorg. Chem.* **1990**, *29*, 1736–1741.
- (18) Bezdek, M. J.; Guo, S.; Chirik, P. J. *Inorg. Chem.* **2016**, *55*, 3117–3127.
- (19) Pal, R.; Cherry, B. R.; Flores, M.; Groy, T. L.; Trovitch, R. J. *Dalton Trans.* **2016**, *45*, 10024–10033.
- (20) Carmo, M.; Fritz, D. L.; Mergel, J.; Stolten, D. *Int. J. Hydrogen Energy* **2013**, *38*, 4901.
- (21) Pal, R.; Laureanti, J. A.; Groy, T. L.; Jones, A. K.; Trovitch, R. J. *Chem. Commun.* **2016**, *52*, 11555–11558.

CHAPTER 1

PREPARATION AND HYDROSILYLATION ACTIVITY OF A MOLYBDENUM CARBONYL COMPLEX FEATURING A PENTADENTATE BIS(IMINO)PYRIDINE LIGAND

1.1. Abstract

Attempts to prepare low-valent molybdenum complexes that feature a pentadentate 2,6-bis(imino)pyridine (or pyridine diimine, PDI) chelate allowed for the isolation of two different products. Refluxing $\text{Mo}(\text{CO})_6$ with the pyridine-substituted PDI ligand, $^{\text{PyEt}}\text{PDI}$, resulted in carbonyl ligand substitution and formation of the respective bis(ligand) compound, $(^{\text{PyEt}}\text{PDI})_2\text{Mo}$ (**1**). This complex was investigated by single crystal X-ray diffraction and density functional theory (DFT) calculations indicated that **1** possesses a $\text{Mo}(0)$ center that backbonds into the π^* -orbitals of the unreduced PDI ligands. Heating an equimolar solution of $\text{Mo}(\text{CO})_6$ and the phosphine-substituted PDI ligand, $^{\text{Ph}_2\text{PPr}}\text{PDI}$, to 120°C allowed for the preparation of $(^{\text{Ph}_2\text{PPr}}\text{PDI})\text{Mo}(\text{CO})$ (**2**), which is supported by a κ^5 - N,N,N,P,P - $^{\text{Ph}_2\text{PPr}}\text{PDI}$ chelate. Notably, this complex has been found to catalyze the hydrosilylation of aldehydes with turnover frequencies (TOFs) of up to 330 h^{-1} at 90°C . Considering additional experimental observations, the potential mechanism of **2**-mediated carbonyl hydrosilylation is discussed.

Reprinted with the permission from Pal, R.; Groy, T. L.; Bowman, A. C.; Trovitch, R. J. *Inorganic Chemistry* **2014**, *53*, 9357-9365. Copyright 2014 American Chemical Society.

1.2. Introduction^{1a}

Homogeneous transition metal complexes capable of mediating the efficient and selective reduction of C=C and C=O bonds have long been sought and studied by coordination chemists.^{1b} While hydrogenation catalysts have become vastly utilized for the synthesis of pharmaceuticals and other fine chemicals,² hydrosilylation catalysts have enabled the production of a wide range of silicone coatings, paints, and adhesives.³ Most industrial-scale hydrosilylation processes rely on precious metal catalysts due to their activity and stability;⁴ however, such catalysts are not always desirable because of their high cost and inherent toxicity.⁵ These characteristics have inspired the search for non-precious metal hydrosilylation catalysts that operate with competitive activities, selectivities, and catalyst lifetimes.⁶ This motivation has led researchers to develop numerous inexpensive and sustainable Mn,⁷ Fe,⁸ Co,⁹ and Ni¹⁰ hydrosilylation catalysts.

While the focus on late first-row transition metal hydrosilylation catalysis continues to intensify,¹¹ the investigation of homogenous Mo-based reduction catalysis has remained relatively overlooked, even though this metal is non-toxic¹² and relatively abundant in the earth's crust (1.2 mg/kg).¹³ Well-defined Mo complexes that mediate the hydrogenation of C=C^{14,15} and C=O bonds^{16,17} have been studied; however, the activity of these catalysts has remained limited to $<50 \text{ h}^{-1}$ at 100 °C, which was reported for Mo(CO)₃(NCMe)(PPh₃)₂-mediated olefin hydrogenation.¹⁵ Mo-based alkene hydrosilylation catalysts have also been described;^{14,18} however, coordination chemists have been far more successful in developing robust and highly active Mo catalysts that mediate C=O bond hydrosilylation. In 2003, Dioumaev and Bullock reported that [CpMo(CO)₂(IMes)][B(C₆F₅)₄] is active for

the hydrosilylation of 3-pentanone at 23 °C; however, the initial TOF of 10 h⁻¹ recorded for this transformation was inferior to the TOFs observed for the tungsten congener of this complex (370 h⁻¹).¹⁹ Research conducted by the Royo²⁰ and Abu-Omar²¹ groups has demonstrated that Mo(IV) dioxo complexes can catalyze the hydrosilylation of aldehydes and ketones with TOFs of up to 80 h⁻¹ at 25 °C.^{20b} Similar TOFs for the hydrosilylation of aldehydes using several related Mo(IV) imido complexes have since been reported by the Nikonov group.²² Mo(0) hydrosilylation catalysts have also been described²³ and Berke and co-workers recently revealed that [(DPEphos)Mo(NO)(NCMe)₃][BAR^F₄] can mediate the hydrosilylation of aldehydes with TOFs of up to 4,864 h⁻¹ and the hydrosilylation of ketones with initial TOFs of up to 32,000 h⁻¹ at 120 °C.²⁴

With this precedent in mind, we hypothesized that it might be possible to design a low-valent Mo hydrosilylation catalyst that is bound to a single donor-substituted PDI ligand, rather than the set of bidentate and monodentate ligands that comprise [(DPEphos)Mo(NO)(NCMe)₃][BAR^F₄]. Our group has utilized this methodology²⁵ to prepare a formally zerovalent Mn complex, (^{Ph₂PPr}PDI)Mn,⁷ⁱ that catalyzes ketone hydrosilylation with TOFs of up to 76,800 h⁻¹ at ambient temperature. Herein, we describe our efforts to prepare Mo complexes that feature a pentadentate PDI ligands, as well as the hydrosilylation activity of one such complex.

1.3. Results and Discussion^{1a}

This project commenced with the synthesis of 2,6-bis[1-(2-ethylpyridylimino)ethyl]pyridine (^{Py^{Et}}PDI), which we hoped would coordinate to low-valent Mo in a κ^5 -*N,N,N,N,N*-fashion. Although (^{Py^{Et}}PDI) had previously been prepared in

low yield (24.6%) by heating a benzene solution of 2,6-diacetylpyridine and 2-aminoethylpyridine,²⁶ it was discovered that yields of up to 96% could be obtained upon heating a toluene solution of these starting materials, a catalytic amount of *p*-toluene sulfonic acid, and 4 Å molecular sieves in a thick-walled glass bomb to 80 °C. With ^{PyEt}PDI in hand, a stoichiometric amount of this ligand was added to a *m*-xylene solution of Mo(CO)₆ and heating to 130 °C for 2 days produced a brown colored solution that offered evidence for ^{PyEt}PDI metallation by ¹H NMR spectroscopy. Because appreciable amounts of the newly formed product could not be isolated from this reaction, the stoichiometry was modified such that 2 equivalents of ^{PyEt}PDI were added per Mo(CO)₆ equivalent. This adjustment allowed the isolation and full characterization of the respective bis(ligand) compound, (^{PyEt}PDI)₂Mo (Fig. 1.1, **1**). Alternatively, this complex has been prepared by reducing (py)₃MoCl₃²⁷ with excess Na amalgam in the presence of 2 equivalents of ^{PyEt}PDI.

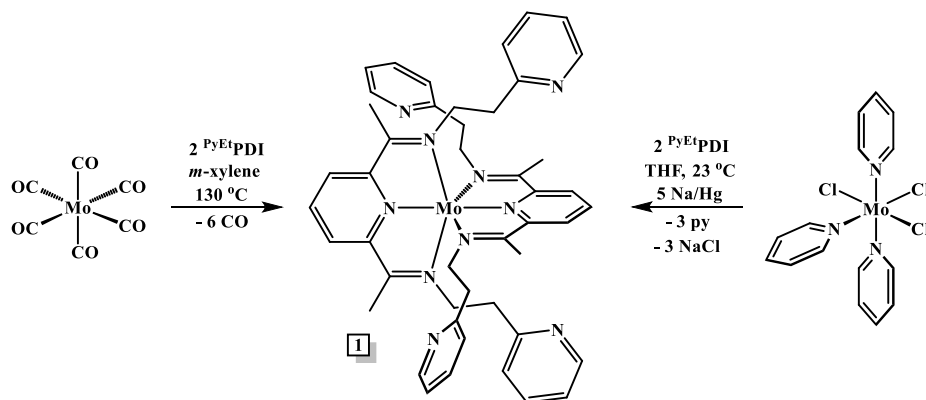


Figure 1.1. Synthetic scheme of (^{PyEt}PDI)₂Mo (**1**).

To confirm the identity of **1**, single crystals of this complex were grown from a concentrated pentane solution at -35 °C and further analyzed by X-ray diffraction. The solid state structure of **1** (Fig. 1.2) confirmed that each ^{PyEt}PDI chelate is coordinated to the

metal center in a terdentate fashion and that the overall geometry about Mo is best described as distorted octahedral, with N(2)-Mo(1)-N(2A) and N(1)-Mo(1)-N(3) angles of 179.7(2) and 147.55(15)°, respectively. Although several reports have demonstrated the coordination of bis(imino)pyridine chelates to Mo,²⁸ only one other complex featuring κ^3 -*N,N,N*-PDI ligation has been crystallographically characterized to date, (^{Et}₂ArPDI)MoCl₃.²⁹ This complex was found to have chelate bond distances that are consistent with minimal backbonding from the Mo(III) center to the π^* orbitals of ^{Et}₂ArPDI (N_{imine}-C_{imine} = 1.24(2), 1.31(2) Å; C_{imine}-C_{pyridine} = 1.49(3), 1.51(3) Å). In contrast, the bond distances established for the bis(imino)pyridine framework of **1** (Table 1.1) indicate that a significant amount of electron density is being transferred from the metal center to the π -system of each chelate, as might be expected for a formally zerovalent Mo complex. This is most apparent when considering the elongated N(1)-C(2) and N(3)-C(8) distances of 1.335(6) and 1.351(6) Å, as well as the contracted C(2)-C(3) and C(7)-C(8) distances of 1.419(7) and 1.420(7) Å, determined for **1**.

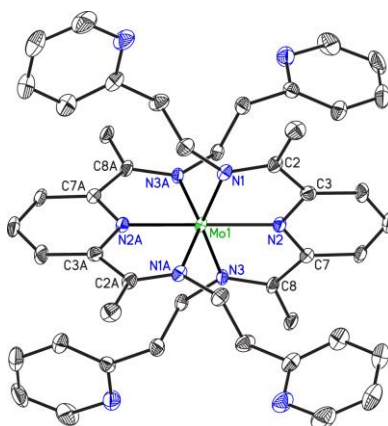


Figure 1.2. The solid state structure of **1** shown at 30% probability ellipsoids. Hydrogen atoms and co-crystallized pentane molecule are omitted for clarity.

Table 1.1. Experimental and calculated (RKS and RKS/COSMO) bond lengths (Å) and angles (°) for **1**.

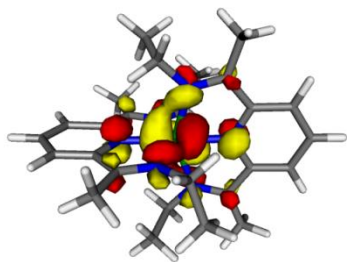
| | 1 | RKS | RKS/COSMO |
|------------------|------------|------------|------------------|
| Mo(1)-N(1) | 2.078(4) | 2.115 | 2.093 |
| Mo(1)-N(2) | 2.026(4) | 2.040 | 2.038 |
| Mo(1)-N(3) | 2.074(4) | 2.113 | 2.086 |
| N(1)-C(2) | 1.335(6) | 1.340 | 1.337 |
| N(3)-C(8) | 1.351(6) | 1.341 | 1.340 |
| C(2)-C(3) | 1.419(7) | 1.423 | 1.421 |
| C(7)-C(8) | 1.420(7) | 1.423 | 1.420 |
| N(2)-C(3) | 1.407(6) | 1.400 | 1.402 |
| N(2)-C(7) | 1.405(6) | 1.400 | 1.403 |
| | | | |
| N(1)-Mo(1)-N(1A) | 86.8(2) | 87.34 | 91.11 |
| N(1)-Mo(1)-N(3) | 147.55(15) | 147.44 | 147.26 |
| N(1)-Mo(1)-N(3A) | 102.09(15) | 101.58 | 97.16 |
| N(2)-Mo(1)-N(2A) | 179.7(2) | 179.71 | 176.40 |

Since the redox non-innocent nature of bis(imino)pyridine ligands has been widely publicized,³⁰⁻³² one must consider whether **1** is best described as having a Mo(0) center that simply backbonds into the π -system of each ^{PyEt}PDI ligand or as having an oxidized Mo center that is supported by radical monoanion or dianionic chelates. Although the bond distances determined for **1** might suggest that each chelate is reduced by at least one electron (one electron reduction: $C_{\text{imine}}-N_{\text{imine}} = 1.32 \text{ \AA}$, $C_{\text{imine}}-C_{\text{pyridine}} = 1.44 \text{ \AA}$; two electron reduction: $C_{\text{imine}}-N_{\text{imine}} = 1.36 \text{ \AA}$, $C_{\text{imine}}-C_{\text{pyridine}} = 1.40 \text{ \AA}$),³¹ recent work to determine the electronic structure of related (^{Me³Ar}DI)₂Mo(CO)₂ (DI = α -diimine) complexes has revealed that they possess Mo(0) metal centers, even though the DI structural parameters are consistent with single electron reduction.³³ To further investigate the electronic structure of **1**, density functional theory (DFT) calculations were performed at the B3LYP level of theory. The bond distances and angles found within the restricted

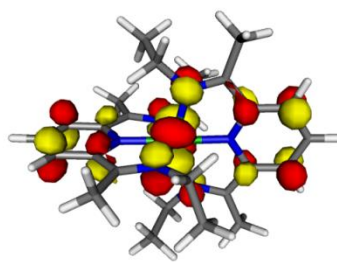
Kohn-Sham (RKS, closed shell) and RKS with applied Conductor-like Screening Model (RKS/COSMO, accounts for solvent effects) solutions for **1** (Table 1.1) are consistent with the experimentally determined values. The Mo-based HOMO, HOMO-1 and HOMO-2 orbitals (Fig. 1.3) are highly covalent and indicate significant metal to ligand backbonding. Furthermore, attempts to calculate the open shell singlet (unrestricted Kohn-Sham, UKS with $S = 0$) converged to the closed-shell solution, while the open shell triplet (UKS with $S = 1$) was geometrically distorted and found to be approximately 20 kcal/mol higher in energy than the RKS solution. These results indicate that **1** can best be described as having a zerovalent metal center that engages in backbonding with each ^{PyEt}PDI ligand.

Table 1.2. Relative orbital energies calculated for (^{PyEt}PDI)₂Mo.

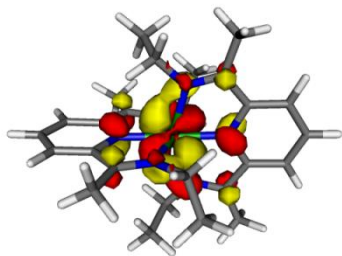
| Orbital | Occupation | Relative Energy (E_h) | Relative Energy (eV) | Relative Energy (kJ/mol) |
|----------------|-------------------|--|---------------------------------|-------------------------------------|
| 136 | 2 | -0.142016 | -3.8645 | -372.86747 |
| 137 | 2 | -0.140444 | -3.8217 | -368.7379 |
| 138 | 2 | -0.132727 | -3.6117 | -348.47599 |
| 139 | 0 | -0.053274 | -1.4497 | -139.87475 |
| 140 | 0 | -0.027016 | -0.7352 | -70.935998 |
| 141 | 0 | -0.022927 | -0.6239 | -60.197183 |
| 142 | 0 | -0.019290 | -0.5249 | -50.645138 |



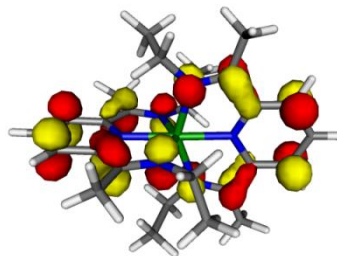
Orbital 142 – LUMO+3 – 45% Mo (d_{yz})



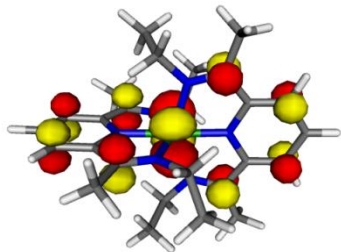
Orbital 141 – LUMO+2 – 30% Mo ($d_{x^2-y^2}$)



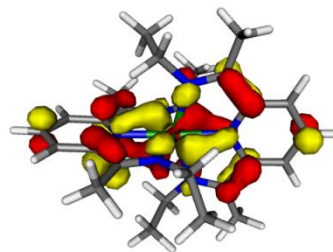
Orbital 140 – LUMO+1 – 42.1% Mo (d_{xz})



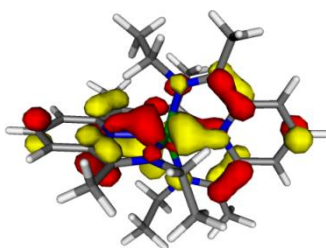
Orbital 139 – LUMO – Ligand π^*



Orbital 138 – HOMO – 39% Mo ($d_{x^2-y^2}$)



Orbital 137 – HOMO-1 – 26.1% Mo (d_{xz})



Orbital 136 – HOMO-2 – 24.8% Mo (d_{yz})

Figure 1.3. Orbital representations for (Py^{Et}PDI)₂Mo (1).

Having determined that PyEt^iPDI displaces the carbonyl ligands of $\text{Mo}(\text{CO})_6$, we hypothesized that incorporating high field strength donors within each imine substituent might allow the preparation of a zerovalent Mo complex featuring κ^5 -, rather than κ^3 -PDI coordination. Knowing that the phosphine-substituted chelate, Ph_2PPrPDI (equation 2), can coordinate to low-valent Rh^{34} and Mn^{7i} in a pentadentate fashion, a stoichiometric quantity of this chelate was added to a toluene solution of $\text{Mo}(\text{CO})_6$ and the reaction was heated to $120\text{ }^\circ\text{C}$ for 48 h. The resulting pink product was analyzed by multinuclear NMR spectroscopy and was found to exhibit a single ^{31}P NMR resonance at 34.88 ppm. Furthermore, this complex was found to possess six ligand methylene environments by ^1H NMR spectroscopy (expected for a complex that contains a C_2 rotation axis and top-to-bottom chelate inequivalence),³⁴ confirming that Ph_2PPrPDI chelate was coordinated in a pentadentate fashion. Analysis of this complex by IR spectroscopy revealed a single CO stretch at $1,740\text{ cm}^{-1}$, suggesting that the newly formed complex retains one CO ligand that is accepting a significant amount of electron density via π -backbonding from the Mo center. Taken together, this data suggested that the newly prepared complex was six-coordinate, $(\text{Ph}_2\text{PPrPDI})\text{Mo}(\text{CO})$ (**2**, Fig. 1.4).

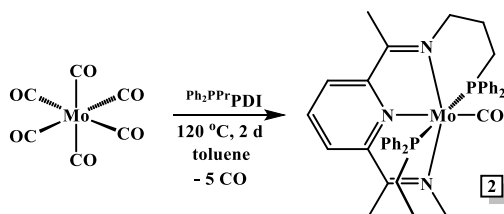


Figure 1.4. Synthesis of $(\text{Ph}_2\text{PPrPDI})\text{Mo}(\text{CO})$ (**2**) from $\text{Mo}(\text{CO})_6$.

An isolated crystal of **2** was then analyzed by single crystal X-ray diffraction to determine the overall geometry about Mo, as well as the existing degree of metal to Ph_2PPrPDI π -backbonding. The solid state structure (Fig 1.5) and metrical parameters (Table 1.3) determined for **2** reveal a few surprising characteristics. The geometry about the Mo center in **2** is significantly distorted from an idealized octahedron with N(1)-Mo(1)-N(3) and P(1)-Mo(1)-P(2) angles of 147.91(15) and 155.46(5) $^\circ$, respectively. More importantly, the carbonyl ligand is not linearly oriented with the pyridine functionality of Ph_2PPrPDI . In turn, the N(2)-Mo(1)-C(40) and N(1)-Mo(1)-C(40) angles of 171.43(18) and 97.74(18) $^\circ$, respectively, appear to dictate how the Mo center in **2** engages in π -backbonding. It is believed that the solid state positioning of the carbonyl ligand serves to maximize its ability to participate in π -backdonation together with the N(1)-C(2) PDI imine arm [*i.e.*, both N(1) and C(40) appear to lie on principal Mo bonding axes since these atoms form an angle of close to 90 $^\circ$]. Upon examining the $C_{\text{imine}}\text{-N}_{\text{imine}}$ and $C_{\text{imine}}\text{-C}_{\text{pyridine}}$ chelate distances, it is clear that the electron density transferred to Ph_2PPrPDI via backdonation is localized between N(1) and N(2), as N(1)-C(2) and N(2)-C(3) are elongated to 1.362(6) and 1.390(6) Å, respectively, while C(2)-C(3) is significantly shortened to 1.402(7) Å.³¹ This contrasts the distances found for N(3)-C(8), C(7)-C(8), and N(2)-C(7), which indicate poorer Mo-PDI π -overlap. These parameters suggest that **2** can best be described as having a Mo(0) center that participates in π -backbonding since a PDI chelate that is reduced by one or more electrons would likely exhibit complete electron delocalization.³⁵

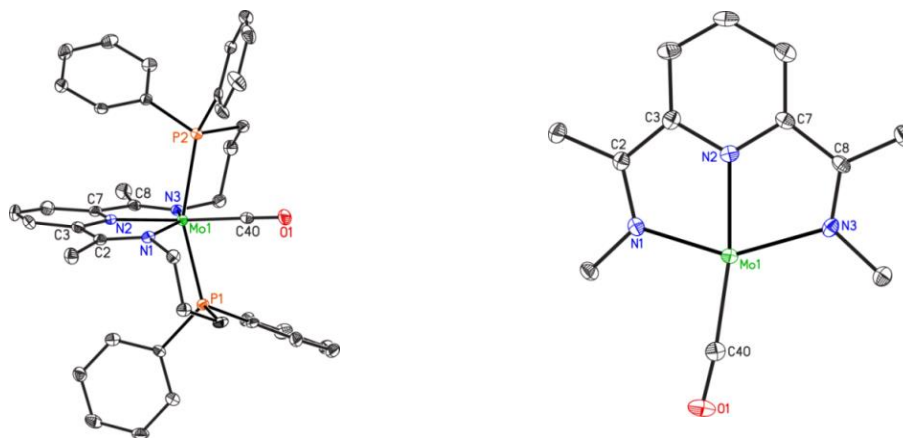


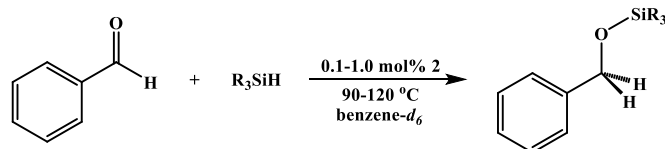
Figure 1.5. The solid state structure of **2** shown at 30% probability ellipsoids (left). A view of the bis(imino)pyridine/carbonyl plane with the chelate ligand arms removed for clarity (right). Hydrogen atoms and a disordered, co-crystallized diethyl ether molecule have been omitted from each rendering.

Table 1.3. Experimental bond lengths (Å) and angles (°) determined for **2**.

| 2 | |
|------------------|------------|
| Mo(1)-N(1) | 2.070(4) |
| Mo(1)-N(2) | 2.072(4) |
| Mo(1)-N(3) | 2.186(4) |
| Mo(1)-P(1) | 2.4301(13) |
| Mo(1)-P(2) | 2.4825(13) |
| Mo(1)-C(40) | 1.955(5) |
| C(40)-O(1) | 1.183(6) |
| N(1)-C(2) | 1.362(6) |
| N(3)-C(8) | 1.323(6) |
| C(2)-C(3) | 1.402(7) |
| C(7)-C(8) | 1.453(7) |
| N(2)-C(3) | 1.390(6) |
| N(2)-C(7) | 1.368(6) |
| | |
| N(1)-Mo(1)-N(3) | 147.91(15) |
| N(1)-Mo(1)-N(2) | 74.79(15) |
| N(1)-Mo(1)-C(40) | 97.74(18) |
| N(2)-Mo(1)-C(40) | 171.43(18) |
| P(1)-Mo(1)-P(2) | 155.46(5) |

Having characterized **2**, the hydrosilylation activity of this complex was investigated. Heating an equimolar benzene-*d*₆ solution of benzaldehyde and phenylsilane with 1.0 mol% of **2** to 90 °C allowed for complete substrate reduction and formation of a 4:1 ratio of PhSiH(OCH₂Ph)₂ to PhSiH₂(OCH₂Ph) after 4.5 h (Table 1.4, Entry 1). Modifying the reductant was found to dramatically impact the rate of benzaldehyde hydrosilylation. For example, heating a benzene-*d*₆ solution of benzaldehyde and diphenylsilane containing 1.0 mol% of **2** to 90 °C gave only 32% conversion after 4.5 h (Entry 2), while the use of Ph₃SiH completely shut down catalysis (Entry 3). While a similar effect was noted for Et₃SiH, quaternary silyl ethers could be prepared when using unhindered ethoxysilanes (Entries 4-6). Although conducting the hydrosilylation of benzaldehyde with phenylsilane at 120 °C resulted in near complete conversion after only 1 h (TOF = 90 h⁻¹), it was found that running the reaction at 0.1 mol% **2** in the absence of solvent at 90 °C resulted in an improved TOF of 323 h⁻¹ (Entry 9). These conditions were determined to be ideal for exploring the synthetic utility of **2**, as minimizing energy input and solvent use are important considerations from a sustainability standpoint.

Table 1.4. The hydrosilylation of benzaldehyde using **2** as a catalyst.



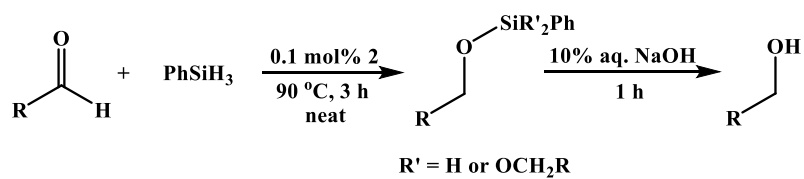
| Entry | Temp. (°C) | Cat. Loading (mol%) | Silane | Product (Ratio) | Time (h) | Conv. (%) ^a |
|----------------|------------|---------------------|----------------------------------|---|----------|------------------------|
| 1 | 90 | 1.0 | PhSiH ₃ | PhSiH(OCH ₂ Ph) ₂ PhSiH ₂ (OCH ₂ Ph) (4:1) ^b | 4.5 | >99 |
| 2 | 90 | 1.0 | Ph ₂ SiH ₂ | Ph ₂ SiH(OCH ₂ Ph) | 4.5 | 32 |
| 3 | 90 | 1.0 | Ph ₃ SiH | - | 4.5 | - |
| 4 | 90 | 1.0 | (EtO) ₃ SiH | (EtO) ₃ SiOCH ₂ Ph | 4.5 | 14 |
| 5 | 90 | 1.0 | (EtO) ₂ (Me)SiH | (EtO) ₂ (Me)SiOCH ₂ Ph | 4.5 | 45 |
| 6 | 90 | 1.0 | (EtO)(Me) ₂ SiH | (EtO)(Me) ₂ SiOCH ₂ Ph | 4.5 | 27 |
| 7 | 90 | 1.0 | Et ₃ SiH | - | 4.5 | - |
| 8 | 120 | 1.0 | PhSiH ₃ | PhSiH(OCH ₂ Ph) ₂ PhSiH ₂ (OCH ₂ Ph) (2:1) ^b | 1 | 90 |
| 9 ^c | 90 | 0.1 | PhSiH ₃ | PhSiH(OCH ₂ Ph) ₂ PhSi(OCH ₂ Ph) ₃ (2:1) ^d | 3 | 97 |

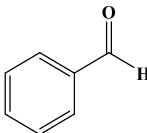
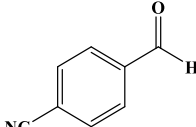
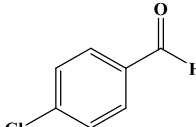
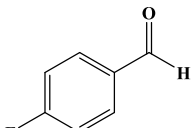
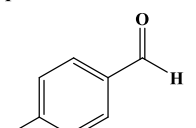
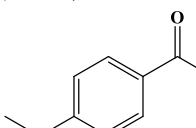
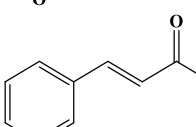
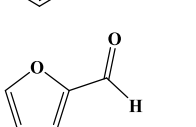
| | | | | | | |
|-----------------|----|-----|--------------------|--|---|----|
| 10 ^c | 60 | 0.1 | PhSiH ₃ | PhSiH(OCH ₂ Ph) ₂ PhSiH ₂ (OCH ₂ Ph) (2:1) | 3 | 29 |
|-----------------|----|-----|--------------------|--|---|----|

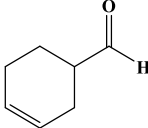
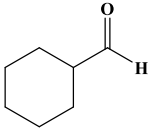
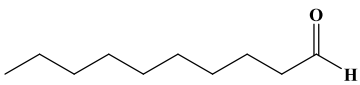
^aPercent conversion was determined by ¹H NMR spectroscopy. ^bA small amount of PhSi(OCH₂Ph)₃ was observed. ^cTrial was conducted without added benzene-*d*₆ (neat). ^dA minimal amount of PhSiH₂(OCH₂Ph) was observed.

Our efforts to investigate the substrate scope of **2**-catalyzed aldehyde hydrosilylation are summarized in Table 1.5. Since both PhSiH(OCH₂Ph)₂ and PhSiH₂(OCH₂Ph) had formed following benzaldehyde hydrosilylation, the conversion of silyl ethers to their parent alcohols was conducted for several trials by treating the reaction mixture with aqueous 10% NaOH, in order to simplify product isolation.⁸¹ As shown in Entries 1-5, modifying the electronic properties of benzaldehyde had little influence on the observed TOFs. Importantly, these trials also indicate that aryl cyanide, chloride, and fluoride substituents appear to be tolerated by **2**. Although the reaction did not reach completion, the hydrosilylation of *trans*-cinnamaldehyde to yield cinnamyl alcohol (Entry 7) revealed that α,β -unsaturation is tolerated by **2** and that the olefin is not reduced during the course of aldehyde hydrosilylation. The inability of **2** to mediate olefin hydrosilylation was further confirmed by following the hydrosilylation of 3-cyclohexene-1-carboxaldehyde (Entry 9). Attempts to achieve 1-hexene or cyclohexene hydrosilylation under similar conditions were unsuccessful.

Table 1.5. The preparation of alcohols from aldehydes via **2**-mediated hydrosilylation.



| Entry | Substrate | % Conversion ^a (Isolated) ^b | TOF ^c (h ⁻¹) |
|-------|---|--|--|
| 1 |  | 97 (80) | 323 |
| 2 |  | >99 ^d | 330 |
| 3 |  | 87 (68) | 290 |
| 4 |  | 90 (74) | 300 |
| 5 |  | 99 (78) | 330 |
| 6 |  | 60 ^e | 200 |
| 7 |  | 52 ^e | 173 |
| 8 |  | >99 (93) | 330 |

| | | | |
|----|---|----------|-----|
| 9 |  | 95 (61) | 317 |
| 10 |  | 99 (82) | 330 |
| 11 |  | >99 (89) | 330 |

^aPercent conversion was determined by ¹H NMR spectroscopy. ^bIsolated yield of alcohol relative to aldehyde. ^cTOF calculated from percent conversion. ^dNaOH treatment resulted in conversion of the nitrile substituent to a carboxylic acid. ^eNaOH treatment afforded a mixture of starting aldehyde and alcohol.

Unfortunately, attempts to catalyze the hydrosilylation of ketones (including cyclohexanone, 2-hexanone, acetophenone, and diisopropyl ketone) under the conditions used to generate Table 1.4 were also unsuccessful. When conducting each of the ketone hydrosilylation trials, no color change was observed upon substrate addition. In contrast, preparing aldehyde or equimolar aldehyde/PhSiH₃ solutions of **2** resulted in a series of color changes whereby the starting pink solution turned bluish-purple, before reverting back to a pink-colored solution within minutes at room temperature. This observation prompted a series of experiments to further probe the interaction of the precatalyst with both PhSiH₃ and aldehydes. Adding 5 eq. of PhSiH₃ to **2** in benzene-*d*₆ solution resulted in no change after 24 h at either 25 °C or 90 °C. However, adding 5 eq. of benzaldehyde to **2** resulted in partial formation of a Mo-containing product featuring an uncoordinated Ph₂PPrPDI phosphine substituent after 1 h at 25 °C, as judged by ³¹P NMR spectroscopy (Fig. 1.6). After 48 h at 25 °C, an intractable mixture of Mo-containing products with one or both ligand phosphine arms dissociated had formed. A similarly complex mixture of Mo

compounds was observed by ^{31}P spectroscopy following aldehyde hydrosilylation. Finally, conducting the hydrosilylation of benzaldehyde in the presence of Hg did not influence hydrosilylation TOF, indicating that heterogeneous Mo species are not responsible for the observed catalysis.

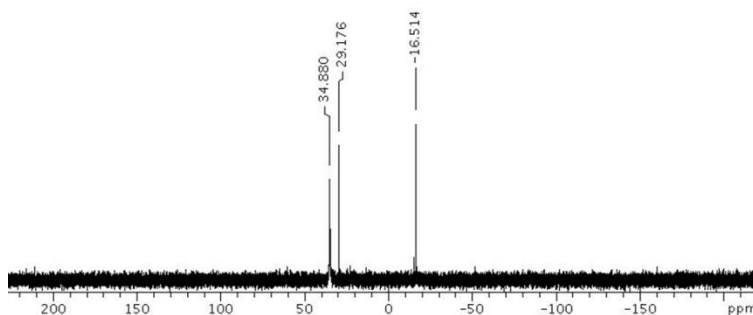


Figure 1.6. ^{31}P NMR spectrum of 5 eq. benzaldehyde addition to **2** after 1 h at 25 °C in benzene- d_6 .

These experiments shed light on the mechanism of **2**-catalyzed aldehyde hydrosilylation and offer clues as to how improved (PDI)Mo hydrosilylation catalysts might be developed. Since the facile coordination of aldehydes to **2** has been observed, it is proposed that this complex mediates hydrosilylation through the mechanism displayed in Fig. 1.7. Starting with **2**, the substitution of one Ph_2PPrPDI chelate arm by an aldehyde ligand is shown; however, it is possible that aldehydes displace both phosphine substituents to form $(\kappa^3\text{-}N,N,N\text{-Ph}_2\text{PPrPDI})\text{Mo}(\text{CO})(\text{aldehyde})$ during the reaction. Incoming aldehydes might coordinate in either an η^1 - or η^2 -fashion and are more likely to displace Ph_2PPrPDI phosphine moieties than ketones since they are less sterically demanding.³⁶ After substrate binding, the oxidative addition of PhSiH_3 would result in formation of the 7-coordinate Mo(II) complex shown at the bottom right of Fig. 1.7. As suggested for

[(DPEphos)Mo(NO)(NCMe)₃][BAR^F₄],²⁴ silane oxidative addition is likely the rate-limiting step of this transformation, in part because PhSiH₃ does not independently react with **2**, even after 24 h at 90 °C. Migratory insertion of the substrate into the Mo-H bond with concomitant phosphine coordination would lead to a monoalkoxide silyl complex that undergoes reductive elimination to regenerate **2** (or an aldehyde-coordinated analogue). While the oxidative addition and insertion steps may proceed in a concerted fashion (a non-hydride pathway has been established for tetravalent Mo hydrosilylation catalysts),^{22d} our proposed mechanism differs from the carbonyl hydrosilylation mechanism proposed by Ojima³⁷ and Berke²⁴ in that it does not rely on the formation of a high-energy tertiary alkyl complex. It is also unlikely that **2** operates by way of a silylene mechanism,³⁸ since tertiary silanes were proven capable of mediating benzaldehyde hydrosilylation (Table 1.3, Entries 4-6).

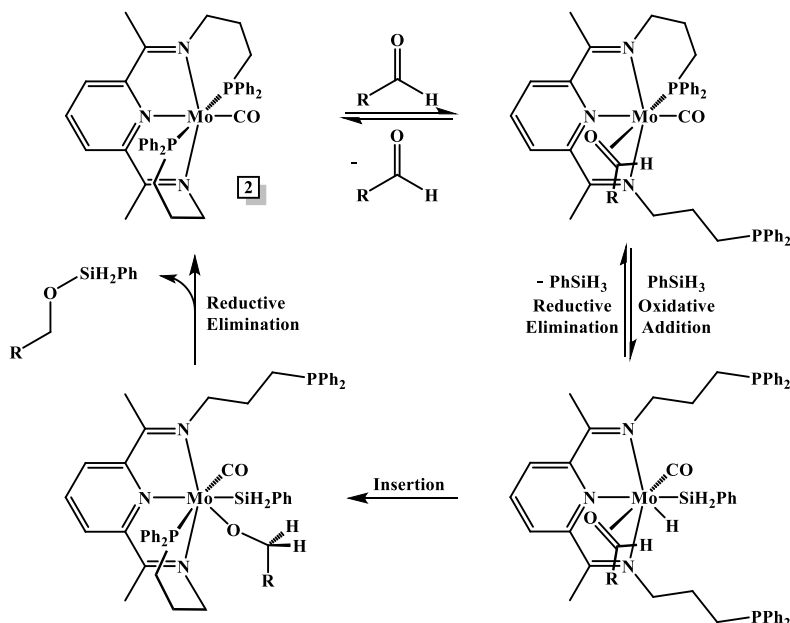


Figure 1.7. Proposed mechanism for **2**-catalyzed aldehyde hydrosilylation.

Ultimately, it must be stated that **2** has been shown to exhibit somewhat disappointing carbonyl hydrosilylation activity when compared to [(DPEphos)Mo(NO)(NCMe)₃][BAr^F₄]. Although its aldehyde hydrosilylation reactions reported by Berke and co-workers were conducted at 120 °C, initial TOFs of up to 4,864 h⁻¹ were observed.²⁴ At 120 °C, **2**-catalyzed benzaldehyde reduction proceeded with a TOF of only 90 h⁻¹. One reason for this difference in activity may be that [(DPEphos)Mo(NO)(NCMe)₃][BAr^F₄] possesses three acetonitrile ligands which are more easily displaced than the CO ligand or the phosphine arms of **2**. To render the metal center more accessible, we are currently working to prepare (κ^5 -PDI)Mo catalysts that have a weak field ligand occupying their sixth coordination site. Additionally, it can be predicted that complexes of the general formula (κ^3 -*N,N,N*-PDI)Mo(L)₃ (where L is a monodentate, weak-field σ -donor) might exhibit improved hydrosilylation activity when compared to **2**.

1.4. Conclusion^{1a}

While attempts to prepare a formal Mo(0) complex featuring κ^5 -^{PyEt}PDI coordination resulted in the formation of (κ^3 -^{PyEt}PDI)₂Mo (**1**), refluxing a toluene solution of ^{Ph₂PPr}PDI and Mo(CO)₆ afforded (κ^5 -^{Ph₂PPr}PDI)Mo(CO) (**2**). The X-ray crystallographic investigation of both products revealed that electron density is being transferred from the metal to the chelate via π -backbonding in each complex; however, actual PDI ligand reduction does not appear to occur. Upon determining that **2** acts a precatalyst for the hydrosilylation of benzaldehyde at 90 °C, the reaction conditions were optimized and then applied to the reduction of 11 different aldehydes (TOFs = 173-330 h⁻¹ at 0.1 mol% catalyst loading). Furthermore, investigating the reactivity of **2** towards phenylsilane and benzaldehyde

revealed that the dissociation of ligand phosphine substituents likely accompanies catalytic turnover. In addition to demonstrating the importance of co-donor field strength in catalyst design, it is believed that the efforts described herein may guide the preparation of improved low-valent Mo hydrosilylation catalysts.

1.5. Experimental Procedures^{1a}

1.5.1. General Considerations

Unless otherwise stated, all chemicals and synthetic reactions were handled under an atmosphere of purified nitrogen, either in an MBraun glove box or using standard Schlenk line techniques. Pentane, toluene, diethyl ether, and tetrahydrofuran were purchased from Sigma-Aldrich, dried using a Pure Process Technology solvent system, and stored in a glove box over activated 4Å molecular sieves and metallic sodium (from Alfa Aesar) before use. Benzene-*d*₆ was obtained from Cambridge Isotope Laboratories and dried over 4Å molecular sieves and metallic sodium prior to use. 2,6-Diacetylpyridine, 2-(2-aminoethyl)pyridine, triethoxysilane, decanal, 4-chlorobenzaldehyde, 3-cyclohexene-1-carboxaldehyde, and *trans*-cinnamaldehyde were purchased from TCI America. 4-Cyanobenzaldehyde, phenylsilane, diphenylsilane, and triphenylsilane were purchased from Oakwood Products. Cyclohexanecarboxaldehyde, *p*-tolualdehyde, furfural, pyridine, triethylsilane, diethoxymethylsilane, dimethoxyethylsilane, benzaldehyde, and *p*-anisaldehyde were purchased from Sigma-Aldrich. Celite, anhydrous sodium sulfate, sodium hydroxide, *m*-xylene, and *p*-fluorobenzaldehyde were purchased from Acros and used as received. Mo(CO)₆ and 3-(diphenylphosphino)propylamine were purchased from

Strem Chemicals and used as received. $\text{Ph}_2\text{PPrPDI}^{34}$ and $(\text{py})_3\text{MoCl}_3^{27}$ were prepared according to literature procedure.

Solution phase ^1H , ^{13}C , and ^{31}P nuclear magnetic resonance (NMR) spectra were recorded at room temperature on either a 400 MHz or 500 MHz Varian NMR Spectrometer. All ^1H and ^{13}C NMR chemical shifts are reported relative to $\text{Si}(\text{CH}_3)_4$ using ^1H (residual) and ^{13}C chemical shifts of the solvent as secondary standards. ^{31}P NMR data is reported relative to H_3PO_4 . Solid-state IR spectroscopy was conducted on a Bruker Vertex 70 spectrometer. Elemental analyses were performed at Robertson Microlit Laboratories Inc. (Ledgewood, NJ) and Arizona State University CLAS Goldwater Environmental Laboratory (Tempe, AZ).

1.5.2. X-ray Crystallography

Single crystals suitable for X-ray diffraction were coated with polyisobutylene oil in the glovebox and transferred to glass fiber with Apiezon N grease, which was then mounted on the goniometer head of a Bruker APEX Diffractometer (Arizona State University), equipped with Mo $\text{K}\alpha$ radiation. A hemisphere routine was used for data collection and determination of the lattice constants. The space group was identified and the data was processed using the Bruker SAINT+ program and corrected for absorption using SADABS. The structures were solved using direct methods (SHELXS) completed by subsequent Fourier synthesis and refined by full-matrix, least-squares procedures on $[F^2]$ (SHELXL). The solid-state structure of **2** was found to possess a disordered diethyl ether molecule.

1.5.3. Calculations

All DFT calculations were carried out using the ORCA program,³⁹ and all compounds were optimized with the B3LYP functional.⁴⁰ The Conductor-like Screening Model (COSMO) was used where indicated, with THF as the solvent.⁴¹ Empirical Van der Waals corrections were included in the geometry optimizations of all molecules.⁴² The self-consistent field (SCF) calculations were tightly converged ($1 \times 10^{-8} E_h$ in energy, $1 \times 10^{-7} E_h$ in the density charge). Ahlrichs triple- ξ valence basis sets (relativistically recontracted) with one set of first polarization functions (def2-TZVP-ZORA) were used for the molybdenum and nitrogen atoms.⁴³ Ahlrichs split valence basis sets (relativistically recontracted) with one set of first polarization functions (def2-SVP-ZORA) were used for the carbon and hydrogen atoms.⁴³ Auxiliary basis sets were chosen to match the orbital basis sets used. Molecular orbitals were visualized using the Molekel program.⁴⁴

1.5.4. Improved Preparation of 2,6-((2-NC₅H₄)CH₂CH₂N=C(CH₃))₂C₅H₃N (Py^{Et}PDI)

Although previously reported,²⁶ an improved synthesis of this ligand is provided. A 100 mL thick-walled reaction bomb containing 0.20 g of 4 Å molecular sieves was charged with 10 mL of toluene, 1.00 g (6.13 mmol) of 2,6-diacetylpyridine, and 0.019 g (0.11 mmol) of *p*-toluenesulfonic acid and the mixture was stirred at ambient temperature for 15 min. To it, 1.49 g (12.21 mmol) of 2-(2-aminoethyl)pyridine was added dropwise. The bomb was then sealed and heated to 80 °C for two days. The resulting orange solution was cooled to ambient temperature and filtered through Celite to remove the sieves and precipitated *p*-toluenesulfonic acid. The solvent was then evacuated to obtain 2.20 g (96%) of a deep orange oil identified as Py^{Et}PDI. Elemental analysis for C₂₃H₂₅N₅: Calcd. C,

74.36; H, 6.78; N, 18.85. Found C, 74.21; H, 6.92; N, 18.31. ^1H NMR (benzene- d_6 , 400 MHz): δ 8.58 (d, 4.3 Hz, 2H, ^aPy), 8.30 (d, 7.7 Hz, 2H, $m\text{-}^c\text{Py}$), 7.23 (t, 7.7 Hz, 1H, $p\text{-}^c\text{Py}$), 7.05 (t, 6.9 Hz, 2H, ^aPy), 6.94 (d, 7.8 Hz, 2H, ^aPy), 6.62 (m, 2H, ^aPy), 3.94 (t, 7.2 Hz, 4H, $\text{CH}_2\text{CH}_2\text{N}$), 3.35 (t, 7.2 Hz, 4H, $\text{CH}_2\text{CH}_2\text{N}$), 2.18 (s, 6H, CH_3). ^{13}C NMR (benzene- d_6 , 100.49 MHz): δ 166.77 (C=N), 161.63 (^aPy), 156.73 (^cPy), 150.11 (^aPy), 136.51 (^cPy), 135.96 (^aPy), 123.87 (^aPy), 121.65 (^aPy), 121.41 (^cPy), 52.95 ($\text{CH}_2\text{CH}_2\text{N}$), 40.58 ($\text{CH}_2\text{CH}_2\text{N}$), 13.71 (CH_3).

1.5.5. Preparation of ($\text{Py}^{\text{Et}}\text{PDI}$) $_2\text{Mo}$ (1)

Method A. In a nitrogen filled glove box, a 20 mL reaction vial was charged with 4.6 g of metallic mercury and 3 mL of THF. To the vial, 0.023 g of freshly cut sodium was added and stirred for 30 min to form clear sodium amalgam solution. To the stirring solution, 0.147 g (0.394 mmol) of $\text{Py}^{\text{Et}}\text{PDI}$ in 5 mL of THF and 0.087 g of $(\text{py})_3\text{MoCl}_3$ (0.198 mmol) in 5 mL of THF were added and the mixture was allowed to stir at ambient temperature for 18 h. The brown solution was then filtered through Celite and the solvent was removed *in vacuo* to yield a brown solid. After washing with pentane and drying, 0.098 g (59%) of **1** was isolated. Suitable crystals for X-ray diffraction were grown from pentane. **Method B.** In a nitrogen filled glove box, a 100 mL thick-walled reaction bomb was charged with 0.016 g (0.06 mmol) of $\text{Mo}(\text{CO})_6$ dissolved in 10 mL of *m*-xylene, 0.045 g (0.121 mmol) of $\text{Py}^{\text{Et}}\text{PDI}$ dissolved in 10 mL of *m*-xylene, and a magnetic stir bar. The bomb was sealed, the solution was frozen with liquid nitrogen, and the reaction was degassed on a Schlenk line. Upon warming to room temperature, the reaction was set to reflux in an oil bath that was preheated to 130 °C. A color change from light yellow to brown was observed within

4 h of stirring. After 24 h, the solution was cooled to room temperature, frozen with liquid nitrogen, and degassed. Once the liberated CO was removed, the reaction bomb was allowed to reflux for another 24 h at 130 °C to ensure reaction completion. After once again removing CO, the bomb was brought inside the glove box and the resulting brown solution was filtered through Celite. After removing the *m*-xylene under vacuum, washing with 2 mL of pentane, and drying, recrystallization from an ether/pentane solution yielded 0.027 g (0.032 mmol, 53%) of a dark crystalline solid identified as (^{PyEt}PDI)₂Mo. Elemental analysis for C₄₆H₅₀N₁₀Mo: Calcd. C, 65.85%, H, 6.00%, N, 16.69%. Found, C, 65.76%, H, 5.95%, N, 15.72%. Elemental analysis on C₄₆H₅₀N₁₀Mo consistently produced low N% values and the ¹H and ¹³C NMR spectra of this complex are provided as Figures 1.8 and 1.9 as a measure of purity. ¹H NMR (benzene-*d*₆): δ 8.27 (d, *J* = 3.6 Hz, 2H, ^aPy), 7.85 (d, *J* = 7.6 Hz, 2H, *m*-^cPy), 7.36 (t, *J* = 7.6 Hz, 1H, *p*-^cPy), 6.97 (m, 2H, ^aPy), 6.46 (d, *J* = 4.8 Hz, 2H, ^aPy), 5.98 (m, 2H, ^aPy), 2.98 (t, *J* = 8.4 Hz, 4H, CH₂CH₂N), 2.77 (s, 6H, CH₃), 1.72 (t, *J* = 8.4 Hz, 4H, CH₂CH₂N). ¹³C NMR (benzene-*d*₆): δ 160.06 (C=N), 149.31 (py), 147.54 (py), 139.58 (py), 135.74 (py), 122.89 (py), 120.88 (py), 112.98 (py), 112.71 (py), 55.05 (NCH₂CH₂), 38.89 (NCH₂CH₂), 13.67 (CH₃).

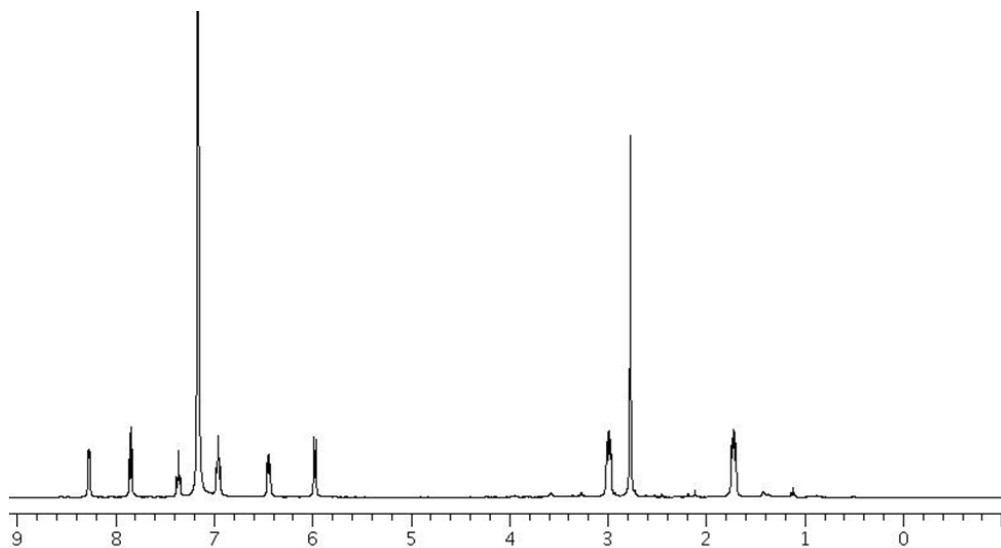


Figure 1.8. ^1H NMR spectrum of $(^{\text{PyEt}}\text{PDI})_2\text{Mo}$ (**1**) in benzene- d_6 .

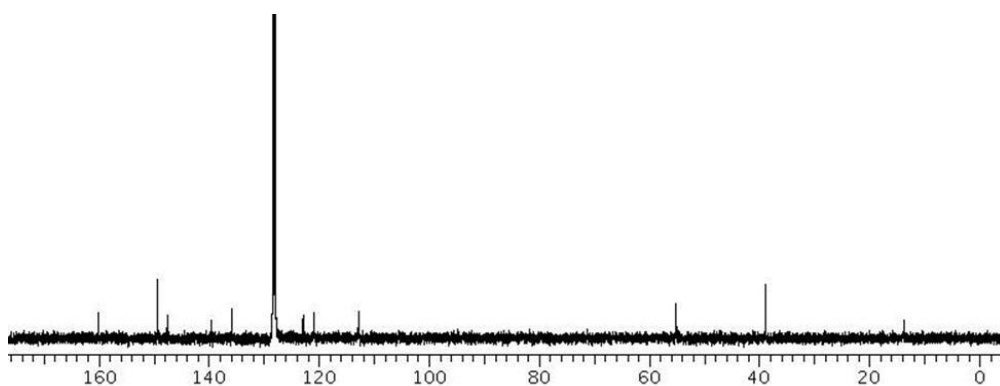


Figure 1.9. ^{13}C NMR spectrum of $(^{\text{PyEt}}\text{PDI})_2\text{Mo}$ (**1**) in benzene- d_6 .

1.5.6. Preparation of $(^{\text{Ph}_2\text{PPr}}\text{PDI})\text{Mo}(\text{CO})$ (**2**)

In a nitrogen filled glove box, a 100 mL thick-walled reaction bomb was charged with 0.025 g (0.095 mmol) of $\text{Mo}(\text{CO})_6$ dissolved in 10 mL of toluene, 0.058 g (0.095 mmol) of $^{\text{Ph}_2\text{PPr}}\text{PDI}$ dissolved in 10 mL of toluene and a magnetic stir bar. The sealed bomb was attached to a Schlenk line, submerged under liquid nitrogen, and degassed. After warming to ambient temperature, the reaction was refluxed to 120 °C in a preheated oil bath. A color

change from light yellow to deep pink was observed within 30 min of stirring. After 24 h, the solution was allowed to cool to room temperature and then frozen in liquid nitrogen before the vessel was degassed on the Schlenk line. Once the liberated CO gas was removed, the solution was allowed to reflux for another 24 h at 120 °C to ensure completion of the reaction. After removal of CO, the bomb was brought inside the glove box and the resulting pink solution was filtered through Celite. The solvent was removed *in vacuo*, the resulting solid was washed with 2 mL of pentane, and then dried to yield 0.06 g (0.081 mmol, 86%) of a deep pink microcrystalline solid identified as **2**. Single crystals suitable for X-ray diffraction were grown from concentrated solution of ether layered with pentane at -35 °C. Elemental analysis for C₄₀H₄₁N₃MoP₂O: Calcd. C, 65.13; H, 5.60; N, 5.70; Found: C, 65.25; H, 5.63; N, 5.45. ¹H NMR (benzene-*d*₆, 400 MHz): δ 7.74 (d, 7.2 Hz, 4H, *Ph*), 7.11 (t, 7.6 Hz, 4H, *Ph*), 6.98 (t, 7.2 Hz, 2H, *Ph*), 6.85 (m, 4H, *Ph*), 6.80 (m, 2H, *Ph*), 6.65 (m, 4H, *Ph*), 6.59 (t, 8.0 Hz, 1H, *p-Py*), 6.22 (d, 8.0 Hz, 2H, *m-Py*), 4.67 (m, 2H, CH₂), 4.63 (m, 2H, CH₂), 2.70 (m, 2H, CH₂), 2.35 (m, 2H, CH₂), 1.92 (m, 2H, CH₂), 1.73 (m, 2H, CH₂) overlaps with a peak at 1.70 (s, 6H, CH₃). ¹³C NMR (benzene-*d*₆, 100.49 MHz): δ 272.19 (t, 20.5 Hz, CO), 157.19 (C=N), 145.86 (*o-py*), 139.54 (t, 17.5 Hz, Ph), 134.92 (t, 7.6 Hz, Ph), 132.80 (t, 5.5 Hz, Ph), 132.47 (t, 5.5 Hz, Ph), 124.86 (*p-py*), 105.34 (*m-py*), 60.41 (NCH₂CH₂), 28.86 (PCH₂CH₂), 27.60 (t, 13.4 Hz, PCH₂CH₂), 12.65 (CH₃). ³¹P NMR (benzene-*d*₆, 161.78 MHz): δ 34.88 (s). IR (KBr): ν_{CO} = 1740 cm⁻¹.

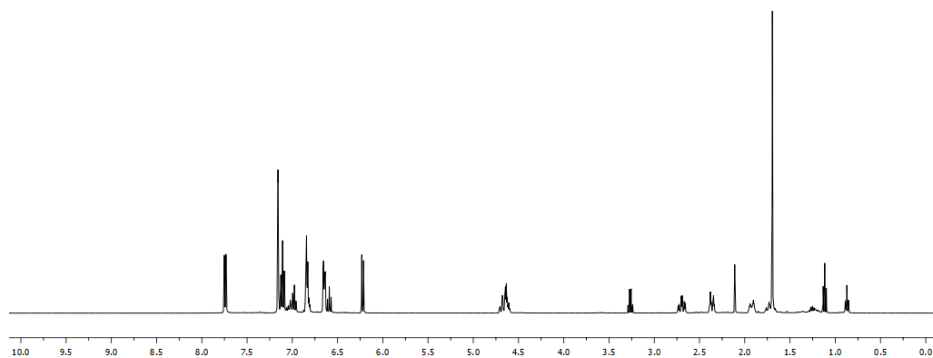


Figure 1.10. ¹H NMR spectrum of (^{Ph}₂PPrPDI)Mo(CO) in benzene-*d*₆.

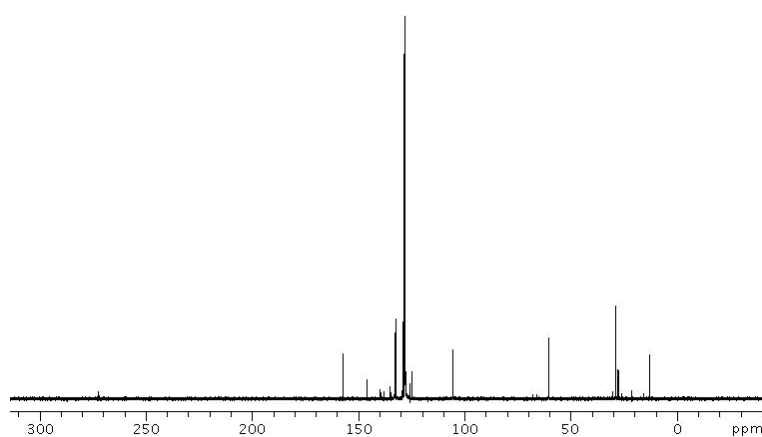


Figure 1.11. ¹³C NMR spectrum of (^{Ph}₂PPrPDI)Mo(CO) in benzene-*d*₆.

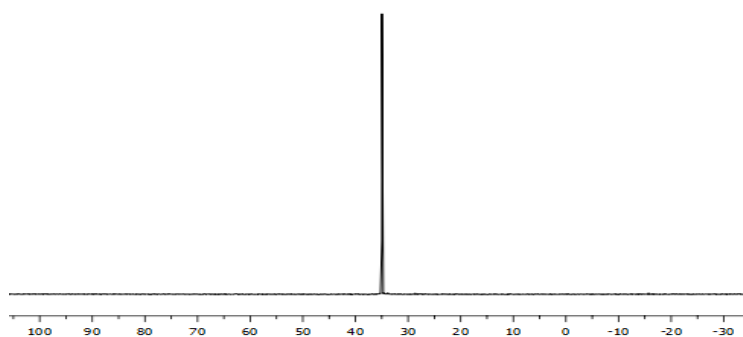


Figure 1.12. ³¹P NMR spectrum of (^{Ph}₂PPrPDI)Mo(CO) in benzene-*d*₆.

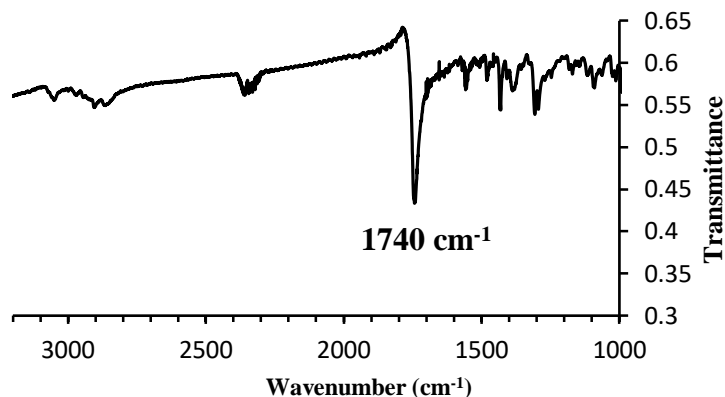


Figure 1.13. IR spectrum of (Ph_2PPrPDI)Mo(CO) in KBr.

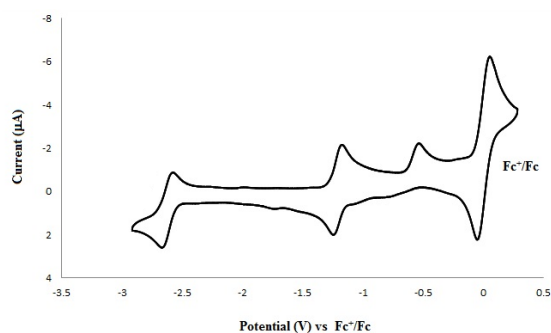


Figure 1.14. Cyclic voltammogram of (Ph_2PPrPDI)Mo(CO) relative to Fc^+/Fc^0 (internal standard) in THF (scan rate = 25 mV/s).

1.5.7. General procedure for silane screening

In the glovebox, a solution of silane (0.017 mL, 0.14 mmol) and benzaldehyde (0.014 mL, 0.14 mmol) in benzene- d_6 (approximately 0.7 mL) was added to a 20 mL scintillation vial containing 0.001 g (0.0014 mmol) of complex **2**. A transient color change from pink to bluish-purple to purple was observed. The resulting solution was transferred into a J. Young tube and the sealed tube was allowed to heat at 90 °C for 4.5 h in an oil bath. The progress of the reaction was determined following analysis by ^1H NMR spectroscopy.

1.6. Catalytic Experiments^{1a}

1.6.1. General procedure for aldehyde hydrosilylation

In the glovebox, a 20 mL scintillation vial containing 0.0014 mmol of **2** was charged with PhSiH₃ (0.14 mmol) and aldehyde (0.14 mmol). A momentary color change from pink to bluish-purple to pink was observed. The vial was sealed under nitrogen and the reaction was heated to 90 °C for 3 h before being opened to air to deactivate the catalyst. The resulting colorless solution was filtered into an NMR tube using 0.7 mL of benzene-*d*₆ solvent and hydrosilylation conversion was assayed by ¹H NMR spectroscopy. After evaporating the NMR solvent, the silylated products were hydrolyzed with 10 % NaOH (2 mL) while stirring at ambient temperature for 1 h. Upon extracting the organic layer with diethyl ether (3 × 2 mL) and drying over anhydrous Na₂SO₄, the product was isolated under reduced pressure. A control experiment was performed in a similar fashion by adding 0.14 mmol of PhSiH₃ and 0.14 mmol of benzaldehyde to 0.7 mL of benzene-*d*₆ in the absence of complex **2**. The solution was monitored by ¹H NMR spectroscopy over time and no reaction was observed after 3 h at 90 °C.

1.6.2. Hydrosilylation of benzaldehyde using PhSiH₃ at 90 °C (1.0 mol %)

In the glovebox, a 20 mL scintillation vial was charged with PhSiH₃ (0.0217 mL, 0.176 mmol), benzaldehyde (0.018 mL, 0.176 mmol), and 0.7 mL of benzene-*d*₆ solution containing 0.00176 mmol of **2**. The reaction mixture was transferred into a J. Young NMR tube, sealed under nitrogen, and heated to 90 °C in a preheated oil bath for 4.5 h. The resulting light-brown solution was then cooled to ambient temperature and the progress of the reaction was monitored using ¹H NMR spectroscopy. By integration, it was observed

that more than 99% of the starting benzaldehyde had been hydrosilylated to form a 4:1 ratio of $\text{PhSiH}(\text{OCH}_2\text{Ph})_2$ to $\text{PhSiH}_2(\text{OCH}_2\text{Ph})$.

1.6.3. Hydrosilylation of benzaldehyde using Ph_2SiH_2 at 90 °C (1.0 mol %)

In the glovebox, a 20 mL scintillation vial was charged with Ph_2SiH_2 (0.0277 mL, 0.149 mmol), benzaldehyde (0.0152 mL, 0.149 mmol), and 0.7 mL of benzene- d_6 solution containing 0.00149 mmol of **2**. The reaction mixture was transferred into a J. Young NMR tube, sealed under nitrogen, and heated to 90 °C in a preheated oil bath for 4.5 h. The resulting light-brown solution was then cooled to ambient temperature and the progress of the reaction was monitored using ^1H NMR spectroscopy. By integration, it was observed that 32% of the starting benzaldehyde had been hydrosilylated to form $\text{Ph}_2\text{SiH}(\text{OCH}_2\text{Ph})$.

1.6.4. Hydrosilylation of benzaldehyde using Ph_3SiH at 90 °C (1.0 mol%)

In the glovebox, a 20 mL scintillation vial was charged with Ph_3SiH (0.060 g, 0.231 mmol), benzaldehyde (0.0235 mL, 0.231 mmol), and 0.7 mL of benzene- d_6 solution containing 0.00231 mmol of **2**. The reaction mixture was transferred into a J. Young NMR tube, sealed under nitrogen, and heated to 90 °C in a preheated oil bath for 4.5 h. The resulting light-brown solution was then cooled to ambient temperature and the progress of the reaction was monitored using ^1H NMR spectroscopy. No hydrosilylation products were observed.

1.6.5. Hydrosilylation of benzaldehyde using $(\text{EtO})_3\text{SiH}$ at 90 °C (1.0 mol%)

In the glovebox, a 20 mL scintillation vial was charged with $(\text{EtO})_3\text{SiH}$ (0.030 mL, 0.163 mmol), benzaldehyde (0.0166 mL, 0.163 mmol), and 0.7 mL of benzene- d_6 solution containing 0.00163 mmol of **2**. The reaction mixture was transferred into a J. Young NMR

tube, sealed under nitrogen, and heated to 90 °C in a preheated oil bath for 4.5 h. The resulting light-brown solution was then cooled to ambient temperature and the progress of the reaction was monitored using ^1H NMR spectroscopy. By integration, it was observed that 14% of the starting benzaldehyde had been hydrosilylated to form $(\text{EtO})_3\text{SiOCH}_2\text{Ph}$.

1.6.6. Hydrosilylation of benzaldehyde using $(\text{EtO})_2\text{MeSiH}$ at 90 °C (1.0 mol%)

In the glovebox, a 20 mL scintillation vial was charged with $(\text{EtO})_2\text{MeSiH}$ (0.0326 mL, 0.200 mmol), benzaldehyde (0.0208 mL, 0.200 mmol), and 0.7 mL of benzene- d_6 solution containing 0.002 mmol of **2**. The reaction mixture was transferred into a J. Young NMR tube, sealed under nitrogen, and heated to 90 °C in a preheated oil bath for 4.5 h. The resulting light-brown solution was then cooled to ambient temperature and the progress of the reaction was monitored using ^1H NMR spectroscopy. By integration, it was observed that 45% of the starting benzaldehyde had been hydrosilylated to form $(\text{EtO})_2\text{MeSiOCH}_2\text{Ph}$.

1.6.7. Hydrosilylation of benzaldehyde using $(\text{EtO})\text{Me}_2\text{SiH}$ at 90 °C (1.0 mol %)

In the glovebox, a 20 mL scintillation vial was charged with $(\text{EtO})\text{Me}_2\text{SiH}$ (0.015 mL, 0.108 mmol), benzaldehyde (0.0111 mL, 0.108 mmol), and 0.7 mL of benzene- d_6 solution containing 0.00108 mmol of **2**. The reaction mixture was transferred into a J. Young NMR tube, sealed under nitrogen, and heated to 90 °C in a preheated oil bath for 4.5 h. The resulting light-brown solution was then cooled to ambient temperature and the progress of the reaction was monitored using ^1H NMR spectroscopy. By integration, it was observed that 27% of the starting benzaldehyde had been hydrosilylated to form $(\text{EtO})\text{Me}_2\text{SiOCH}_2\text{Ph}$.

1.6.8. Hydrosilylation of benzaldehyde using Et₃SiH at 90 °C (1.0 mol%)

In the glovebox, a 20 mL scintillation vial was charged with Et₃SiH (0.0195 mL, 0.122 mmol), benzaldehyde (0.0125 mL, 0.122 mmol), and 0.7 mL of benzene-*d*₆ solution containing 0.00122 mmol of **2**. The reaction mixture was transferred into a J. Young NMR tube, sealed under nitrogen, and heated to 90 °C in a preheated oil bath for 4.5 h. The resulting light-brown solution was then cooled to ambient temperature and the progress of the reaction was monitored using ¹H NMR spectroscopy. No hydrosilylation products were observed.

1.6.9. Hydrosilylation of benzaldehyde at 120 °C (1.0 mol%)

In the glovebox, a 20 mL scintillation vial was charged with PhSiH₃ (0.0217 mL, 0.176 mmol), benzaldehyde (0.018 mL, 0.176 mmol), and 0.7 mL of a benzene-*d*₆ solution containing 0.00176 mmol of **2**. The reaction mixture was transferred into a J. Young NMR tube, sealed under nitrogen, and heated at 120 °C in a preheated oil bath for 1 hour. The resulting light-brown solution was then cooled to ambient temperature and the progress of the reaction was monitored by ¹H NMR spectroscopy. By integration, it was observed that 90% of the starting benzaldehyde had been hydrosilylated to form a 2:1 ratio of PhSiH(OCH₂Ph)₂ to PhSiH₂(OCH₂Ph).

1.6.10. Hydrosilylation of benzaldehyde at 90 °C (0.1 mol%)

In the glovebox, a 20 mL scintillation vial was charged with PhSiH₃ (0.168 mL, 1.36 mmol), benzaldehyde (0.139 mL, 1.36 mmol), and 0.001 g (0.00136 mmol) of **2**. A momentary color change from pink to bluish-purple to pink was observed. The vial was then sealed under nitrogen and heated at 90 °C in a preheated oil bath for 3 hours. The

resulting light-brown solution was then cooled to ambient temperature and opened to the air to deactivate the catalyst. The resulting colorless solution was dissolved in 0.7 mL of benzene-*d*₆ and filtered through Celite into an NMR tube. By integrating the ¹H NMR spectrum of this solution, it was determined that 97% of the starting benzaldehyde had been hydrosilylated. The resulting hydrosilylation products were hydrolyzed in 10% NaOH solution (3 mL) upon stirring for 1 hour. The organic contents were extracted with diethylether (3 × 2 mL), dried over anhydrous Na₂SO₄, and the solvent was removed under reduced pressure. The product was analyzed by ¹H NMR spectroscopy and identified as benzylalcohol (0.118 g, 80% isolated yield).

1.6.11. Hydrosilylation of benzaldehyde at 60 °C (0.1 mol%)

In the glovebox, a 20 mL scintillation vial was charged with PhSiH₃ (0.234 mL, 1.89 mmol) and a benzaldehyde (0.194 mL, 1.89 mmol) solution containing 0.0014 g (0.00189 mmol) of **2**. A momentary color change from pink to bluish-purple to pink was observed. The vial was then sealed under nitrogen and heated at 60 °C in a preheated oil bath for 3 hours. The resulting light-brown solution was then cooled to ambient temperature and opened to the air to deactivate the catalyst. The resulting colorless solution was dissolved in 0.7 mL of benzene-*d*₆ and filtered through Celite into an NMR tube. By integration, it was observed that 29% of the starting benzaldehyde had been hydrosilylated to form a 2:1 ratio of PhSiH(OCH₂Ph)₂ to PhSiH₂(OCH₂Ph).

1.6.12. Hydrosilylation of 4-cyanobenzaldehyde (0.1 mol%)

In the glovebox, a 20 mL scintillation vial was charged with PhSiH₃ (0.100 mL, 0.8 mmol), 4-cyanobenzaldehyde (0.107 mg, 0.8 mmol), and 0.0006 g (0.0008 mmol) of **2**. A

momentary color change from pink to bluish-purple to pink was observed. The vial was then sealed under nitrogen and heated at 90 °C in a preheated oil bath for 3 hours. The resulting light-brown solution was then cooled to ambient temperature and opened to the air to deactivate the catalyst. The resulting colorless solution was dissolved in 0.7 mL of benzene-*d*₆ and filtered through Celite into an NMR tube. By integrating the ¹H NMR spectrum of this solution, it was determined that 99% of the starting 4-cyanobenzaldehyde had been hydrosilylated. Hydrolysis of this product mixture in 10% NaOH solution (2 mL) did not result in a diethylether soluble product, presumably due to nitrile group conversion into a carboxylic acid.

1.6.13. Hydrosilylation of 4-chlorobenzaldehyde (0.1 mol%)

In the glovebox, a 20 mL scintillation vial was charged with PhSiH₃ (0.184 mL, 1.49 mmol), 4-chlorobenzaldehyde (0.210 mg, 1.49 mmol), and 0.0011 g (0.00149 mmol) of **2**. A momentary color change from pink to bluish-purple to pink was observed. The vial was then sealed under nitrogen and heated at 90 °C in a preheated oil bath for 3 hours. The resulting light-brown solution was then cooled to ambient temperature and opened to the air to deactivate the catalyst. The resulting colorless solution was dissolved in 0.7 mL of benzene-*d*₆ and filtered through Celite into an NMR tube. By integrating the ¹H NMR spectrum of this solution, it was determined that 87% of the starting 4-chlorobenzaldehyde had been hydrosilylated. The resulting hydrosilylation products were hydrolyzed in 10% NaOH solution (3 mL) upon stirring for 1 hour. The organic contents were extracted with diethylether (3 × 2 mL), dried over anhydrous Na₂SO₄, and the solvent was removed under

reduced pressure. The product was analyzed by ^1H NMR spectroscopy and identified as 4-chlorobenzylalcohol (0.109 g, 68% isolated yield).

1.6.14. Hydrosilylation of 4-fluorobenzaldehyde (0.1 mol%)

In the glovebox, a 20 mL scintillation vial was charged with PhSiH_3 (0.168 mL, 1.36 mmol), 4-fluorobenzaldehyde (0.145 mL, 1.36 mmol), and 0.001 g (0.00136 mmol) of **2**. A momentary color change from pink to bluish-purple to pink was observed. The vial was then sealed under nitrogen and heated at 90 °C in a preheated oil bath for 3 hours. The resulting light-brown solution was then cooled to ambient temperature and opened to the air to deactivate the catalyst. The resulting colorless solution was dissolved in 0.7 mL of benzene- d_6 and filtered through Celite into an NMR tube. By integrating the ^1H NMR spectrum of this solution, it was determined that 90% of the starting 4-fluorobenzaldehyde had been hydrosilylated. The resulting hydrosilylation products were hydrolyzed in 10% NaOH solution (3 mL) upon stirring for 1 hour. The organic contents were extracted with diethylether (3 \times 2 mL), dried over anhydrous Na_2SO_4 , and the solvent was removed under reduced pressure. The product was analyzed by ^1H NMR spectroscopy and identified as 4-fluorobenzylalcohol (0.101 g, 74% isolated yield).

1.6.15. Hydrosilylation of *p*-tolualdehyde (0.1 mol%)

In the glovebox, a 20 mL scintillation vial was charged with PhSiH_3 (0.201 mL, 1.63 mmol), *p*-tolualdehyde (0.192 mL, 1.63 mmol), and 0.0012 g (0.00163 mmol) of **2**. A momentary color change from pink to bluish-purple to pink was observed. The vial was then sealed under nitrogen and heated at 90 °C in a preheated oil bath for 3 hours. The resulting light-brown solution was then cooled to ambient temperature and opened to the

air to deactivate the catalyst. The resulting colorless solution was dissolved in 0.7 mL of benzene- d_6 and filtered through Celite into an NMR tube. By integrating the ^1H NMR spectrum of this solution, it was determined that 99% of the starting *p*-tolualdehyde had been hydrosilylated. The resulting hydrosilylation products were hydrolyzed in 10% NaOH solution (3 mL) upon stirring for 1 hour. The organic contents were extracted with diethylether (3×2 mL), dried over anhydrous Na_2SO_4 , and the solvent was removed under reduced pressure. The product was analyzed by ^1H NMR spectroscopy and identified as 4-methylbenzylalcohol (0.155 g, 78% isolated yield).

1.6.16. Hydrosilylation of *p*-anisaldehyde (0.1 mol%)

In the glovebox, a 20 mL scintillation vial was charged with PhSiH_3 (0.285 mL, 2.3 mmol) and a *p*-anisaldehyde (0.281 mL, 2.3 mmol) solution containing 0.0017 g (0.0023 mmol) of **2**. A momentary color change from pink to bluish-purple to pink was observed. The vial was then sealed under nitrogen and heated at 90 °C in a preheated oil bath for 3 hours. The resulting light-brown solution was then cooled to ambient temperature and opened into the air to deactivate the catalyst. The resulting colorless solution was dissolved in 0.7 mL of benzene- d_6 and filtered through Celite into an NMR tube. By integrating the ^1H NMR spectrum of this solution, it was determined that 60% of the starting *p*-anisaldehyde had been hydrosilylated. The resulting hydrosilylation products were hydrolyzed in 10% NaOH solution (3 mL) upon stirring for 1 hour. The organic contents were extracted with diethylether (3×2 mL), dried over anhydrous Na_2SO_4 , and the solvent was removed under reduced pressure. The product was analyzed by ^1H NMR spectroscopy

and was identified as 4-methoxybenzylalcohol; however, a significant amount of *p*-anisaldehyde remained.

1.6.17. Hydrosilylation of *trans*-cinnamaldehyde (0.1 mol%)

In the glovebox, a 20 mL scintillation vial was charged with PhSiH₃ (0.100 mL, 0.81 mmol), *trans*-cinnamaldehyde (0.102 mL, 0.81 mmol), and 0.0006 g (0.00081 mmol) of **2**. A momentary color change from pink to bluish-purple to pink was observed. The vial was then sealed under nitrogen and heated at 90 °C in a preheated oil bath for 3 hours. The resulting light-brown solution was then cooled to ambient temperature and opened to the air to deactivate the catalyst. The resulting colorless solution was dissolved in 0.7 mL of benzene-*d*₆ and filtered through Celite into an NMR tube. By integrating the ¹H NMR spectrum of this solution, it was determined that 52% of the starting *trans*-cinnamaldehyde had been hydrosilylated. The resulting hydrosilylation products were hydrolyzed in 10% NaOH solution (3 mL) upon stirring for 1 hour. The organic contents were extracted with diethylether (3 × 2 mL), dried over anhydrous Na₂SO₄, and the solvent was removed under reduced pressure. The product was analyzed by ¹H NMR spectroscopy and was identified as *trans*-cinnamylalcohol; however, a significant amount of *trans*-cinnamaldehyde remained.

1.6.18. Hydrosilylation of furfural (0.1 mol%)

In the glovebox, a 20 mL scintillation vial was charged with PhSiH₃ (0.150 mL, 1.22 mmol), furfural (0.101 mL, 1.22 mmol), and 0.0009 g (0.00122 mmol) of **2**. A momentary color change from pink to bluish-purple to pink was observed. The vial was then sealed under nitrogen and heated at 90 °C in a preheated oil bath for 3 hours. The resulting light-

brown solution was then cooled to ambient temperature and opened to the air to deactivate the catalyst. The resulting colorless solution was dissolved in 0.7 mL of benzene-*d*₆ and filtered through Celite into an NMR tube. By integrating the ¹H NMR spectrum of this solution, it was determined that >99% of the starting furfural had been hydrosilylated. The resulting hydrosilylation products were hydrolyzed in 10% NaOH solution (3 mL) upon stirring for 1 hour. The organic contents were extracted with diethylether (3 × 2 mL), dried over anhydrous Na₂SO₄, and the solvent was removed under reduced pressure. The product was analyzed by ¹H NMR spectroscopy and identified as 2-furanmethanol (0.111 g, 93% isolated yield).

1.6.19. Hydrosilylation of 3-cyclohexene-1-carboxaldehyde (0.1 mol%)

In the glovebox, a 20 mL scintillation vial was charged with PhSiH₃ (0.134 mL, 1.1 mmol), 3-cyclohexene-1-carboxaldehyde (0.127 mL, 1.11 mmol), and 0.0008 g (0.0011 mmol) of **2**. A momentary color change from pink to bluish-purple to pink was observed. The vial was then sealed under nitrogen and heated at 90 °C in a preheated oil bath for 3 hours. The resulting light-brown solution was then cooled to ambient temperature and opened to the air to deactivate the catalyst. The resulting colorless solution was dissolved in 0.7 mL of benzene-*d*₆ and filtered through Celite into an NMR tube. By integrating the ¹H NMR spectrum of this solution, it was determined that 95% of the starting 3-cyclohexene-1-carboxaldehyde had been hydrosilylated. The resulting hydrosilylation products were hydrolyzed in 10% NaOH solution (3 mL) upon stirring for 1 hour. The organic contents were extracted with diethylether (3 × 2 mL), dried over anhydrous Na₂SO₄, and the solvent was removed under reduced pressure. The product was analyzed

by ^1H NMR spectroscopy and identified as 3-cyclohexene-1-methanol (0.075 g, 61% isolated yield).

1.6.20. Hydrosilylation of cyclohexanecarboxaldehyde (0.1 mol%)

In the glovebox, a 20 mL scintillation vial was charged with PhSiH_3 (0.151 mL, 1.22 mmol), cyclohexanecarboxaldehyde (0.148 mL, 1.22 mmol), and 0.0009 g (0.00122 mmol) of **2**. A momentary color change from pink to bluish-purple to pink was observed. The vial was then sealed under nitrogen and heated at 90 °C in a preheated oil bath for 3 hours. The resulting light-brown solution was then cooled to ambient temperature and opened to the air to deactivate the catalyst. The resulting colorless solution was dissolved in 0.7 mL of benzene- d_6 and filtered through Celite into an NMR tube. By integrating the ^1H NMR spectrum of this solution, it was determined that 99% of the starting cyclohexanecarboxaldehyde had been hydrosilylated. The resulting hydrosilylation products were hydrolyzed in 10% NaOH solution (3 mL) upon stirring for 1 hour. The organic contents were extracted with diethylether (3 \times 2 mL), dried over anhydrous Na_2SO_4 , and the solvent was removed under reduced pressure. The product was analyzed by ^1H NMR spectroscopy and identified as cyclohexylmethanol (0.115 g, 82% isolated yield).

1.6.21. Hydrosilylation of decanal (0.1 mol%)

In the glovebox, a 20 mL scintillation vial was charged with PhSiH_3 (0.100 mL, 0.81 mmol), decanal (0.153 mL, 0.81 mmol), and 0.0006 g (0.00081 mmol) of **2**. A momentary color change from pink to bluish-purple to pink was observed. The vial was then sealed under nitrogen and heated at 90 °C in a preheated oil bath for 3 hours. The resulting light-

brown solution was then cooled to ambient temperature and opened to the air to deactivate the catalyst. The resulting colorless solution was dissolved in 0.7 mL of benzene-*d*₆ and filtered through Celite into an NMR tube. By integrating the ¹H NMR spectrum of this solution, it was determined that >99% of the starting decanal had been hydrosilylated. The resulting hydrosilylation products were hydrolyzed in 10% NaOH solution (3 mL) upon stirring for 1 hour. The organic contents were extracted with diethylether (3 × 2 mL), dried over anhydrous Na₂SO₄, and the solvent was removed under reduced pressure. The product was analyzed by ¹H NMR spectroscopy and identified as 1-decanol (0.115 g, 89% isolated yield).

1.7. Addition of 5 eq. benzaldehyde to 2

In the glovebox, a 20 mL scintillation vial was charged with benzaldehyde (0.00346 mL, 0.035 mmol) and 0.7 mL of benzene-*d*₆ solution containing 0.007 mmol of **2**. The reaction mixture was stirred for an hour under nitrogen at ambient temperature. The resulting pink solution was then transferred into a J. Young NMR tube and progress of the reaction was monitored by ¹H NMR and ³¹P NMR spectroscopy. Free chelate arms were observed along with unreacted **2** after 1h. After 48 h, the reaction mixture was filtered through Celite and the volatile organics were removed under reduced pressure to obtain a pink solid. A majority of the chelate phosphine substituents were no longer coordinated to Mo, as judged by ³¹P NMR spectroscopy.

1.8. Hydrosilylation of benzaldehyde using PhSiH₃ at 90 °C (10 mol%)

In the glovebox, a 20 mL scintillation vial was charged with PhSiH₃ (0.016.6 mL, 0.135 mmol), (0.0138 mL, 0.135 mmol), and 0.5 mL of benzene-*d*₆ solution containing 0.0135

mmol of **2**. The reaction mixture was transferred into a J. Young NMR tube, sealed under nitrogen, and heated to 90 °C in a preheated oil bath for 3 h. The resulting light-brown solution was then cooled to ambient temperature and the reaction was monitored using ¹H NMR and ³¹P NMR spectroscopy. Complete conversion of starting benzaldehyde resonances were observed by ¹H NMR spectroscopy and the formation of multiple unidentified Mo compounds were observed by ³¹P NMR spectroscopy.

1.9. Test for Catalyst Homogeneity

In the glovebox, a 20 mL scintillation vial was charged with Hg (11.25 g, 56.25 mmol), PhSiH₃ (0.150 mL, 1.22 mmol), benzaldehyde (0.125 mL, 1.22 mmol), and 0.0009 g (0.00122 mmol) of **2**. A momentary color change from pink to bluish-purple to pink was observed. The vial was sealed under nitrogen and heated at 90 °C in a preheated oil bath for 3 h. The resulting light-brown solution was then cooled to ambient temperature and opened to air to deactivate the catalyst. The resulting colorless solution was dissolved in 0.7 mL of benzene-*d*₆ and filtered through Celite into an NMR tube. By integrating the ¹H NMR spectrum of this solution, it was determined that 97% of the starting benzaldehyde had been hydrosilylated.

1.10. References

- (1)(a) Pal, R.; Groy, T. L.; Bowman, A. C.; Trovitch, R. J. *Inorg. Chem.* **2014**, *53*, 9357-9365. (b) Collman, J. P.; Hegedus, L. S.; Norton, J. R.; Finke, R. G. *Principles and Applications of Organotransition Metal Chemistry*; University Science Books: Sausalito, CA, 1987; pp 523-575.
- (2)(a) Noyori, R. *Angew. Chem. Int. Ed.* **2002**, *41*, 2008-2022. (b) Carey, J. S.; Laffan, D.; Thomson, C.; Williams, M. T. *Org. Biomol. Chem.* **2006**, *4*, 2337-2347.
- (3) Parshall, G. W.; Ittel, S. D. in *Homogeneous Catalysis: The Applications and Chemistry of Catalysis by Soluble Transition Metal Complexes*, 2nd Edition, John Wiley & Sons, Inc., New York, 1992, pp. 39-41.
- (4) For examples of commonly used hydrosilylation catalysts see: (a) Speier, J. L.; Webster, J. A.; Barnes, G. H. *J. Am. Chem. Soc.* **1957**, *79*, 974-979. (b) Hitchcock, P. B.; Lappert, M. F.; Warhurst, N. J. W. *Angew. Chem. Int. Ed.* **1991**, *30*, 438-440.
- (5)(a) Enthaler, S.; Junge, K.; Beller, M. *Angew. Chem. Int. Ed.* **2008**, *47*, 3317-3321. (b) Czaplik, W. M.; Mayer, M.; Cvengroš, J.; van Wangelin, A. J. *Chem. Sus. Chem.* **2009**, *2*, 396-417.
- (6)(a) Gaillard, S.; Renaud, J.-L. *Chem. Sus. Chem.* **2008**, *1*, 505-509. (b) Troegel, D.; Stohrer, J. *Coord. Chem. Rev.* **2011**, *255*, 1440-1459.
- (7)(a) Pratt, S. L.; Faltynek, R. A. *J. Organomet. Chem.* **1983**, *258*, C5-C8. (b) Hilal, H. S.; Abu-Eid, M.; Al-Subu, M.; Khalaf, S. *J. Mol. Catal.* **1987**, *39*, 1-11. (c) Mao, Z.; Gregg, B. T.; Cutler, A. R. *J. Am. Chem. Soc.* **1995**, *117*, 10139-10140. (d) Cavanaugh; M. D.; Gregg, B. T.; Cutler, A. R. *Organometallics* **1996**, *15*, 2764-2769. (e) Son, S. U.; Paik, S.-J.; Lee, I. S.; Lee, Y.-A.; Chung, Y. K.; Seok, W. K.; Lee, H. N. *Organometallics* **1999**, *18*, 4114-4118. (f) Son, S. U.; Paik, S.-J.; Chung, Y. K. *J. Mol. Catal. A: Chem.* **2000**, *151*, 87-90. (g) Chidara, V. K.; Du, G. *Organometallics* **2013**, *32*, 5034-5037. (h) Zheng, J.; Chevance, S.; Darcel, C.; Sortais, J.-B. *Chem. Commun.* **2013**, *49*, 10010-10012. (i) Mukhopadhyay, T. K.; Flores, M.; Groy, T. L.; Trovitch, R. J. *J. Am. Chem. Soc.* **2014**, *136*, 882-885.
- (8) For representative Fe hydrosilylation catalysts see: (a) Brunner, H.; Fisch, K. *Angew. Chem. Int. Ed.* **1990**, *29*, 1131-1132. (b) Tondreau, A. M.; Lobkovsky, E.; Chirik, P. J. *Org. Lett.* **2008**, *10*, 2789-2792. (c) Langlotz, B. K.; Wadepohl, H.; Gade, L. H. *Angew. Chem. Int. Ed.* **2008**, *47*, 4670-4674. (d) Tondreau, A. M.; Darmon, J. M.; Wile, B. M.; Floyd, S. K.; Lobkovsky, E.; Chirik, P. J. *Organometallics* **2009**, *28*, 3928-3940. (e) Inagaki, T.; Ito, A.; Ito, J.; Nishiyama, H. *Angew. Chem. Int. Ed.* **2010**, *49*, 9384-9387. (f) Kandepi, V. V. K. M.; Cardoso, J. M. S.; Peris, E.; Royo, B. *Organometallics* **2010**, *29*,

2777-2782. (g) Yang, J.; Tilley, T. D. *Angew. Chem. Int. Ed.* **2010**, *49*, 10186-10188. (h) Bhattacharya, P.; Krause, J. A.; Guan, H. *Organometallics* **2011**, *30*, 4720-4729. (i) Atienza, C. C. H.; Tondreau, A. M.; Weller, K. J.; Lewis, K. M.; Cruse, R. W.; Nye, S. A.; Boyer, J. L.; Delis, J. G. P.; Chirik, P. J. *ACS Catal.* **2012**, *2*, 2169-2172. (j) Tondreau, A. M.; Atienza, C. C. H.; Darmon, J. M.; Milsmann, C.; Hoyt, H. M.; Weller, K. J.; Nye, S. A.; Lewis, K. M.; Boyer, J.; Delis, J. G. P.; Lobkovsky, E.; Chirik, P. J. *Organometallics* **2012**, *31*, 4886-4893. (k) Tondreau, A. M.; Atienza, C. C. H.; Weller, K. J.; Nye, S. A.; Lewis, K. M.; Delis, J. G. P.; Chirik, P. J. *Science* **2012**, *335*, 567-570. (l) Ruddy, A. J.; Kelly, C. M.; Crawford, S. M.; Wheaton, C. A.; Sydora, O. L.; Small, B. L.; Stradiotto, M.; Turculet, L. *Organometallics* **2013**, *32*, 5581-5588. (m) Peng, D.; Zhang, Y.; Du, X.; Zhang, L.; Leng, X.; Walter, M. D.; Huang, Z. *J. Am. Chem. Soc.* **2013**, *135*, 19154-19166.

(9) For representative Co hydrosilylation catalysts see: (a) Brunner, H.; Amberger, K. *J. Organomet. Chem.* **1991**, *417*, C63-C65. (b) Brookhart, M.; Grant, B. E. *J. Am. Chem. Soc.* **1993**, *115*, 2151-2156. (c) Tojo, S.; Isobe, M. *Tetrahedron Lett.* **2005**, *46*, 381-384. (d) Yong, L.; Kirleis, K.; Butenschön, H. *Adv. Synth. Catal.* **2006**, *348*, 833-836. (e) Konno, T.; Taku, K.; Yamada, S.; Moriyasu, K.; Ishihara, T. *Org. Biomol. Chem.* **2009**, *7*, 1167-1170. (f) Inagaki, T.; Phong, L. T.; Furuta, A.; Ito, J.; Nishiyama, H. *Chem. Eur. J.* **2010**, *16*, 3090-3096. (g) Yu, F.; Zhang, X.-C.; Wu, F.-F.; Zhou, J.-N.; Fang, W.; Wu, J.; Chan, A. S. C. *Org. Biomol. Chem.* **2011**, *9*, 5652. (h) Sauer, D. C.; Wadepohl, H.; Gade, L. H. *Inorg. Chem.* **2012**, *51*, 12948-12958. (i) Niu, Q.; Sun, H.; Li, X.; Klein, H.-F.; Flörke, U. *Organometallics* **2013**, *32*, 5235-5238.

(10) For representative Ni hydrosilylation catalysts see: (a) Tamao, K.; Miyake, N.; Kiso, Y.; Kumada, M. *J. Am. Chem. Soc.* **1975**, *97*, 5603-5605. (b) Tamao, K.; Kobayashi, K.; Ito, Y. *J. Am. Chem. Soc.* **1989**, *111*, 6478-6480. (c) Chakraborty, S.; Krause, J. A.; Guan, H. *Organometallics* **2009**, *28*, 582-586. (d) Tran, B. L.; Pink, M.; Mindiola, D. J. *Organometallics* **2009**, *28*, 2234-2243. (e) Porter, T. M.; Hall, G. B.; Groy, T. L.; Trovitch, R. J. *Dalton Trans.* **2013**, *42*, 14689-14692. (f) Miller, Z. D.; Li, W.; Belderrain, T. R.; Montgomery, J. *J. Am. Chem. Soc.* **2013**, *135*, 15282-15285.

(11) (a) Morris, R. H. *Chem. Soc. Rev.* **2009**, *38*, 2282-2291. (b) Bullock, R. M. *Catalysis without Precious Metals*; Wiley-VCH: Weinheim, Germany, 2010. (c) Junge, K.; Schroeder, K.; Beller, M. *Chem. Commun.* **2011**, *47*, 4849-4859.

(12) Molybdenum is the only second row metal that is widely utilized in biological systems. For a recent review see: Hille, R.; Hall, J.; Basu, P. *Chem. Rev.* **2014**, *114*, 3963-4038.

(13) Haynes, W. M. *CRC Handbook of Chemistry and Physics: A Ready-reference Book of Chemical and Physical Data*, 94th ed.; Taylor & Francis, Boca Raton, FL, 2013-2014.

(14) Fuchikami, T.; Ubukata, Y.; Tanaka, Y. *Tetrahedron Lett.* **1991**, *32*, 1199-1202.

- (15) Baricelli, P. J.; Melean, L. G.; Ricardes, S.; Guanipa, V.; Rodriguez, M.; Romero, C.; Pardey, A. J.; Moya, S.; Rosales, M. *J. Organomet. Chem.* **2009**, *694*, 3381-3385.
- (16) (a) Bullock, R. M.; Voges, M. H. *J. Am. Chem. Soc.* **2000**, *122*, 12594-12595. (b) Voges, M. H.; Bullock, R. M. *J. Chem. Soc., Dalton Trans.* **2002**, 759-770. (c) Kimmich, B. F. M.; Fagan, P. J.; Hauptman, E.; Bullock, R. M. *Chem. Commun.* **2004**, 1014-1015. (d) Kimmich, B. F. M.; Fagan, P. J.; Hauptman, E.; Marshall, W. J.; Bullock, R. M. *Organometallics* **2005**, *24*, 6220-6229.
- (17) Namorado, S.; Antunes, M. A.; Veiros, L. F.; Ascenso, J. R.; Duarte, M. T.; Martins, A. M. *Organometallics* **2008**, *27*, 4589-4599.
- (18) (a) Adams, K. P.; Joyce, J. A.; Nile, T. A.; Patel, A. I.; Reid, C. D.; Walters, J. M. *J. Mol. Catal.* **1985**, *29*, 201-208. (b) Keinan, E.; Perez, D. *J. Org. Chem.* **1987**, *52*, 2576-2580. (c) Abdelquader, W.; Ozkar, S.; Peynircioglu, N. B. *Z. Naturforsch. B: Chem. Sci.* **1993**, *48*, 539-540. (d) Schmidt, T. *Tetrahedron Lett.* **1994**, *35*, 3513-3516. (e) Kayran, C.; Rouzi, P. *Z. Naturforsch. B: Chem. Sci.* **2001**, *56*, 1138-1142. (f) Stosur, M.; Symańska-Buzar, T. *J. Mol. Catal. A: Chem.* **2008**, *286*, 98-105.
- (19) Dioumaev, V. K.; Bullock, R. M. *Nature* **2003**, *424*, 530-532.
- (20) (a) Fernandes, A. C.; Fernandes, R.; Romão, C. C.; Royo, B. *Chem. Commun.* **2005**, 213-214. (b) Reis, P. M.; Romão, C. C.; Royo, B. *Dalton Trans.* **2006**, 1842-1846. (c) Pontes da Costa, A.; Reis, P. M.; Gamelas, C.; Romão, C. C.; Royo, B. *Inorg. Chim. Acta* **2008**, *361*, 1915-1921.
- (21) Ziegler, J. E.; Du, G.; Fanwick, P. E.; Abu-Omar, M. M. *Inorg. Chem.* **2009**, *48*, 11290-11296.
- (22) (a) Khalimon, A. Y.; Simionescu, R.; Kuzmina, L. G.; Howard, J. A. K.; Nikonov, G. I. *Angew. Chem. Int. Ed.* **2008**, *47*, 7701-7704. (b) Oeterson, E.; Khalimon, A. Y.; Simionescu, R.; Kuzmina, L. G.; Howard, J. A. K.; Nikonov, G. I. *J. Am. Chem. Soc.* **2009**, *131*, 908-909. (c) Shirobokov, O. G.; Gorelsky, S. I.; Simionescu, R.; Kuzmina, L. G.; Nikonov, G. I. *Chem. Commun.* **2010**, *46*, 7831-7833. (d) Shirobokov, O. G.; Kuzmina, L. G.; Nikonov, G. I. *J. Am. Chem. Soc.* **2011**, *133*, 6487-6489. (e) Khalimon, A. Y.; Ignatov, S. K.; Simionescu, R.; Kuzmina, L. G.; Howard, J. A. K.; Nikonov, G. I. *Inorg. Chem.* **2012**, *51*, 754-756. (f) Khalimon, A. Y.; Shirobokov, O. G.; Peterson, E.; Simionescu, R.; Kuzmina, L. G.; Howard, J. A. K.; Nikonov, G. I. *Inorg. Chem.* **2012**, *51*, 4300-4313. (g) Khalimon, A. Y.; Ignatov, S. K.; Okhapkin, A. I.; Simionescu, R.; Kuzmina, L. G.; Howard, J. A. K.; Nikonov, G. I. *Chem. Eur. J.* **2013**, *19*, 8573-8590.

- (23) (a) Arias-Ugarte, R.; Sharma, H. K.; Morris, A. L. C.; Pannell, K. H. *J. Am. Chem. Soc.* **2012**, *134*, 848-851. (b) Sharma, H. K.; Arias-Ugarte, R.; Tomlinson, D.; Gappa, R.; Metta-Magaña, A. J.; Ito, H.; Pannell, K. H. *Organometallics* **2013**, *32*, 3788-3794.
- (24) Chakraborty, S.; Blacque, O.; Fox, T.; Berke, H. *ACS Catal.* **2013**, *3*, 2208-2217.
- (25) Trovitch, R. J. *Synlett* **2014**, *25*, 1638-1642.
- (26) Chiericato Jr., G.; Arana, C. R.; Casado, C.; Cusdrado, I.; Abruña, H. D. *Inorg. Chim. Acta* **2000**, *300-302*, 32-42.
- (27) Zeng, D.; Hampden-Smith, M. J. *Polyhedron* **1992**, *11*, 2585-2589.
- (28) Several complexes featuring κ^2 -*N,N*-PDI coordination have been identified. For crystallographically characterized examples, see: (a) Lu, S.; Selbin, J. *Inorg. Chim. Acta* **1987**, *134*, 229-232. (b) Heard, P. J.; Tocher, D. A. *J. Chem. Soc., Dalton Trans.* **1998**, 2169-2176. (c) Cosquer, N.; Le Gall, B.; Conan, F.; Kerbaol, J.-M.; Sala-Pala, J.; Kubicki, M. M.; Vigier, E. *Inorg. Chim. Acta* **2006**, *359*, 4311-4316.
- (29) Hiya, K.; Nakayama, Y.; Yasuda, H. *Macromolecules* **2003**, *36*, 7916-7922.
- (30) de Bruin, B.; Bill, E.; Bothe, E.; Weyhermüller, T.; Wieghardt, K. *Inorg. Chem.* **2000**, *39*, 2936-2947.
- (31) Knijnenberg, Q.; Gambarotta, S.; Budzelaar, P. H. M. *Dalton Trans.* **2006**, 5442-5448.
- (32) PDI redox-activity has proven to be important for enabling first-row metal catalyzed transformations. For a leading example see: Chirik, P. J.; Wieghardt, K. *Science* **2010**, *327*, 794-795.
- (33) Corn, I. R.; Astudillo-Sánchez, P. D.; Zdilla, M. J.; Fanwick, P. E.; Shaw, M. J.; Miller, J. T.; Evans, D. H.; Abu-Omar, M. M. *Inorg. Chem.* **2013**, *52*, 54657-54663.
- (34) Ben-Daat, H.; Hall, G. B.; Groy, T. L.; Trovitch, R. J. *Eur. J. Inorg. Chem.* **2013**, 4430-4442.
- (35) Complete delocalization would be expected if the electron(s) is(are) delocalized across the LUMO of the κ^3 -*N,N,N*-PDI chelate (see ref. 31). It is also possible that κ^2 -*N,N*-PDI chelates can behave as redox non-innocent ligands. For α -iminopyridine reduction see: Lu, C. C.; Weyhermüller, T.; Bill, E.; Wieghardt, K. *Inorg. Chem.* **2009**, *48*, 6055-6064.
- (36) If η^1 -substrate binding occurs, the steric hinderance of the carbonyl substituents would be further removed from the metal center.

- (37) Ojima, I.; Kogure, T. *Organometallics* **1982**, *1*, 1390-1399.
- (38) Schneider, N.; Finger, M.; Haferkemper, C.; Bellemin-Laponnaz, S.; Hofmann, P.; Gade, L. H. *Chem. Eur. J.* **2009**, *15*, 11515-11529.
- (39) Neese, F. *Orca, an Ab Initio, Density Functional and Semiempirical Electronic Structure Program Package*, version 2.9.1; Max Planck Institute for Bioinorganic Chemistry: Mülheim an der Ruhr, Germany, 2012.
- (40) (a) Becke, A. D. *J. Chem. Phys.* **1993**, *98*, 5648-5652. (b) Lee, C. T.; Yang, W. T.; Parr, R. G. *Phys. Rev. B* **1988**, *37*, 785-789.
- (41) (a) Klamt, A.; Schüürmann, G. *J. Chem. Soc., Perkin Trans. 2* **1993**, 799-805. (b) Sinnecker, S.; Rajendran, A.; Klamt, A.; Diedenhofen, M.; Neese, F. *J. Phys. Chem. A* **2006**, *110*, 2235-2245.
- (42) Grimme, S. *J. Comput. Chem.* **2006**, *27*, 1787-1799.
- (43) Pantazis, D. A.; Chen, X. Y.; Landis, C. R.; Neese, F. *J. Chem. Theory Comput.* **2008**, *4*, 908-919.
- (44) *Molekel*, Advanced Interactive 3D-Graphics for Molecular Sciences, Swiss National Supercomputing Center. <http://www.cscs.ch/molekel>.

CHAPTER 2

CONVERSION OF CARBON DIOXIDE TO METHANOL USING A C-H ACTIVATED BIS(IMINO)PYRIDINE MOLYBDENUM HYDROBORATION CATALYST

2.1. Abstract

Using a multistep synthetic pathway, a bis(imino)pyridine (or pyridine diimine, PDI) molybdenum catalyst for the selective conversion of carbon dioxide into methanol has been developed. Starting from $(\text{Ph}^{2\text{PPr}}\text{PDI})\text{Mo}(\text{CO})$, I_2 addition afforded $[(\text{Ph}^{2\text{PPr}}\text{PDI})\text{MoI}(\text{CO})][\text{I}]$, which features a seven-coordinate Mo(II) center. Heating this complex to 100 °C under vacuum resulted in CO loss and the formation of $[(\text{Ph}^{2\text{PPr}}\text{PDI})\text{MoI}][\text{I}]$. Reduction of $[(\text{Ph}^{2\text{PPr}}\text{PDI})\text{MoI}][\text{I}]$ in the presence of excess K/Hg yielded $(\kappa^6\text{-}P,N,N,N,C,P\text{-}\text{Ph}^{2\text{PPr}}\text{PDI})\text{MoH}$ following methylene group C–H activation at the α -position of one PDI imine substituent. The addition of CO_2 to $(\kappa^6\text{-}P,N,N,N,C,P\text{-}\text{Ph}^{2\text{PPr}}\text{PDI})\text{MoH}$ resulted in facile insertion to generate the respective η^1 -formate complex, $(\kappa^6\text{-}P,N,N,N,C,P\text{-}\text{Ph}^{2\text{PPr}}\text{PDI})\text{Mo}(\text{OCOH})$. When low pressures of CO_2 were added to solutions of $(\kappa^6\text{-}P,N,N,N,C,P\text{-}\text{Ph}^{2\text{PPr}}\text{PDI})\text{MoH}$ containing pinacolborane, the selective formation of H_3COBPin and $\text{O}(\text{BPin})_2$ was observed along with precatalyst regeneration. When HBPin was limited, $\text{H}_2\text{C}(\text{OBPin})_2$ was observed as an intermediate and $(\kappa^6\text{-}P,N,N,N,C,P\text{-}\text{Ph}^{2\text{PPr}}\text{PDI})\text{Mo}(\text{OCOH})$ remained present throughout CO_2 reduction. The hydroboration of CO_2 to H_3COBPin was optimized and 97% HBPin utilization by 0.1 mol % $(\kappa^6\text{-}P,N,N,N,C,P\text{-}\text{Ph}^{2\text{PPr}}\text{PDI})\text{MoH}$ was demonstrated over 8 h at 90 °C, resulting in a methoxide formation turnover frequency (TOF) of 40.4 h^{-1} (B–H utilization TOF = 121.2 h^{-1}). Hydrolysis of the products and distillation at 65 °C allowed for MeOH isolation. The mechanism of $(\kappa^6\text{-}P,N,N,N,C,P\text{-}\text{Ph}^{2\text{PPr}}\text{PDI})\text{MoH}$ mediated CO_2 hydroboration is presented

in the context of these experimental observations. Notably, (κ^6 -*P,N,N,N,C,P*-Ph₂PP_rPDI)MoH is the first Mo hydroboration catalyst capable of converting CO₂ to MeOH, and the importance of this study as it relates to previously described catalysts is discussed.

Reprinted with the permission from Pal, R.; Groy, T. L.; Trovitch, R. J. *Inorganic Chemistry* **2015**, *54*, 7506-7515. Copyright 2015 American Chemical Society.

2.2. Introduction^{1a}

For more than a century, developed nations have relied on fossil fuel combustion to satisfy a large fraction of their energy demands.^{1b} As a result, atmospheric CO₂ concentrations have climbed by 36% over 250 years² and an additional 30 Gt of CO₂ are released into the atmosphere annually.³ Moreover, increasing atmospheric CO₂ concentrations have been linked to environmental consequences that include higher global temperatures,⁴ rising sea levels,⁵ and ocean acidification.⁶ Diverse and complimentary approaches to mitigating these effects by reducing CO₂ emissions are being considered^{7,8} and the conversion of CO₂ into value-added products has become an increasingly relevant area of chemical research.⁹⁻¹¹ Syntheses that rely on CO₂ as a carbon-based feedstock are industrially desirable since this molecule is abundant, inexpensive, and renewable.¹² These characteristics have led to CO₂ utilization for the production of urea (70 Mt/yr), inorganic carbonates (30 Mt/yr), and salicylic acid (20 Mt/yr);¹³ however, the efficient and selective reduction of CO₂ into suitable fossil fuel alternatives is an unresolved challenge that continues to draw interest from the scientific community.¹⁴

Efficient homogeneous catalysts for the conversion of CO₂ into formic acid,¹⁵ formaldehyde (or formaldehyde-derived oligomers and derivatives),¹⁶ methanol,¹⁷⁻²⁶ and methane²⁷ have only recently been developed. Of these products, methanol is the most appropriate transportation fuel for our existing energy infrastructure since it is a liquid under ambient conditions with an energy density of 22.7 MJ/kg.²⁸ Although H₂ is an ideal reductant in terms of cost and atom efficiency, the hydrogenation of CO₂ to MeOH using homogeneous Ru catalysts has been hindered by a lack of selectivity¹⁷ and activity at elevated temperatures (140-155 °C).¹⁸ Silanes have been used to achieve Ir-¹⁹ and Ru-

catalyzed²⁰ conversion of CO₂ into methoxysilanes; however, a limited turnover number (TON) for selective methoxide group formation was reported in each case (TON = 3 for Ir¹⁹; 32 for Ru²⁰). Free *N*-heterocyclic carbenes have also been found to mediate the reduction of CO₂ into Ph₂Si(OMe)₂ and Ph₂HSiOSiHPh₂ at ambient temperature (methoxide formation TON of 6 over 24 h).²¹

While reducing CO₂ to the methoxide level using H₂ and silanes has been met with limited success, borane reagents have proven to be highly effective for this transformation. Depending on the nature of the borane, frustrated Lewis pairs,²² alkali metal²³ and alkaline earth metal²⁴ reagents have all been found to catalyze the hydroboration of CO₂ to the respective methoxyborane. To date, only two well-defined transition metal catalyst systems have been found to selectively mediate this transformation, (^RPOCOP)NiH²⁵ [R = ^tBu²⁵ (Fig. 2.1, A), ⁱPr,^{25b,c} or ^cPe^{25b,c}] and [(κ⁵-*P,P,N,N,O*-(ⁱPr₂PNH(CH₂)₂)₂N((CH₂)₂NPⁱPr₂CO₂)Ru)][BPh₄]²⁶ (Fig. 2.1, B). Using 0.2 mol% A relative to HBPi_n under 1 atm CO₂, complete conversion to H₃COBPi_n and O(BPi_n)₂ was observed within 1 h at ambient temperature (methoxide formation TOF = 165 h⁻¹, B-H utilization TOF = 495 h⁻¹).^{25a} Complex B was found to be a comparatively inefficient catalyst for this transformation (TON = 9 after 96 h at 50 °C).²⁶

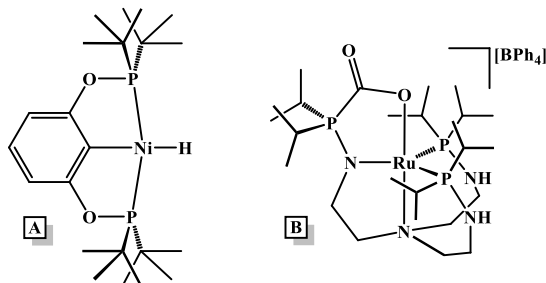


Figure 2.1. Previously described transition metal catalysts for the hydroboration of CO₂ to methoxyborane.^{25,26}

In the previous chapter, we reported that (Ph_2PPrPDI)Mo(CO) (**2**) catalyzes C=O bond hydrosilylation with TOFs of up to 330 h^{-1} at $90 \text{ }^\circ\text{C}$.³⁰ Having determined that this transformation occurs by way of phosphine substituent dissociation, we hypothesized that ($\kappa^5\text{-P,P,P,N,N-Ph}_2\text{PPrPDI}$)Mo-L (L = weakly coordinating neutral ligand) complexes may exhibit superior carbonyl reduction activity relative to **2**.³⁰ Continuing our investigation of (Ph_2PPrPDI)Mo complexes, this contribution describes the preparation of a 7-coordinate Mo hydride complex following chelate C-H activation, in addition to its utility as a CO_2 reduction catalyst.

2.3. Results and Discussion^{1a}

2.3.1. Synthesis and Characterization

Having recently reported the preparation of **2**³⁰ (Fig. 2.2) from Ph_2PPrPDI ³¹ and $\text{Mo}(\text{CO})_6$, a synthetic pathway for CO-free analogues was sought. Refluxing toluene solutions of **2** under vacuum for days failed to result in CO loss.³⁰ Therefore, we hypothesized that oxidizing **2** would diminish Mo-CO backbonding and render this ligand susceptible to dissociation. Addition of stoichiometric I_2 to a toluene solution of **2** resulted in precipitation of a purple solid within hours of stirring at ambient temperature. Isolation of the product and analysis by ^{31}P NMR spectroscopy revealed two doublets centered at 37.92 and 37.52 ppm, indicating that both phosphine arms remain coordinated to the Mo center. The ^1H and ^{13}C NMR spectra collected for this complex were also indicative of left-to-right Ph_2PPrPDI inequivalence. Importantly, a pseudo triplet was observed at 238.4 ppm ($J_{\text{PC}} = 20.5 \text{ Hz}$) in the ^{13}C NMR spectrum and infrared spectroscopy revealed a single CO stretch at 1826 cm^{-1} . Taken together, this data suggests that I_2 addition to **2** results in formation of the seven-coordinate Mo(II) complex, [$(\text{Ph}_2\text{PPrPDI})\text{MoI}(\text{CO})$][I] (**3**, Fig. 2.2).³²

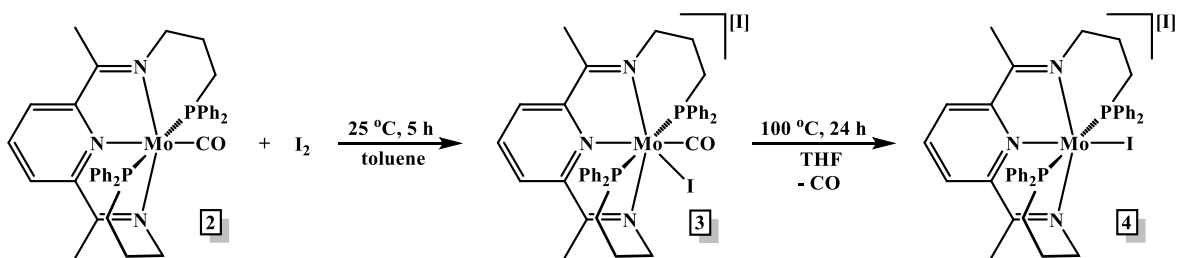


Figure 2.2. Synthetic scheme for $[(\text{Ph}_2\text{PPrPDI})\text{MoI}][\text{I}]$ (**4**) from $(\text{Ph}_2\text{PPrPDI})\text{Mo}(\text{CO})$ (**2**).

Relative to **2** ($\nu_{\text{CO}} = 1740\text{ cm}^{-1}$),³⁰ complex **3** ($\nu_{\text{CO}} = 1826\text{ cm}^{-1}$) exhibits significantly weakened Mo-CO backbonding and heating a THF solution of the latter to $100\text{ }^\circ\text{C}$ for 24 h resulted in CO dissociation and formation of an amber-colored complex identified as $[(\text{Ph}_2\text{PPrPDI})\text{MoI}][\text{I}]$ (**4**, Fig. 2.2). Analysis by IR and ^{13}C NMR spectroscopy revealed no evidence of CO coordination and the ^{31}P NMR spectrum of **4** was found to feature a single resonance at 6.18 ppm, indicating equivalent phosphine environments. Furthermore, complexes **2** (bright pink), **3** (purple), and **4** (amber) are readily distinguishable by UV-visible spectroscopy (Fig. 2.3 and Table 2.1). The spectrum of **2** is dominated by charge transfer bands with maxima at 299, 345, 399, and 537 nm; all of which have molar absorptivity values of greater than $10,000\text{ M}^{-1}\text{cm}^{-1}$. Two-electron oxidized **3** features comparatively weak charge transfer bands at 328 ($\epsilon = 5,410$), 410 ($\epsilon = 2,580$), and 541 nm ($\epsilon = 7,250$). Finally, complex **4** exhibits a predominant charge transfer band at 452 nm ($\epsilon = 2,210$) with a shoulder at 527 nm ($\epsilon = 1,072$).

The solid state structure of **4** (Fig. 2.4) was determined by single crystal X-ray diffraction and noteworthy metrical parameters are provided in Table 2.2. The geometry about Mo can best be described as distorted octahedral with N(1)-Mo(1)-N(3) and P(1)-Mo(1)-P(2) angles of $141.6(4)$ and $169.30(7)^\circ$, respectively. Inspection of the PDI chelate imine N=C distances reveals considerable elongation [$1.324(15)$ and $1.332(16)\text{ \AA}$] relative

to unreduced PDI ligands (1.28 Å).³³ The C(2)-C(3) and C(7)-C(8) distances determined for **4** of 1.442(17) and 1.401(18) Å, respectively, are also significantly contracted from the C_{imine}-C_{pyridine} bond lengths found for unreduced chelates (1.50 Å).³³ Comparable C_{imine}-C_{pyridine} distances reported for [(ⁱPr₂ArBPDI)Mo(N₂)]₂(μ₂,η¹,η¹-N₂) of 1.421(5) and 1.437(5) Å have recently been assigned to two-electron reduction of the chelate;³⁴ however, this complex features a geometry in which Mo does not lie in the idealized PDI chelate plane.

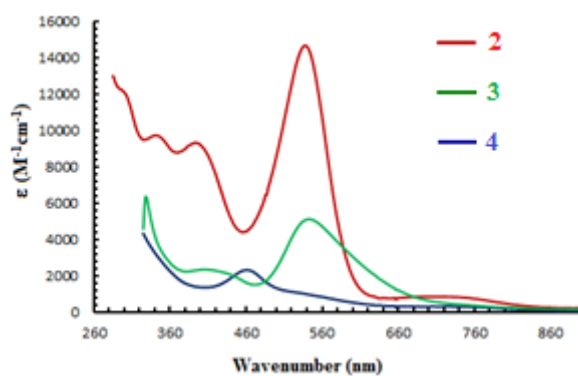


Figure 2.3. Absorption spectra comparison of **2**, **3**, and **4**. Molar absorptivity values have been determined from 5 independent concentrations and are tabulated in Table 2.1.

Table 2.1. Wavelengths of maximum absorption (λ_{max}) and extinction coefficients (ϵ) for each complex analyzed by UV-vis spectroscopy.

| Complex | λ_{max} (nm) | ϵ ($\text{M}^{-1} \text{cm}^{-1}$) |
|---|-----------------------------|---|
| (Ph₂PPrPDI)Mo(CO) | 299 | 17,770 |
| | 345 | 10,520 |
| | 399 | 10,030 |
| | 537 | 13,550 |
| | 723 | 1,619 |
| [(Ph₂PPrPDI)MoI(CO)][I] | 328 | 5,410 |
| | 410 | 2,580 |
| | 541 | 7,250 |
| [(Ph₂PPrPDI)MoI][I] | 452 | 2,210 |
| | 527 | 1,070 |
| | 735 | 280 |

As we have previously described, d-orbital radial expansion enhances second-row metal backbonding such that redox non-innocent ligand LUMOs are greatly destabilized, rendering their population unlikely.^{30,31,35} For this reason, we refrain from assigning the Ph₂PPrPDI chelate of **4** as redox-active (i.e., reduced by one or more electrons), even though Ph₂PPrPDI is known to be redox-active when coordinated to formally zerovalent Mn.³⁶⁻³⁷

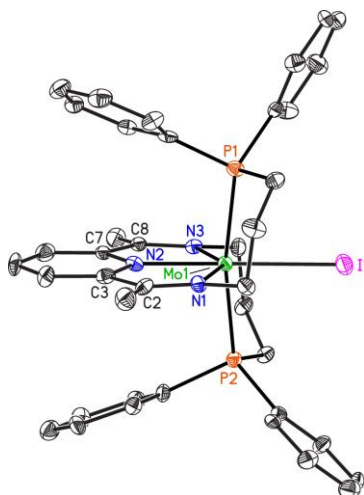


Figure 2.4. The solid state structure of **4** shown at 30% probability ellipsoids. Hydrogen atoms and I⁻ counterion are omitted for clarity.

Table 2.2. Notable bond lengths (Å) and angles (°) determined for **4**.

| 3 | |
|-----------------|------------|
| Mo(1)-N(1) | 2.036(11) |
| Mo(1)-N(2) | 2.112(10) |
| Mo(1)-N(3) | 2.077(10) |
| Mo(1)-P(1) | 2.472(3) |
| Mo(1)-P(2) | 2.453(3) |
| Mo(1)-I(1) | 2.7810(17) |
| N(1)-C(2) | 1.332(16) |
| N(3)-C(8) | 1.324(15) |
| C(2)-C(3) | 1.442(17) |
| C(7)-C(8) | 1.401(18) |
| N(1)-Mo(1)-N(3) | 141.6(4) |
| P(1)-Mo(1)-P(2) | 169.30(7) |
| N(2)-Mo(1)-I(1) | 178.2(3) |

Having isolated and characterized **4**, its reduction to an appropriate catalyst precursor **r** was explored. Adding an excess of K/Hg to **4** in THF afforded a green solution after 2 d at ambient temperature. Upon workup, the resulting product was analyzed by multinuclear NMR spectroscopy. The ¹H NMR spectrum of this complex was found to feature two unique backbone methyl resonances at 2.88 and 2.50 ppm, indicating left-to-right ^{Ph}2PP^rPDI

inequivalence. A set of methylene-derived resonances was also shifted downfield to 4.85 and 4.77 ppm. Further inspection by gHSQCAD revealed that the ^1H resonance at 4.77 ppm was correlated to a newly formed C–H environment (54.9 ppm, suggesting concomitant Mo–H formation) while ^1H resonances at 5.44 and 4.85 ppm were associated with a ^{13}C NMR resonance at 57.8 ppm (Fig. 2.25). Collecting ^1H -coupled ^{13}C data confirmed that the resonance centered at 54.9 ppm is a doublet ($J_{\text{CH}} = 171.12$ Hz), indicating it is bound to a single hydrogen atom (Fig. 2.26).³⁹ Attempts to locate a Mo–H resonance by COSY or NOESY NMR spectroscopy were unsuccessful. The ^{31}P NMR spectrum of this product featured two sets of doublets at 46.93 and 57.94 ppm ($J_{\text{PP}} = 97.2$ Hz), further supporting static left-to-right Ph_2PPrPDI inequivalence. Taken together, NMR spectroscopic data indicates that reduction of **4** using K/Hg affords the C–H activated Mo(II) product, $(\kappa^6\text{-}P,N,N,N,C,P\text{-Ph}_2\text{PPrPDI})\text{MoH}$ (**5**, Fig. 2.5).

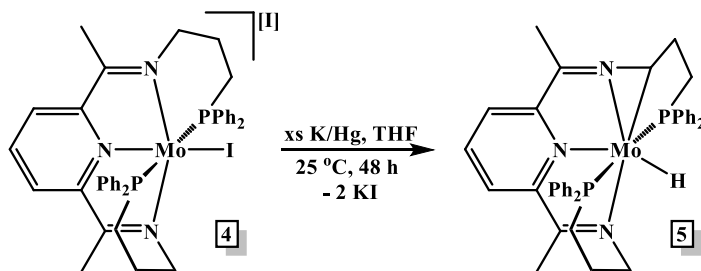


Figure 2.5. Synthesis of $(\kappa^6\text{-}P,N,N,N,C,P\text{-Ph}_2\text{PPrPDI})\text{MoH}$ (**5**) from $[(\text{Ph}_2\text{PPrPDI})\text{MoII}][\text{I}]$ (**4**).

To confirm the unusual coordination environment proposed for **5**, the solid state structure of this complex was determined by single crystal X-ray diffraction. As illustrated in Fig. 2.6, the geometry about Mo can best be described as distorted pentagonal bipyramidal. Due to the rigidity of the C–H activated propylene arm of Ph_2PPrPDI , the phosphine donors are restricted from linearity with a P(1)–Mo(1)–P(2) angle of $152.91(7)^\circ$. The N(1)–Mo(1)–N(3) angle of $144.3(2)^\circ$ is similar to the one observed for **4**; however,

the angle defined by N(1)-Mo(1)-C(10) is only 38.0(2) °. Interestingly, C-H activation affords a Mo(1)-C(10) bond distance of 2.259(8) Å and the *trans*-influence of this alkyl is responsible for a relatively long Mo(1)-N(3) contact of 2.121(6) Å. The C(10)-N(1) distance of 1.399(9) Å is indicative of a single bond and the proximity of C(10) to Mo(1) forces a fairly short Mo(1)-N(1) contact of 1.940(7) Å. Although the in-plane PDI bond precision determined for **5** is poorer than desired for electronic structure discussion, the C(2)-C(3) and C(7)-C(8) distances of 1.406(10) and 1.408(11) Å, respectively, indicate that a significant amount of electron density is being transferred from Mo to the ligand framework.

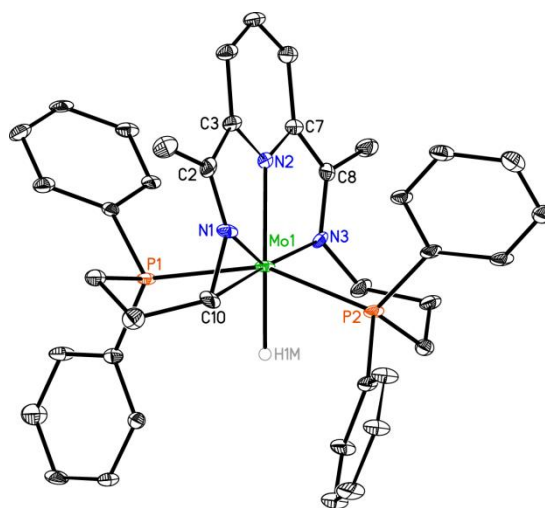


Figure 2.6. The solid state structure of **5** shown at 30% probability ellipsoids. Hydrogen atoms other than H1M and a partially occupied toluene molecule are omitted for clarity.

Table 2.3. Notable bond lengths (Å) and angles (°) determined for **5**.

| 5 | |
|------------------|-----------|
| Mo(1)-N(1) | 1.940(7) |
| Mo(1)-N(2) | 2.072(5) |
| Mo(1)-N(3) | 2.121(6) |
| Mo(1)-P(1) | 2.448(2) |
| Mo(1)-P(2) | 2.433(2) |
| Mo(1)-H(1M) | 1.75(8) |
| Mo(1)-C(10) | 2.259(8) |
| C(10)-N(1) | 1.399(9) |
| N(1)-C(2) | 1.324(9) |
| N(3)-C(8) | 1.374(9) |
| C(2)-C(3) | 1.406(10) |
| C(7)-C(8) | 1.408(11) |
| | |
| N(1)-Mo(1)-C(10) | 38.0(2) |
| N(1)-Mo(1)-N(3) | 144.3(2) |
| P(1)-Mo(1)-P(2) | 152.91(7) |
| N(3)-Mo(1)-C(10) | 176.8(3) |

2.3.2. CO₂ Functionalization

Considering that CO₂ insertion into Mo-H bonds has been well-documented,³⁹ its addition to **5** was investigated. When 0.2 atm of CO₂ was admitted to a J. Young tube containing a frozen benzene-*d*₆ solution of **5** (0 °C), complete conversion to a new complex was observed by multinuclear NMR spectroscopy after 10 min at 25 °C (Fig. 2.7).

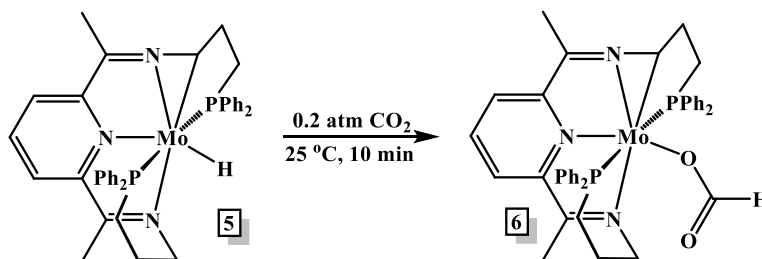


Figure 2.7. Synthesis of (κ^6 -*P,N,N,N,C,P*-Ph₂PPrPDI)Mo(OCOH) (**6**) from (κ^6 -*P,N,N,N,C,P*-Ph₂PPrPDI)MoH (**5**).

The ^1H NMR spectrum of the product featured resonances consistent with left-to-right chelate inequivalence in addition to a sharp singlet at 9.14 ppm. This resonance, along with a newly observed ^{13}C NMR resonance at 169.7 ppm,^{39a} is consistent with formation of the respective formate complex, $(\kappa^6\text{-}P,N,N,N,C,P\text{-Ph}_2\text{PPrPDI})\text{Mo}(\text{OCOH})$ (**6**, Fig. 2.7). Complex **6** is believed to possess a η^1 -formate ligand since this binding mode renders it an 18-electron complex. Infrared spectroscopy revealed a formate C=O stretch at 1625 cm^{-1} (KBr), providing further support for η^1 -coordination. In the absence of reducing agent, the addition of more than 0.2 atm CO_2 to **5** at 0 °C has been found to result in decomposition by way of chelate loss.

Having determined that CO_2 insertion into the Mo–H bond of **5** is facile, the stoichiometric reduction of CO_2 was attempted in the presence of excess HBPIn. Upon adding 20 eq. of HBPIn relative to **5** in benzene- d_6 and exposing the solution to 0.2 atm of CO_2 , reaction progress was monitored by NMR spectroscopy. After 3 d at 25 °C, small quantities of H_3COBPIn and $\text{O}(\text{BPIn})_2$ were identified (Fig. 2.8). Realizing that reduction beyond the formate level was slow under these conditions (**6** remained observable by ^{31}P NMR spectroscopy, Fig. 2.9), the reaction was heated to 60 °C and continued monitoring over 2 d revealed near quantitative conversion of CO_2 to H_3COBPIn and $\text{O}(\text{BPIn})_2$ by ^1H NMR spectroscopy (Fig. 2.10). The collection of ^{31}P NMR spectroscopic data confirmed that **5** is regenerated in the absence of CO_2 (Fig. 2.11).

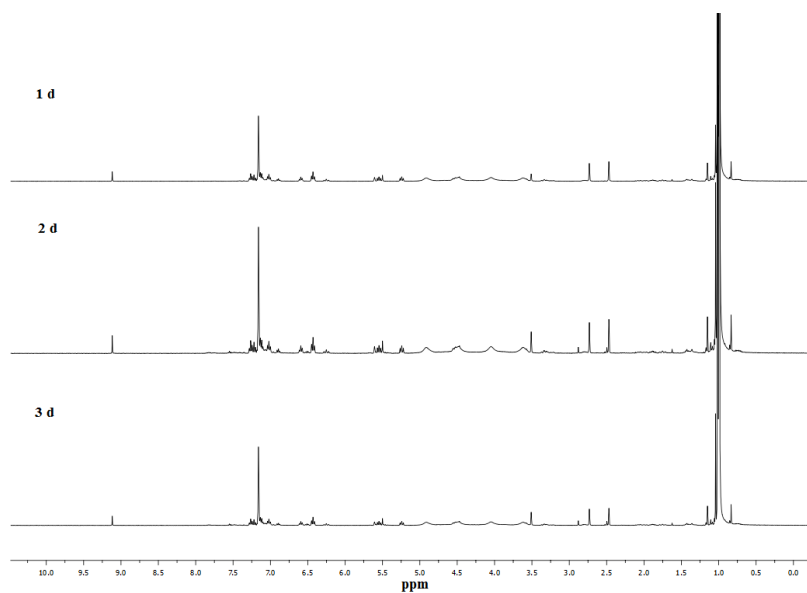
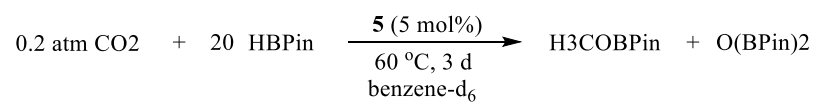


Figure 2.8. ¹H NMR spectra illustrating the slow conversion of CO₂ to H₃COBPin and O(BPin)₂ over 3 d at 25 °C using **5**.

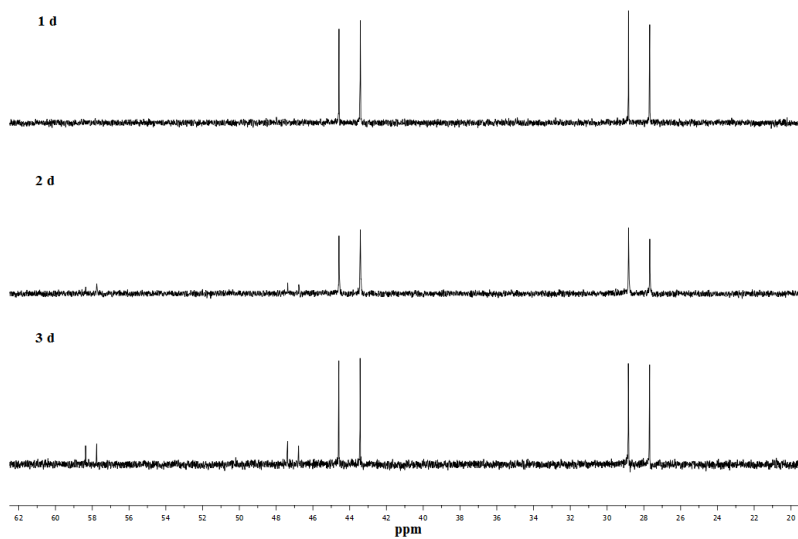


Figure 2.9. ¹H NMR spectra illustrating the slow conversion of **6** to **5** over 3 d at 25 °C.

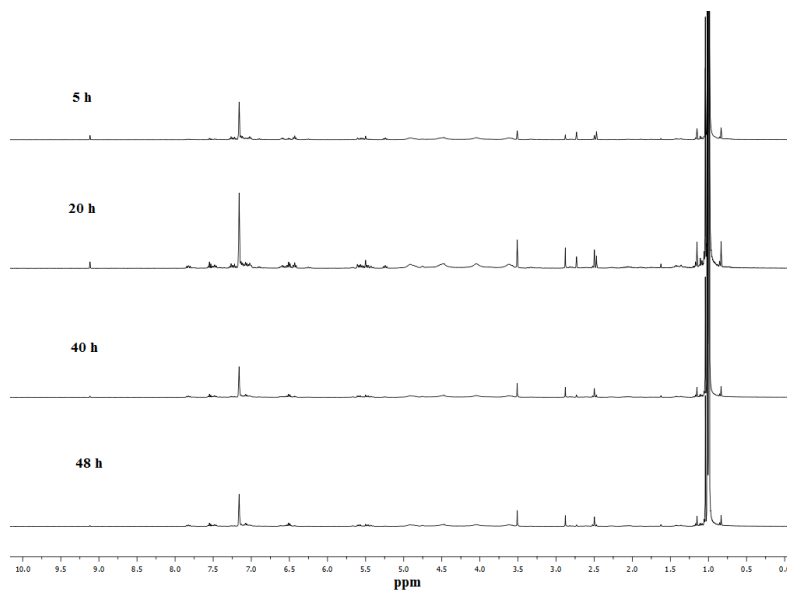


Figure 2.10. ^1H NMR spectra illustrating the stoichiometric conversion of CO_2 to H_3COBPIn and $\text{O}(\text{BPin})_2$ over 2 d at $60\text{ }^\circ\text{C}$ using **5**.

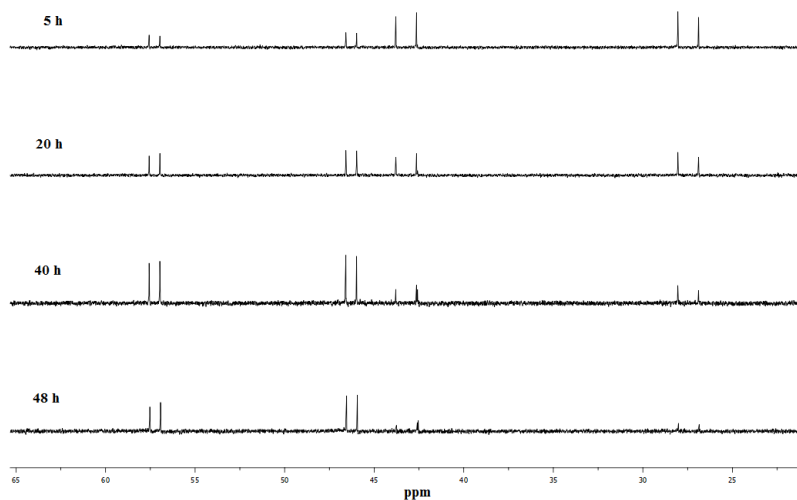


Figure 2.11. ^{31}P NMR spectra illustrating the conversion of **6** to **5** over 2 d at $60\text{ }^\circ\text{C}$.

Since conversion remained slow at $60\text{ }^\circ\text{C}$ and CO_2 was the limiting reagent at 0.2 atm, attempts were made to optimize this transformation. Upon adding 1 atm of CO_2 to a J. Young tube containing a benzene- d_6 solution of 100 eq. HBPIn relative to **5** at $-70\text{ }^\circ\text{C}$, the reaction was heated to $90\text{ }^\circ\text{C}$ and monitored spectroscopically. After 2 h, most of the HBPIn had been consumed and a mixture of $\text{H}_2\text{C}(\text{OBPin})_2$, H_3COBPIn , and $\text{O}(\text{BPin})_2$ was

observed in a 2:1:2 ratio by ^1H NMR spectroscopy (Fig. 2.12). After 5 h at 90 °C, the product mixture consisted only of H_3COBPin and $\text{O}(\text{BPin})_2$ as judged by ^1H (Fig. 2.12) and ^{11}B NMR spectroscopy (Fig. 2.14). Repeating the reaction in the absence of **5** did not result in CO_2 reduction. Since phosphine-promoted CO_2 hydroboration has been reported in the presence of 9-BBN,^{22c,d} a control experiment employing 1 mol% Ph_2PPrPDI was conducted. This experiment did not afford H_3COBPin ; however, a minimal amount (3%) of HCO_2BPin was detected by ^1H and ^{11}B NMR spectroscopy after 5 h at 90 °C (Fig. 2.15 and 2.16). Employing 1 mol% **5** under these conditions affords a methoxide formation TON of 33 (99 based on B-H) and TOF of 6.6 h^{-1} (B-H utilization TOF = 19.8 h^{-1}). The observation of $\text{H}_2\text{C}(\text{OBPin})_2$ under excess CO_2 at low HBPIn concentrations is also important from a mechanistic standpoint.

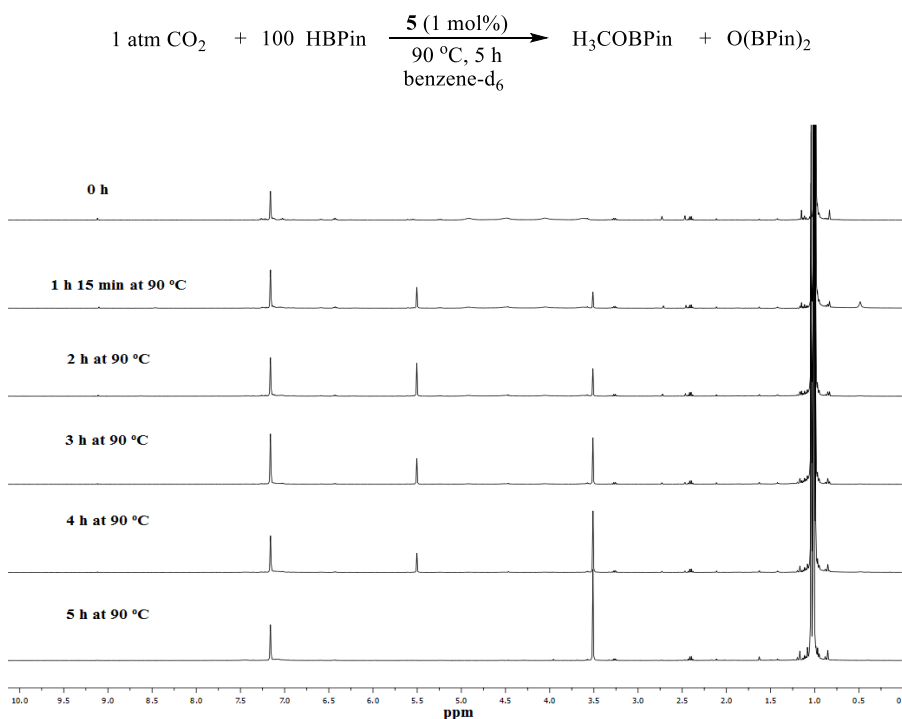


Figure 2.12. ^1H NMR spectra of **5**-mediated CO_2 hydroboration over the course of 5 h at 90 °C.

To explore the full synthetic utility of this transformation, a thick-walled glass bomb was charged with 0.1 mol% **5** in neat HBPIn and 1 atm of CO₂ was added at -70 °C (Fig. 2.13). After heating to 90 °C for 8 h, analysis by ¹H NMR spectroscopy revealed greater than 99% B-H bond utilization to selectively generate H₃COBPIn and O(BPin)₂, equating to a **5**-mediated CO₂ to methoxide TOF of 41.3 h⁻¹ (123.8 h⁻¹ relative to B-H; TON = 330) (Fig. 2.17). The product mixture was then treated with deionized H₂O, and upon stirring for 24 h, fractional distillation at 65 °C yielded MeOH (0.022 g, 58% isolated yield relative to HBPIn, Fig. 2.18 and 2.19). The low catalyst loading and solvent-free conditions used to achieve this transformation are advantageous from a sustainability perspective.

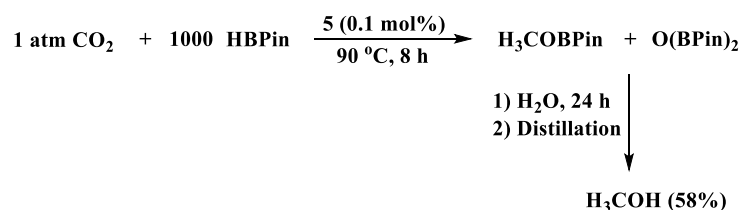


Figure 2.13. Overall reaction of **5**-mediated CO₂ hydroboration over the course of 8 h at 90 °C.

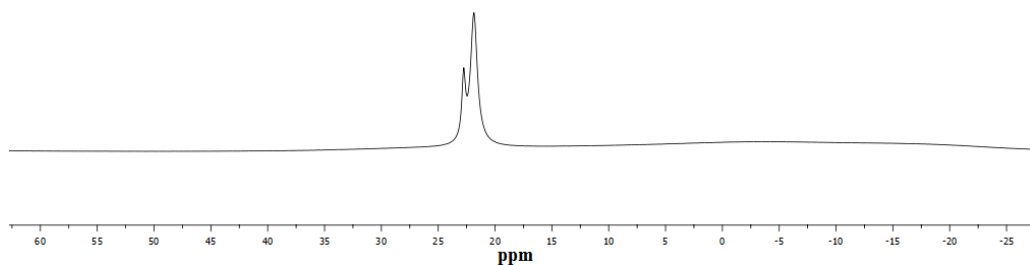


Figure 2.14. ¹¹B NMR spectrum of CO₂ hydroboration using 0.1 mol% **5** after 8 h at 90 °C.

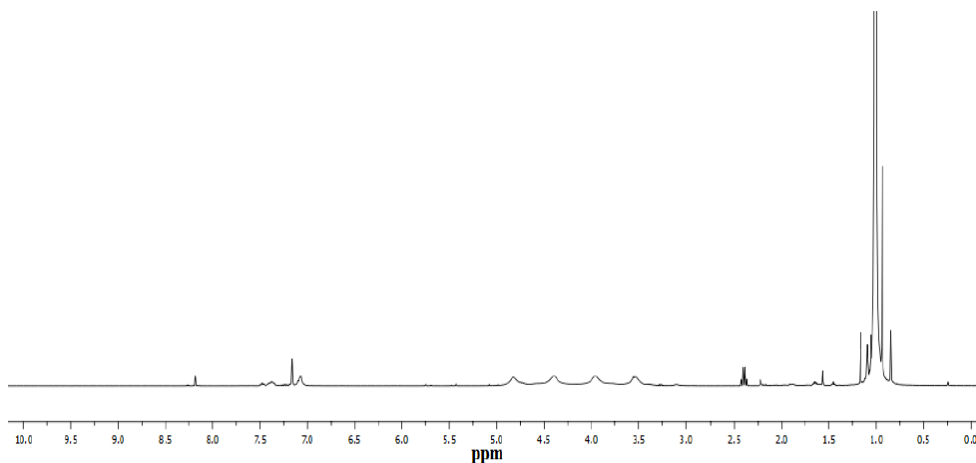


Figure 2.15. ^1H NMR spectrum of attempted CO_2 hydroboration using 1.0 mol% Ph_2PPrPDI as a catalyst in benzene- d_6 .

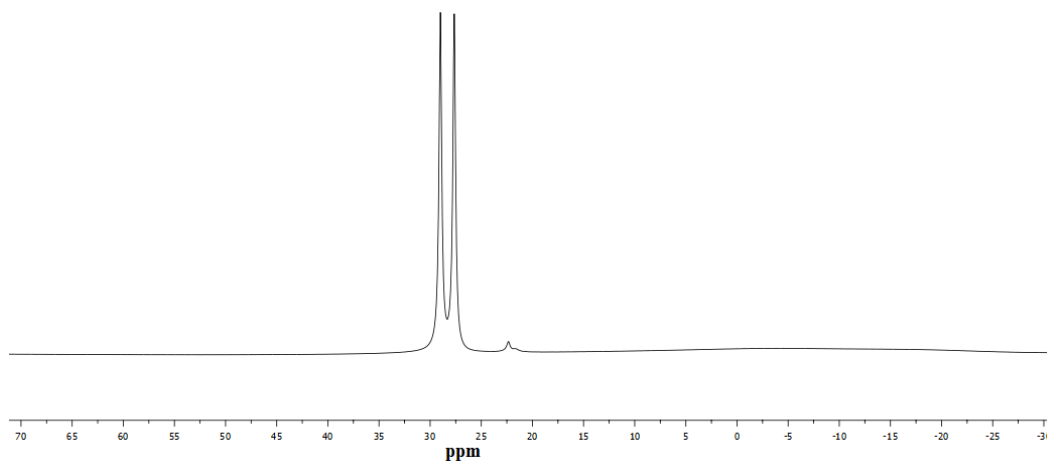


Figure 2.16. ^{11}B NMR spectrum of attempted CO_2 hydroboration using 1.0 mol% Ph_2PPrPDI as a catalyst in benzene- d_6 .

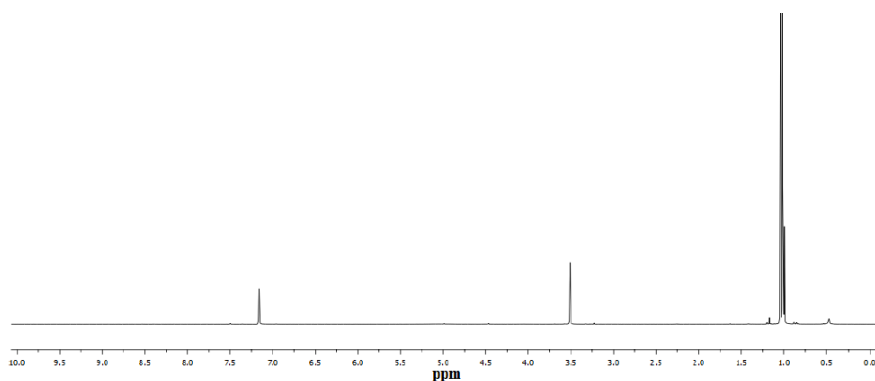


Figure 2.17. ^1H NMR spectrum of CO_2 hydroboration using 0.1 mol% **5** after 8 h at 90 $^\circ\text{C}$ in benzene- d_6 .

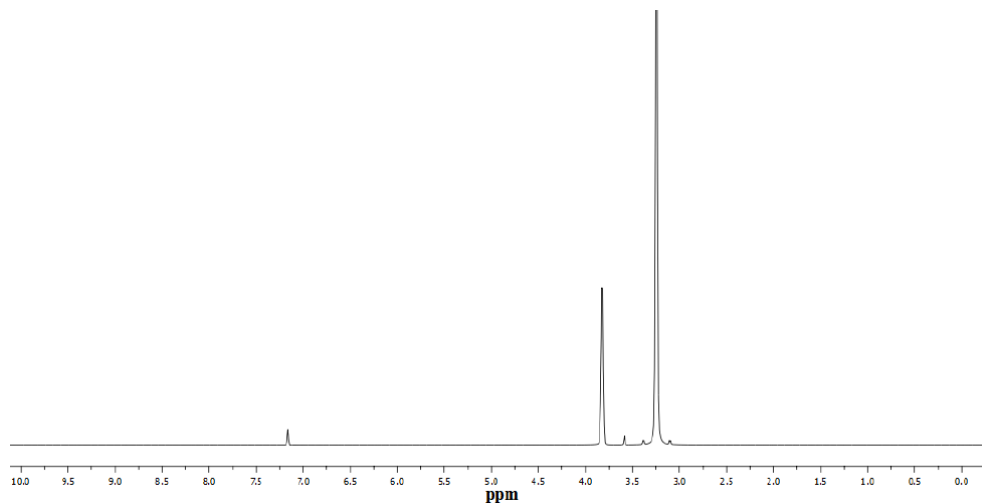


Figure 2.18. ^1H NMR spectrum of distilled methanol from the hydrolysis of CO_2 hydroboration products using 0.1 mol% **5** in benzene- d_6 .

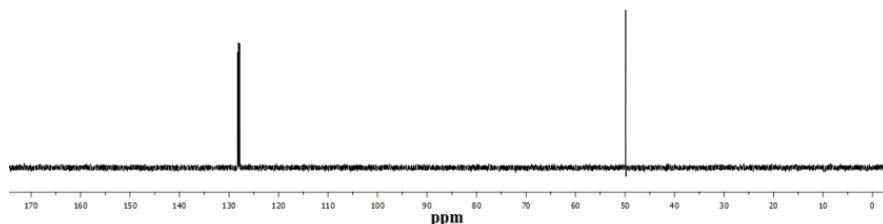


Figure 2.19. ^{13}C NMR spectrum of distilled methanol from the hydrolysis of CO_2 hydroboration products using 0.1 mol% **5** in benzene- d_6 .

2.4. Mechanism of Hydroboration^{1a}

Upon investigating the **5**-mediated hydroboration of CO_2 to methoxyborane under a range of conditions, a mechanistic pathway consistent with our experimental observations is proposed (Fig. 2.20). Starting from **5**, the insertion of CO_2 generates catalyst resting state **6**. Incoming HBPIn undergoes σ -bond metathesis with the Mo-O bond of **6** to regenerate **5** and yield the respective borylformate, HCO_2BPIn . The carbonyl functionality of this intermediate may competitively coordinate since it remains in solution, and its insertion into the Mo-H bond of **5** results in the respective alkoxide intermediate, $(\kappa^6\text{-}P,N,N,N,C,P\text{-Ph}_2\text{PPPrPDI})\text{Mo}(\text{OCH}_2\text{OBPin})$ (Fig. 2.20, bottom right). This complex has not been observed while monitoring CO_2 hydroboration in the presence of low HBPIn concentrations,

suggesting that σ -bond metathesis with HBPIn to generate $\text{H}_2\text{C}(\text{OBPin})_2$ is facile. The methoxyborane product, H_3COBPIn , may then be prepared by way of σ -bond metathesis between the Mo-H bond of **5** and a C-O bond of $\text{H}_2\text{C}(\text{OBPin})_2$. This pathway would also result in the formation of $(\kappa^6\text{-}P,N,N,N,C,P\text{-Ph}_2\text{PP}r\text{PDI})\text{Mo}(\text{OBPin})$ (Fig. 2.20, bottom left). This complex is also not observed and is proposed to react with HBPIn to liberate $\text{O}(\text{BPIn})_2$ and reform **5**.

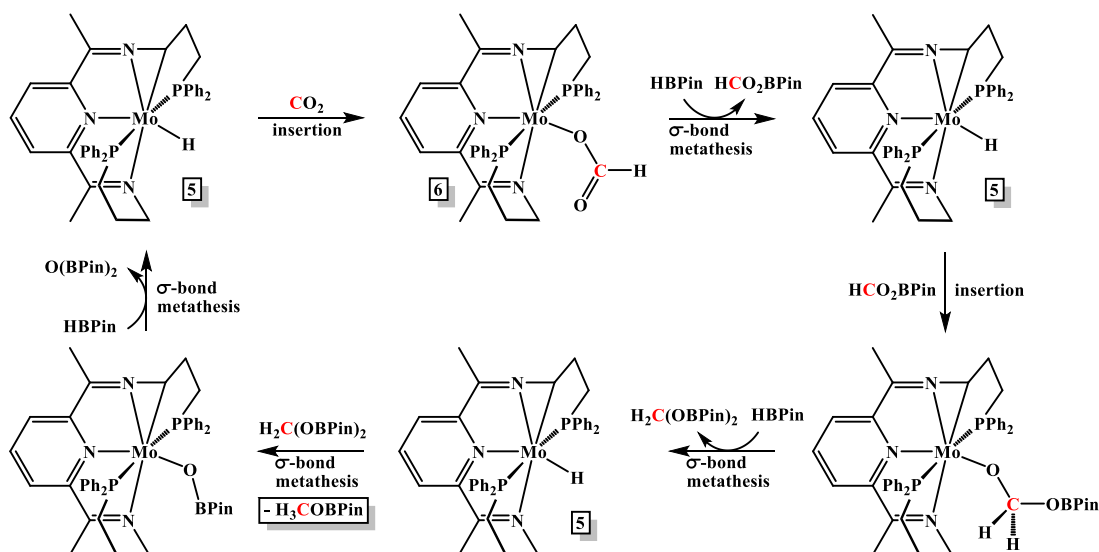


Figure 2.20. Proposed mechanism of **5**-mediated CO_2 hydroboration.

Although the mechanism presented in Fig. 2.20 is similar to those proposed for alkaline earth metal²⁴ and Ni ^{25,40} catalyzed CO_2 hydroboration, our observations suggest that H_3COBPIn is formed through a slightly different reaction pathway. Hall and co-workers suggested that heating $\text{H}_2\text{C}(\text{OBPin})_2$ to $60\text{ }^\circ\text{C}$ might result in its conversion to formaldehyde and $\text{O}(\text{BPIn})_2$ by way of 1,2-elimination.²⁴ Alternatively, computational efforts by Wang and Guan have indicated that β -boroxide elimination from $(\text{PCP})\text{Ni}(\text{OCH}_2\text{OBCat})$ is responsible for the formation of OCH_2 and $(\text{PCP})\text{Ni}(\text{OBCat})$.⁴⁰ It must also be mentioned that OCH_2 has been observed during Ru-catalyzed CO_2

hydroboration, allowing for the isolation of formalin.^{16a} The possibility that OCH₂ is formed during **5**-mediated CO₂ reduction cannot be discounted; however, spectroscopic evidence of its formation has not been observed under a range of conditions. When **5**-catalyzed hydroboration was conducted at low HBPIn concentration, a buildup of H₂C(OBPIn)₂ was noted (Fig. 2.12), suggesting that alkoxide intermediate (κ^6 -*P,N,N,N,C,P*-Ph²PPrPDI)Mo(OCH₂OBPIn) does not undergo β -boroxide elimination to give OCH₂ and (κ^6 -*P,N,N,N,C,P*-Ph²PPrPDI)Mo(OBPIn). Since accumulation of H₂C(OBPIn)₂ occurs at 90 °C, the breakdown of this intermediate to yield OCH₂ is either slow or not occurring under our reaction conditions. Rather, it is proposed that σ -bond metathesis between H₂C(OBPIn)₂ and the Mo-H bond of **5** to yield H₃COBPIn is slow in the presence of excess CO₂ since **6** is observed spectroscopically.

2.5. Catalyst Comparison and Intricacies^{1a}

To put the utility of **5** as a CO₂ to MeOH conversion catalyst into context, a comparison to previously reported hydroboration catalysts is warranted. Considering well-defined transition metal catalysts, (^tBuPOCOP)NiH²⁵ (Fig. 2.1, A) remains the most efficient for the conversion of CO₂ to H₃COBCat, exhibiting a methoxide formation TOF of 165 h⁻¹ at ambient temperature.²⁵ Comparatively, **5** was found to mediate slow methoxide formation at ambient temperature and heating to 90 °C was required to reach an appreciable methoxide formation TOF (41.3 h⁻¹). The methoxide formation TON of 330 achieved using 0.1 mol% **5** relative to borane is far greater than the TON of 9 achieved using the tris(aminophosphine)Ru hydroboration catalyst reported by Sgro and Stephan (Fig. 2.1, B),²⁶ however, the efficacy of the latter catalyst was not assayed at 90 °C. Finally, Sabo-

Etienne and co-workers have demonstrated that $(\text{Cy}_3\text{P})_2\text{RuH}_2(\text{H}_2)_2$ is capable of producing small quantities of H_3COBP in under mild conditions, albeit in a non-selective fashion.¹⁶

Although **5** is less efficient than the Ni hydroboration catalysts developed by Guan,²⁵ the chemistry described herein is rather unique. Surprisingly, Ph_2PPrPDI chelate C-H activation was found to result in the formation of an alkyl ligand that possesses a β -methylene group. The H atoms of this group do not participate in β -hydride elimination, even at temperatures up to 90 °C. We believe that the Mo center is simply unable to access these atoms due to the rigidity of the metallacyclopentane ring which they are a part of.⁴¹ It is also notable that the Mo-C bond of **5** is inert towards carbonyl insertion pathways and B-H σ -bond metathesis throughout the course CO_2 hydroboration. It must be stressed that the synthesis and reactivity of **5** are made possible by the diphenylphosphinopropyl arms of Ph_2PPrPDI . These substituents have enabled distinct reduction chemistry from that reported for aryl-substituted (PDI)Mo complexes,³⁴ and the high degree of modularity achievable for donor-substituted PDI chelates is expected to yield unprecedented structures and reactivity in future catalyst development studies.

2.6. Conclusion^{1a}

The synthesis, characterization, and catalytic properties of the first well-defined Mo catalyst for the reduction of CO_2 to MeOH have been established. The oxidative addition of I_2 to **2** was found to weaken metal-to-ligand backbonding, enabling CO dissociation and concomitant preparation of the respective diiodide complex, **4**. The reduction of **4** using K/Hg resulted in intramolecular C-H activation of the chelate to yield **5**. By single crystal X-ray diffraction, this precatalyst was found to possess a distorted pentagonal bipyramidal geometry due to the formation of a persistent metallacyclopentane. The addition of CO_2 to

5 revealed facile insertion to yield **6**, which possesses an η^1 -formate ligand. The utilization of **5** as a CO₂ reduction catalyst in the presence of HBPIn resulted in the selective formation of H₃COBPIn and O(BPin)₂ over a range of temperatures. This reaction was optimized such that 0.1 mol% **5** was employed in the absence of solvent at 90 °C, allowing a methoxide formation turnover frequency (TOF) of 41.6 h⁻¹ (B-H utilization TOF = 125 h⁻¹) and the isolation of MeOH following hydrolysis. Finally, the mechanism of **5**-mediated CO₂ hydroboration has been proposed to proceed through a series of insertion and σ -bond metathesis events which are enabled by chelate C-H activation.

2.7. Experimental Details^{1a}

2.7.1. General Considerations

All synthetic manipulations were performed in an MBraun glovebox under an atmosphere of purified nitrogen. Pentane, toluene, diethyl ether and tetrahydrofuran were purchased from Sigma Aldrich, dried using a Pure Process Technology (PPT) solvent system, and stored in the glove box over activated 4Å molecular sieves and metallic sodium (Alfa Aeser) before use. Benzene-*d*₆, acetone-*d*₆, and acetonitrile-*d*₃ were obtained from Cambridge Isotope Laboratories and dried over 4Å molecular sieves and metallic potassium (purchased from Sigma-Aldrich) prior to use. 2,6-Diacetylpyridine and Celite were purchased from TCI America and Acros, respectively. Mo(CO)₆ and 3-(diphenylphosphino)propylamine were purchased from Strem Chemicals and 4,4,5,5-tetramethyl-1,2,3-dioxaborolane (HPin) was used as received from Sigma-Aldrich. Carbon dioxide was used as received from Praxair. ^{Ph}2PPrPDI³¹ and (^{Ph}2PPrPDI)Mo(CO) (**2**)³⁰ were prepared according to literature procedures. Solution phase ¹H, ¹³C, ¹¹B, and ³¹P nuclear magnetic resonance (NMR) spectra were recorded at room temperature on either a 400

MHz or 500 MHz Varian NMR Spectrometer. All ^1H and ^{13}C NMR chemical shifts are reported relative to $\text{Si}(\text{CH}_3)_4$ using ^1H (residual) and ^{13}C chemical shifts of the solvent as secondary standards. ^{31}P and ^{11}B NMR data are reported relative to H_3PO_4 and 0.01 M boric acid in water respectively. IR spectroscopy was conducted on Bruker VERTEX 70 spectrometer with an MCT detector. Elemental analyses were performed at Robertson Microlit Laboratories Inc. (Ledgewood, NJ). UV-visible spectra were collected on an Agilent 8453 spectrophotometer.

2.7.2. X-ray Crystallography

Single crystals suitable for X-ray diffraction were coated with polyisobutylene oil in the glovebox and transferred to glass fiber with Apiezon N grease before mounting on the goniometer head of a Bruker APEX Diffractometer (Arizona State University) equipped with Mo $K\alpha$ radiation. A hemisphere routine was used for data collection and determination of the lattice constants. The space group was identified and the data was processed using the Bruker SAINT+ program and corrected for absorption using SADABS. The structures were solved using direct methods (SHELXS) completed by subsequent Fourier synthesis and refined by full-matrix, least-squares procedures on $[F^2]$ (SHELXL). Attempts to refine an inversion twin for **4** resulted in a twin fraction of 0.00166, which was therefore removed from the final refinement. The solid state structure of **5** features a disordered phenyl ring that has been modelled as two partially occupied rings with restrictions placed on thermal parameters and bond distances. For **5**, two large electron density peaks were located within 1.2 Å of Mo but were not modelled as H atoms due to their proximity to existing Mo-N bonds.

2.7.3. Synthesis of [(^{Ph}2PPrPDI)MoI(CO)]**[I]** (**3**)

In a nitrogen filled glove box, a 20 mL reaction vial was charged with 0.10 g (0.135 mmol) of **2** and 10 mL of toluene. To the pink solution, 0.036 g (0.135 mmol) of iodine dissolved in 5 mL of toluene was slowly added while stirring. A purple solid precipitated within 5 min of stirring. After 5 h, the reaction mixture was filtered through a sintered frit to remove the purple solid. After washing with toluene and ether and drying under vacuum, 0.127 g (0.128 mmol, 95%) of a purple solid identified as **3** was isolated. Anal. calcd. for C₄₀H₄₁N₃I₂OMoP₂·C₄H₈O: C, 49.68, H, 4.64, N, 3.95. Found: C, 49.81; H, 4.38; N, 4.30. ¹H NMR (acetone-*d*₆, 400 MHz): 8.46 (d, 8.0 Hz, 1H, *Py*), 8.33 (d, 8.0 Hz, 1H, *Py*), 8.01 (t, 8.0 Hz, 1H, *Py*), 7.77 (t, 6.8 Hz, 2H, *Ph*), 7.57 (m, 2H, *Ph*), 7.48 (t, 8.4 Hz, 2H, *Ph*), 7.36 (m, 2H, *Ph*), 7.20 (m, 6H, *Ph*), 6.99 (t, 8.0 Hz, 2H, *Ph*), 6.92 (t, 8.4 Hz, 2H, *Ph*), 6.31 (t, 8.8 Hz, 2H, *Ph*), 4.48 (d, 12.0 Hz, 1H, *CH*₂), 4.24 (d, 12.0 Hz, 1H, *CH*₂), 4.03 (t, 12.0 Hz, 1H, *CH*₂), 3.41 (t, 12.0 Hz, 1H, *CH*₂), 2.98 (m, 3H, *CH*₂), 2.64 (d, 2.4 Hz, 3H, *CH*₃), 2.57 (m, 1H, *CH*₂), 2.34 (m, 2H, *CH*₂), 2.31 (s, 3H, *CH*₃), 2.19 (m, 2H, *CH*₂). ¹³C NMR (acetone-*d*₆, 100.49 MHz): 238.4 (pseudo t, *J*_{CP} = 20.5 Hz, CO), 176.6 (*Py*), 175.8 (*Py*), 155.4 (C=N), 153.8 (C=N), 142.8 (d, *J*_{CP} = 161.0, *Ph*), 135.4 (d, *J*_{CP} = 15.0 Hz, *Ph*), 133.7 (d, *J*_{CP} = 13.8 Hz, *Ph*), 133.5 (d, *J*_{CP} = 10.8 Hz, *Ph*), 133.2 (*Py*), 132.3 (d, *J*_{CP} = 26.2 Hz, *Ph*), 130.8 (d, *J*_{CP} = 13.3 Hz, *Ph*), 130.5 (d, *J*_{CP} = 15.2 Hz, *Ph*), 130.5 (d, *J*_{CP} = 30.3 Hz, *Ph*), 129.1 (d, *J*_{CP} = 14.7 Hz, *Ph*), 128.2 (*Py*), 128.1 (d, *J*_{CP} = 7.9 Hz, *Ph*), 127.2 (*Py*), 61.4 (NCH₂), 59.3 (NCH₂), 28.2 (d, *J*_{CP} = 46.6 Hz, CH₂CH₂P), 26.9 (d, *J*_{CP} = 3.9 Hz, CH₂CH₂P), 26.1 (d, *J*_{CP} = 5.2 Hz, CH₂CH₂P), 25.9 (d, *J*_{CP} = 36.7 Hz, CH₂CH₂P), 17.3 (CH₃), 17.13 (t, *J*_{CP} = 4.0 Hz, CH₃). ³¹P NMR (acetone-*d*₆, 161.78 MHz): δ 39.6 (d, *J*_{PP} = 13.7 Hz), 39.2 (d, *J*_{PP} = 13.7 Hz). IR (KBr pellet): ν_{CO} = 1826 cm⁻¹.

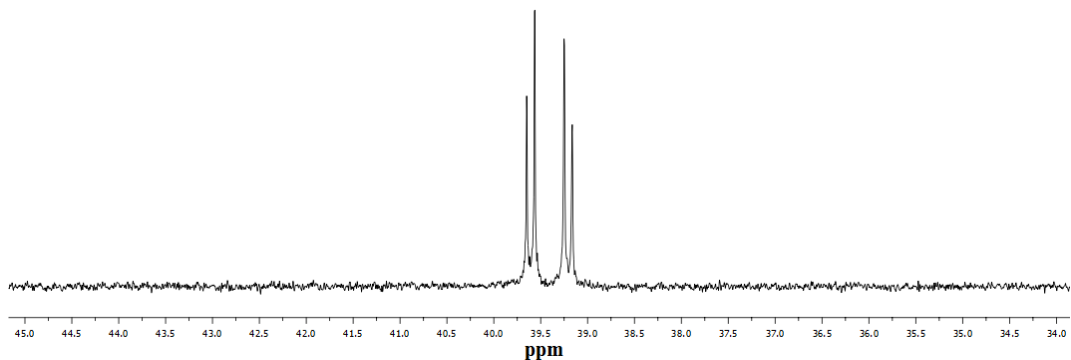


Figure 2.21. ^{31}P NMR spectrum of $[(\text{Ph}^2\text{PPrPDI})\text{MoI}(\text{CO})][\text{I}]$ (**3**) in acetone- d_6 .

2.7.4. Synthesis of $[(\text{Ph}^2\text{PPrPDI})\text{MoI}][\text{I}]$ (**4**)

In a nitrogen filled glove box, a 100 mL thick-walled reaction bomb was charged with 0.080 g (0.080 mmol) of **3** dissolved in 20 mL THF and a magnetic stir bar. The sealed bomb was frozen in liquid nitrogen and degassed on a Schlenk line before being refluxed at 100 °C in a preheated oil bath. A brownish-amber color solid began to precipitate within 2 h of stirring. After 12 h, the reaction mixture was allowed to cool at room temperature and was once again degassed on the Schlenk line. Once the liberated CO gas was removed, the reaction was allowed to reflux for 24 h at 100 °C to ensure reaction completion. After removing CO in the same way, the bomb was brought inside the glove box and an amber solid was isolated on top of a sintered frit. The product was washed with THF, ether, and pentane, and dried under vacuum to yield 0.053 g (0.055 mmol, 68%) of an amber solid identified as **4**. Single crystals suitable for X-ray diffraction were grown from a concentrated solution in acetone/THF at -35 °C. Anal. calcd. for $\text{C}_{39}\text{H}_{41}\text{N}_3\text{I}_2\text{MoP}_2$: C, 48.61, H, 4.29; N, 4.36; Found: C, 48.35; H, 4.13; N, 4.13. ^1H NMR (acetonitrile- d_3 , 400 MHz): δ 7.46 (t, 8.0 Hz, 1H, *Py*), 7.30 (m, 7H, *Ph*), 6.92 (t, 7.2 Hz, 2H, *Ph*), 6.72 (t, 7.6 Hz, 4H, *Ph*), 6.45 (d, 8.0 Hz, 2H, *Py*), 6.01 (d, 7.2 Hz, 3H, *Ph*), 5.55 (t, 14.4 Hz, 2H, *Ph*),

5.01 (d, 14.4 Hz, 2H, *Ph*), 3.98 (s, 6H, *CH*₃), 3.51 (m, 1H, *CH*₂), 3.28 (t, 7.2 Hz, 1H, *CH*₂), 3.14 (m, 2H, *CH*₂), 2.93 (m, 2H, *CH*₂), 2.81 (m, 2H, *CH*₂), 2.62 (m, 2H, *CH*₂), 1.88 (m, 2H, *CH*₂). ¹³C NMR (acetonitrile-*d*₃, 100.49 MHz): δ 156.9 (*C=N*), 138.4 (*Py*), 133.6 (*Ph*), 131.4 (*Py*), 130.3 (*Ph*), 129.6 (*Ph*), 128.7 (*Py*), 127.2 (*Ph*), 118.8 (*Py*), 57.2 (*NCH*₂*CH*₂), 28.1 (*PCH*₂*CH*₂), 26.4 (*PCH*₂*CH*₂), 15.4 (*CH*₃). ³¹P NMR (acetonitrile-*d*₃, 161.78 MHz): δ 6.18 (s).

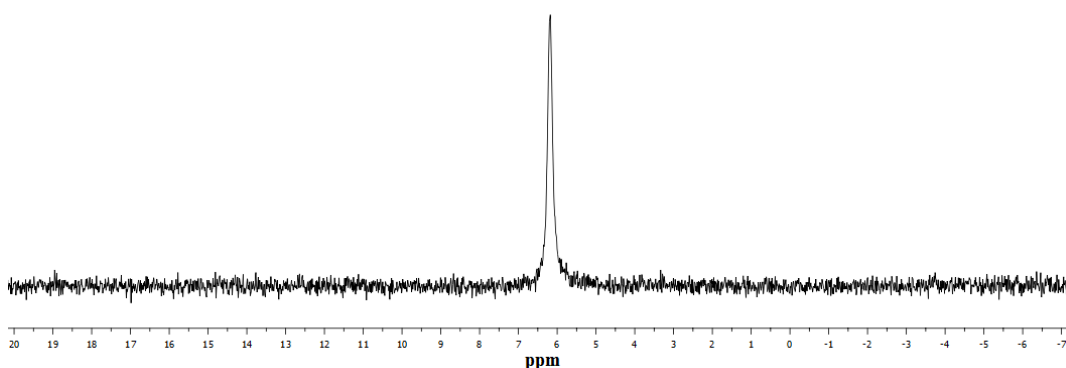


Figure 2.22. ³¹P NMR spectrum of [(^{Ph2PPr}PDI)MoI][I] (**4**) in acetonitrile-*d*₃.

2.7.5. Synthesis of (κ^6 -*P,N,N,N,C,P*-^{Ph2PPr}PDI)MoH (**5**)

In a nitrogen filled glove box, a 20 mL reaction vial was charged with 4.2 g of mercury and 3 mL of THF. To it, 0.016 g of freshly cut metallic potassium was added and stirred for 30 min to form clear potassium amalgam solution. To the solution, 0.078 g (0.081 mmol) of **4** in 10 mL of THF was slowly added and the mixture was allowed to stir at ambient temperature for 3 d. The resulting green solution was filtered through Celite and the solvent was removed *in vacuo* to yield a green solid. After washing with pentane and drying, 0.051 g (87%) of a dark green solid identified as **5** was isolated. Single crystals suitable for X-ray diffraction were grown from a concentrated toluene solution at -35 °C. Anal. calcd. for C₃₉H₄₁N₃MoP₂: Calcd. C, 66.00%, H, 5.82%, N, 5.92%; Found: C,

65.88%, H, 5.57%, N, 5.64%. ^1H NMR (benzene- d_6 , 400 MHz): δ 7.83 (t, 8.4 Hz, 2H, *Ar*), 7.56 (m, 3H, *Ar*), 7.49 (t, 8.0 Hz, 2H, *Ar*), 7.07 (m, 3H, *Ar*), 7.02 (m, 1H, *Ar*), 6.62 (m, 1H, *Ar*), 6.51 (m, 5H, *Ar*), 5.60 (t, 8.4 Hz, 2H, *Ar*), 5.49 (m, 2H, *Ar*), 5.44 (t, 11.9 Hz, 1H, *NCH}_2*), 4.85 (d, 10.8 Hz, 1H, *NCH}_2*), 4.77 (b, 1H, *HCMo*), 2.88 (s, 3H, CH_3), 2.82 (m, 1H, CH_2), 2.62 (m, 2H, CH_2), 2.50 (s, 3H, CH_3), 2.27 (m, 1H, CH_2), 2.06 (m, 2H, CH_2), 1.39 (m, 1H, CH_2), 1.18 (m, 1H, CH_2), Mo–H peak not located. ^{13}C NMR (benzene- d_6 , 125.00 MHz): δ 147.3 (C=N), 145.5 (C=N), 139.3 (*Py*), 138.7 (d, $J_{\text{CP}} = 57$ Hz, *Ph*), 134.3 (d, $J_{\text{CP}} = 33.53$ Hz, *Ph*), 133.96 (d, $J_{\text{CP}} = 34$ Hz, *Ph*), 132.7 (d, $J_{\text{CP}} = 2.5$ Hz, *Ph*), 132.6 (d, $J_{\text{CP}} = 9.2$ Hz, *Ph*), 132.2 (*Py*), 131.9 (d, $J_{\text{CP}} = 16.2$ Hz, *Ph*), 131.0 (d, $J_{\text{CP}} = 19.9$ Hz, *Ph*), 129.0 (d, $J_{\text{CP}} = 30.6$ Hz, *Ph*), 117.1 (*Py*), 106.5 (*Py*), 104.2 (*Py*), 57.8 (*NCH}_2*), 54.9 (d, $J_{\text{CP}} = 7.5$ Hz, *NCHMo*), 33.8 (d, $J_{\text{CP}} = 47.9$ Hz, $\text{CH}_2\text{CH}_2\text{P}$), 31.4 (d, $J_{\text{CP}} = 33.4$ Hz, CH_2), 30.5 (d, $J_{\text{CP}} = 55.7$ Hz, CH_2), 29.6 (d, $J_{\text{CP}} = 42.1$ Hz, CH_2), 17.1 (CH_3), 13.2 (CH_3). ^{31}P NMR (benzene- d_6 , 161.78 MHz): 57.9 (d, 97.2 Hz, PPh_2), 46.9 (d, 97.2 Hz, PPh_2).

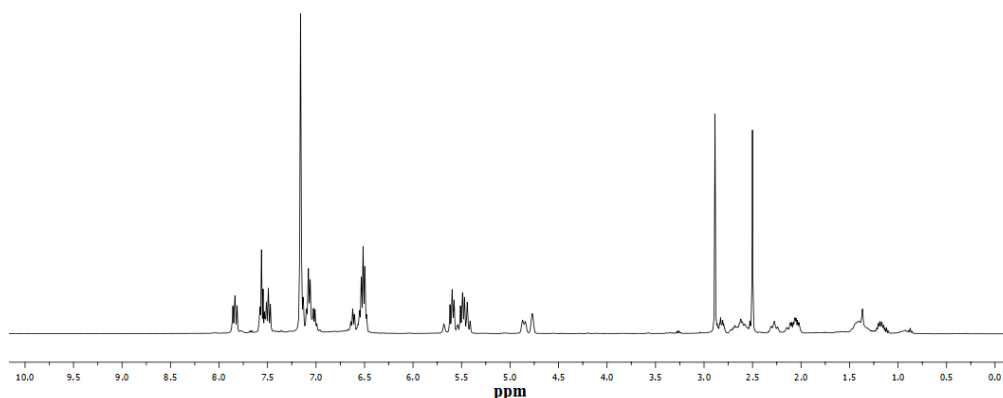


Figure 2.23. ^1H NMR spectrum of (κ^6 -*P,N,N,N,C,P*- Ph_2PPrPDI)MoH (**5**) in benzene- d_6 .

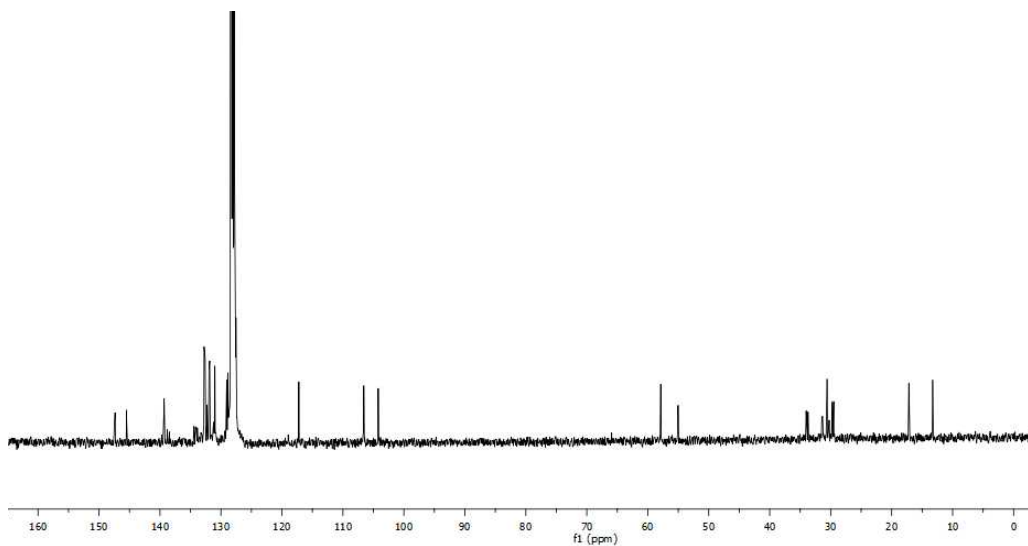


Figure 2.24. ^{13}C NMR spectrum of $(\kappa^6\text{-}P,N,N,N,C,P\text{-Ph}_2\text{PPrPDI})\text{MoH}$ (**5**) in benzene- d_6 .

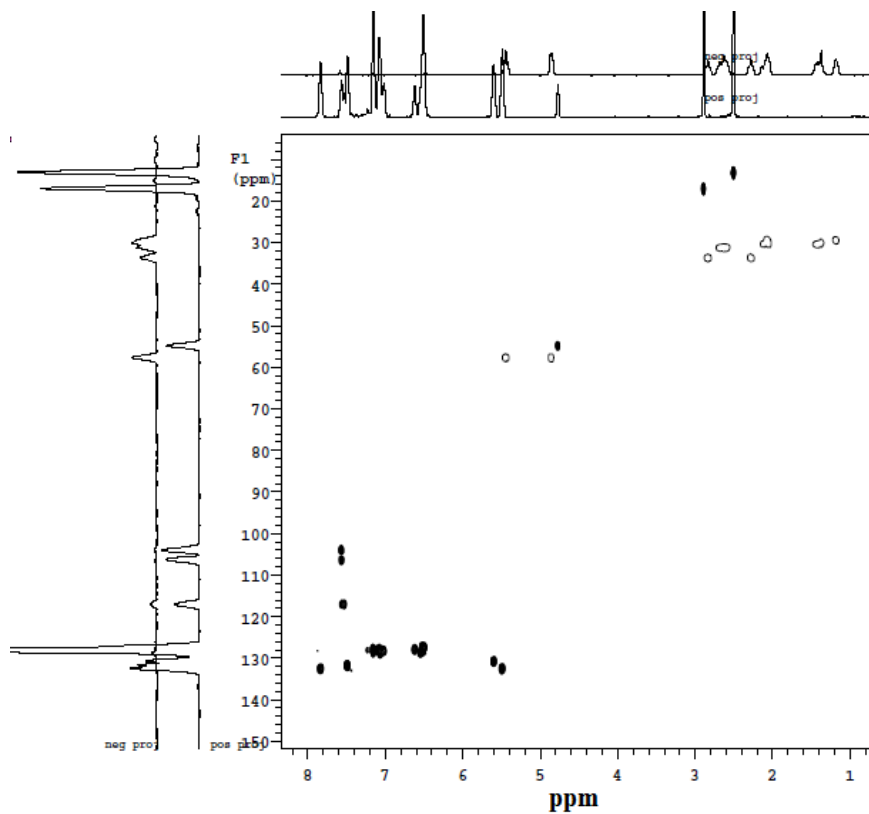


Figure 2.25. gHSQCAD NMR spectrum of $(\kappa^6\text{-}P,N,N,N,C,P\text{-Ph}_2\text{PPrPDI})\text{MoH}$ (**5**) in benzene- d_6 .

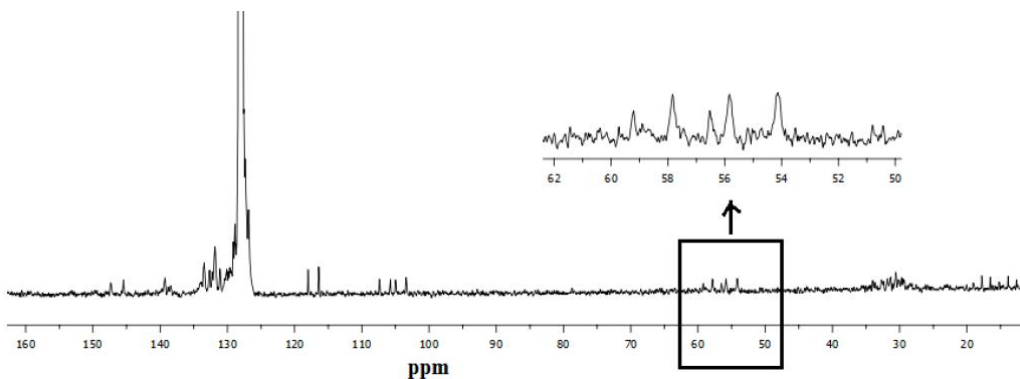


Figure 2.26. ^1H -coupled ^{13}C NMR spectrum of $(\kappa^6\text{-P,N,N,N,C,P-Ph}_2\text{PPrPDI})\text{MoH}$ (**5**) in benzene- d_6 .

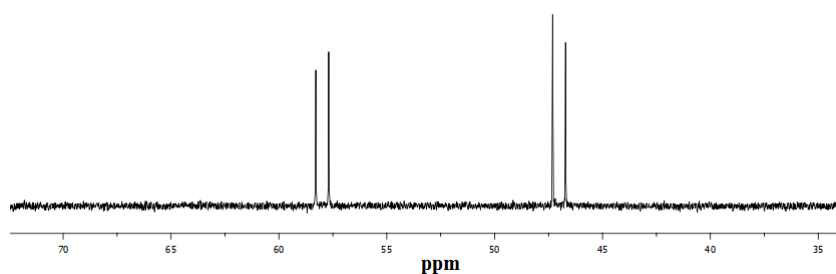


Figure 2.27. ^{31}P NMR spectrum of $(\kappa^6\text{-P,N,N,N,C,P-Ph}_2\text{PPrPDI})\text{MoH}$ (**5**) in benzene- d_6 .

2.7.6. Synthesis of $(\kappa^6\text{-P,N,N,N,C,P-Ph}_2\text{PPrPDI})\text{Mo}(\text{OCOH})$ (**6**)

In a nitrogen filled glove box, a J. Young NMR tube was charged with 0.012 g (0.014 mmol) of **5** dissolved in 0.7 mL of C_6D_6 . The tube was frozen at 0°C , degassed, and 0.2 atm of CO_2 was added. Within 10 min, formation of a new compound identified as **6** was observed by multinuclear NMR spectroscopy. Upon removal of excess CO_2 and solvent, 0.009 g (0.012 mmol, 85%) of a green solid identified as **6** was isolated. Anal. calcd. for $\text{C}_{40}\text{H}_{41}\text{N}_3\text{MoO}_2\text{P}_2$: Calcd. C, 63.74%; H, 5.48%; N, 5.57%. Found: C, 63.51%, H, 5.42%, N, 5.28%. ^1H NMR (benzene- d_6 , 400 MHz): 9.14 (s, 1H, CHO), 7.25 (m, 4H, Ar), 7.12 (m, 5H, Ar), 7.02 (t, 7.2 Hz, 3H, Ar), 6.90 (t, 7.6 Hz, 1H, Ar), 6.59 (t, 7.6 Hz, 2H, Ar), 6.43 (t, 7.6 Hz, 4H, Ar), 6.26 (t, 12.0 Hz, 1H, NCH_2), 5.62 (s, 1H, NCHMo), 5.56 (t, 7.8 Hz, 2H, Ar), 5.25 (t, 8.4 Hz, 2H, Ar), 4.55 (d, 12.0 Hz, 1H, NCH_2), 3.34 (m, 2H, CH_2), 2.80 (m,

1H, CH₂), 2.73 (s, 3H, CH₃), 2.47 (s, 3H, CH₃), 2.04 (m, 1H, CH₂), 1.87 (m, 1H, CH₂), 1.76 (t, 14.4 Hz, 1H, CH₂), 1.39 (m, 3H, CH₂), 0.74 (m, 1H, CH₂). ¹³C NMR (benzene-*d*₆, 100.49 MHz): 169.7 (MoOCOH), 148.1 (C=N), 148.1 (C=N), 144.6 (*Ar*), 132.8 (d, *J*_{CP} = 17.8 Hz, *Ar*), 132.2 (d, *J*_{CP} = 20.0 Hz, *Ar*), 131.3 (d, *J*_{CP} = 17.2 Hz, *Ar*), 130.9 (d, *J*_{CP} = 18.9 Hz, *Ar*), 129.4 (*Ar*), 128.6 (d, *J*_{CP} = 7.6 Hz, *Ar*), 128.5 (d, *J*_{CP} = 10.0 Hz, *Ar*), 127.6 (d, *J*_{CP} = 10.0 Hz, *Ar*), 117.5 (*Ar*), 106.8 (*Ar*), 106.1 (*Ar*), 57.4 (NHCMo), 50.2 (NCH₂), 30.5 (d, *J*_{CP} = 14.9 Hz, CH₂), 28.8 (CH₂), 23.9 (d, *J*_{CP} = 30.6 Hz, CH₂), 20.9 (d, *J*_{CP} = 34.2 Hz, CH₂), 16.6 (CH₃), 13.5 (CH₃). ³¹P NMR (benzene-*d*₆, 161.78 MHz): 43.80 (d, 186.2 Hz, PPh₂), 28.10 (d, 186.2 Hz, PPh₂). IR (KBr pellet): ν_{COH} = 1625 cm⁻¹.

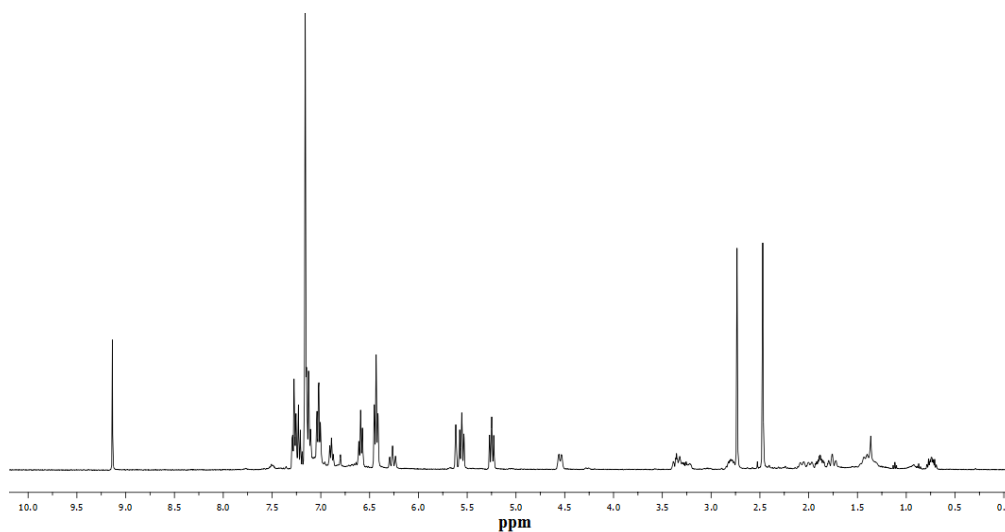


Figure 2.28. ¹H NMR spectrum of (κ⁶-*P,N,N,N,C,P*-Ph₂PPrPDI)Mo(OCOH) (**6**) in benzene-*d*₆.

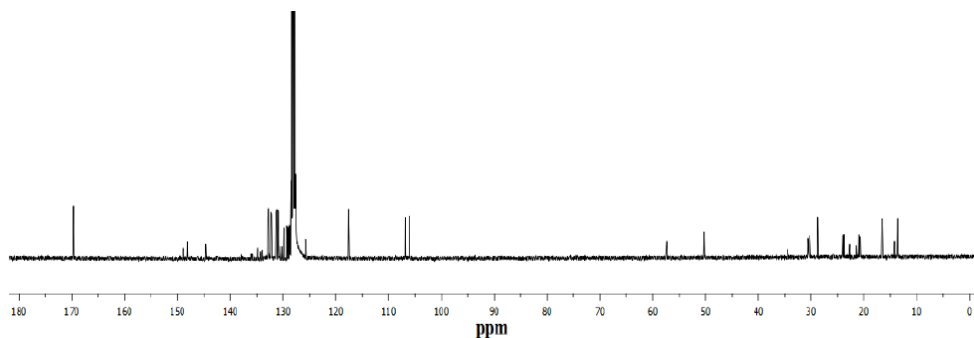


Figure 2.29. ^{13}C NMR spectrum of $(\kappa^6\text{-}P,N,N,N,C,P\text{-Ph}_2\text{PPrPDI})\text{Mo}(\text{OCOH})$ (**6**) in benzene- d_6 .

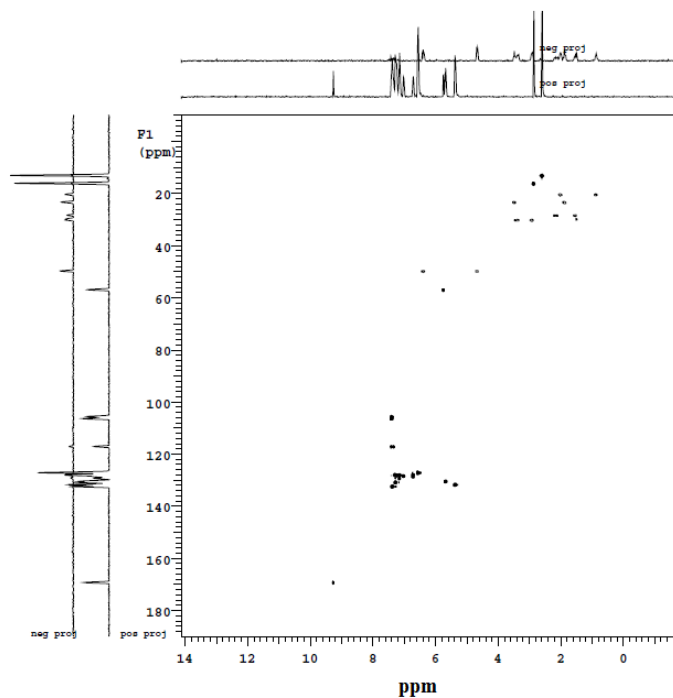


Figure 2.30. gHSQCAD NMR spectrum of $(\kappa^6\text{-}P,N,N,N,C,P\text{-Ph}_2\text{PPrPDI})\text{Mo}(\text{OCOH})$ (**6**) in benzene- d_6 .

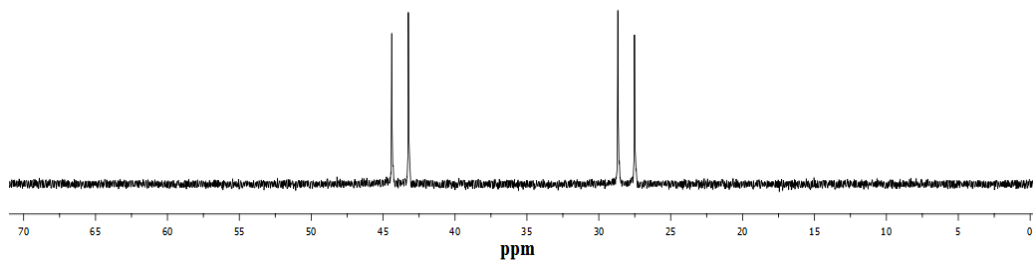


Figure 2.31. ^{31}P NMR spectrum of $(\kappa^6\text{-}P,N,N,N,C,P\text{-Ph}_2\text{PPrPDI})\text{Mo}(\text{OCOH})$ (**6**) in benzene- d_6 .

2.7.7. Hydroboration of CO₂ using 5 mol% **5**

In the glovebox, a 20 mL scintillation vial containing 0.014 mmol of **5** was charged with pinacolborane (0.28 mmol) in 0.7 mL of benzene-*d*₆. The mixture was transferred into a J. Young NMR tube and sealed under nitrogen. After degassing the tube, an atmosphere of CO₂ gas was purged into the frozen solution at 0 °C, and the tube was placed in an oil bath preheated to 60 °C. The reaction was monitored over time using multinuclear NMR spectroscopy.

2.7.8. Hydroboration of CO₂ using 1 mol% **5**

In the glovebox, a 20 mL scintillation vial containing 0.0011 mmol of **5** was charged with pinacolborane (0.11 mmol) in 0.7 mL of benzene-*d*₆. The mixture was transferred into a J. Young NMR tube and sealed under nitrogen. After degassing the tube, an atmosphere of CO₂ gas was purged into the frozen solution at -70 °C, and the tube was placed in an oil bath preheated at 90 °C for 5 h. The reaction was monitored over time using multinuclear NMR spectroscopy.

2.7.9. Hydroboration of CO₂ using 0.1 mol% **5**

In the glovebox, a 20 mL scintillation vial containing 0.0035 mmol of **5** was charged with pinacolborane (3.5 mmol) in 0.7 mL of benzene-*d*₆. The mixture was transferred into a 100 mL reaction bomb, and was sealed under nitrogen. After degassing the bomb, an atmosphere of CO₂ gas added at -70 °C. Upon thawing, the tube was placed in a 90 °C oil bath for 8 h. A few drops of the reaction mixture were dissolved in C₆D₆ and complete consumption of starting borane was observed by ¹H, ¹³C and ¹¹B NMR spectroscopy. After recombining fractions and removing the NMR solvent *in vacuo*, the borylated products were hydrolyzed with water (2 mL) while stirring at ambient temperature for 24 h. The

volatile components were separated by short path fractional distillation and methanol was recovered (58% isolated yield, relative to HBPin).

2.7.10. Control Reaction between Pinacolborane and CO₂

In the glovebox, a 20 mL scintillation vial was charged with 0.016 mL of pinacolborane and 0.7 mL of benzene-*d*₆. The mixture was transferred into a J. Young NMR tube and sealed under nitrogen. After degassing the tube, an atmosphere of CO₂ gas was added at -70 °C, and the tube was placed in an oil bath preheated at 90 °C for 4 h. The reaction was monitored using ¹H NMR spectroscopy and transformation of the reactants was not observed.

2.7.11. Control Reaction Employing ^{Ph}2PPrPDI as a Catalyst

In the glovebox, a 20 mL scintillation vial containing 0.0045 mmol of ^{Ph}2PPrPDI was charged with pinacolborane (0.45 mmol) in 0.7 mL of benzene-*d*₆. The mixture was transferred into a J. Young NMR tube, and was sealed under nitrogen. After degassing the tube, an atmosphere of CO₂ gas was purged into the frozen solution at -70 °C, and the tube was allowed to heat in an oil bath preheated at 90 °C for 4 h. The reaction was monitored using multinuclear NMR spectroscopy. No trace of methoxide was observed; however, 3% of pinacolboryl formate was identified by ¹H and ¹¹B NMR spectroscopy (Fig. 2.15 and 2.16).

2.8. References

- (1) (a) Pal, R.; Groy, T. L.; Trovitch, R. J. *Inorganic Chemistry* **2015**, *54*, 7506-7515. (b) van Aardenne, J. A.; Dentener, F. J.; Oliver, J. G. J.; Goldewijk, M. K.; Lelieveld, J. *Global Biogeochem. Cy.* **2001**, *15*, 909-928. (c) Sims, R. E. H.; Schock, R. N.; Adegbululgbé, A.; Fenhann, J.; Konstantinaviciute, I.; Moomaw, W.; Nimir, H. B.; Schlamadinger, B.; Torres-Martínez, J.; Turner, C.; Uchiyama, Y.; Vuori, S. J. V.; Wamukonya, N.; Zhang, X. 2007: Energy supply. In *Climate Change 2007: Mitigation. Contribution of Working Group III to the Fourth Assessment Report of the Intergovernmental Panel on Climate Change*, Edited by Metz, B.; Davidson, O. R.; Bosch, P. R.; Dave, R.; Meyer, L. A., Cambridge University Press, Cambridge, United Kingdom and New York, NY, USA.
- (2) (a) Keeling, C. D.; Whorf, T. P.; Wahlen, M.; van der Plicht, J. *Nature* **1995**, *375*, 666-670. (b) Forster, P.; Ramaswamy, V.; Artaxo, P.; Berntsen, T.; Betts, R.; Fahey, D. W.; Haywood, J.; Lean, J.; Lowe, D. C.; Myhre, G.; Nganga, J.; Prinn, R.; Raga, G.; Schulz, M.; Van Dorland, R. 2007: Changes in Atmospheric Constituents and in Radiative Forcing. In: *Climate Change 2007: The Physical Science Basis. Contribution of Working Group I to the Fourth Assessment Report of the Intergovernmental Panel on Climate Change*, Edited by Solomon, S.; Qin, D.; Manning, M.; Chen, Z.; Marquis, M.; Averyt, K. B.; Tignor, M.; Miller, H. L., Cambridge University Press, Cambridge, United Kingdom and New York, NY, USA.
- (3) (a) Raupach, M. R.; Marland, G.; Ciais, P.; Le Quéré, C.; Canadell, J. G.; Klepper, G.; Field, C. B. *Proc. Natl. Acad. Sci. USA* **2007**, *104*, 10288-10293. (b) IPCC, 2007: Summary for Policymakers. In: *Climate Change 2007: Mitigation. Contribution of Working Group III to the Fourth Assessment Report of the Intergovernmental Panel on Climate Change*, Edited by Metz, B.; Davidson, O. R.; Bosch, P. R.; Dave, R.; Meyer, L. A., Cambridge University Press, Cambridge, United Kingdom and New York, NY, USA.
- (4) Meinshausen, M.; Meinshausen, N.; Hare, W.; Raper, S. C. B.; Frieler, K.; Knutti, R.; Frame, D. J.; Allen, M. R. *Nature* **2009**, *458*, 1158-1162.
- (5) Solomon, S.; Plattner, G.-P.; Knutti, R.; Friedlingstein, P. *Proc. Natl. Acad. Sci. USA* **2009**, *106*, 1704-1709.
- (6) (a) Caldeira, K.; Wickett, M. E. *Nature* **2003**, *425*, 365. (b) Bindoff, N. L.; Willebrand, J.; Artale, V.; Cazenave, A.; Gregory, J.; Gulev, S.; Hanawa, K.; Le Quéré, C.; Levitus, S.; Nojiri, Y.; Shum, C. K.; Talley, L. D.; Unnikrishnan, A. 2007: Observations: Oceanic Climate Change and Sea Level. In: *Climate Change 2007: The Physical Science Basis. Contribution of Working Group I to the Fourth Assessment Report of the Intergovernmental Panel on Climate Change*, Edited by Solomon, S.; Qin, D.; Manning, M.; Chen, Z.; Marquis, M.; Averyt, K. B.; Tignor, M.; Miller, H. L., Cambridge University Press, Cambridge, United Kingdom and New York, NY, USA.
- (7) Rogelj, J.; McCollum, D. L.; Reisinger, A.; Meinshausen, M.; Riahi, K. *Nature* **2013**, *493*, 79-83.

(8) For CO₂ capture and geologic storage see: (a) Markewitz, P.; Kuckshinrichs, W.; Leitner, W.; Linssen, J. Zapp, P.; Bongartz, R.; Schreiber, A.; Müller, T. E. *Energy Environ. Sci.* **2012**, *5*, 7281-7305. (b) Figueroa, J. D.; Fout, T.; Plasynski, S.; McIlvried, H.; Srivastava, R. D. *Int. J. Greenh. Gas Con.* **2008**, *2*, 9-20. (c) Davison, J. *Energy* **2007**, *32*, 1163-1176. (d) Steeneveldt, R.; Berger, B.; Torp, T. A. *Chem. Eng. Res. Des.* **2006**, *84*, 739-763.

(9) For general CO₂ fixation pathways see: (a) Martin, R.; Kleij, A. W. *ChemSusChem*. **2011**, *4*, 1259-1263. (b) Riduan, S. N.; Zhang, Y. *Dalton Trans.* **2010**, *39*, 3347-3357. (c) Yu, K. M. K.; Curcic, I.; Gabriel, J.; Tsang, S. C. E. *ChemSusChem* **2008**, *1*, 893-899. (d) Sakakura, T.; Choi, J.-C.; Yasuda, H. *Chem. Rev.* **2007**, *107*, 2365-2387.

(10) For examples of C-H carboxylation see: (a) Boogaerts, I. I. F.; Nolan, S. P. *Chem. Commun.* **2011**, *47*, 3021-3024. (b) Boogaerts, I. I. F.; Nolan, S. P. *J. Am. Chem. Soc.* **2010**, *132*, 8858-8859. (c) Boogaerts, I. I. F.; Fortman, G. C.; Furst, M. R. L.; Cazin, C. S. J.; Nolan, S. P. *Angew. Chem. Int. Ed.* **2010**, *49*, 8674-8677. (d) Zhang, L.; Cheng, J.; Ohishi, Z.; Hou, Z. *Angew. Chem. Int. Ed.* **2010**, *49*, 8670-8673. (e) Vechorkin, O.; Hirt, N.; Hu, X. *Org. Lett.* **2010**, *12*, 3567-3569.

(11) For polycarbonates from CO₂ see: (a) Kember, M. R.; Buchard, A.; Williams, C. K. *Chem. Commun.* **2011**, *47*, 141-163. (b) Sakakura, T.; Kohno, K. *Chem. Commun.* **2009**, 1312-1330. (c) Darensbourg, D. J.; *Chem. Rev.* **2007**, *107*, 2388-2410. (d) Coates, G. W.; Moore, D. R. *Angew. Chem. Int. Ed.* **2004**, *43*, 6618-6639.

(12) Mikkelsen, M.; Jørgensen, M.; Krebs, F. C. *Energy Environ. Sci.* **2010**, *3*, 43-81.

(13) Aresta, M. In *Activation of Small Molecules*, Edited by Tolman, W. B., Wiley-VCH, Weinheim, 2006, pp 1-42.

(14) For electrocatalytic CO₂ reduction see: (a) Windle, C. D.; Peruta, R. N. *Coord. Chem. Rev.* **2012**, *256*, 2562-2570, and references therein. (b) Benson, E. E.; Kubiak, C. P.; Sathrum, A. J.; Smieja, J. M. *Chem. Soc. Rev.* **2009**, *38*, 89-99. (c) Morris, A. J.; Meyer, G. J.; Fujita, E. *Acc. Chem. Res.* **2009**, *42*, 1983-1994.

(15) (a) Drake, J. L.; Manna, C. M.; Byers, J. A. *Organometallics* **2013**, *32*, 6891-6894. (b) Jeletic, M. S.; Mock, M. T.; Appel, A. M.; Linehan, J. C. *J. Am. Chem. Soc.* **2013**, *135*, 11533-11536. (c) Ono, T.; Planas, N.; Miró, P.; Ertem, M. Z.; Escudero-Adán, E. C.; Benet-Buchholtz, J.; Gagliardi, L.; Cramer, C. J.; Llobet, A. *ChemCatChem* **2013**, *5*, 3897-3903. (d) Jiang, Y.; Blacque, O.; Fox, T.; Berke, H. *J. Am. Chem. Soc.* **2013**, *135*, 7751-7760. (e) Ziebart, C.; Federsel, C.; Anbarasan, P.; Jackstell, R.; Baumann, W.; Spannenberg, A.; Beller, M. *J. Am. Chem. Soc.* **2012**, *134*, 20701-20704. (f) Langer, R.; Diskin-Posner, Y.; Leitius, G.; Shimon, L. J. W.; Ben-David, Y.; Milstein, D. *Angew. Chem. Int. Ed.* **2011**, *50*, 9948-9952. (g) Federsel, C.; Boddien, A.; Jackstell, R.; Jennerjahn, R.; Dyson, P. J.; Scopelliti, R.; Laurenczy, G.; Beller, M.; *Angew. Chem. Int. Ed.* **2010**, *49*, 977-9780. (h) Tanaka, R.; Yamashita, M.; Nozaki, K. *J. Am. Chem. Soc.* **2009**, *131*, 14168-14169. (i) Himeda, Y.; Onozawa-Komatsuzaki, N.; Sugihara, H.; Kasuga, K.

Organometallics **2007**, *26*, 702-712. (j) Munshi, P.; Main, A. D.; Linehan, J. C.; Tai, C.-C.; Jessop, P. G. *J. Am. Chem. Soc.* **2002**, *124*, 7963-7971. (k) Jessop, P. G.; Ikariya, T.; Noyori, R. *Nature* **1994**, *368*, 231-233. (l) Gassner, F.; Leitner, W. *J. Chem. Soc., Chem. Commun.* **1993**, 1465-1466.

(16) (a) Bontemps, S.; Vendier, L.; Sabo-Etienne, S. *J. Am. Chem. Soc.* **2014**, *136*, 4419-4425. (b) LeBlanc, F. A.; Piers, W. E.; Parvez, M. *Angew. Chem. Int. Ed.* **2014**, *53*, 789-792. (c) Bontemps, S.; Sabo-Etienne, S. *Angew. Chem. Int. Ed.* **2013**, *52*, 10253-10255. (d) Berkefeld, A.; Piers, W. E.; Parvez, M.; Castro, L.; Maron, L.; Eisenstein, O. *Chem. Sci.* **2013**, *4*, 2152-2162. (e) Bontemps, S.; Vendier, L.; Sabo-Etienne, S. *Angew. Chem. Int. Ed.* **2012**, *51*, 1671-1674.

(17) (a) Tominaga, K.; Sasaki, Y.; Watanabe, T.; Saito, M. *Bull. Chem. Soc. Jpn.* **1995**, *68*, 2837-2842. (b) Tominaga, K.; Sasaki, Y.; Kawai, M.; Watanabe, T.; Saito, M. *J. Chem. Soc., Chem. Commun.* **1993**, 629-631.

(18) (a) Rezayee, N. M.; Huff, C. A.; Sanford, M. S. *J. Am. Chem. Soc.* **2015**, *137*, 1028-1031. (b) Wesselbaum, S. Moha, V.; Meuresch, M.; Broninski, S.; Thenert, K. M.; Kothe, J.; von Stein, T.; Englert, U.; Hölscher, M.; Klankermayer, J.; Leitner, W. *Chem. Sci.* **2015**, *6*, 693-704. (c) Wesselbaum, S.; von Stein, T.; Klankermayer, J.; Leitner, W. *Angew. Chem. Int. Ed.* **2012**, *51*, 7499-7502. (d) Huff, C. A.; Sanford, M. S. *J. Am. Chem. Soc.* **2011**, *133*, 18122-18125.

(19) Eisenschmid, T. C.; Eisenberg, R. *Organometallics* **1989**, *8*, 1822-1824.

(20) Metsänen, T. T.; Oestreich, M. *Organometallics* **2015**, *34*, 543-546.

(21) Riduan, S. N.; Zhang, Y.; Ying, J. Y. *Angew. Chem.* **2009**, *121*, 3372-3375.

(22) (a) Courtemanche, M.-A.; Légaré, M.-A.; Maron, L.; Fontaine, F.-G. *J. Am. Chem. Soc.* **2013**, *135*, 9326-9329. (b) Wang, T.; Stephan, D. W. *Chem. Eur. J.* **2014**, *20*, 3036-3039. (c) Gomes, C. D. N.; Blondiaux, E.; Thuéry, P.; Cantat, T. *Chem. Eur. J.* **2014**, *20*, 7098-7106. (d) Wang, T.; Stephan, D. W. *Chem. Commun.*, **2014**, *50*, 7007-7010.

(23) Fujiwara, K.; Yasuda, S.; Mizuta, T. *Organometallics* **2014**, *33*, 6692-6695.

(24) Anker, M. D.; Arrowsmith, M.; Bellham, P.; Hill, M. S.; Kociok-Köhn, G.; Liptrot, D. J.; Mahon, M. F.; Weetman, C. *Chem. Sci.* **2014**, *5*, 2826-2830.

(25) (a) Chakraborty, S.; Zhang, J.; Krause, J. A.; Guan, H. *J. Am. Chem. Soc.* **2010**, *132*, 8872-8873. (b) Chakraborty, S.; Patel, Y. J.; Krause, J. A.; Guan, H. *Polyhedron* **2012**, *32*, 30-34. (c) Chakraborty, S.; Zhang, J.; Patel, Y. J.; Krause, J. A.; Guan, H. *Inorg. Chem.* **2013**, *52*, 37-47.

(26) Sgro, M. J.; Stephan, D. W. *Angew. Chem. Int. Ed.* **2012**, *51*, 11343-11345.

(27) (a) Wehmschulte, R. J.; Saleh, M.; Powell, D. R. *Organometallics* **2013**, *32*, 6812-6819. (b) Mitton, S. J.; Turculet, L. *Chem. Eur. J.* **2012**, *18*, 15258-15262. (c) Park, S.; Bézier, D.; Brookhart, M. *J. Am. Chem. Soc.* **2012**, *134*, 11404-11407. (d) Khandelwal, M.; Wehmschulte, R. J. *Angew. Chem. Int. Ed.* **2012**, *51*, 7323-7326. (e) Berkefeld, A.; Piers, W. E.; Parvez, M. *J. Am. Chem. Soc.* **2010**, *132*, 10660-10661. (f) Matsuo, T.; Kawaguchi, H. *J. Am. Chem. Soc.* **2006**, *128*, 12362-12363.

(28) Haynes, W. M. *CRC Handbook of Chemistry and Physics: A Ready-reference Book of Chemical and Physical Data*, 94th ed.; Taylor & Francis, Boca Raton, FL, 2013-2014.

(29) Pal, R.; Groy, T. L.; Bowman, A. C.; Trovitch, R. J. *Inorg. Chem.* **2014**, *53*, 9357-9365.

(30) Ben-Daat, H.; Hall, G. B.; Groy, T. L.; Trovitch, R. J. *Eur. J. Inorg. Chem.* **2013**, 4430-4442.

(31) The oxidation addition of I₂ to **1** occurs in an ionic fashion, a pathway commonly observed for 18-electron precursors and electrophilic reagents. For a discussion see: Collman, J. P.; Hegedus, L. S.; Norton, J. R.; Finke, R. G. *Principles and Applications of Organotransition Metal Chemistry*; University Science Books: Sausalito, CA, 1987; pp 279-322.

(32) Knijnenburg, Q.; Gambarotta, S.; Budzelaar, P. H. M. *Dalton Trans.* **2006**, 5442-5448.

(33) Margulieux, G. W.; Turner, Z. R.; Chirik, P. J. *Angew. Chem. Int. Ed.* **2014**, *53*, 14211-14215.

(34) Mukhopadhyay, T. K.; Flores, M.; Feller, R. K.; Scott, B. L.; Taylor, R. D.; Paz-Pasternak, M.; Henson, N. J.; Rein, F. N.; Smythe, N. C.; Trovitch, R. J.; Gordon, J. C. *Organometallics* **2014**, *33*, 7101-7112.

(35) Mukhopadhyay, T. K.; Flores, M.; Groy, T. L.; Trovitch, R. J. *J. Am. Chem. Soc.* **2014**, *136*, 882-885.

(36) Trovitch, R. J. *Synlett* **2014**, *25*, 1638-1642.

(37) This is strong evidence against the formation of a complex featuring a static or fluxional agnostic interaction, which are known to exhibit J_{CH} values between 80-100 Hz. Our inability to observe a second J_{CH} coupling constant is consistent with C-H bond oxidative addition. For more information, see: Brookhart, M.; Green, M. L. H. *J. Organomet. Chem.* **1983**, *250*, 395-408.

(38) (a) Zhang, Y.; Hanna, B. S.; Dineen, A.; Williard, P. G.; Bernskoetter, W. H. *Organometallics* **2013**, *32*, 3969-3979. (b) Minato, M.; Zhou, D.-Y.; Sumiura, K.; Oshima, Y.; Mine, S.; Ito, T.; Kakeya, M.; Hoshino, K.; Asaeda, T.; Nakada, T.; Osakada, K. *Organometallics* **2012**, *31*, 4941-4949. (c) Ito, T.; Matsubara, T. *J. Chem. Soc., Dalton*

Trans. **1988**, 2241-2242. (d) Ellis, R.; Henderson, R. A.; Hills, A.; Hughes, D. L. *J. Organomet. Chem.* **1987**, 333, C6-C10. (e) Fong, L. K.; Fox, J. R.; Cooper, N. J. *Organometallics* **1987**, 6, 223-231. (f) Lyons, D.; Wilkinson, G.; Thornton-Pett, M.; Hursthouse, M. B. *J. Chem. Soc., Dalton Trans.* **1984**, 695-700. (g) Darensbourg, D. J.; Rokicki, A.; Darensbourg, M. Y. *J. Am. Chem. Soc.* **1981**, 103, 3223-3224.

(39) Huang, F.; Zhang, C.; Jiang, J.; Wang, Z.-X.; Guan, H. *Inorg. Chem.* **2011**, 50, 3816-3825.

(40) (a) Miller, T. M.; Whitesides, G. M. *Organometallics* **1986**, 5, 1473-1480. (b) Chappell, S. D.; Cole-Hamilton, D. J. *Polyhedron* **1982**, 1, 739-777.

CHAPTER 3

ISOLATION OF A BIS(IMINO)PYRIDINE MOLYBDENUM(I) IODIDE COMPLEX THROUGH CONTROLLED REDUCTION AND INTERCONVERSION OF ITS REACTION PRODUCTS

3.1. Abstract

Analysis of [$(\text{Ph}^2\text{PPrPDI})\text{MoI}][\text{I}]$] by cyclic voltammetry revealed a reversible wave at -1.20 V vs. $\text{Fc}^{+/0}$, corresponding to the $\text{Mo}^{\text{II/I}}$ redox couple. Reduction of [$(\text{Ph}^2\text{PPrPDI})\text{MoI}][\text{I}]$] using stoichiometric potassium naphthalenide ($\text{K}/\text{C}_{10}\text{H}_8$) resulted in ligand deprotonation rather than reduction to yield a Mo(II) monoiodide complex featuring a Mo-C bond to the α -position of one imine substituent, $(\kappa^6\text{-}P,N,N,N,C,P\text{-Ph}^2\text{PPrPDI})\text{MoI}$. Successful isolation of the inner-sphere Mo(I) monoiodide complex, $(\text{Ph}^2\text{PPrPDI})\text{MoI}$, was achieved via reduction of [$(\text{Ph}^2\text{PPrPDI})\text{MoI}][\text{I}]$] with equimolar $\text{Na}/\text{C}_{10}\text{H}_8$. This complex was found to have a near octahedral coordination geometry by single crystal X-ray diffraction and electron paramagnetic resonance (EPR) spectroscopy revealed an unpaired Mo-based electron which is highly delocalized onto the PDI chelate core. Attempts to prepare a Mo(I) monohydride complex upon adding NaEt_3BH to $(\text{Ph}^2\text{PPrPDI})\text{MoI}$ resulted in disproportionation to yield an equimolar quantity of $(\kappa^6\text{-}P,N,N,N,C,P\text{-Ph}^2\text{PPrPDI})\text{MoH}$ and newly identified $(\text{Ph}^2\text{PPrPDI})\text{MoH}_2$. Independent synthesis of $(\text{Ph}^2\text{PPrPDI})\text{MoH}_2$ was achieved by adding 2 equivalents of NaEt_3BH to [$(\text{Ph}^2\text{PPrPDI})\text{MoI}][\text{I}]$] and a minimum hydride resonance T_1 of 176 ms suggests that the Mo-bound H atoms are best described as classical hydrides. Interestingly, $(\text{Ph}^2\text{PPrPDI})\text{MoH}_2$ can be converted to $(\kappa^6\text{-}P,N,N,N,C,P\text{-Ph}^2\text{PPrPDI})\text{MoI}$ upon iodomethane addition, while $(\text{Ph}^2\text{PPrPDI})\text{MoH}_2$ is prepared from $(\kappa^6\text{-}P,N,N,N,C,P\text{-Ph}^2\text{PPrPDI})\text{MoI}$ in the presence of excess NaEt_3BH . Similarly, $(\kappa^6\text{-}$

$P,N,N,N,C,P\text{-}^{\text{Ph}_2\text{PPr}}\text{PDI})\text{MoI}$ can be converted to $(\kappa^6\text{-}P,N,N,N,C,P\text{-}^{\text{Ph}_2\text{PPr}}\text{PDI})\text{MoH}$ with 1 equivalent of NaEt_3BH , while the opposite transformation occurs following iodomethane addition to $(\kappa^6\text{-}P,N,N,N,C,P\text{-}^{\text{Ph}_2\text{PPr}}\text{PDI})\text{MoH}$. Facile interconversion between $[(^{\text{Ph}_2\text{PPr}}\text{PDI})\text{MoI}][\text{I}]$, $(\kappa^6\text{-}P,N,N,N,C,P\text{-}^{\text{Ph}_2\text{PPr}}\text{PDI})\text{MoI}$, $(\kappa^6\text{-}P,N,N,N,C,P\text{-}^{\text{Ph}_2\text{PPr}}\text{PDI})\text{MoH}$, and $(^{\text{Ph}_2\text{PPr}}\text{PDI})\text{MoH}_2$ is expected to guide future reactivity studies on this unique set of compounds.

Parts of this chapter have been reproduced from Pal, R.; Cherry, B. R.; Flores, M.; Groy, T. L.; Trovitch, R. J. *Dalton Transactions* **2016**, 45, 10024-10033 with the permission of *Royal Society of Chemistry*.

3.2. Introduction^{1a}

Over the last half century, the advancement of molybdenum coordination chemistry has contributed to seminal discoveries including non-classical dihydrogen coordination,^{1b} dinitrogen reduction,² and the development of well-defined olefin metathesis catalysts.³ Notably, these developments have relied on complexes which possess diverse Mo oxidation states. For example, Kubas and co-workers first observed dihydrogen coordination following H₂ addition to zerovalent Mo(CO)₃(PCy₃)₂.⁴ While Mo(0) dinitrogen complexes contributed to early Chatt cycle development⁵ and have recently regained favor,⁶ the Mo(III) complexes [({3,5-(CH₃)₂C₆H₃}N{C(CD₃)₂(CH₃)}₃Mo)⁷ and ({3,5-(2,4,6-ⁱPr₃C₆H₂)₂C₆H₃NCH₂CH₂}₃N)Mo(N₂)⁸ were first found to cleave the triple bond of dinitrogen and catalyze its reduction to NH₃, respectively. Furthermore, olefin metathesis catalysts popularized by Schrock operate via [2+2] addition at hexavalent Mo.⁹ Considering the rich chemistry of Mo(II)¹⁰ and Mo(III)¹¹ precursors, as well as the biological importance of mononuclear Mo(IV), Mo(V), and Mo(VI) cofactors,¹² the common oxidation states of Mo are largely accepted to be 0, 2+, 3+, 4+, 5+ and 6+.¹³

Well-defined complexes of Mo(I) are omitted from this list, although several have been reported. One thoroughly studied and structurally characterized example is [(Cp)Mo(CO)₃]₂,¹⁴ which is known to undergo M-M bond cleavage following photoactivation.¹⁵ The addition of I₂ to [Et₄N]₂[Mo₂(CO)₈(SCH₂CO₂Et)₂] in acetonitrile solution has allowed isolation of the thiolate bridged Mo(I) dimer, Mo₂(CO)₆(SCH₂CO₂Et)₂(NCCH₃)₂.¹⁶ The solid-state structures of monomeric (Tp)Mo^I(CO)₃¹⁷ and (Tp')Mo^I(CO)₂(η²-PhC≡CPh)¹⁸ (Tp = hydrotris(pryazoly)borate; Tp' = hydrotris(3,5-dimethylpryazoly)borate) have also been described and related Mo(I)

complexes have been characterized by EPR spectroscopy.¹⁹⁻²¹ Wieghardt and co-workers reported the synthesis and solid-state structure of $[(\text{Bn}_3\text{tacn})\text{Mo}(\text{CO})_3][\text{PF}_6]$ ($\text{Bn}_3\text{tacn} = 1,4,7\text{-tribenzyl-}1,4,7\text{-triazacyclononane}$)²² and their more recent efforts to elucidate the electronic structures of formally monovalent $[(\text{bpy})_3\text{Mo}][\text{PF}_6]$ ²³ and $[(4\text{-OMePhPDI})_2\text{Mo}][\text{PF}_6]$ ²⁴ suggest that $[(\text{bpy})_3\text{Mo}][\text{PF}_6]$ is best described as having a Mo(III) center that is antiferromagnetically coupled to two bipyridine radical anions,²³ while $[(4\text{-OMePhPDI})_2\text{Mo}][\text{PF}_6]$ consists of a Mo(IV) center, an antiferromagnetically coupled PDI radical anion, and one singlet PDI dianion.²⁴ Moreover, oxidation state discrepancies exist for several half-sandwich 1,3,5-cycloheptatriene Mo complexes.²⁵

We hypothesized that pentadentate coordination of donor-substituted bis(imino)pyridine (or pyridine diimine, PDI) chelates might allow for the preparation of complexes and catalysts that are not isolable when employing a set of monodentate ligands.²⁶ Since 2014, we have extended this methodology to study the Mo coordination chemistry of the diphenylphosphinopropyl-substituted PDI chelate, Ph_2PPrPDI .²⁷ Refluxing this ligand in the presence of $\text{Mo}(\text{CO})_6$ allowed for the displacement of five carbonyl ligands to yield the monocarbonyl complex, $(\text{Ph}_2\text{PPrPDI})\text{Mo}(\text{CO})$ (**2**, Fig. 3.1).²⁷ Ionic oxidative addition of I_2 to **2** afforded 7-coordinate $[(\text{Ph}_2\text{PPrPDI})\text{MoI}(\text{CO})][\text{I}]$ (**3**, Fig. 3.1), which was ultimately converted to $[(\text{Ph}_2\text{PPrPDI})\text{MoI}][\text{I}]$ (**4**, Fig. 3.1) upon heating at 100 °C for 24 h.²⁸ Reduction of this complex in the presence of excess K/Hg allowed the preparation of $(\kappa^6\text{-}P,N,N,N,C,P\text{-Ph}_2\text{PPrPDI})\text{MoH}$ (**5**, Fig. 3.1), which catalyzes the hydroboration of CO_2 to methoxyborane.²⁸ In this effort, we describe a one-step synthesis of **4**, its controlled reduction to yield the respective Mo(I) monoiodide complex, and the interconversion between **4** and two newly observed $(\text{Ph}_2\text{PPrPDI})\text{Mo}$ complexes.

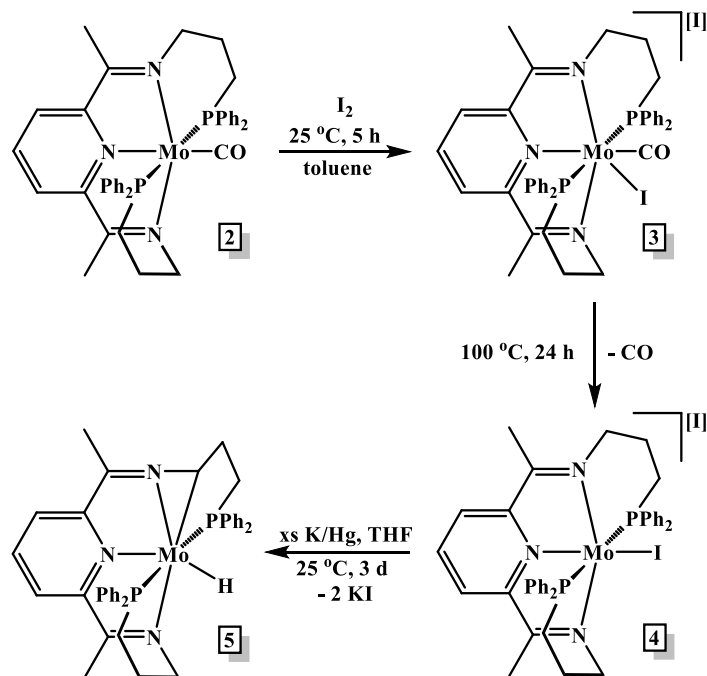


Figure 3.1. Previously described synthesis of $(\text{Ph}_2\text{PPrPDI})\text{Mo}$ complexes 3-5 from 2.²⁸

3.3. Results and Discussion^{1a}

Having recently reported the two-step synthesis of **4**²⁸ (Fig. 3.1) from **2**,²⁷ a simpler preparation of **4** was desired to facilitate further study of its reactivity. For this purpose, the Mo(II) diiodide precursor, $(\text{CO})_3\text{MoI}_2(\text{NCCH}_3)_2$ (Fig. 3.2), was prepared according to literature procedure²⁹ and added directly to Ph_2PPrPDI .²⁶ When heated to $110\text{ }^\circ\text{C}$ under vacuum, ligand substitution results in monodentate ligand loss and formation of **4** in 92% yield.

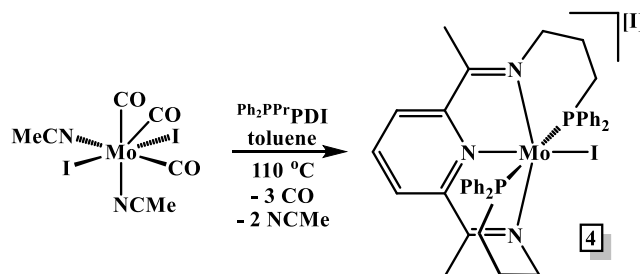


Figure 3.2. Synthesis of $[(\text{Ph}_2\text{PPrPDI})\text{MoI}][\text{I}]$ (**4**) from $(\text{CO})_3\text{MoI}_2(\text{NCCH}_3)_2$.²⁹

With significant quantities of **4** in hand, we set out to further explore its behavior under reducing conditions. Upon scanning towards negative potentials, the cyclic voltammogram of **4** in acetonitrile solution was found to feature a reversible wave at -1.20 V vs. $\text{Fc}^{+/0}$ (Fig. 3.3). Irreversible waves were also observed at -2.65 and -2.77 V vs. $\text{Fc}^{+/0}$. These waves, which are not due to solvent reduction, have been assigned to the reduction of Mo(I) to Mo(0) and Mo(0) to Mo(-I), respectively. The reversible wave at -1.20 V vs. $\text{Fc}^{+/0}$ is consistent with previously reported Mo(II)/Mo(I) redox potentials,³⁰ suggesting that it may be possible to isolate a persistent, well-defined Mo(I) complex following one electron reduction of **4**.

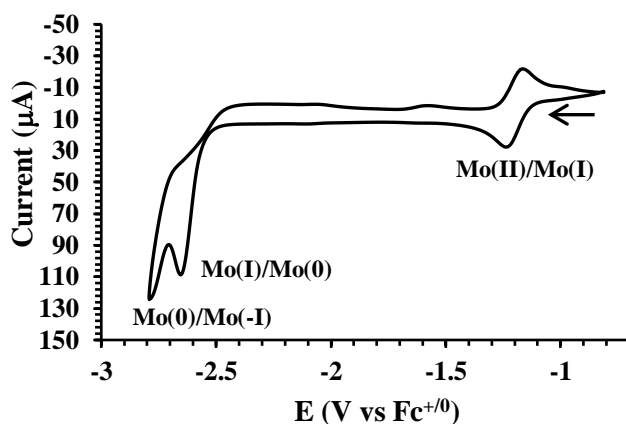


Figure 3.3. Cyclic voltammogram of 3.0 mM **4** in dry acetonitrile (0.1 M TBAPF₆; scan rate = 0.05 V s⁻¹). Arrow indicates the initiation point and direction of cycling.

We previously reported that excess K/Hg addition to **4** affords complex **5** (Fig. 3.1) following C-H activation at the α -position of one imine substituent.²⁸ With this in mind, reduction of **4** was attempted using a stoichiometric quantity of *in situ* generated potassium naphthalenide. Work-up of the resulting greenish-brown solution followed by multinuclear NMR spectroscopic analysis revealed a diamagnetic reaction product. This complex was found to feature ³¹P NMR doublets at 40.22 and 16.20 ppm ($J_{\text{PP}} = 162.5$ Hz), indicating

side-to-side chelate inequivalence. Moreover, gHSQCAD NMR spectroscopy revealed a methine ^1H resonance at 5.51 ppm, signifying that Ph_2PPrPDI methylene group deprotonation has taken place. Considering that the α -position of Ph_2PPrPDI is prone to activation,²⁸ the diamagnetic product has been assigned as the seven-coordinate monoiodide complex, (κ^6 - P,N,N,N,C,P - Ph_2PPrPDI)MoI (**7**, Fig. 3.4).

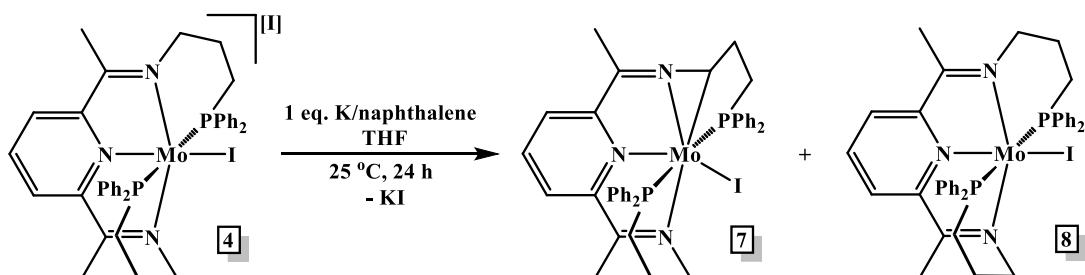


Figure 3.4. Synthesis of (κ^6 - P,N,N,N,C,P - Ph_2PPrPDI)MoI (**7**) from [$(\text{Ph}_2\text{PPrPDI})\text{MoI}$][I] (**4**).

To confirm the position of chelate deprotonation, the solid-state structure of **7** (Fig. 3.5) was determined by single crystal X-ray diffraction. The overall geometry about Mo is distorted pentagonal bipyramidal and the experimentally determined metrical parameters of **7** (Table 3.1) are strongly correlated to isostructural **5**.²⁸ The Mo(1)-C(10) distance of 2.257(8) Å is consistent with single bond formation, confirming that deprotonation occurred at the chelate α -methylene group. The distances and angles defined by the metal center and Ph_2PPrPDI N-atoms are closely matched to those determined for **5**.²⁸ In contrast, the Mo(1)-P(1) and Mo(1)-P(2) distances of 2.471(2) and 2.488(2) Å found for **7** are approximately 0.04 Å longer than those of **5**. These contacts, along with the larger P(1)-Mo(1)-P(2) angle of 164.06(7)°, are likely due to the weak field nature of the iodide ligand of **7** which serves to weaken phosphine σ -donation.

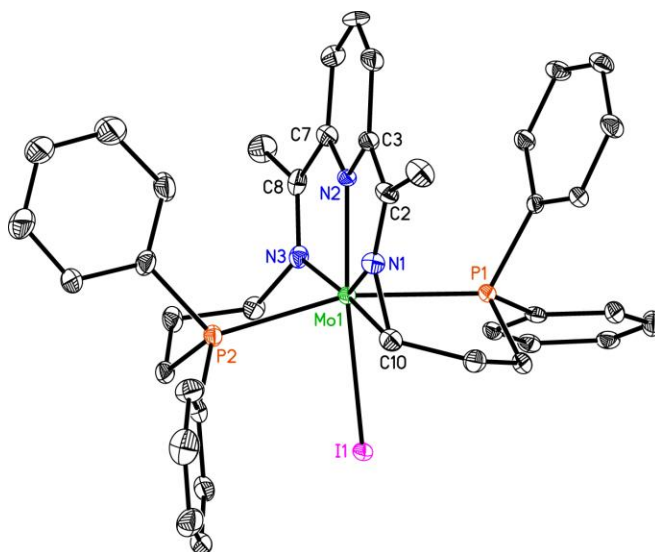


Figure 3.5. The solid state structure of **7** shown at 30% probability ellipsoids. Hydrogen atoms and co-crystallized ether are removed for clarity.

Table 3.1. Notable bond lengths (Å) and angles (°) determined for **7**, along with values previously reported for **5**.²⁸

| | 7 | 5 ²⁸ |
|------------------|-----------|------------------------|
| Mo(1)-N(1) | 1.952(7) | 1.940(7) |
| Mo(1)-N(2) | 2.055(6) | 2.072(5) |
| Mo(1)-N(3) | 2.141(7) | 2.121(6) |
| Mo(1)-P(1) | 2.471(2) | 2.448(2) |
| Mo(1)-P(2) | 2.488(2) | 2.433(2) |
| Mo(1)-C(10) | 2.257(8) | 2.259(8) |
| Mo(1)-I(1) | 2.8954(8) | - |
| Mo(1)-H(1M) | - | 1.75(8) |
| C(10)-N(1) | 1.386(11) | 1.399(9) |
| N(1)-C(2) | 1.322(11) | 1.324(9) |
| N(3)-C(8) | 1.328(12) | 1.374(9) |
| C(2)-C(3) | 1.412(13) | 1.406(10) |
| C(7)-C(8) | 1.408(13) | 1.408(11) |
| | | |
| N(1)-Mo(1)-C(10) | 37.6(3) | 38.0(2) |
| N(1)-Mo(1)-N(3) | 143.5(3) | 144.3(2) |
| P(1)-Mo(1)-P(2) | 164.06(7) | 152.91(7) |
| N(3)-Mo(1)-C(10) | 176.4(3) | 176.8(3) |

Given the propensity of PDI chelates to accept one or more electrons from low-valent first-row metal centers,³¹ it should be noted that the N=C distances found for **7** are

elongated [1.322(11) and 1.328(12) Å] relative to unreduced PDI ligands (1.28 Å).³² Furthermore, the neighboring C(2)-C(3) and C(7)-C(8) distances of 1.412(13) and 1.408(13) Å, respectively, are greatly contracted relative to the C_{imine}-C_{pyridine} bond lengths of unreduced PDI chelates (1.50 Å).³² Even though these distances are suggestive of chelate reduction, the nature of the metal must be considered when assaying chelate non-innocence. Since Mo is a second-row metal, its expanded d-orbitals efficiently overlap with the ^{Ph₂PPr}PDI chelate LUMOs of **7**, allowing electron density transfer and delocalization through backbonding. This mixing lowers the energy of the Mo-derived orbital while greatly destabilizing the ^{Ph₂PPr}PDI LUMOs, rendering their population unlikely. For this reason, we do not believe that the PDI chelate of **7** is reduced by one or more electrons.

In the process of purifying complex **7** following potassium naphthalenide addition to **4**, a small quantity of a dark red side product was isolated. After determining this complex to be NMR silent, a selective synthesis was desired to facilitate its characterization. When a stoichiometric quantity of milder sodium naphthalenide was added to **4**, chelate deprotonation was not observed and the dark red complex was the sole isolated product. This complex was determined to have an ambient temperature magnetic moment of 1.4(1) μ_B (Evans method), consistent with one electron reduction and formation of the respective Mo(I) monoiodide complex, (^{Ph₂PPr}PDI)MoI (**8**, Fig. 3.6).

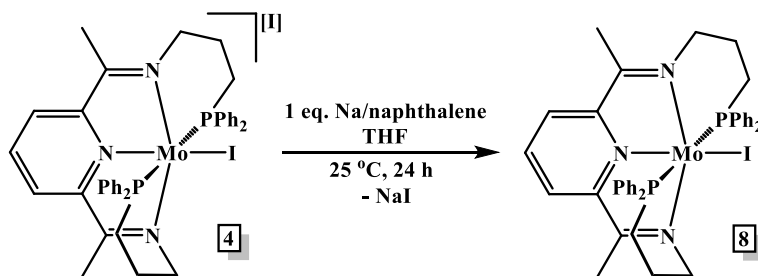


Figure 3.6. Synthesis of (^{Ph₂PPr}PDI)MoI (**8**) from [(^{Ph₂PPr}PDI)MoI][I].

To further characterize **8**, a toluene solution of this complex was prepared and analyzed by X-band EPR spectroscopy at 108 K and 296 K (Fig. 3.7). The spectral features observed at 108 K are consistent with the presence of Mo(I), i.e. the spectrum is an overlap of two signals, a broad signal corresponding to $^{95,97}\text{Mo}$ ($I = 5/2$) and a large narrow signal corresponding to ^{96}Mo ($I = 0$) (Fig. 3.7A). In addition, the signal corresponding to ^{96}Mo shows a multiline pattern due to hyperfine coupling (hfc) interactions between the magnetic moment of the unpaired electron and the magnetic moment of neighboring ^{14}N ($I = 1$) nuclei. To simplify the EPR spectrum observed at 108 K, a toluene solution of **8** was measured at 296 K (Fig. 3.7B). The EPR spectrum at 296 K also shows contributions from $^{95,97}\text{Mo}$ ($I = 5/2$) and ^{96}Mo ($I = 0$), although the intensity of the signal corresponding to $^{95,97}\text{Mo}$ is barely above the noise level. The signal corresponding to ^{96}Mo shows a five-line splitting and resembles those associated with the hfc between the magnetic moment of one unpaired electron and the magnetic moment of two equivalent nitrogens (\mathbf{A}^{N_i}).

Thus, the EPR spectrum of **8** at 296 K was well-fit ($\sigma = 3.0\%$, see Experimental Section) considering a low-spin Mo(I) center ($S = 1/2$) with an isotropic g value of 2.001 and an isotropic hfc, between the unpaired electron and two equivalent nitrogen atoms, of 48 MHz (Table 3.2). This finding is consistent with the crystallographically determined structure of **8** which shows two imine nitrogen atoms which are symmetrically coordinated to Mo (Fig. 3.8). The principal components of the \mathbf{g} and \mathbf{A}^{N_i} tensors were obtained from the simulation of the signal corresponding to ^{96}Mo ($I = 0$) at 108 K (Fig. 3A and Table 3.2). Consistently, the signal corresponding to $^{95,97}\text{Mo}$ ($I = 5/2$) at 108 K shows two different splittings (inset in Fig. 3.7A); one due to the hfc's of the $^{95,97}\text{Mo}$ nucleus (\mathbf{A}^{Mo}) and a second one due to the hfc's of the two equivalent nitrogens (\mathbf{A}^{N_i}). The principal components of the \mathbf{A}^{Mo} tensor

were obtained from the simulation of the broad signal observed at 108 K. The EPR data of **6** show that its paramagnetic properties are due to the presence of a low-spin Mo(I) center ($S = 1/2$). Additionally, the data show significant delocalization of the unpaired electron into the Ph_2PPrPDI ligand of **8**, reflected in the isotropic hfc (i.e. the contact interaction) of the two symmetrically coordinated imines.

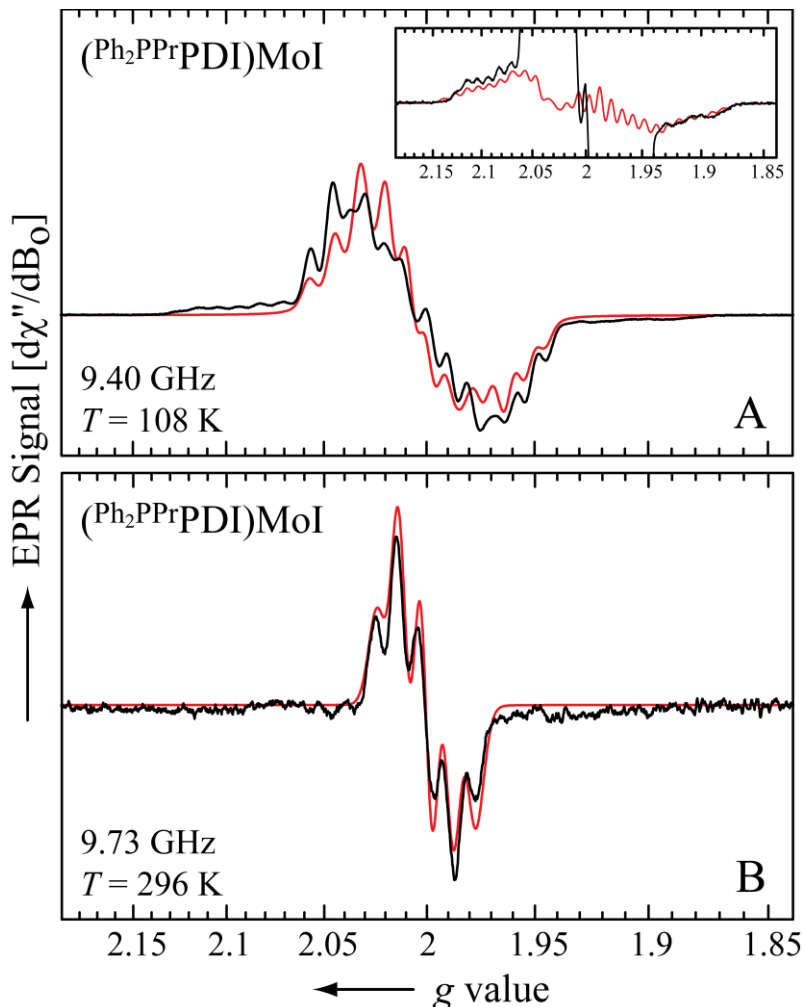


Figure 3.7. Experimental (black) and simulated (red) X-band EPR spectra of **8** in toluene at 108 K (frozen solution) (**A**) and at 296 K (liquid solution) (**B**). The EPR spectrum at 108 K is an overlap of two signals (see text), one attributed to ^{96}Mo ($I = 0$) (large signal) and another attributed to $^{95,97}\text{Mo}$ ($I = 5/2$) (small signal). The inset shows a closer view of the signal attributed to $^{95,97}\text{Mo}$ ($I = 5/2$) (**A**). The EPR spectrum at 296 K shows mostly the signal attributed to ^{96}Mo ($I = 0$). The observed five-line splitting was attributed to the hyperfine coupling between the unpaired electron and two equivalent nitrogen atoms.

Table 3.2. Parameters used to fit the EPR spectra of **8** at 108 K and 296 K.

| Parameter ^a | 8 | |
|------------------------|----------------|-----------------|
| | T=108 K | T= 296 K |
| g_x | 2.032 | |
| g_y | 2.008 | |
| g_z | 1.964 | |
| g_{iso} | | 2.001 |
| $ A_x^{Mo} $ | 146 MHz | |
| $ A_y^{Mo} $ | 60 MHz | |
| $ A_z^{Mo} $ | 135 MHz | |
| $ A_{iso}^{Mo} $ | 114 MHz | |
| $ A_x^{Ni} $ | 55 MHz | |
| $ A_y^{Ni} $ | 44 MHz | |
| $ A_z^{Ni} $ | 45 MHz | |
| $ A_{iso}^{Ni} $ | | 48 MHz |

The molecular structure of **8** was determined by single crystal X-ray diffraction (Fig. 3.8) and relevant metrical parameters are provided in Table 3.3. Relative to diiodide precursor **4**,²⁸ monoiodide **8** was found to possess a geometry closer to an idealized octahedron, with N(1)-Mo(1)-N(1A) and P(1)-Mo(1)-P(2) angles of 148.4(6) and 172.76(15) °, respectively. The Mo(1)-I(I) contact distance of 2.8993(18) Å for **8** is significantly longer than the distance of 2.7810(17) Å reported for the inner-sphere iodide of **4**.²⁸ The lengthened Mo-N and Mo-P distances determined for **8** relative to **4** (Table 3.3) are also consistent with a reduction in oxidation state from Mo(II) to Mo(I); however, the Mo(1)-N(2) distance of 1.984(11) Å found for **8** is noticeably shorter. This may be due to increased backbonding from Mo into the π^* -orbitals of PDI.³² Based on our EPR spectroscopic results and the N_{imine}-C_{imine} and C_{imine}-C_{pyridine} distances in Table 3.3, the SOMO of **8** is likely to possess both metal and chelate character; however, computational work is needed to definitively establish the electronic structure of this complex.

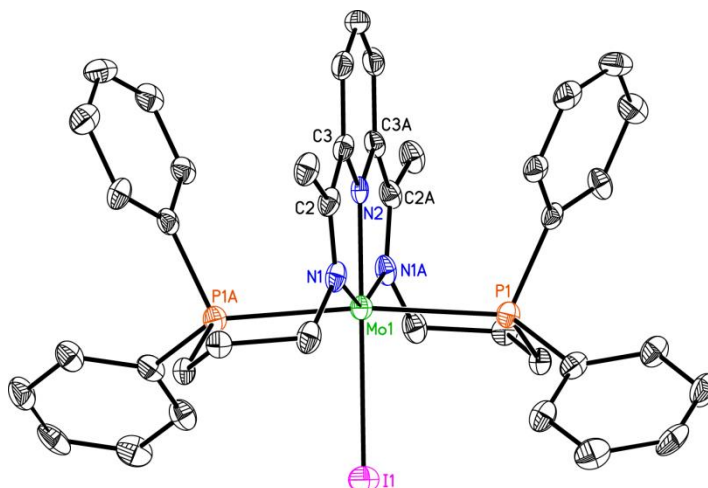


Figure 3.8. The solid state structure of **8** shown at 30% probability ellipsoids. Atoms with labels ending in “A” have been generated by symmetry. Hydrogen atoms are omitted for clarity.

Table 3.3. Notable bond lengths (Å) and angles (°) determined for **8** and **9**, compared with those reported for **4**.²⁸

| | 8 | 9 | 4 ²⁸ |
|--------------------|------------|-----------|------------------------|
| Mo(1)-N(1) | 2.122(9) | 2.098(2) | 2.036(11) |
| Mo(1)-N(2) | 1.984(11) | 2.056(2) | 2.112(10) |
| Mo(1)-N(1A/3) | 2.122(9) | 2.098(2) | 2.077(10) |
| Mo(1)-P(1) | 2.488(3) | 2.4123(6) | 2.472(3) |
| Mo(1)-P(1A/2) | 2.488(3) | 2.4103(6) | 2.453(3) |
| Mo(1)-I(1) | 2.8993(18) | - | 2.7810(17) |
| N(1)-C(2) | 1.305(15) | 1.345(3) | 1.332(16) |
| N(1A/3)-C(2A/8) | 1.305(15) | 1.349(3) | 1.324(15) |
| C(2)-C(3) | 1.436(16) | 1.416(4) | 1.442(17) |
| C(2A/7)-C(3A/8) | 1.436(16) | 1.407(4) | 1.401(18) |
| N(1)-Mo(1)-N(1A/3) | 148.4(6) | 147.13(8) | 141.6(4) |
| P(1)-Mo(1)-P(2) | 172.76(15) | 138.15(2) | 169.30(7) |
| N(2)-Mo(1)-I(1) | 180.00(6) | - | 178.2(3) |

With **8** in hand, its conversion to the respective Mo(I) hydride was attempted. Upon adding a stoichiometric quantity of NaEt₃BH to **8**, analysis by multinuclear NMR spectroscopy revealed an approximate 1:1 ratio of two products: previously described **5**²⁸ and a newly identified product featuring a {¹H}³¹P NMR singlet at 43.15 ppm.

Furthermore, the new complex was found to feature a well-resolved ^1H NMR triplet with $J_{\text{HP}} = 36.0$ Hz at 4.20 ppm. Given the observed chelate equivalence, and that the ^1H NMR resonance at 4.20 ppm integrates to two hydrogen atoms, this product was assigned as the dihydride complex, $(^{\text{Ph}_2\text{PPr}}\text{PDI})\text{MoH}_2$ (**9**, Fig. 3.9). The identification of **5** and **9** in an equimolar ratio is consistent with disproportionation following formation of the suspected short-lived intermediate, $(^{\text{Ph}_2\text{PPr}}\text{PDI})\text{MoH}$.

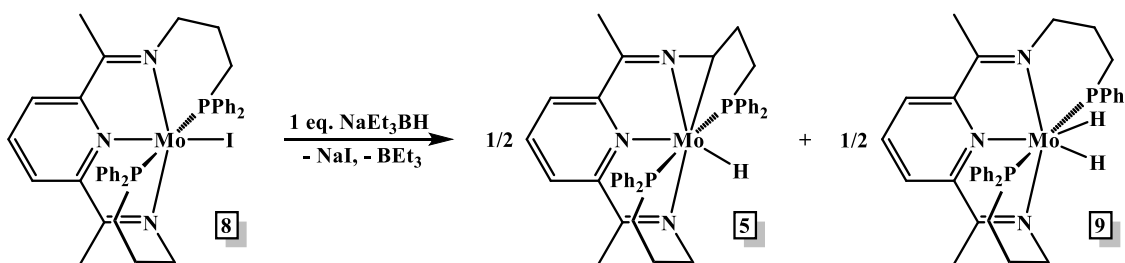


Figure 3.9. Attempt to isolate $(^{\text{Ph}_2\text{PPr}}\text{PDI})\text{MoH}$ from $(^{\text{Ph}_2\text{PPr}}\text{PDI})\text{MoI}$.

Having identified **9**, a selective synthesis was desired so that the characterization and reactivity of this complex could be more thoroughly investigated. Its preparation directly from **4** was achieved following the addition of 2 equivalents of NaEt_3BH in 86 % yield (Fig. 3.10). Complex **9** was also prepared by adding 1 atm. of H_2 to **5** (Fig. 3.10). Solutions of **9** stored under N_2 atmosphere are fairly persistent; however, when left at ambient temperature for several days, partial reversion to **5** is observed following H_2 loss and chelate C-H activation. To determine whether **9** can appropriately be considered a dihydride (as opposed to a dihydrogen complex),¹ attempts were made to determine the solid-state structure by X-ray diffraction. Suitable single crystals were grown from a concentrated ether solution at -35 °C and a high-resolution structure with $R_1 = 0.0332$ was obtained (Fig. 3.11). The metrical parameters determined for **9** are provided in Table 3.3;

however, the Mo-bound hydrogen atoms could not be located in the difference map. The solid state structure of this complex possesses a distorted trigonal bipyramidal chelate coordination environment with a P(1)-Mo(1)-P(2) angle of $138.15(2)^\circ$. This angle is much smaller than the angles of $169.30(7)^\circ$ and $172.76(15)^\circ$ observed for six-coordinate **4** and **8**, respectively, an observation which highlights the coordinative flexibility of Ph_2PPrPDI .

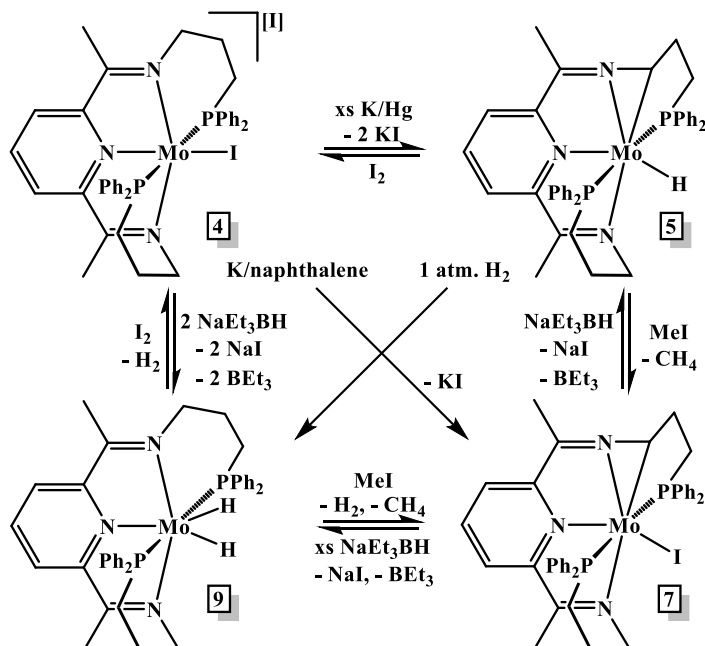


Figure 3.10. Interconversion of $(\text{Ph}_2\text{PPrPDI})\text{Mo}$ complexes **4**, **5**, **7**, and **9**.

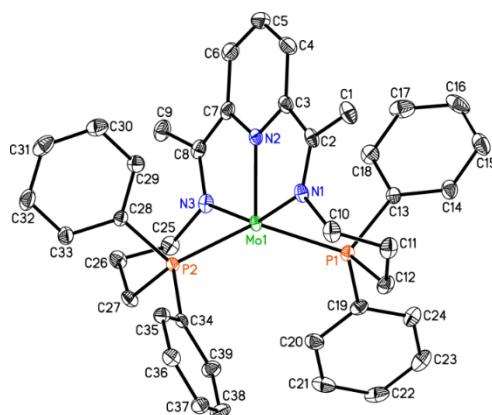


Figure 3.11. The molecular structure of **9** displayed at 30% probability ellipsoids. Hydrogen atoms omitted for clarity (Note: the hydride ligands of **9** were not located in the difference map).

Since information regarding the degree of H₂ activation could not be gained through X-ray diffraction, a variable temperature experiment was conducted to assay relaxation of the hydride ¹H NMR resonance at 4.20 ppm. A minimum T₁ value of 176 ms (400 MHz) was observed at -20 °C. This suggests that the Mo-bound hydrogen atoms of **9** are most appropriately described as hydrides, although minimal H-H bonding character may remain.³³ Given the C-H activated chelate of **5**, we were interested to see if D₂ addition would result in Mo-C bond hydrogenation to give the corresponding MoH(D) complex with one or more D-labelled α-methylene positions. Instead, clean conversion to the dideuteride complex, (^{Ph₂PP_r}PDI)MoD₂ (**9-d₂**, Fig. 3.12), was observed by ¹H and ²H NMR spectroscopy with no evidence of HD formation or methylene group labelling (Fig. 3.21). This observation suggests that C-H reductive elimination is likely to precede D₂ coordination and oxidative addition.

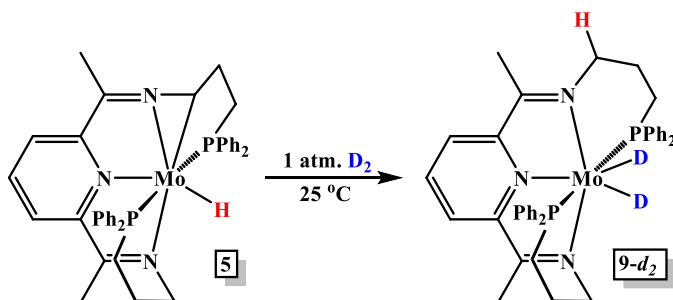


Figure 3.12. Synthesis of (^{Ph₂PP_r}PDI)MoD₂ (**9-d₂**) from **5**.

Since **5** and **9** have both been prepared from **4**, the conversion of these complexes back into **4** was explored. Adding a stoichiometric quantity of I₂ to either **5** or **9** resulted in the immediate formation of **4** (Fig. 3.10), as determined by multinuclear NMR spectroscopy. Complexes **5** and **9** have also been used as precursors for the formation of deprotonated monoiodide complex **7**. The stoichiometric addition of iodomethane to a toluene solution

of either **5** or **9** allowed for the isolation of **7** in 95% and 76% yield, respectively (Fig. 3.10). Conducting the same reactions in a J. Young tube allowed for the direct observation of CH₄ by ¹H NMR spectroscopy. Finally, complex **7** was determined to be a suitable synthon for both **5** and **9** upon addition of either 1 equiv. or an excess of NaEt₃BH, respectively (Fig. 3.10). Since **4** can be readily prepared from ^{Ph₂PPr}PDI and (CO)₃MoI₂(NCCH₃)₂, the synthetic pathways illustrated in Fig. 3.10 represent convenient ways to access complexes **5**, **7**, and **9**.

3.4. Conclusion^{1a}

In summary, varying the reagent used to reduce [^{(Ph₂PPr}PDI)MoI][I] enabled isolation of both (κ⁶-*P,N,N,N,C,P*-^{Ph₂PPr}PDI)MoI and (^{Ph₂PPr}PDI)MoI, in addition to (κ⁶-*P,N,N,N,C,P*-^{Ph₂PPr}PDI)MoH. Persistent Mo(I) complexes such as (^{Ph₂PPr}PDI)MoI remain rare, and this complex is believed to be the first crystallographically characterized Mo(I) monoiodide. Although an attempt to prepare the analogous Mo(I) monohydride complex resulted in disproportionation, it allowed for the observation and eventual isolation of the respective dihydride complex, (^{Ph₂PPr}PDI)MoH₂. The dihydride was converted back to either [^{(Ph₂PPr}PDI)MoI][I] or (κ⁶-*P,N,N,N,C,P*-^{Ph₂PPr}PDI)MoI following addition of either I₂ or MeI, respectively, and analogous reactivity has been noted for (κ⁶-*P,N,N,N,C,P*-^{Ph₂PPr}PDI)MoH. The straightforward interconversion between this unique set of (PDI)Mo complexes is expected to facilitate future efforts to study their reactivity and catalytic competency.

3.5. Experimental Details^{1a}

3.5.1. General Considerations

All synthetic manipulations were performed in an MBraun glovebox under an atmosphere of purified nitrogen. Diethyl ether, pentane, tetrahydrofuran, and toluene were purchased from Sigma Aldrich, dried using a Pure Process Technology (PPT) solvent purification system, and stored in the glove box over activated 4Å molecular sieves and metallic sodium (Alfa Aesar) before use. Acetonitrile was purchased from VWR, dried over 3 Å molecular sieves, and distilled from CaH₂ prior to use. Benzene-*d*₆ was obtained from Cambridge Isotope Laboratories and dried over 4Å molecular sieves and metallic potassium (from Sigma-Aldrich) prior to use. 2,6-Diacetylpyridine and Celite were purchased and used as received from TCI America and Acros, respectively. Mo(CO)₆ and 3-(diphenylphosphino)propylamine were purchased from Strem Chemicals and 1.0 M toluene solution of sodium triethyl borohydride was used as received from Sigma-Aldrich. Hydrogen gas was used as received from Praxair and deuterium gas was used as received from Specialty Gases of America. Ph₂PPrPDI,²⁶ **5**,²⁸ and (CO)₃MoI₂(NCCH₃)₂²⁹ were prepared according to literature procedure. Solution phase ¹H, ¹³C, and ³¹P nuclear magnetic resonance (NMR) spectra were recorded at room temperature on either a 400 MHz or 500 MHz Varian NMR Spectrometer. All ¹H and ¹³C NMR chemical shifts are reported relative to Si(CH₃)₄ using ¹H (residual) and ¹³C chemical shifts of the solvent as secondary standards. ²H NMR chemical shifts are reported relative to Si(CD₃)₄ using benzene-*d*₆ as an internal reference. ³¹P NMR resonances are reported relative to H₃PO₄. Elemental analyses were performed at Robertson Microlit Laboratories Inc. (Ledgewood, NJ) and at Arizona State University.

3.5.2. Electrochemistry

Electrochemical analysis was carried out under a nitrogen atmosphere using a CH Instruments handheld potentiostat. A conventional three-electrode cell was used for recording the cyclic voltammogram of **4**. A glassy carbon working electrode (3 mm diameter) was prepared by successive polishing with 1.0, 0.3, and 0.05 μm alumina slurries, followed by sonication (5 min) in ultrapure water after each polishing step. The supporting electrolyte was 0.1 M TBAPF₆ in acetonitrile. The Ag/Ag⁺ pseudoreference electrode was prepared by immersing a silver wire into 1.0 M HCl, washing with acetonitrile, and air drying. A platinum wire was used as the counter electrode. All potentials are reported to the ferrocene/ferrocenium (Fc⁺⁰) couple as an internal reference.

3.5.3. X-ray crystallography

Single crystals suitable for X-ray diffraction were coated with polyisobutylene oil in the glovebox and transferred to glass fiber with Apiezon N grease before mounting on the goniometer head of a Bruker APEX Diffractometer (Arizona State University) equipped with Mo K α radiation. A hemisphere routine was used for data collection and determination of the lattice constants. The space group was identified and the data was processed using the Bruker SAINT+ program and corrected for absorption using SADABS. The structures were solved using direct methods (SHELXS) completed by subsequent Fourier synthesis and refined by full-matrix, least-squares procedures on [F²] (SHELXL). For **7**, A-level alerts remain following refinement due to close contacts between the main molecule and four partially occupied ether molecules which were modelled as rigid bodies. Diffraction of **8** yielded weak high resolution data, and ultimately, poor bond precision. The hydrides

of **9** could not be located due to their proximity to Mo. Crystallographic parameters for **7**, **8**, and **9** are located in Table S1 of the Supporting Information.

3.5.4. Electron Paramagnetic Resonance Spectroscopy

3.5.4.1. Instrumentation

Studies were performed at the EPR Facility of Arizona State University. Continuous wave (CW) EPR spectra were recorded, at 108 K and 296 K, using a Bruker ELEXSYS E580 CW X-band spectrometer (Bruker, Rheinstetten, Germany). A standard resonator (ER 4102ST) attached to a liquid nitrogen temperature control system (ER 4131VT), and quartz sample tubes type 707-SQ-250M (Wilma-LabGlass, Vineland, NJ) (OD 4 mm, ID 3 mm), were used at 108 K. Whereas, a cylindrical mode resonator (ER 4103TM) and quartz sample tubes type 712-SQ-100M (OD 2 mm, ID 1 mm) were used at 296 K. The magnetic field modulation frequency was 100 kHz with a field modulation of 0.5 mT (at 108 K) and 0.2 mT (at 296 K) peak-to-peak. The microwave power was 1 mW, the microwave frequency was 9.40 GHz (at 108 K) and 9.73 GHz (at 296 K), and the sweep time was 84 seconds (at 108 K) and 168 seconds (at 296 K).

3.5.4.2. Spin Hamiltonian

The EPR spectra of **8** were interpreted using a spin Hamiltonian, H , containing the electron Zeeman interaction with the applied magnetic field B_0 and the hyperfine coupling (hfc) interactions with a single $^{95,97}\text{Mo}$ ($I = 5/2$) and two equivalent ^{14}N ($I = 1$):³⁴

$$H = \beta_e \mathbf{S} \cdot \mathbf{g} \cdot \mathbf{B}_0 + h \mathbf{S} \cdot \mathbf{A}^{\text{Mo}} \cdot \mathbf{I}^{\text{Mo}} + \sum_{i=1}^2 h \mathbf{S} \cdot \mathbf{A}^{N_i} \cdot \mathbf{I}^{N_i} \quad (6)$$

where \mathbf{S} is the electron spin operator, \mathbf{I}^{Mo} and \mathbf{I}^{N_i} are the nuclear spin operators of the single $^{95,97}\text{Mo}$ and the two equivalent ^{14}N , respectively, \mathbf{A}^{Mo} and \mathbf{A}^{N_i} are the corresponding hfc tensors in frequency units, \mathbf{g} is the electronic g -tensor, β_e is the electron magneton, and h is Planck's constant.

3.5.4.3. Fitting of EPR spectra

To quantitatively compare experimental and simulated spectra, we divided the spectra into N intervals, i.e. we treated the spectrum as an N -dimensional vector \mathbf{R} . Each component R_j has the amplitude of the EPR signal at a magnetic field B_j , with j varying from 1 to N . The amplitudes of the experimental and simulated spectra were normalized so that the span between the maximum and minimum values of R_j is 1. We compared the calculated amplitudes R_j^{calc} of the signal with the observed values R_j^{exp} defining a root-mean-square deviation σ by: $\sigma(p_1, p_2, \dots, p_n) = [\sum_j (R_j^{\text{calc}}(p_1, p_2, \dots, p_n) - R_j^{\text{exp}})^2/N]^{1/2}$, where the sums are over the N values of j , and p 's are the fitting parameters that produced the calculated spectrum. For our simulations, N was set equal to 1024. The EPR spectra were simulated using EasySpin (v 5.0.2), a computational package developed by Stoll and Schweiger³⁵ and based on Matlab (The MathWorks, Natick, MA, USA). EasySpin calculates EPR resonance fields using the energies of the states of the spin system obtained by direct diagonalization of the spin Hamiltonian. The EPR fitting procedure used a Monte Carlo type iteration to minimize the root-mean-square deviation, σ between measured and simulated spectra. We searched for the optimum values of the following parameters: the principal components of \mathbf{g} (i.e. g_x, g_y, g_z), the principal components of the hfc tensors \mathbf{A}^{Mo} (i.e. $A_x^{\text{Mo}}, A_y^{\text{Mo}}, A_z^{\text{Mo}}$) and \mathbf{A}^{Ni} (i.e. $A_x^{\text{Ni}}, A_y^{\text{Ni}}, A_z^{\text{Ni}}$) and the peak-to-peak line-width (ΔB).

3.5.5. Alternative synthesis of [(^{Ph}2PPrPDI)MoI][I] (**4**)

Method 1. Although previously reported,²⁸ a simplified synthesis of **4** was utilized. In a nitrogen filled glovebox, a 100 mL thick-walled reaction bomb was charged with 0.150 g (0.291 mmol) of $(\text{CO})_3\text{MoI}_2(\text{NCMe})_2$ dissolved in 5 mL of toluene, 0.180 g (0.294 mmol)

of Ph^2PPrPDI dissolved in 10 mL of toluene, and a magnetic stir-bar. The bomb was sealed, the solution was frozen with liquid nitrogen, and the reaction was degassed on a Schlenk line. Upon warming to room temperature, the reaction was set to reflux in an oil bath that was preheated to 110 °C. An amber solid started to precipitate within 3 h. After 12 h, the solution was cooled to room temperature, frozen with liquid nitrogen, and degassed. Once the liberated CO was removed, the reaction bomb was allowed to reflux for another 12 h at 110 °C to ensure reaction completion. After once again removing CO, the bomb was brought inside the glovebox and the resulting amber solid was filtered and collected on top of a sintered frit. After washing with 2 mL of THF and ether, and drying under vacuum, 0.257 g (0.267 mmol, 92%) of previously reported **4** was isolated. *Method 2.* In a nitrogen filled glovebox, a 20 mL reaction vial was charged with 0.011 g (0.015 mmol) of **5** and dissolved in 3 mL of benzene. To this solution, 0.004 g (0.016 mmol) of I₂ dissolved in 3 mL of benzene was added while stirring. Immediate precipitation of an amber solid, identified as **4** was observed. *Method 3.* In a nitrogen filled glovebox, a 20 mL reaction vial was charged with 0.012 g (0.017 mmol) of **9** and dissolved in 3 mL of benzene. To this solution, 0.0046 g (0.0181 mmol) of I₂ dissolved in 3 mL of benzene was added while stirring. Immediate precipitation of an amber solid, identified as **4** was observed.

3.5.6. Preparation of ($\kappa^6\text{-P,N,N,N,C,P-Ph}^2\text{PPrPDI}$)MoI (**7**)

Method 1. In a nitrogen filled glovebox, a 20 mL reaction vial was charged with 0.050 g (0.071 mmol) of **5** and dissolved in 3 mL of toluene. To this solution, 0.005 mL (0.080 mmol) of iodomethane was added while stirring. The reaction turned olive green within 1 h, at which time the solution was filtered through Celite and dried under vacuum. After washing with pentane, 0.056 g (95%) of an olive-green solid identified as **7** was isolated.

Suitable crystals for X-ray diffraction were grown from a concentrated solution of ether.

Method 2. In a nitrogen filled glovebox, a 20 mL reaction was charged with 0.030 g (0.042 mmol) of **9** and dissolved in 3 mL of toluene. To this solution, 0.003 mL (0.048 mmol) of iodomethane was added while stirring. The reaction turned olive-green within an hour, at which time the solution was filtered through Celite and dried under vacuum. After washing with pentane, 0.027 g (76%) of an olive-green solid identified as **7** was isolated.

Method 3. In a nitrogen filled glovebox, a 20 mL reaction vial was charged with 0.002 g (0.051 mmol) of freshly cut metallic potassium, 0.006 g (0.047 mmol) of naphthalene, and 3 mL of THF. The solution was stirred for 30 min to form green potassium naphthalenide solution. To it, 0.050 g (0.052 mmol) of **4** in 10 mL of THF was slowly added and the mixture was allowed to stir at ambient temperature for 24 h. The resulting greenish-brown solution was filtered through Celite and the solvent was removed *in vacuo*. After washing with pentane and drying, 0.022 g of a brownish-green solid identified as a mixture of **7** and **8** was isolated.

Elemental analysis for C₃₉H₄₀N₃MoP₂I: Calcd. C, 56.06%; H, 4.83%; N, 5.03%. (Calcd. for C₃₉H₄₀N₃MoP₂I·C₄H₁₀O: Calcd. C, 56.77%; H, 5.54%; N, 4.62%). Found: C, 56.61%; H, 5.36%; N, 4.68%. ¹H NMR (benzene-*d*₆, 400 MHz): 7.58 (t, 8.2 Hz, 2H, *Ar*), 7.41 (t, 12.3 Hz, 1H, *CH*₂), 7.30 (t, 8.2 Hz, 2H, *Ar*), 7.06 (d, 12.6 Hz, 1H, *Ar*), 6.99 (m, 5H, *Ar*), 6.91 (m, 2H, *Ar*), 6.73 (d, 7.5 Hz, 1H, *Ar*), 6.62 (t, 7.3 Hz, 1H), 6.57 (t, 7.3 Hz, 1H, *Ar*), 6.43 (t, 7.0 Hz, 2H, *Ar*), 6.37 (t, 7.0 Hz, 2H, *Ar*), 5.66 (t, 8.2 Hz, 2H, *Ar*), 5.51 (s, 1H, *HCMo*), 5.37 (t, 8.5 Hz, 2H, *Ar*), 4.93 (d, 9.3 Hz, 1H, *CH*₂), 4.02 (t, 13.7 Hz, 1H, *CH*₂), 3.32 (m, 1H, *CH*₂), 3.08 (m, 1H, *CH*₂), 2.92 (m, 1H, *CH*₂), 2.48 (s, 3H, *CH*₃), 2.40 (s, 3H, *CH*₃), 2.07 (m, 2H, *CH*₂), 1.85 (m, 1H, *CH*₂), 1.65 (m, 1H, *CH*₂). ¹³C NMR (benzene-*d*₆, 125.00 MHz): 151.4 (C=N), 148.6 (C=N), 143.7 (*Ar*), 136.8 (*Ar*), 136.3 (d, *J*_{CP} = 24.1 Hz,

Ar), 136.0 (d, $J_{CP} = 12.1$ Hz, Ar), 134.3 (d, $J_{CP} = 11.0$ Hz, Ar), 132.6 (d, $J_{CP} = 9.6$ Hz, Ar), 131.6 (d, $J_{CP} = 12.0$ Hz, Ar), 131.5 (d, $J_{CP} = 28.5$ Hz, Ar), 130.9 (d, $J_{CP} = 31.0$ Hz, Ar), 129.8 (d, $J_{CP} = 10.0$ Hz, Ar), 129.3 (d, $J_{CP} = 2.1$ Hz, Ar), 129.0 (d, $J_{CP} = 2.1$ Hz, Ar), 128.3 (Ar), 128.1 (Ar), 128.0 (Ar), 127.3 (d, $J_{CP} = 8.7$ Hz, Ar), 127.2 (Ar), 127.1 (d, $J_{CP} = 8.0$ Hz, Ar), 118.0 (Ar), 107.9 (Ar), 106.3 (Ar), 56.8 (t, 4.8 Hz, NCHMo), 53.4 (d, 2.4 Hz, NCH₂), 31.6 (d, $J_{CP} = 7.8$ Hz, CH₂), 29.0 (CH₂), 27.5 (d, $J_{CP} = 25.7$ Hz, CH₂), 26.1 (t, 21.8 Hz, CH₂), 17.1 (CH₃), 13.7 (CH₃). ³¹P NMR (benzene-*d*₆, 161.78 MHz): 40.22 (d, 162.6 Hz, PPh₂), 16.20 (d, 162.6 Hz, PPh₂).

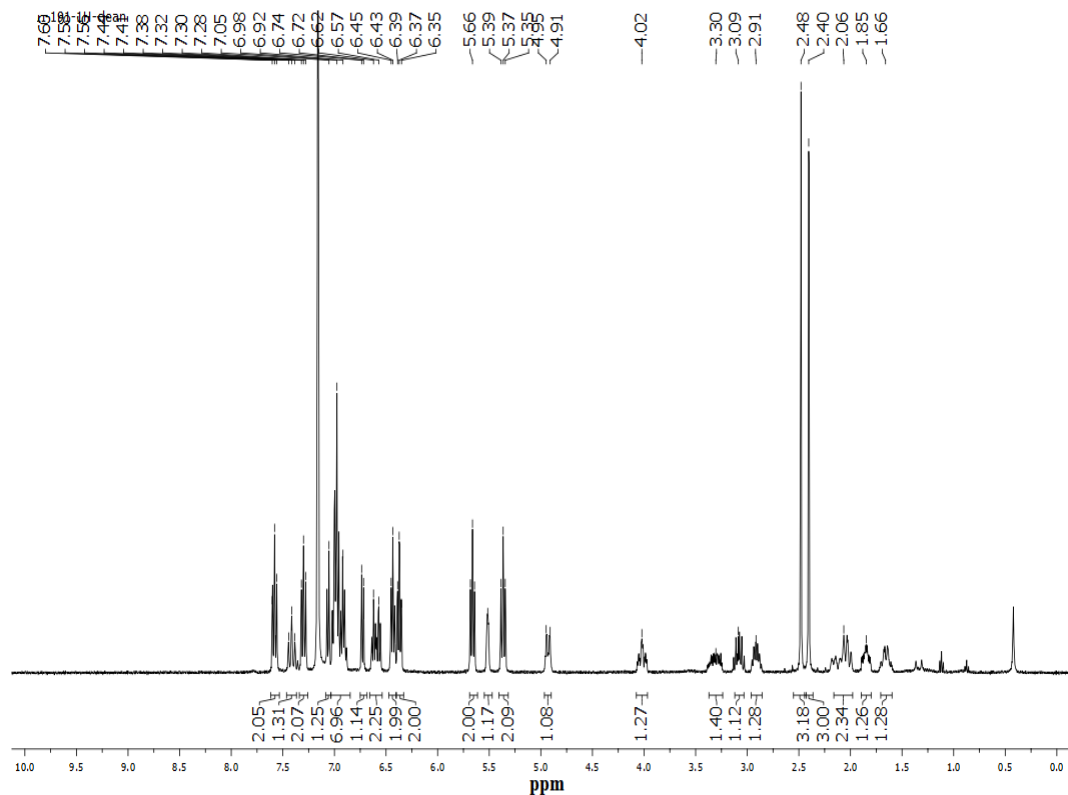


Figure 3.13. ¹H NMR spectrum of (κ⁶-P,N,N,N,C,P-Ph₂PPrPDI)MoI (7) in benzene-*d*₆.

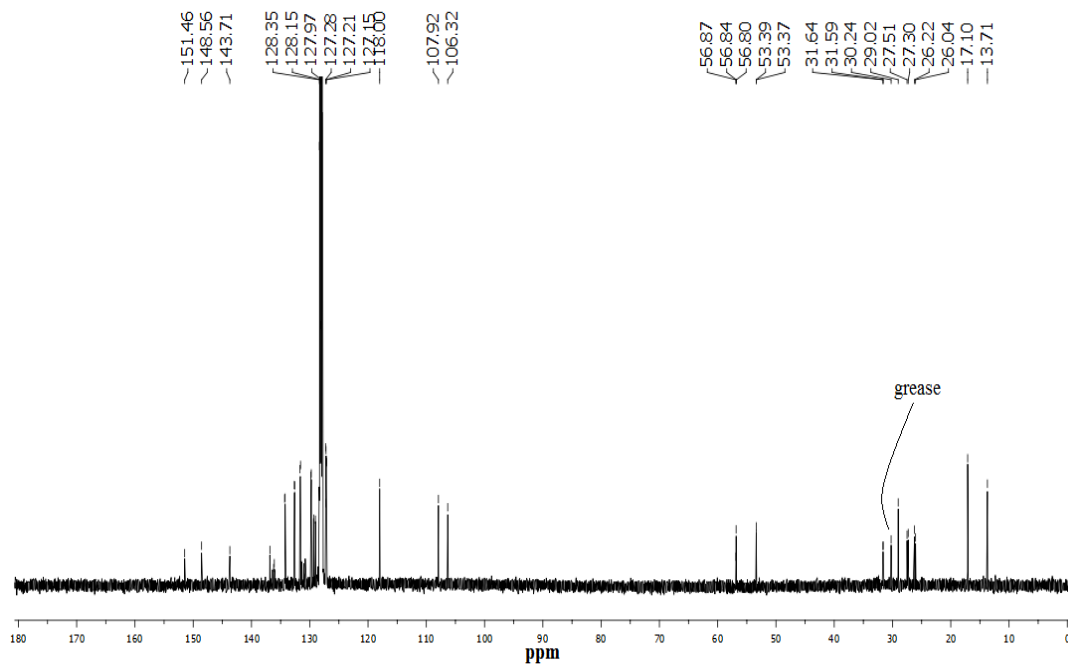


Figure 3.14. ^{13}C NMR spectrum of $(\kappa^6\text{-}P,N,N,N,C,P\text{-Ph}_2\text{PPrPDI})\text{MoI}$ (**7**) in benzene- d_6 .

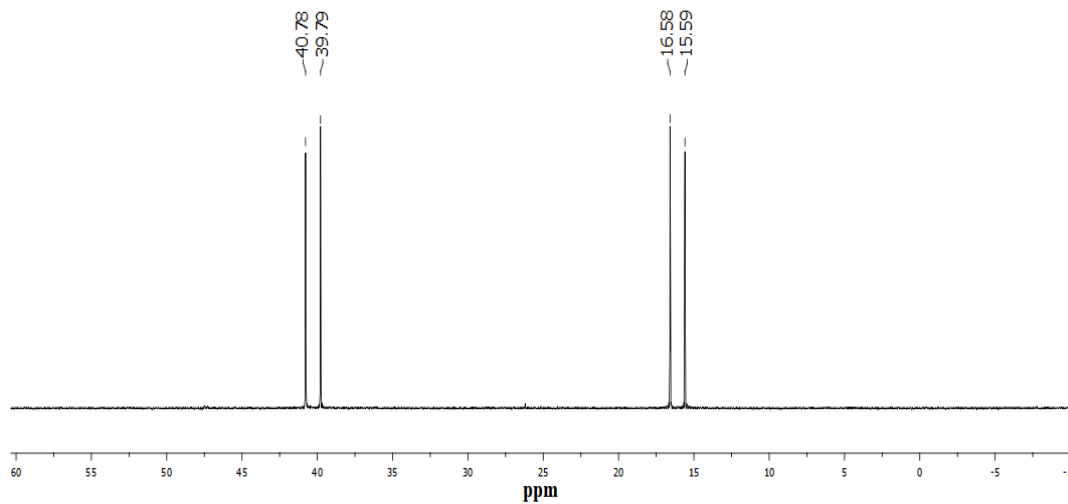


Figure 3.15. ^{31}P NMR spectrum of $(\kappa^6\text{-}P,N,N,N,C,P\text{-Ph}_2\text{PPrPDI})\text{MoI}$ (**7**) in benzene- d_6 .

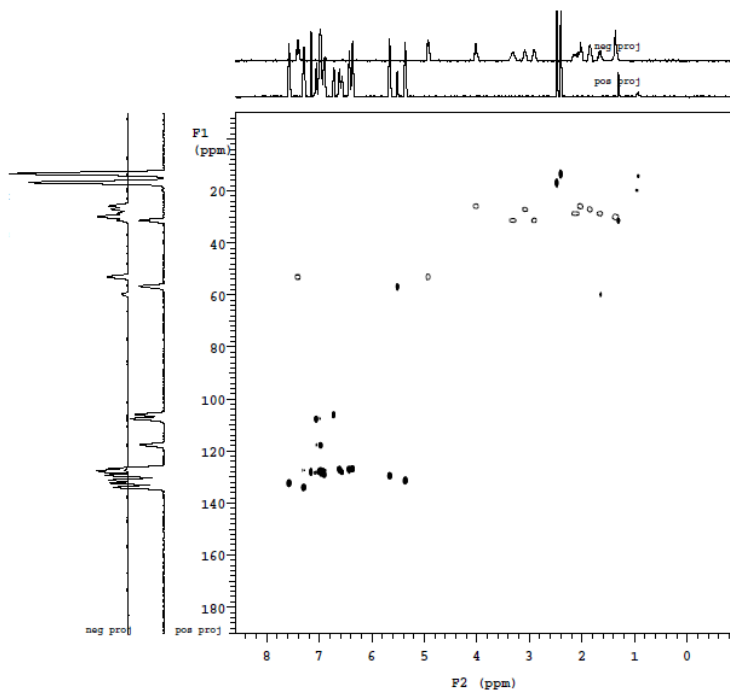


Figure 3.16. gHSQCAD NMR spectrum of **7** in benzene- d_6 .

3.5.7. Preparation of (Ph^2PPrPDI)MoI (**8**)

In a nitrogen filled glovebox, a 20 mL reaction vial was charged with 0.002 g (0.083 mmol) of freshly cut metallic sodium, 0.010 g (0.078 mmol) of naphthalene, and 3 mL of THF. The solution was stirred for 30 min to generate a green sodium naphthalenide solution. To the solution, 0.075 g (0.078 mmol) of **4** in 10 mL of THF was slowly added and the mixture was allowed to stir at ambient temperature for 24 h. The resulting brown solution was filtered through Celite and the solvent was removed *in vacuo* to yield a reddish-brown solid. After washing with pentane and drying, 0.049 g (75%) of a dark red solid identified as **8** was isolated. Single crystals suitable for X-ray diffraction were grown from a concentrated THF/toluene solution at $-35\text{ }^\circ\text{C}$. Elemental analysis for $\text{C}_{39}\text{H}_{41}\text{N}_3\text{IMoP}_2$: Calcd. C, 55.99%; H, 4.94%; N, 5.02%. Found: C, 56.10%; H, 4.70%; N, 4.53%. Magnetic susceptibility: $\mu_{\text{eff}} = 1.4(1)\ \mu_{\text{B}}$ (acetone- d_6 , $25\text{ }^\circ\text{C}$). ^1H NMR (benzene- d_6 ,

400 MHz, 25 °C): No resonances located. ^{31}P NMR (benzene- d_6 , 168.78 MHz, 25 °C): No resonances located.

3.5.8. Preparation of (Ph^2PPrPDI) MoH_2 (**9**)

Method 1. In a nitrogen filled glovebox, a 20 mL reaction vial was charged with 0.080 g (0.083 mmol) of **4** and 5 mL of toluene, and was placed in a liquid N_2 chilled cold well for 15 min. To it, 0.220 mL of 1.0 M NaEt_3BH in toluene solution dissolved in an additional 5 mL of toluene was added slowly and the mixture was allowed to stir at room temperature for 48 h. The resulting green solution was filtered through Celite and solvent was removed under vacuum. After washing with pentane and drying, 0.051 g (86%) of a green solid identified as **9** was isolated. Single crystals suitable for X-ray diffraction were obtained from a concentrated ether solution at -35 °C. *Method 2.* In a nitrogen filled glovebox, a 20 mL reaction vial was charged with 0.022 g (0.0263 mmol) of **7** and 3 mL of toluene, and was placed in a liquid N_2 chilled cold well for 15 min. To it, 0.090 mL of 1.0 M of toluene solution of NaEt_3BH in 5 mL of toluene was added slowly and the mixture was allowed to stir at room temperature for 48 h. The resulting green solution was filtered through Celite and solvent was removed under vacuum. After washing with pentane and drying, 0.010 g (55%) of a green solid identified as **9** was isolated. *Method 3.* In a nitrogen filled glovebox, a J. Young NMR tube was charged with 0.015 g (0.0211 mmol) of **5** dissolved in 0.7 mL of C_6D_6 . The solution was frozen in liquid nitrogen and degassed on a Schlenk line, and 1 atm of H_2 was added. After heating at 65 °C for 12 h, formation of **9** was observed by multinuclear NMR spectroscopy. Elemental analysis for $\text{C}_{39}\text{H}_{43}\text{N}_3\text{MoP}_2$: Calcd. C, 65.82%; H, 6.09%; N, 5.90%. Found: C, 66.12%; H, 6.42%; N, 5.96%. ^1H NMR (benzene- d_6 , 500 MHz): 7.77 (br, 4H, *Ph*), 7.51 (d, 8.0 Hz, 2H, *py*), 7.41 (t, 8.0 Hz, 1H, *py*), 7.13 (br,

2H, *Ph*), 7.06 (m, 4H, *Ph*), 6.58 (t, 7.0 Hz, 2H, *Ph*), 6.51 (t, 7.0 Hz, 4H, *Ph*), 5.68 (br, 4H, *Ph*), 5.44 (t, 12.0 Hz, 2H, NCH₂), 5.04 (d, 11.0 Hz, 2H, CH₂), 4.20 (t, 36.0 Hz, 2H, MoH₂), 2.53 (s, 6H, CH₃), 2.42 (t, 13.0 Hz, 2H, CH₂), 2.31 (m, 2H, CH₂), 2.02 (m, 2H, CH₂), 1.57 (m, 2H, CH₂). ¹³C NMR (benzene-*d*₆, 100.49 MHz): 143.8 (C=N), 142.6 (*Ar*), 138.5 (*Ar*), 135.3 (*Ar*), 132.7 (*Ar*), 132.0 (*Ar*), 131.8 (*Ar*), 130.9 (*Ar*), 130.5 (*Ar*), 128.5 (*Ar*), 127.4 (*Ar*), 115.6 (*Ar*), 106.9 (*Ar*), 64.8 (NCH₂), 32.5 (t, *J*_{CP} = 14.0 Hz, PCH₂), 29.9 (PCH₂CH₂), 13.7 (CH₃). ³¹P NMR (benzene-*d*₆, 161.78 MHz): 43.15 ppm. The following *T*₁ values (ms) for the hydride resonance of **7** were obtained via inversion recovery: 249 (20 °C), 204 (0 °C), 187 (-10 °C), 176 (-20 °C), 195 (-30 °C), 225 (-40 °C).

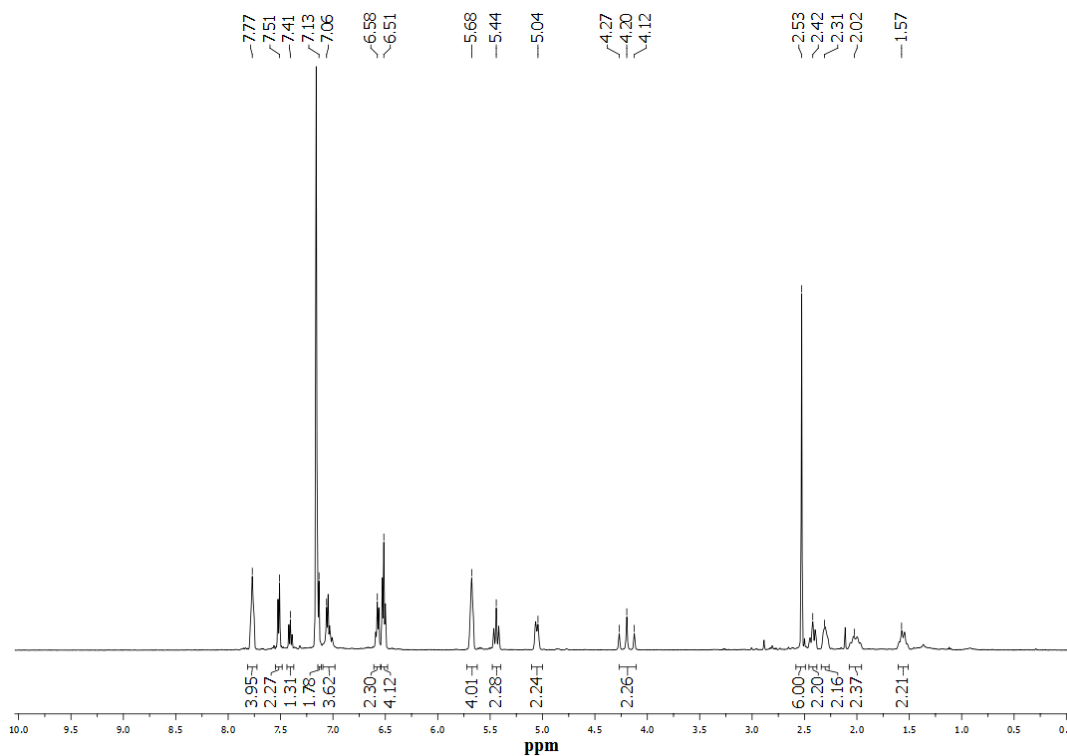


Figure 3.17. ¹H NMR spectrum of (Ph₂PPrPDI)MoH₂ (**9**) in benzene-*d*₆.

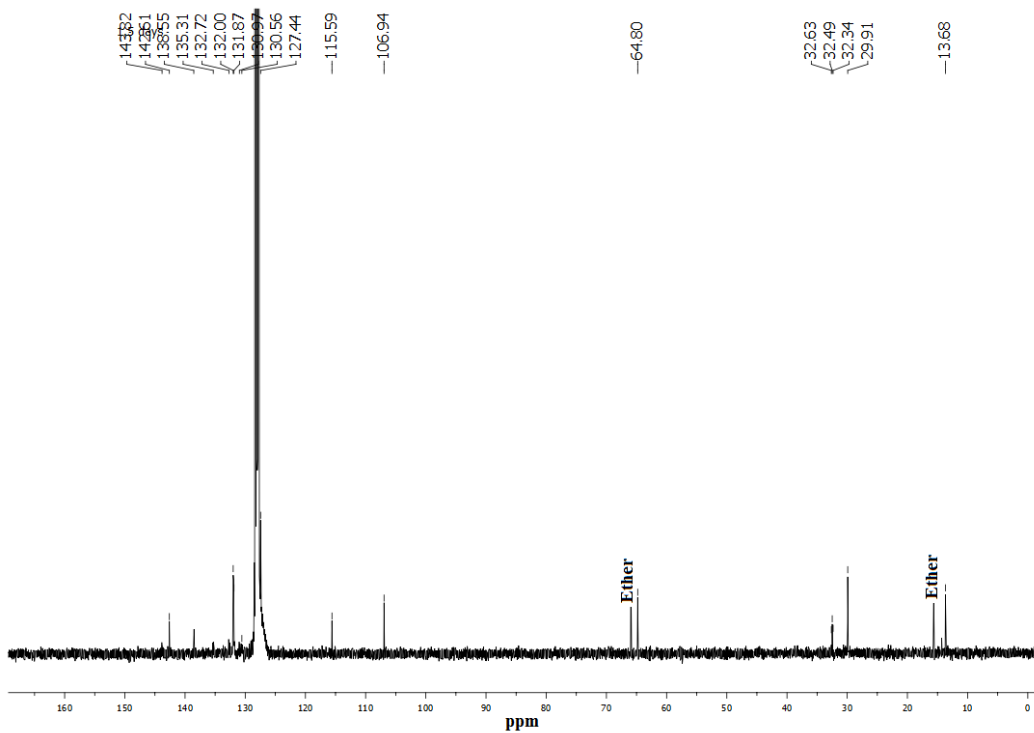


Figure 3.18. ^{13}C NMR spectrum of $(\text{Ph}^2\text{PPrPDI})\text{MoH}_2$ (**9**) in benzene- d_6 .

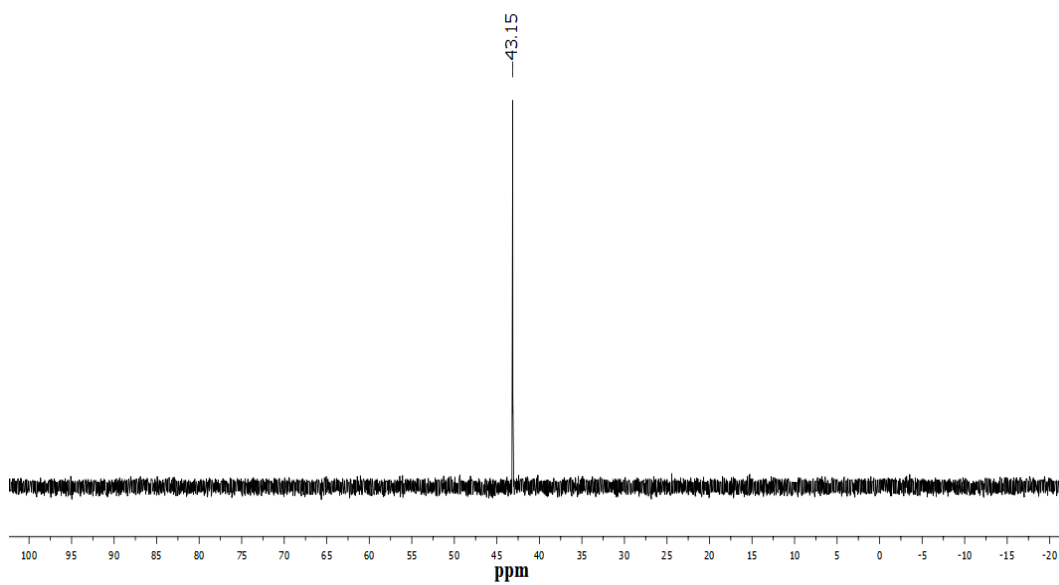


Figure 3.19. ^{31}P NMR spectrum of $(\text{Ph}^2\text{PPrPDI})\text{MoH}_2$ (**9**) in benzene- d_6 .

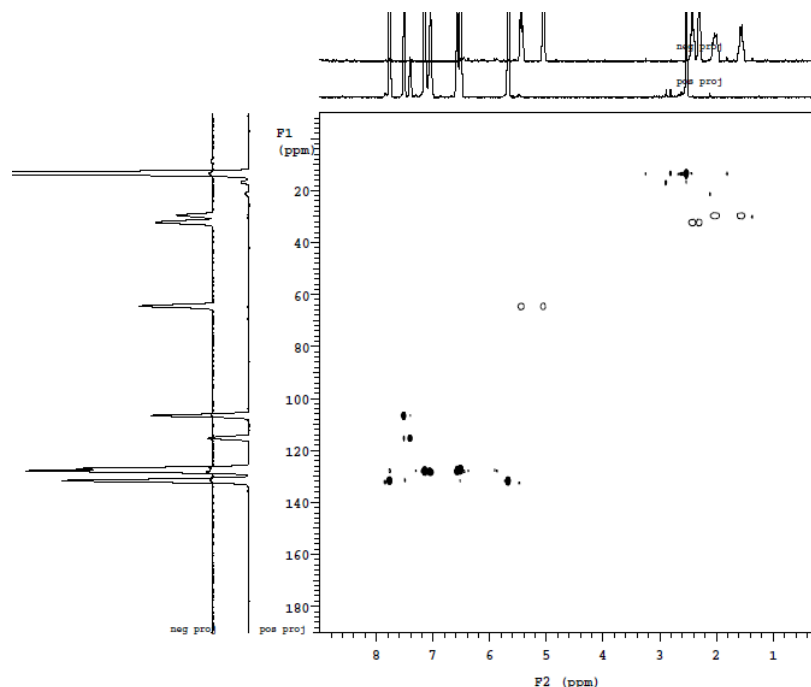


Figure 3.20. gHSQCAD NMR spectrum of (Ph_2PPrPDI) MoH_2 (**9**) in benzene- d_6 .

3.5.9. Observation of (Ph_2PPrPDI) MoD_2 (**9-d₂**)

In a nitrogen filled glovebox, a J. Young NMR tube was charged with **5** dissolved in 0.7 mL of C_6D_6 . The solution was frozen in liquid nitrogen, degassed on a Schlenk line, and 1 atm of D_2 was added. After heating at 65 °C for 12 h, formation of **9-d₂** was observed by multinuclear NMR spectroscopy. ^2H NMR (benzene- d_6 , 61.40 MHz): 4.13 (pseudo t, $J_{\text{DP}} = 4.9$ Hz, MoD_2). ^{31}P NMR (benzene- d_6 , 161.78 MHz): 43.50 ppm (m, PPh_2).

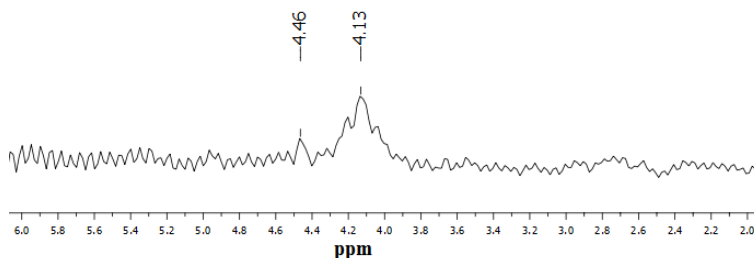


Figure 3.21. ^2H NMR spectrum of **7-d₂** in benzene- d_6 .

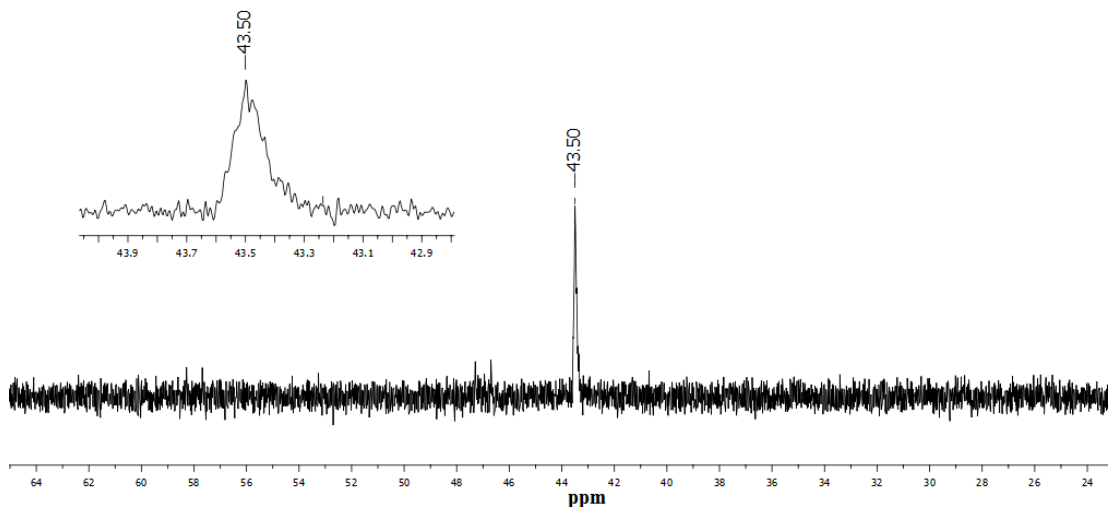


Figure 3.22. ^{31}P NMR spectrum of **9- d_2** in benzene- d_6 .

3.5.10. Alternative synthesis of (κ^6 - P,N,N,N,C,P -Ph 2 PPrPDI)MoH (**5**)

In a nitrogen filled glovebox, a 20 mL reaction vial was charged with 0.035 g (0.042 mmol) of **7** and 3 mL of toluene, and was placed in a liquid N_2 chilled cold well for 15 min. To it, 0.046 mL of 1.0 M toluene solution of NaEt_3BH in 4 mL of toluene was added slowly and the mixture was allowed to stir at room temperature for 36 h. The resulting green solution was filtered through Celite and the solvent was removed under vacuum. After washing with pentane and drying, 0.017 g (57%) of a green compound identified as **5** was isolated.

3.6. References

- (1) (a) Pal, R.; Cherry, B. R.; Flores, M.; Groy, T. L.; Trovitch, R. J. *Dalton Transactions* **2016**, 45, 10024-10033. (b) Kubas, G. J. *J. Organomet. Chem.* **2001**, 635, 37-68.
- (2) Schrock, R. R. *Acc. Chem. Res.* **2005**, 38, 955-962.
- (3) Schrock, R. R. *Chem. Rev.* **2002**, 102, 145-179.
- (4) Kubas, G. J.; Ryan, R. R.; Swanson, B. I.; Vergamini, P. J.; Wasserman, H. J. *J. Am. Chem. Soc.* **1984**, 106, 451-452.
- (5) Chatt, J.; Dilworth, J. R.; Richards, R. L. *Chem. Rev.* **1978**, 78, 589-625.
- (6) (a) Arashiba, K.; Miyake, Y.; Nishibayashi, Y. *Nature Chem.* **2011**, 3, 120-125. (b) Kinoshita, E.; Arashiba, K.; Kuriyama, S.; Miyake, Y.; Shimazaki, R.; Nakanishi, H.; Nishibayashi, Y. *Organometallics* **2012**, 31, 8437-8443.
- (7) Laplaza, C.; Cummins, C. C. *Science* **1995**, 268, 861-863.
- (8) Yandulov, D. V.; Schrock, R. R. *Science* **2003**, 301, 76-78.
- (9) Schrock, R. R. Murdzek, J. S.; Bazan, G. C.; Robbins, J.; DiMare, M.; O'Regan, M. J. *J. Am. Chem. Soc.* **1990**, 112, 3875-3886.
- (10) For an early review of Mo(II) chemistry see: Sheldon, J. C. *Nature* **1959**, 184, 1210-1213.
- (11) For examples of Mo(III) complex reactivity see: (a) Laplaza, C.; Johnson, M. J. A.; Peters, J. C.; Odom, A. L.; Kim, E.; Cummins, C. C.; George, G. N.; Pickering, I. J. *J. Am. Chem. Soc.* **1996**, 118, 8623-8638. (b) Cummins, C. C. *Chem. Commun.* **1998**, 1777-1786.
- (12) Hille, R. *Chem. Rev.* **1996**, 96, 2757-2816.
- (13) Haynes, W. M. *CRC Handbook of Chemistry and Physics: A Ready-reference Book of Chemical and Physical Data*, 94th ed.; Taylor & Francis, Boca Raton, FL, 2013-2014. Like Mo(I), Mo(0) is omitted from this list since it does not occur naturally.
- (14) Wilson, F. C.; Shoemaker, D. P. *J. Chem. Phys.* **1957**, 27, 809.
- (15) (a) Wrighton, M. S.; Ginley, D. S. *J. Am. Chem. Soc.* **1975**, 97, 4246-4251. (b) Hughey, J. L.; Bock, C. B.; Meyer, T. J. *J. Am. Chem. Soc.* **1975**, 97, 4440-4441.
- (16) Xhuang, B.; Huang L.; Yang, Y.; Lu, J. *Inorg. Chim. Acta* **1986**, 116, L41-L43.

- (17) (a) Shiu, K.-B.; Curtis, M. D.; Huffman, J. C. *Organometallics* **1983**, *2*, 936-938. (b) Curtis, M. D.; Shiu, K.-B.; Butler, W. M.; Huffman, J. C. *J. Am. Chem. Soc.* **1986**, *108*, 3335-3343.
- (18) Bartlett, I. A.; Connelly, N. G.; Orpen, A. G.; Quayle, M. J.; Rankin, J. C. *Chem. Commun.* **1996**, 2583-2584.
- (19) McWhillie, S. L. W.; Jones, C. J.; McCleverty, J. A.; Collison, D.; Mabbs, F. E. *J. Chem. Soc., Chem. Commun.* **1990**, 940-942.
- (20) Connelly, N. G.; Geiger, W. E.; Lovelace, S. R.; Metz, B.; Paget, T. J.; Winter, R. *Organometallics* **1999**, *18*, 3201-3207.
- (21) Seidel, W. W.; Arias, M. D. I.; Schaffrath, M.; Jahnke, M. C.; Hepp, A.; Pape, T. *Inorg. Chem.* **2006**, *45*, 4791-4800.
- (22) Beissel, T.; Della Vedova, B. S. P. C.; Wieghardt, K.; Boese, R. *Inorg. Chem.* **1990**, *29*, 1736-1741.
- (23) Wang, M.; Weyhermüller, T.; Wieghardt, K. *Chem. Eur. J.* **2014**, *20*, 9037-9044.
- (24) Wang, M.; Weyhermüller, T.; Wieghardt, K. *Eur. J. Inorg. Chem.* **2015**, 3246-3254.
- (25) Roberts, K. A. E.; Brown, N. J.; Roberts, H. N.; McDouall, J. J. W.; Low, P. J.; Whitely, M. W. *Polyhedron* **2015**, *86*, 89-97.
- (26) Ben-Daat, H.; Hall, G. B.; Groy, T. L.; Trovitch, R. J. *Eur. J. Inorg. Chem.* **2013**, 4430-4442.
- (27) Pal, R.; Groy, T. L.; Bowman, A. C.; Trovitch, R. J. *Inorg. Chem.* **2014**, *53*, 9357-9365.
- (28) Pal, R.; Groy, T. L.; Trovitch, R. J. *Inorg. Chem.* **2015**, *54*, 7506-7515.
- (29) Baker, P. K.; Fraser, S. G.; Keys, E. M. *J. Organomet. Chem.* **1986**, *309*, 319-321.
- (30) DuBois, D. W.; Iwamoto, R. T.; Kleinberg, J. *Inorg. Chem.* **1970**, *9*, 968-970.
- (31) (a) Luca, O. R.; Crabtree, R. H. *Chem. Soc. Rev.* **2013**, *42*, 1440. (b) Lyaskovskyy, V.; de Bruin, B. *ACS Catal.* **2012**, *2*, 270-279. (c) Chirik, P. J.; Wieghardt, K. *Science* **2010**, *327*, 794-795. (d) Bouwkamp, M. W.; Bowman, A. C.; Lobkovsky, E.; Chirik, P. J. *J. Am. Chem. Soc.* **2006**, *128*, 13340-13341.
- (32) Knijnenburg, Q.; Gambarotta, S.; Budzelaar, P. H. M. *Dalton Trans.* **2006**, 5442-5448.

(33) Crabtree, R. H. *Acc. Chem. Res.* **1990**, *23*, 95-101.

(34) Weil, J. A.; Bolton, J. R. *Electron paramagnetic resonance: Elementary theory and practical applications*; Wiley, Hoboken, NJ, 2007.

(35) Stoll, S.; Schweiger, A. *J. Magn. Reson.* **2006**, *178*, 42-55.

CHAPTER 4

HYDROGEN EVOLUTION FROM WATER USING A BIS(IMINO)PYRIDINE MOLYBDENUM OXO COMPLEX

4.1. Abstract

Heating an acetonitrile solution of $[(^{\text{Ph}_2\text{PPr}}\text{PDI})\text{MoI}][\text{I}]$ (**4**) and styrene oxide with two equivalents of AgPF_6 at $60\text{ }^\circ\text{C}$ allowed for the isolation of $[(^{\text{Ph}_2\text{PPr}}\text{PDI})\text{MoO}][\text{PF}_6]_2$ (**10**), which was found to be an active precatalyst for electrocatalytic generation of H_2 from neutral water. Analysis of **10** by cyclic voltammetry revealed two reversible transitions at -0.70 V and -1.26 V vs $\text{Fc}^{+/0}$, corresponding to the $\text{Mo}^{\text{IV/III}}$ and $\text{Mo}^{\text{III/II}}$ redox couples, respectively. Two irreversible redox events corresponding to $\text{Mo}^{\text{II/I}}$ and $\text{Mo}^{\text{I/0}}$ were also observed at -1.53 and -1.95 V vs $\text{Fc}^{+/0}$, respectively. This complex acts as an efficient electrocatalyst for the production of dihydrogen from neutral water with 96% faradaic efficiency at an overpotential of 2.46 V and a rate constant of 55 s^{-1} . Two electron reduction of **10** using $\text{K/C}_{10}\text{H}_8$ afforded the key intermediate $(^{\text{Ph}_2\text{PPr}}\text{PDI})\text{MoO}$ (**11**), a rare example of a $\text{Mo}(\text{II})$ oxo complex. The intermediate **11** likely mediates H_2 evolution through sequential proton-coupled electron transfer steps to form $(^{\text{Ph}_2\text{PPr}}\text{PDI})\text{Mo}(\text{OH}_2)$ (**12**), which releases H_2 following O-H oxidative addition and 1,2-elimination.

Parts of this chapter have been reproduced from Pal, R.; Laureanti, J. A.; Groy, T. L.; Jones, A. K.; Trovitch, R. J. *Chemical Communications* **2016**, 52, 11555-11558 with the permission of *Royal Society of Chemistry*.

4.2. Introduction

The search for a renewable, carbon-neutral, and sustainable energy sources has become a long-standing challenge for scientists in the 21st century.¹⁻³ While technological advances have been made in solar energy conversion, converting electrical energy into high-energy chemical bonds appears to be a promising energy storage methodology.⁴⁻⁶ Due to its eco-friendly combustion to water and high energy density, dihydrogen has emerged as an attractive replacement for fossil fuels.^{5,7} Hence, developing catalysts which can facilitate the reduction of protons to dihydrogen while utilizing earth-abundant, low-cost resources, such as neutral pH water, can offer a potential alternative to address the high energy demands of modern infrastructure.^{4,7,8} Water electrolysis is a mature industrial technology; however, Ni/C cathodes require highly basic conditions while Pt cathodes are costly and operated under highly acidic conditions.⁹⁻¹¹ To be economically practical and deployable on an industrial scale, catalysts comprised of inexpensive and abundant elements are highly desirable.¹² This drive has led researchers to develop numerous molecular electrocatalysts based on low-cost and earth-abundant first row-transition metals.^{7,13-15}

While interest in using first-row transition metal-based homogeneous catalysts for proton reduction has continued to gain momentum, weak organic acids are often required as the proton source and they often suffer from poor solubility, stability, and activity in presence of water.¹⁴ However, there are organometallic compounds which have shown unusual tolerance to water and exhibited interesting water activation chemistry.¹⁶⁻²¹ In particular, the work by Tyler and Yoon²⁰ showed that the low-valent molybdenum cyclopentadienyl compound (Cp₂Mo) undergoes O-H oxidative addition of water followed

by 1,2-elimination of H₂ to yield the corresponding oxo complex (Cp₂Mo=O). Recently, high-valent molybdenum compounds have shown promising catalytic activity, robustness, and sustainability for HER while employing water as the feedstock in either neutral⁸ or acidic solutions.^{22,23} In 2010, Long and coworkers reported a polypyridyl molybdenum(IV) oxo precatalyst, [(PY₅Me₂)MoO][PF₆]₂ which generates dihydrogen from a pH = 7 aqueous solution with a TOF 2.3 s⁻¹ at an overpotential of 1.0 V.⁸ On the other hand, the disulfide analogue, [(PY₅Me₂)Mo(S₂)] [OSO₂CF₃]₂ was found to catalyze hydrogen evolution from pH = 3 solution with TOFs as high as 480 s⁻¹ at an overpotential of 0.78 V.²² Inspired by these literature precedents, this manuscript describes the preparation of a robust Mo(IV) oxo electrocatalyst for H₂ production from neutral pH water and its mechanism of operation.

4.3. Results and Discussion

In the previous chapters, we reported the multi-step synthesis of [(^{Ph}2PPrPDI)MoI][I]₂²⁴ (**4**) starting from (^{Ph}2PPrPDI)Mo(CO) (**2**)²⁵ through oxidation of the metal center by I₂ followed by thermal removal of the CO ligand. Alternatively, an improved, one-step synthesis of **4** has also been reported by heating an equimolar mixture of ^{Ph}2PPrPDI²⁶ and (CH₃CN)₂(CO)₃MoI₂²⁷ at 110 °C.²⁸ Heating an acetonitrile solution of **4** and styrene oxide at 60 °C in the presence of two equivalents of silver hexafluorophosphate (AgPF₆) resulted in a bright orange compound within a few hours of stirring. Isolation of the desired product and analysis by ¹H NMR revealed a C_s-symmetric chelate environment about Mo with six methylene resonances (Figure 4.2). An equivalent ligand environment is also evidenced by ³¹P NMR spectroscopy exhibiting a singlet at 22.9 ppm and a septet at -143.6 ppm which

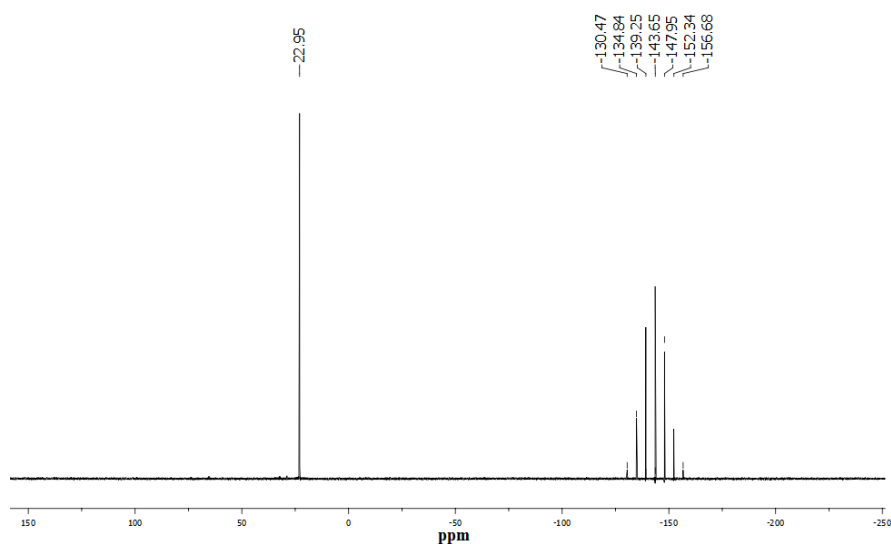


Figure 4.3. ^{31}P NMR spectrum of $[(\text{Ph}_2\text{PPrPDI})\text{MoO}][\text{PF}_6]_2$ (**10**) in acetonitrile- d_3 .

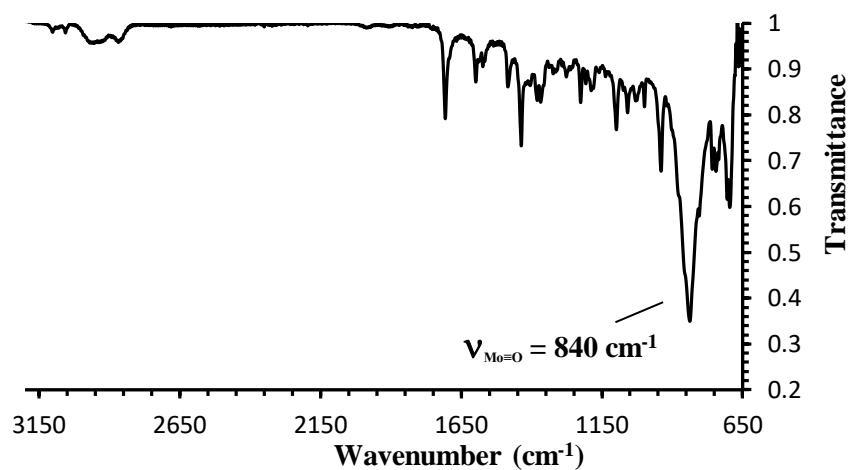


Figure 4.4. Infrared spectrum of $[(\text{Ph}_2\text{PPrPDI})\text{MoO}][\text{PF}_6]_2$ (**10**) in KBr.

A pseudo-octahedral molecular geometry of **10** was confirmed by single crystal X-ray diffraction (Figure 4.5) with N(1)-Mo(1)-N(3) and P(1)-Mo(1)-P(2) angles of 139.92(9) and 176.84(2) $^\circ$, respectively (Table 4.1). The short Mo(1)-O(1) distance of 1.693(2) \AA is consistent with the presence of a triple bond,^{16,24} rendering **10** an 18-electron complex.

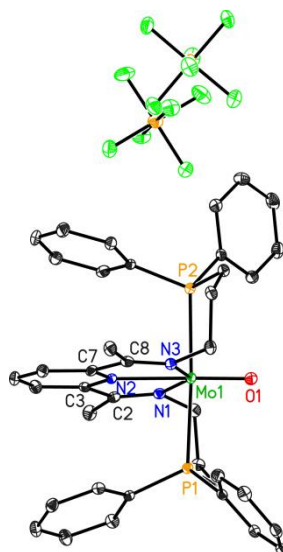


Figure 4.5. The solid-state structure of **10** shown at 30% probability ellipsoids. Hydrogen atoms have been omitted for clarity.

Table 4.1. Notable bond lengths (Å) and angles (°) determined for **10**, compared with those reported for **11**.

| | 10 | 11 |
|-----------------|-----------|------------|
| Mo(1)-N(1) | 2.140(2) | 2.062(4) |
| Mo(1)-N(2) | 2.240(2) | 2.101(3) |
| Mo(1)-N(3) | 2.134(2) | 2.068(4) |
| Mo(1)-P(1) | 2.526(8) | 2.530(14) |
| Mo(1)-P(2) | 2.537(8) | 2.508(14) |
| Mo(1)-O(1) | 1.693(2) | 1.797(3) |
| N(1)-C(2) | 1.294(4) | 1.355(5) |
| N(3)-C(8) | 1.301(4) | 1.363(5) |
| C(2)-C(3) | 1.469(3) | 1.420(7) |
| C(7)-C(8) | 1.480(4) | 1.401(7) |
| N(1)-Mo(1)-N(3) | 139.92(9) | 143.9(14) |
| P(1)-Mo(1)-P(2) | 176.84(2) | 166.80(4) |
| N(2)-Mo(1)-O(1) | 179.10(9) | 176.61(16) |

4.3.1. Cyclic Voltammetry

The redox chemistry of **10** was probed by cyclic voltammetry in 0.1 M tetrabutylammonium hexafluorophosphate (TBAPF₆) in dry acetonitrile. As shown in Figure 4.6, cyclic voltammetry of **10** shows two reversible transitions corresponding to Mo^{IV/III} and Mo^{III/II} at $E_{1/2} = -0.70$ V ($i_p^a/i_p^c = 1.20$, $\Delta E_p = 0.08$ V) and $E_{1/2} = -1.26$ V ($i_p^a/i_p^c = 0.85$, $\Delta E_p = 0.08$ V), respectively. Two irreversible transitions corresponding to Mo^{III/I} and Mo^{I/0} are centered at -1.53 and -1.95 V vs Fc⁺⁰ (Fc = ferrocene), respectively. Cycling to potentials more oxidizing than +0.5 V vs Fc⁺⁰ results in the loss of the peaks attributed to the Mo^{IV/III} and Mo^{III/II} transitions. However, when the potential is maintained at potentials less oxidizing than Fc⁺⁰, the Mo^{IV/III} and Mo^{III/II} transitions do not diminish in reversibility.

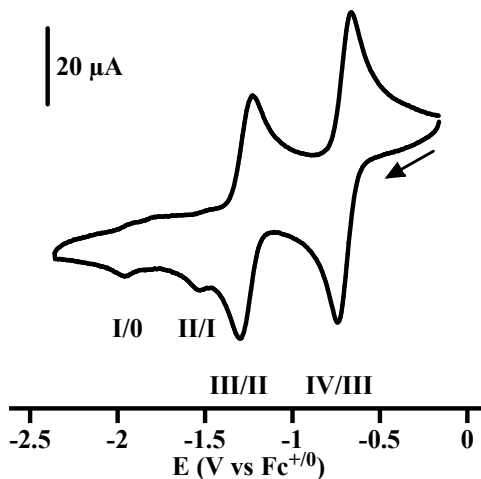


Figure 4.6. Cyclic voltammogram of 2.1 mM **10** in dry acetonitrile. Experimental conditions: 0.1 M TBAPF₆ in acetonitrile with a scan rate of 0.2 V s⁻¹. Arrow indicates the initiation point and direction of the cyclic voltammogram.

4.3.2. Catalysis in the Presence of Water

The electrocatalytic activity of **10** for the reduction of water to dihydrogen was investigated in dry acetonitrile (ACN), within a potential scan window of -1.3 to -2.8 V vs $\text{Fc}^{+/0}$ (Figure 4.7). The ability of the glassy carbon electrode to reduce H_2O to H_2 is negligible in this region (Figure 4.7B). In the presence of **10**, sequential addition of water from 0.1 to 4.0 M, produces a catalytic wave with linear increase in catalytic current as more substrate is introduced (Figure 4.7A). The peak catalytic current, defined here as i_{cat} , in the presence of >4.0 M water, is independent of water concentration (Figure 4.8A). Furthermore, at water concentrations >2.0 M, a pair of reversible redox transitions at $E_{1/2} = -1.96$ V ($i_p^a/i_p^c = 1.07$ $\Delta E_p = 0.09$ V) for $[\text{H}_2\text{O}] = 3.5$ M appear that are not observed at lower concentrations of water (Figure 4.8B). It should be noted that the development of the new transition was independent of time, i.e. the catalyst resting in a low concentration of water did not develop the reversible couple, while a dramatic increase of water from 0 to 2.0 M immediately produced the reversible couple upon electrochemical analysis.

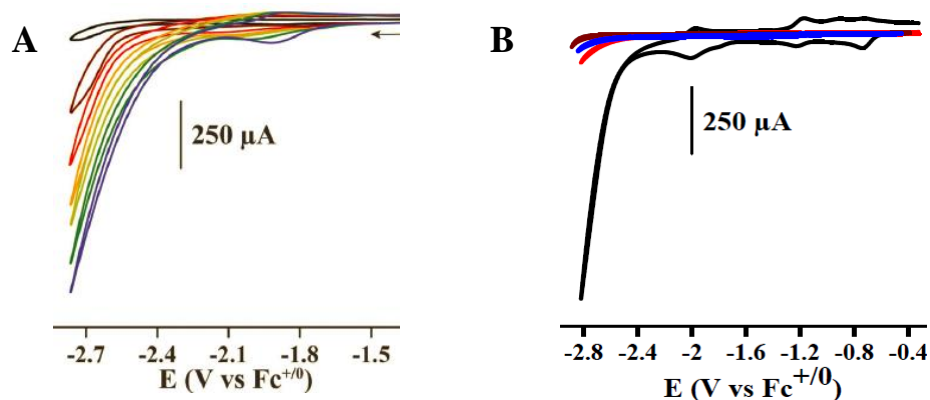


Figure 4.7. **A.** Cyclic voltammograms of 1.25 mM **10** in acetonitrile. $[\text{H}_2\text{O}] = 0.0$ M (black), 0.5 M (dark red), 1.0 M (red), 1.5 M (orange), 2.0 M (yellow-green), 3.0 M (green), and 6.0 M (blue). **B.** Cyclic voltammogram from 2.0 mM **10** in 3.5 M water in acetonitrile

containing 0.1 M TBAPF₆ (black). Control experiments employing a rinsed working electrode immediately following electrocatalysis and transferred to a neat acetonitrile solution containing 0 M (dark red) and 5.0 M water (red). To illustrate that catalysis at a glassy carbon electrode is negligible, a solution of acetonitrile containing 6.0 M water in the absence of catalyst is shown (blue). Potential scan rate is 0.2 V s⁻¹.

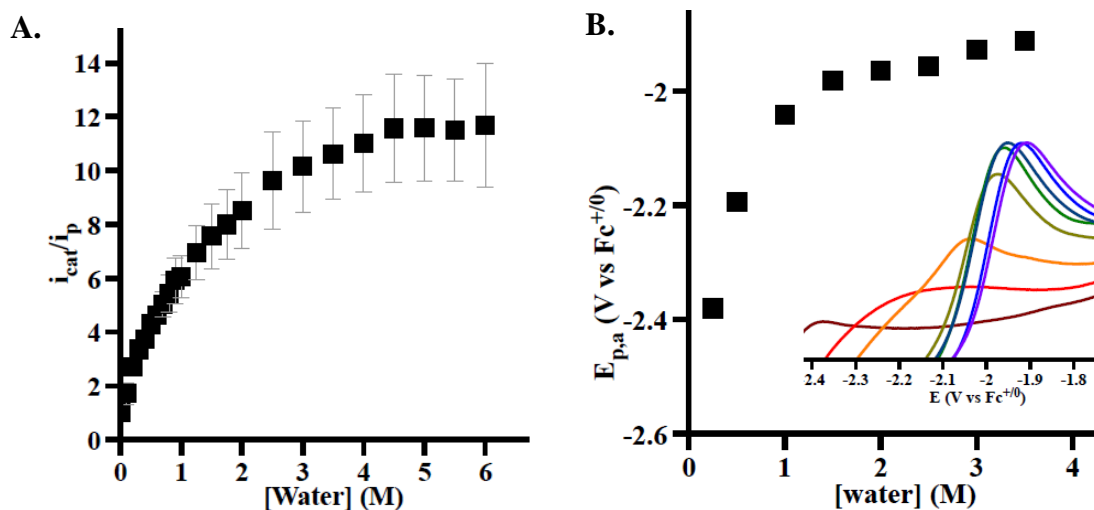


Figure 4.8. **A.** Dependence of catalytic current (i_{cat}/i_p) on concentration of water. Data (squares, $k = 55 \pm 15$ s⁻¹) are averaged from three individual experiments and error bars represent one standard deviation. **B.** Anodic peak that develops at increasing water concentrations. Inset (Figure 4.7B constrained to the potential window of the developing anodic transition) shows the linear sweep voltammograms from which the potentials are derived. Experimental conditions are defined in Figure 4.6.

Production of H₂ was detected experimentally by gas chromatography *via* analysis of the head-space from a sealed electrochemical cell following controlled potential electrolysis at -2.5 V vs Fc⁺⁰. The faradaic efficiency of hydrogen evolution for **10** was calculated to be 96%. The observed overpotential was directly determined for each addition of water to acetonitrile by measuring the open circuit potential (OCP) and further referencing each addition of water to Fc⁺⁰ as described by Roberts and Bullock.²⁹ Table 4.2 summarizes the values for $E_{p/2}$, overpotential, and OCP values, corrected to V vs Fc⁺⁰,

obtained for each concentration of water investigated, where $E_{p/2}$ is the half-wave potential of the catalytic wave. The overpotential ranges from 1.65 to 1.70 V from 0.2 to 6.0 M water, respectively. The “rinse test” shows that **10** does not decompose to form a heterogeneous nanocatalyst on the electrode surface. Immediately following an electrocatalytic experiment with **10**, the working electrode was rinsed with acetonitrile. As shown in Figure 4.7B, cyclic voltammetry in a fresh ACN or 5.0 M H₂O/ACN solution showed no detectable faradaic peaks or electrocatalysis. This indicates **10** remains in solution throughout the electrocatalytic experiments.

Table 4.2 Overpotential calculated from the open circuit potential (OCP) vs $Fc^{+/0}$ and $E_{p/2}$ of the catalytic wave associated with **10** at the specified concentration of water in acetonitrile.

| [H ₂ O] (M) | OCP (V vs $Fc^{+/0}$) | $E_{p/2}$ (V vs $Fc^{+/0}$) | Overpotential OCP – $E_{p/2}$ (V) |
|---------------------------|---------------------------|---------------------------------|---|
| 0.2 | -1.10 | -2.75 | 1.65 |
| 0.4 | -1.07 | -2.74 | 1.67 |
| 0.6 | -1.12 | -2.70 | 1.58 |
| 1.8 | -1.08 | -2.68 | 1.60 |
| 2.0 | -1.08 | -2.69 | 1.61 |
| 3.5 | -1.03 | -2.65 | 1.62 |
| 4.0 | -1.03 | -2.65 | 1.62 |
| 5.0 | -1.01 | -2.64 | 1.63 |
| 6.0 | -0.94 | -2.64 | 1.70 |

The kinetics for the reduction of water to dihydrogen by **10** were evaluated using Equations 1-3, where i_{cat} is the catalytic peak current, i_{cat}/i_p is the ratio of peak catalytic current (i_{cat}) to the peak current (i_p) in the absence of substrate, n is the number of electrons in the reaction, F is Faraday's constant, A is the area of the electrode, D is the diffusional coefficient of the catalyst, k is the rate constant, R is the ideal gas constant, and T is the temperature in Kelvin. Figure 4.9A shows that i_{cat} is linear with respect to the concentration of catalyst in solution from 0.75 to 1.75 mM of **10**. This shows a first order dependence with respect to **10**. Figure 4.9B shows that the catalytic current, defined as i_{cat}/i_p , is linear with respect to the concentration of water in solution. This shows a second order dependence with respect to acid at a scan rate of 0.2 V s^{-1} . Using the average rate for proton reduction calculated by Equation 3 for the acid independent region (4.5 - 6.0 M H_2O) $k = 55 \pm 15 \text{ s}^{-1}$.

$$i_{cat} = nFA[cat]\sqrt{D(k[acid]^x)} \quad (\text{Eq. 1})$$

$$\frac{i_{cat}}{i_p} = \left(\frac{n}{0.4463}\right)\sqrt{RT(k[acid]^x)/Fv} \quad (\text{Eq. 2})$$

$$\frac{i_{cat}}{i_p} = \left(\frac{n}{0.4463}\right)\sqrt{RTk/Fv} \quad (\text{Eq. 3})$$

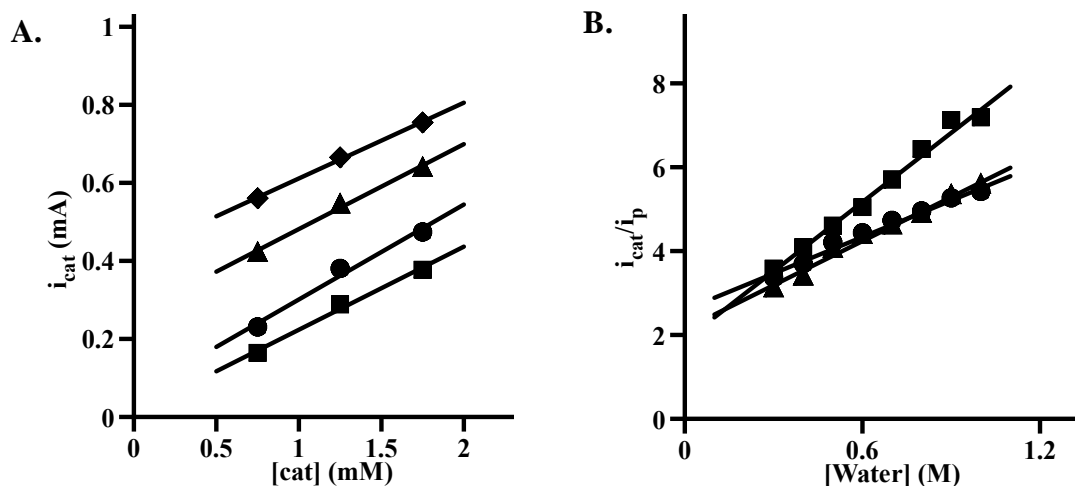


Figure 4.9. **A.** Catalytic current depends linearly on the concentration of **10** present in the experiment irrespective of water concentrations. Squares, circles, triangles, and diamonds refer to 0.3, 0.6, 1.75, and 3.0 M water, respectively. Solid lines are the lines of best fit with $R^2 = 0.99$. **B.** Dependence of normalized catalytic current on water concentration. Triangles, squares, and circles refer to currents extracted from cyclic voltammograms at -2.8 V vs $\text{Fc}^{+/0}$ for solutions containing **10** at 0.75, 1.25, and 1.75 mM, respectively. Solid lines are the lines of best fit ($R^2 = 0.98$). Experimental conditions: acetonitrile containing 0.1 M TBAPF_6 with a scan rate of 0.2 V s^{-1} . Averaging the rate constant obtained from these three individual experiments (in the water concentration range of 0.3 to 1.0 M) yields $k = 25 \pm 5 \text{ s}^{-1}$.

4.4. Mechanism Elucidation

Based on the experimental evidence, we sought to understand the mechanism of catalytic water reduction. Cyclic voltammetry of **10** exhibits two reversible single electron reduction processes and two irreversible reduction events before the initiation of catalytic current. Knowing the first two redox events were reversible, a neutral molybdenum oxo compound, **11** was isolated by chemical reduction of **10** using two equivalents of potassium naphthalenide (Figure 4.10). Work-up of the resulting reddish-brown solution followed by multinuclear NMR spectroscopic analysis revealed a diamagnetic product featuring a ^{31}P NMR singlet at 4.88 ppm (Figure 4.12). Due to the presence of two strong π -acceptor

phosphine donor sites, stabilization and isolation of the low-valent, terminal molybdenum (II) oxo intermediate has been achieved. This observation supports our hypothesis that two successive reversible one-electron reductions of **10** allowed for the formation of **11** (the resting state of the catalysis). The solid-state structure of **11** was determined by single crystal X-ray diffraction (Figure 4.14) and revealed a near octahedral geometry. A significant elongation of the Mo-O bond to 1.797 (3) in **11** compared to 1.693 (2) of **10** confirms the reduction of molybdenum oxidation state to Mo(II) from Mo(IV). This is also evident from significantly elongated PDI chelate of **11** which features N(1)–C(2) and N(3)–C(8) distances of 1.355(5) and 1.363(5) Å, along with contracted C(2)–C(3) and C(7)–C(8) distances of 1.420(7) and 1.401(7) Å, respectively (Table 4.1). These bond lengths are largely consistent with those reported for Ph_2PPrPDI supported Mo(II) complexes.^{24,25,28}

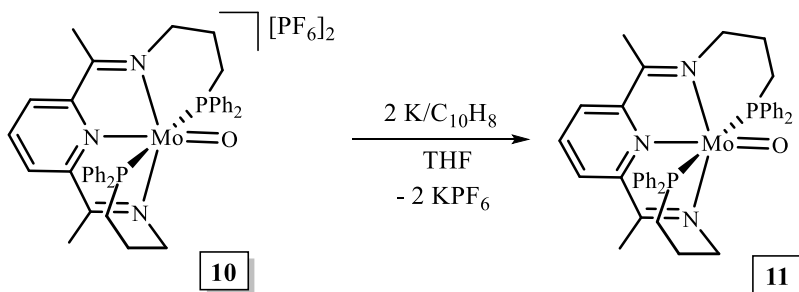


Figure 4.10. Synthesis of $(\text{Ph}_2\text{PPrPDI})\text{MoO}$ (**11**).

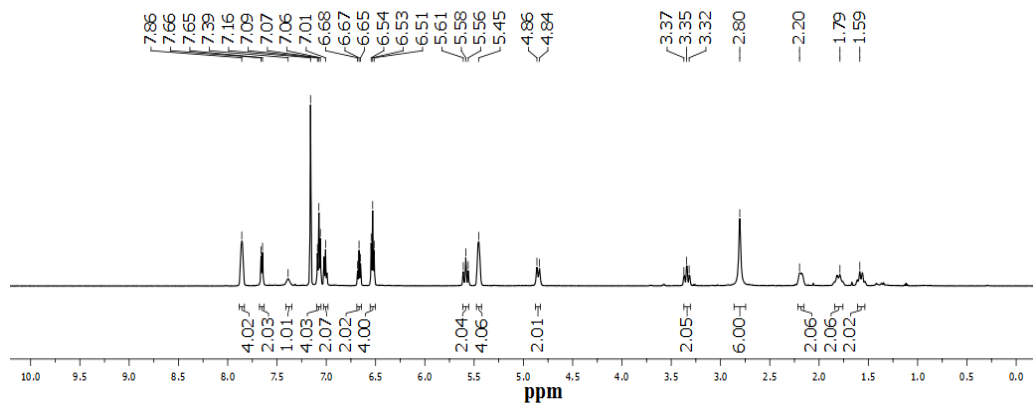


Figure 4.11. ^1H NMR spectrum of $(\text{Ph}_2\text{PPrPDI})\text{MoO}$ (**11**) in benzene- d_6 .

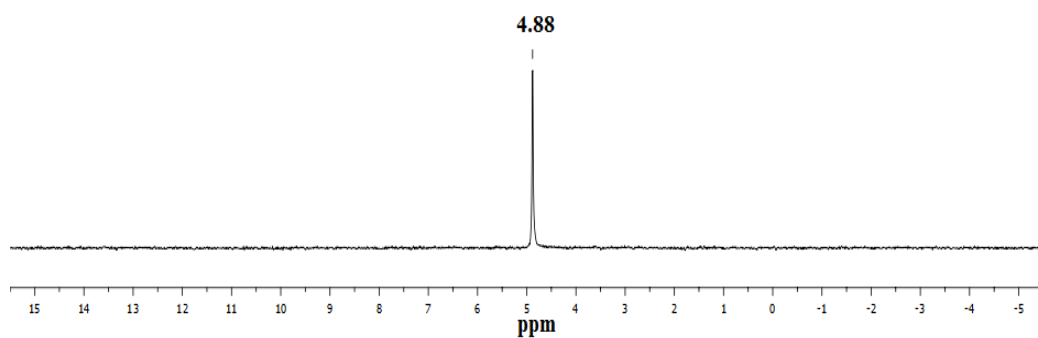


Figure 4.12. ^{31}P NMR spectrum of $(\text{Ph}_2\text{PPrPDI})\text{MoO}$ (**11**) in benzene- d_6 .

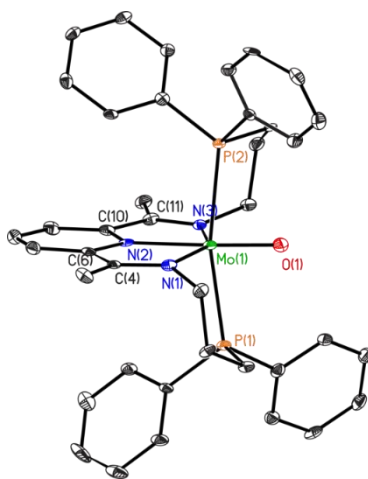


Figure 4.13. The solid-state structure of **11** shown at 30% probability ellipsoids. Hydrogen atoms have been removed for clarity.

Due to the weakened bond strength, Mo=O in compound **11** exerts high nucleophilicity⁸ and undergoes two consecutive proton-coupled single-electron transfer (PCET) processes to form $[(\text{Ph}_2\text{PPrPDI})\text{Mo}^{\text{I}}(\text{OH})]$ and then $[(\text{Ph}_2\text{PPrPDI})\text{Mo}^0(\text{H}_2\text{O})]$. The formation of $[(\text{Ph}_2\text{PPrPDI})\text{Mo}^0(\text{H}_2\text{O})]$ is supported by the accumulation of the reversible transition with $E_{1/2} = -1.96$ V at higher concentrations of water ($>2\text{M}$) during catalytic experiments (Figure 4.8B). However, zerovalent $\text{Ph}_2\text{PPrPDI}\text{Mo}$ is known to undergo C-H activation of the chelate to yield an 18-electron compound.^{24,28} Therefore, there are two possible mechanistic pathways that must be considered: (a) **11**-mediated O-H oxidative addition followed by 1,2-elimination of H_2 (Fig. 4.18) and (b) protonation of chelate-activated $[(\kappa^6\text{-}P,N,N,N,C,P\text{-Ph}_2\text{PPrPDI})\text{MoH}]$ to liberate H_2 followed by 1,2-elimination of the chelate (Fig. 4.19).

To get further insight about the mechanism, stoichiometric water was added to **5** (Figure 4.14). Generation of the neutral oxo compound with concomitant release of dihydrogen gas was observed by ^1H NMR spectroscopy (Figure 4.15). Knowing that the involvement of the ligand arm is possible during the evolution of dihydrogen from water, a controlled potential electrolysis experiment using **10** and excess D_2O was performed. After continuous accumulation of charge for 30 min, the post electrolysis solution was analyzed by multinuclear NMR spectroscopy. While ^{31}P NMR spectrum showed a singlet at 22.9 ppm corresponding to **10** (Figure 4.16), no resonances related to **10** were detected in ^2H NMR; however, H/D exchange of acetonitrile in presence of basic deuteroxide ions is observed (Figure 4.17).³¹ Moreover, a C_2 -symmetric complex presumed to be **12** has also been observed by ^{31}P NMR spectroscopy upon adding 4 atm of H_2 to **11** (Fig. 4.14). When

H₂ is removed under vacuum, this complex converts back to **11**, indicating the 1,2-elimination and O–H oxidative addition steps in Fig. 4.18 are reversible. Taken together all the experimental information, it is evident that the electrochemical hydrogen evolution from water by **10** follows the mechanism shown in Fig. 4.18, not Fig. 4.19.

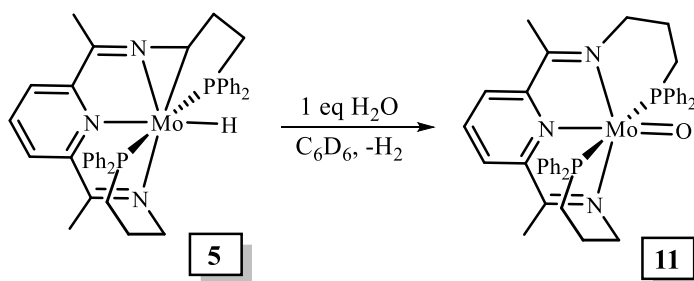


Figure 4.14. Synthesis of **11** from [(κ^6 -*P,P,N,N,N,C*-Ph₂PPrPDI)MoH] (**5**).

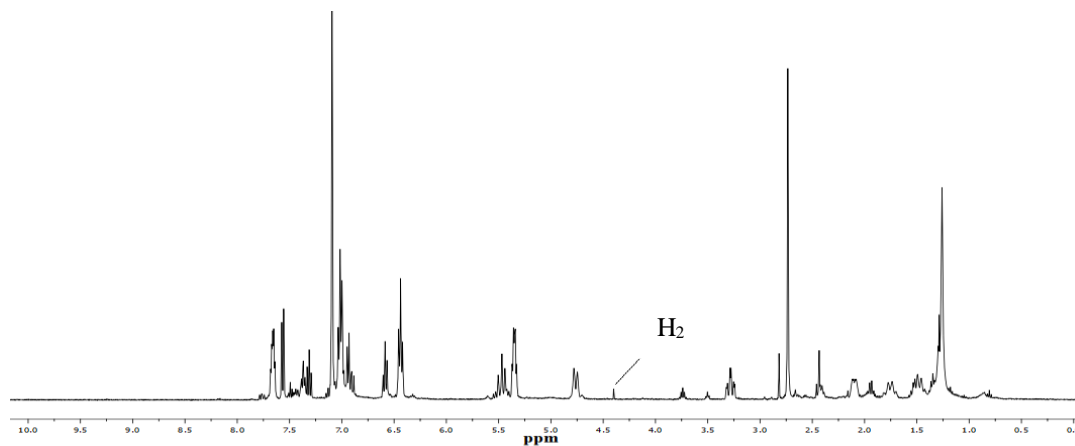


Figure 4.15. ¹H NMR spectrum of **11** in benzene-*d*₆ obtained from stoichiometric H₂O addition to [(κ^6 -*P,P,N,N,N,C*-Ph₂PPrPDI)MoH] (**5**).

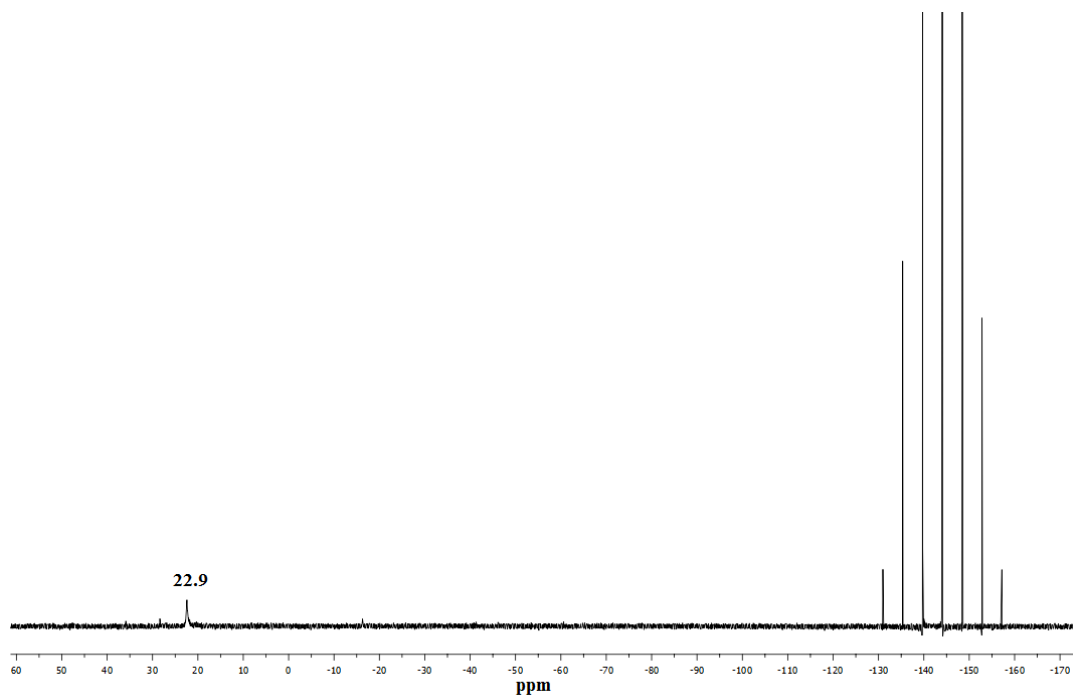


Figure 4.16. ^{31}P NMR spectrum of **10** in acetonitrile after bulk electrolysis with D_2O .

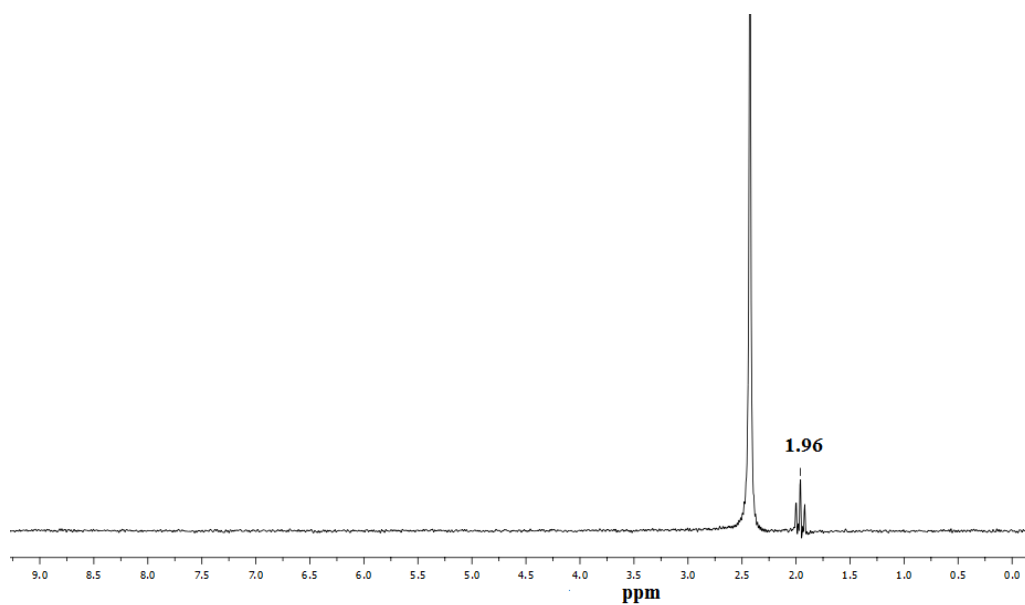


Figure 4.17. ^2H NMR spectrum of **10** in acetonitrile after bulk electrolysis with D_2O . The peak at 1.96 ppm is due to NCCH_2D .

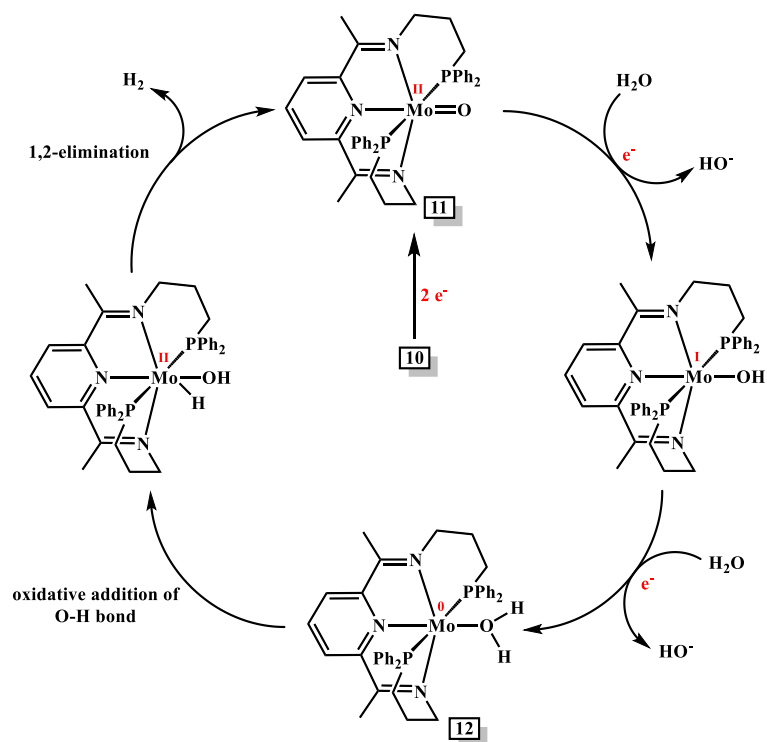


Figure 4.18. Proposed electrocatalytic cycle for hydrogen evolution from water.

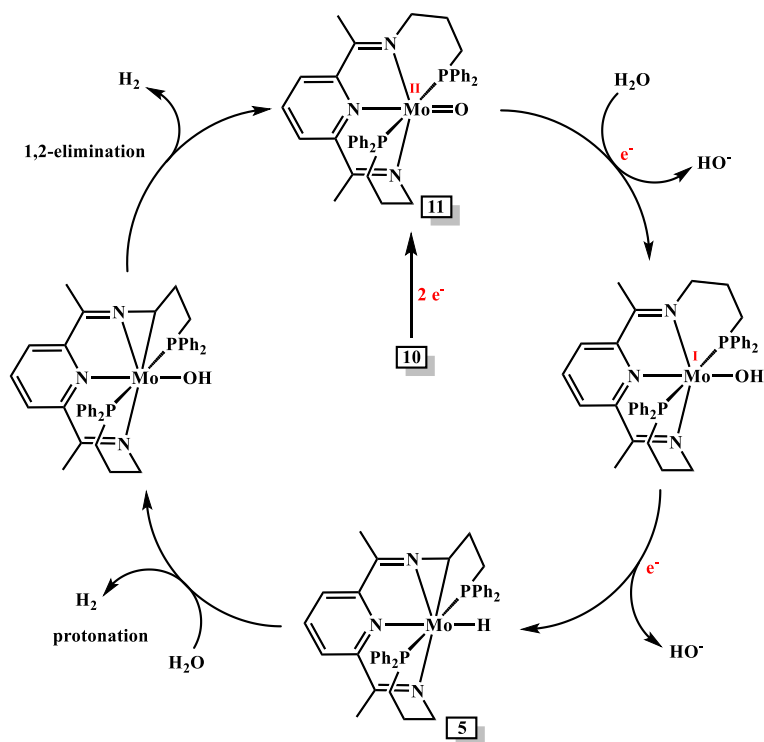


Figure 4.19. Alternative ligand-assisted electrocatalytic cycle for generation of H₂ and hydroxide ions from water.

4.5. Conclusion

The synthesis, characterization, and catalytic properties of a well-defined, redox-active ligand supported Mo oxo compound for the reduction of water to H₂ have been established. Halogen abstraction following AgPF₆ addition to **4**²⁴ in presence of an oxo-donor such as styrene oxide allowed for the isolation of the oxidized molybdenum (IV) oxo compound, **10**. Cyclic voltammetry of compound **10** showed two successive reversible reductions corresponding to Mo^{IV/III} and Mo^{III/II}, respectively. Compound **10** was found to catalyze electrochemical reduction of water to dihydrogen and hydroxide with a rate constant of 55 s⁻¹ at an overpotential of 2.45 V. The reduction of **10** using two equivalents of K/C₁₀H₈ allowed for isolation of the corresponding rare terminal Mo(II) oxo compound, **11**.

Interestingly, stoichiometric water addition to the C-H activated compound **5** resulted in the formation of **11** with concomitant release of dihydrogen. Although, this phenomena sheds light on the possibility of chelate arm involvement during the electrochemical generation of hydrogen, a controlled potential electrolysis experiment was conducted using D₂O as substrate. This experiment did not produce any evidence of deuterium incorporation into the chelate arm. Also, formation of **12** was observed when **11** was exposed to H₂ atmosphere, which reverts back to **11** under vacuum. Taken together, we propose a mechanism for the evolution of dihydrogen from water which includes two successive proton-coupled, two-electron reductions to form the active catalyst, **11** followed by oxidative addition of O-H and 1,2-elimination. It is hoped that the electrochemical reactivity reported herein highlights the promise of high-denticity, redox non-innocent PDI chelates in catalyst design for use in renewable energy production.

4.6. Experimental Details

4.6.1. General Considerations

All chemical manipulations were performed in an MBraun glovebox under an atmosphere of purified nitrogen. Diethyl ether, pentane, tetrahydrofuran, and toluene (Sigma Aldrich: St. Louis, MO) were dried using Pure Process Technology (PPT) solvent system, and stored in the glove box over activated 4Å molecular sieves and metallic sodium (Alfa Aesar: Haverhill, MA) before use. Acetonitrile was dried by distillation over calcium hydride. Acetonitrile-*d*₃, benzene-*d*₆ (Cambridge Isotope Laboratories: Tewksbury, MA) were dried over 3Å and 4Å molecular sieves, respectively, and metallic potassium (Sigma Aldrich: St. Louis, MO) prior to use. 2,6-Diacetylpyridine (TCI America: Portland, OR),

Celite (Acros Organics: Geel, Belgium), Silver hexafluorophosphate (Strem: Newburyport, MA), and tetrabutylammonium hexafluorophosphate (TBAPF₆) (Sigma Aldrich) were used without further manipulation. Ph₂PPrPDI²⁶ and [Ph₂PPrPDIMoI]²⁴ were prepared according to literature procedures. Solution phase ¹H, ¹³C, and ³¹P nuclear magnetic resonance (NMR) spectra were recorded at room temperature on either 400 MHz or 500 MHz Varian NMR spectrometer. All ¹H and ¹³C NMR chemical shifts are reported relative to Si(CH₃)₄ using ¹H (residual) and ¹³C chemical shifts of the solvent as secondary standards. ³¹P NMR data are reported relative to H₃PO₄. Elemental analyses were performed at Robertson Microlit Laboratories Inc. (Ledgewood, NJ).

4.6.2. Electrochemistry

All electrochemical investigations were carried out under a nitrogen atmosphere using a PG-STAT 128N Autolab electrochemical analyzer. A conventional three-electrode cell was used for recording cyclic voltammograms. Glassy carbon working electrodes (3 mm diameter) were prepared by successive polishing with 1.0 and 0.3 μm alumina slurries, followed by sonication (5 min) in ultrapure water after each polishing step. The supporting electrolyte was 0.1 M TBAPF₆ in acetonitrile. The Ag/Ag⁺ pseudoreference electrode was prepared by immersing a silver wire anodized with AgCl in a glass sheath equipped with a CoralPor frit (BASi: West Lafayette, IN) and loaded with 0.1 M TBAPF₆ in acetonitrile. A platinum wire was used as the counter electrode. All potentials are reported to the ferrocene/ferrocenium (Fc⁺⁰) couple as a reference.

Controlled potential experiments were completed in a custom-made, airtight, electrochemical cell equipped with a gas-tight sampling port. The electrochemical cell

mirrored the conventional three-electrode cell described above. The quantity of H₂ produced was determined by sampling the headspace gas via a gastight syringe at the end of the experiment. Headspace gas was injected to an SRI model 310 gas chromatograph (GC) equipped with a thermal conductivity detector (TCD) and a 6' molecular sieve 13X packed column; argon was used as the carrier gas. The GC-TCD was calibrated using the area of the peak resulting from an injection of a known concentration of H₂ in N₂.

4.6.3. Open Circuit Potential Determination

Open circuit potentials (OCP) were determined using the method described by Roberts and Bullock²⁹ in a 10 mL four-neck, airtight electrochemical cell equipped with three electrodes as described above and a gas-tight sampling port. An acetonitrile solution containing 0.1 M TBAPF₆ was purged with 1 atm H₂ gas. The working electrode was then connected to the platinum counter electrode (now the working electrode) and water was introduced to the desired molar concentration. The OCP was recorded following stabilization. Potentials were adjusted to the Fc⁺⁰ reference scale using a cyclic voltammogram of Fc at each water concentration obtained with glassy carbon as the working electrode. Results are provided in Table 4.2.

4.6.4. X-ray Crystallography

Single crystals suitable for X-ray diffraction were coated with polyisobutylene oil in the glovebox and transferred to glass fiber with Apiezon N grease before mounting on the goniometer head of a Bruker APEX Diffractometer (Arizona State University) equipped with Mo K α radiation. A hemisphere routine was used for data collection and determination of the lattice constants. The space group was identified and the data was processed using

the Bruker SAINT+ program and corrected for absorption using SADABS. The structures were solved using direct methods (SHELXS) completed by subsequent Fourier synthesis and refined by full-matrix, least-squares procedures on $[F^2]$ (SHELXL).

4.6.5. Synthesis of [(^{Ph}2PPrPDI)MoO][PF₆]₂ (**10**)

In a nitrogen filled glovebox, a 20 mL reaction vial was wrapped with electrical tape, and charged with 0.090 g (0.093 mmol) of **4**, 0.012 g (0.1 mmol) of styrene oxide, and 3 mL of acetonitrile. To this solution, 0.048 g (0.19 mmol) of AgPF₆ in 5 mL of acetonitrile was added slowly while stirring. The reaction vial was sealed and allowed to heat at 60 °C for 12 h. The orange solution was allowed to cool down to room temperature for complete precipitation of insoluble AgI after which the solution was filtered through Celite and dried under vacuum. A bright orange compound was extracted from acetone and dried under vacuum to isolate 0.069 g (73%) of solid identified as **10**. Suitable crystals were grown from acetone/THF at -15 °C. Elemental analysis for C₃₉H₄₁N₃MoP₄O₁₂: Calcd. C, 46.12%; H, 4.07%; N, 4.14%. Found: C, 46.40%; H, 4.16%; N, 4.05%. ¹H NMR (acetonitrile-*d*₃, 400 MHz): 7.83 (m, 4H, *Ph*), 7.60 (m, 9H, *Ph*), 7.42 (t, 7.6 Hz, 2H, *Ph*), 7.30 (t, 7.6 Hz, 4H, *Ph*), 7.21 (t, 8.0 Hz, 1H, *Py*), 6.30 (d, 8.0 Hz, 2H, *Py*), 4.25 (d, 13.2 Hz, 2H, *CH*₂), 3.65 (m, 2H, *CH*₂), 3.44 (m, 2H, *CH*₂), 2.56 (m, 4H, *CH*₂), 2.35 (m, 2H, *CH*₂), 2.10 (s, 6H, *CH*₃). ¹³C NMR (Acetonitrile-*d*₃, 100.49 MHz): 172.4 (*C=N*), 155.2 (*Ar*), 145.2 (*Ar*), 134.3 (t, 6.7 Hz, *Ph*), 133.3 (*Ar*), 133.2 (t, 2.5 Hz, *Ph*), 132.8 (*Ar*), 131.9 (t, 20.9, *Ph*), 130.8 (t, 5.0 Hz, *Ph*), 130.7 (t, 5.0 Hz, *Ph*), 126.7 (t, 23.1 Hz, *Ph*), 126.2 (*Ar*), 57.3 (*NCH*₂), 29.0 (t, 10.6 Hz, *PCH*₂), 26.8 (*PCH*₂*CH*₂), 16.6 (*CH*₃). ³¹P NMR (benzene-*d*₆, 161.78 MHz): 22.9 ppm (*PPh*₂), -143.6 (sept, 705 Hz, *PF*₆).

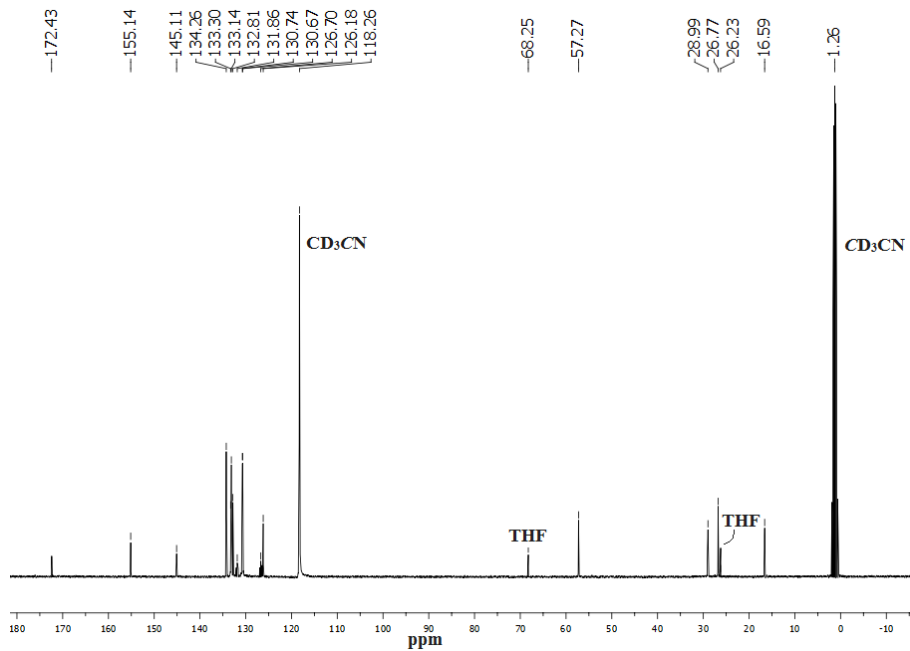


Figure 4.20. ^{13}C NMR spectrum of $[(\text{Ph}_2\text{PPr})\text{PDI}]\text{MoO}[\text{PF}_6]_2$ (**10**) in acetonitrile- d_3 .

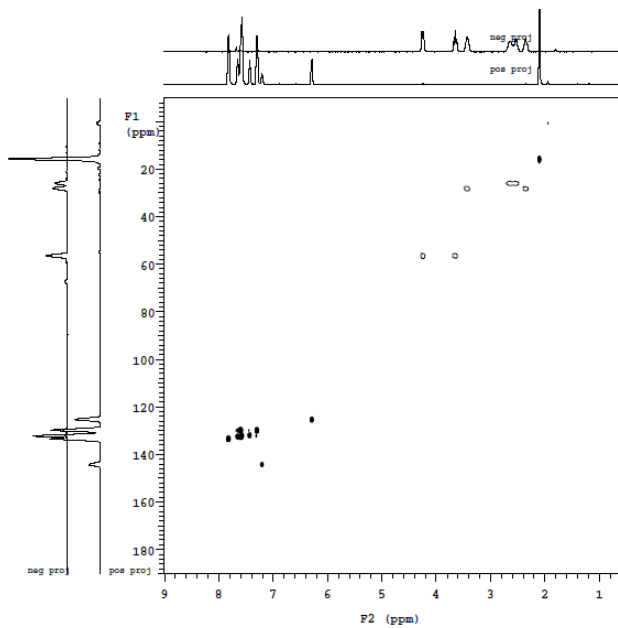


Figure 4.21. gHSQCAD NMR spectrum of $[(\text{Ph}_2\text{PPr})\text{PDI}]\text{MoO}[\text{PF}_6]_2$ (**10**) in acetonitrile- d_3 .

4.6.6. Synthesis of (^{Ph}2PPrPDI)MoO (**11**)

Method 1. In a nitrogen filled glovebox, a 20 mL reaction vial was charged with 0.0038 g (0.098 mmol) of freshly cut metallic potassium, 0.0122 g (0.095 mmol) of naphthalene, and 2 mL of THF. The solution was stirred for 30 min to form green potassium naphthalenide solution. To it, 0.051 g (0.050 mmol) of **10** in 10 mL of THF was slowly added and the mixture was allowed to stir at ambient temperature for 24 h. The resulting brown solution was filtered through Celite and the solvent was removed *in vacuo*. After washing with cold pentane and drying, 0.025 g (68%) of a brownish-red solid identified as **11** was isolated. *Method 2.* In a nitrogen filled glovebox, a 20 mL reaction vial was charged with 0.030 g (0.042 mmol) of **5**, and dissolved in 2 mL of toluene. Followed by addition of 0.001 mL of H₂O, the mixture was stirred at ambient temperature for 12 h. The reddish-brown solution was filtered through Celite, and dried *in vacuo*. After washing with cold pentane, 0.025 g (81%) of brown solid identified as **11** was isolated. Suitable crystals were grown from concentrated ether solution at -35 °C. Elemental analysis for C₃₉H₄₁N₃MoP₂O: Calcd. C, 64.55%; H, 5.69%; N, 5.79%. Found: C, 63.54%; H, 5.60%; N, 5.30%. ¹H NMR (benzene-*d*₆, 500 MHz): 7.88 (m, 4H, *Ph*), 7.66 (d, 8 Hz, 2H, *Py*), 7.39 (br, 1H, *Py*), 7.07 (t, 7.5 Hz, 4H, *Ph*), 7.01 (m, 2H, *Ph*), 6.67 (t, 7.4 Hz, 2H, *Ph*), 6.53 (d, 7.5 Hz, 4H, *Ph*), 5.58 (t, 12.5 Hz, 2H, NCH₂), 5.45 (br, 4H, *Ph*), 4.85 (d, 12.5 Hz, 2H, NCH₂), 3.35 (3, 12.0 Hz, 2H, CH₂), 2.80 (s, 6H, CH₃), 2.20 (br, 2H, CH₂), 1.79 (br, 2H, CH₂), 1.59 (m, 2H, CH₂). ¹³C NMR (benzene-*d*₆, 100.49 MHz): 138.95 (t, 10.0 Hz, *Ph*), 136.64 (*Ar*), 133.07 (t, 7.0 Hz, *Ar*), 132.41 (t, 7.0 Hz, *Ph*), 130.01 (*Ar*), 129.26 (*Ar*), 128.84 (*Ar*), 128.64 (*Ph*), 128.3 (*Ar*), 128.18 (*Ar*), 127.58 (t, 3.0 Hz, *Ph*), 112.60 (*Py*), 109.07 (*Py*), 58.53 (NCH₂),

28.69 (t, 8.0 Hz, PCH₂), 27.41 (PCH₂CH₂), 13.5 (CH₃). ³¹P NMR (benzene-*d*₆, 161.78 MHz): 4.88 ppm (PPh₂).

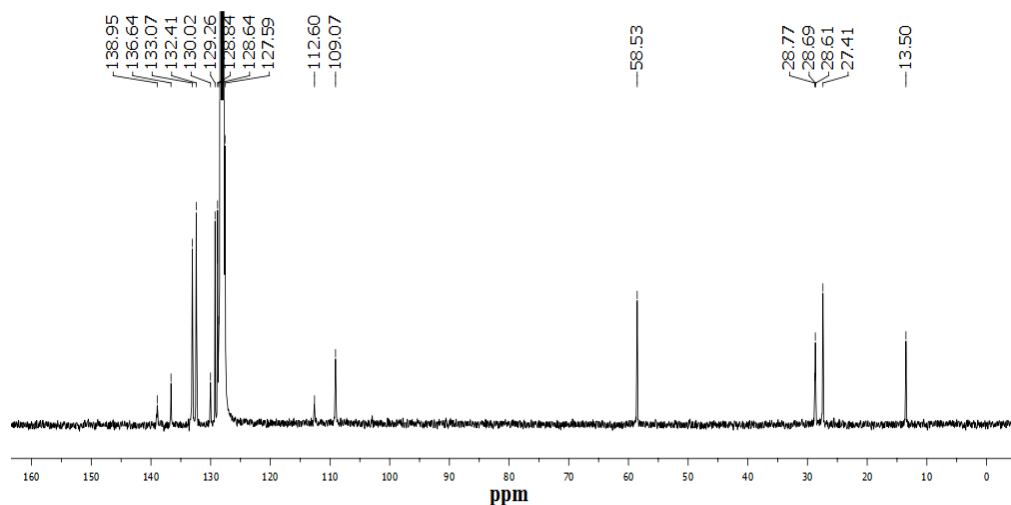


Figure 4.22. ¹³C NMR spectrum of (Ph²PPrPDI)MoO (**11**) in benzene-*d*₆.

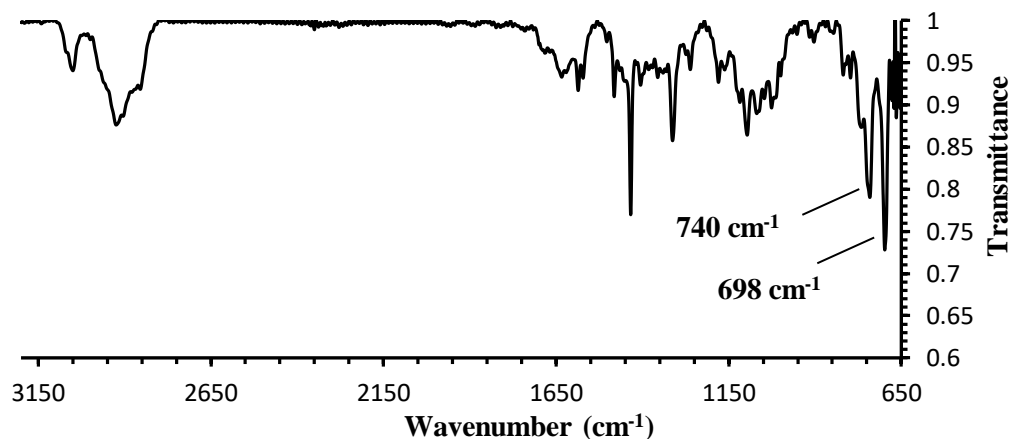


Figure 4.23. Infrared spectrum of (Ph²PPrPDI)MoO (**11**) in KBr.

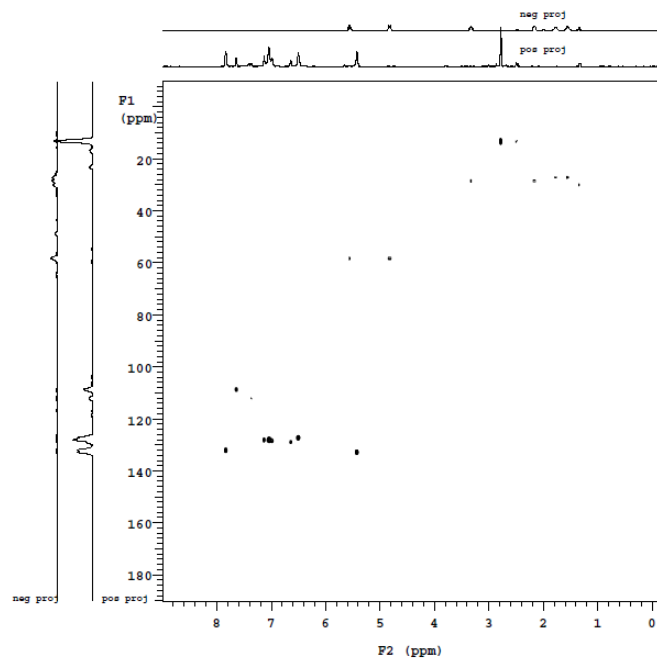


Figure 4.24. gHSQCAD NMR spectrum of **11** in benzene-*d*₆.

4.7. References

- (1) Bard, A. J.; Fox, M. A. *Acc. Chem. Res.* **1995**, *28*, 141–145.
- (2) Gust, D.; Moore, T. A.; Moore, A. L. *Acc. Chem. Res.* **2009**, *42*, 1890–1898.
- (3) Lewis, N. S.; Nocera, D. G. *Proc. Natl. Acad. Sci. U. S. A.* **2006**, *103*, 15729–15735.
- (4) Walter, M. G.; Warren, E. L.; McKone, J. R.; Boettcher, S. W.; Mi, Q.; Santori, E. A.; Lewis, N. S. *Chem. Rev.* **2010**, *110*, 6446–6473.
- (5) Thoi, V. S.; Sun, Y.; Long, J. R.; Chang, C. J. *Chem. Soc. Rev.* **2013**, *42*, 2388–2400.
- (6) Esswein, A. J.; Nocera, D. G. *Chem. Rev.* **2007**, *107*, 4022–4047.
- (7) Zee, D. Z.; Chantarojsiri, T.; Long, J. R.; Chang, C. J. *Acc. Chem. Res.* **2015**, *48*, 2027–2036.
- (8) Karunadasa, H. I.; Chang, C. J.; Long, J. R. *Nature* **2010**, *464*, 1329–1333.
- (9) Steele, B. C. H.; Heinzl, A. *Nature* **2001**, *414*, 345–352.
- (10) Debe, M. K. *Nature* **2012**, *486*, 43–51.
- (11) Ezaki, H.; Morinaga, M.; Watanabe, S. *Electrochim. Acta* **1993**, *38*, 557–564.
- (12) Nocera, D. G. *Acc. Chem. Res.* **2012**, *45*, 767–776.
- (13) Du, P.; Eisenberg, R. *Energy Environ. Sci.* **2012**, *5*, 6012.
- (14) Dubois, D. L. *Inorg. Chem.* **2014**, *53*, 3935–3960.
- (15) Gan, L.; Groy, T. L.; Tarakeshwar, P.; Mazinani, S. K. S.; Shearer, J.; Mujica, V.; Jones, A. K. *J. Am. Chem. Soc.* **2015**, *137*, 1109–1115.
- (16) Baxley, G. T.; Avey, A. A.; Aukett, T. M.; Tyler, D. R. *Inorganica Chim. Acta* **2000**, *300-302*, 102–112.
- (17) Blum, O.; Milstein, D. *J. Am. Chem. Soc.* **2002**, *124*, 11456–11467.
- (18) Parkin, G.; Bercaw, J. E. *J. Am. Chem. Soc.* **1989**, *111*, 391–393.
- (19) Yoon, K.; Parkin, G.; Rheingold, A. L. *J. Am. Chem. Soc.* **1991**, *113*, 1437–1438.

- (20) Yoon, M.; Tyler, D. R. *Chem. Commun.* **1997**, 639–670.
- (21) Silavwe, N. D.; Bruce, M R. M.; Philbin, C. E.; Tyler, D. R. *Inorg. Chem.* **1988**, *27*, 4669–4676.
- (22) Karunadasa, H. I.; Montalvo, E.; Sun, Y.; Majda, M.; Long, J. R.; Chang, C. J. *Science* **2012**, *335*, 698–702.
- (23) Thoi, V. S.; Karunadasa, H. I.; Surendranath, Y.; Long, J. R.; Chang, C. J. *Energy Environ. Sci.* **2012**, *5*, 7762.
- (24) Pal, R.; Groy, T. L.; Trovitch, R. J. *Inorg. Chem.* **2015**, *54*, 7506–7515.
- (25) Pal, R.; Groy, T. L.; Bowman, A. C.; Trovitch, R. J. *Inorg. Chem.* **2014**, *53*, 9357–9365.
- (26) Ben-Daat, H.; Hall, G. B.; Groy, T. L.; Trovitch, R. J. *Eur. J. Inorg. Chem.* **2013**, 4430–4442.
- (27) Baker, P. K.; Fraser, S. G.; Keys, E. M. *J. Organomet. Chem.* **1986**, *309*, 319–321.
- (28) Pal, R.; Cherry, B. R.; Flores, M.; Groy, T. L.; Trovitch, R. J. *Dalton Trans.* **2016**.
- (29) Kilgore, U. J.; Roberts, J. A. S.; Pool, D. H.; Appel, A. M.; Stewart, M. P.; Dubois, M. R.; Dougherty, W. G.; Kassel, W. S.; Bullock, R. M.; Dubois, D. L. *J. Am. Chem. Soc.* **2011**, *133*, 5861–5872.
- (30) Baffert, C.; Artero, V.; Fontecave, M. *Inorg. Chem.* **2007**, *46*, 1817–1824.
- (31) Balaj, O. P.; Siu, C-K.; Balteanu, I.; Fox-Beyer, B. S.; Beyer, M. K.; Bondybey, V. *E. J. Phys. Chem. A* **2004**, *108*, 7506–7512.

CHAPTER 5

DIRECT CONVERSION OF CARBON DIOXIDE TO MOLECULAR OXYGEN AND CARBON MONOXIDE

5.1. Abstract

Global carbon emissions have increased significantly in last two centuries due to the industrial revolution. To combat the projected impacts on world climate, sustainable utilization of CO₂ as a carbon feedstock for renewable organic products is of prime interest. While capture and sequestration can mitigate CO₂ release to the atmosphere, the metal-mediated activation and multi-electron reduction of this greenhouse gas to commodity chemicals and fuels is perhaps the most promising long term solution. In attempt to mimic photosystems, several homogeneous and heterogeneous catalysts have been reported which can reduce CO₂ to CO with concomitant oxidation of water to molecular oxygen (O₂); however, direct conversion of CO₂ to O₂ is rare. While extremely harsh conditions, such as thermal decomposition of CO₂ over a mixed-metal oxide surface at 900 °C, and photodissociation using vacuum ultra-violet (VUV) radiation allowed for formation of O₂ from CO₂, utilization of mild conditions for this transformation has remained a far-reached dream of scientists. Here we report, a molybdenum bis(dinitrogen) complex stabilized by a redox non-innocent diimine chelate, that enables for the first time, direct conversion of CO₂ to O₂ and CO at ambient-temperature. The combination of experimental studies with DFT calculations suggests that this rare two-electron transformation is achieved via a novel tail-to-tail reductive coupling of two CO₂ molecules forming a diformyl peroxide intermediate which spontaneously dissociates into O₂ and the corresponding dicarbonyl complex. We anticipate that this finding may prove valuable in the development of

catalysts for multi-electron reductive coupling of CO₂ in future O₂ generation systems, non-aqueous artificial photosystems, and solar cells. Moreover, the results described herein may stand useful in creating oxygenic atmosphere on Mars, where the atmosphere is 96% CO₂.

5.2. Introduction

Carbon dioxide is one of the main greenhouse gases which is responsible for global warming.¹ However, recent scientific and technological advancements have shown that CO₂ can be used as a renewable C₁-building block in the industrial-scale manufacturing of fine-chemicals, commodity products, and alternative fuels.² In nature, the most important CO₂ reduction process takes place during photosynthesis where CO₂ molecules are enzymatically converted into C_n-sugars with the concomitant oxidation of water to O₂. In order to mimic photosystems, T. J. Meyer and co-workers have recently showed that a homogeneous Ru electrocatalyst reduces CO₂ to CO and oxidizes H₂O to O₂ at the same time.³ However, synthetic chemists have not had great deal of success developing artificial catalysts which can directly reduce CO₂ to CO and O₂ under mild conditions. To overcome the inherent large thermodynamic and kinetic barrier of CO₂ to CO and O₂ transformation,⁴ thermal decomposition of CO₂ over a mixed-metal oxide containing furnace has been reported,⁵ however, a maximum of 20% conversion was achieved at 900 °C. Alternatively, high energy vacuum VUV radiation was shown to enact decomposition of CO₂ to elemental C and O₂,⁶ albeit with only 5% conversion. While the metal-assisted reduction of CO₂ to CO requires external reductants and yields O²⁻,⁷ CO₃²⁻,⁸ or H₂O⁹ as the oxygenated by

products; reductant-free direct conversion of CO₂ to CO and O₂ using a metal complex at room-temperature has not been reported.

Despite the inherent thermodynamic stability of CO₂,^{4,10} an aptly designed metal complex can activate and reduce CO₂.² Although $\eta^1\text{-C}^{11}$ and $\eta^2\text{-C,O}^{12}$ are the most common modes of CO₂ coordination to a transition metal complex, $\eta^1\text{-O}^{13}$ and polymetallic binding of CO₂ are also known.¹⁰ While the coordination chemistry of CO₂ with transition metals is diverse and well explored, reductive coupling of two CO₂ molecules at a single metal-site are limited.^{14,15} Although CO₂ molecules can couple in a head-to-head, head-to-tail, or tail-to-tail fashion (Fig. 5.1), the reported metal-mediated CO₂ coupling processes have exclusively proceeded in head-to-head (C-C bond formation)¹⁴ or head-to-tail (C-O bond formation)^{9d,8c,15} fashion, with the later often known to undergo subsequent disproportionation to generate CO₃²⁻ and CO.^{15a,b} The tail-to-tail reductive coupling of two CO₂ molecules at a single metal site by means of O-O bond formation, has remained elusive till date.

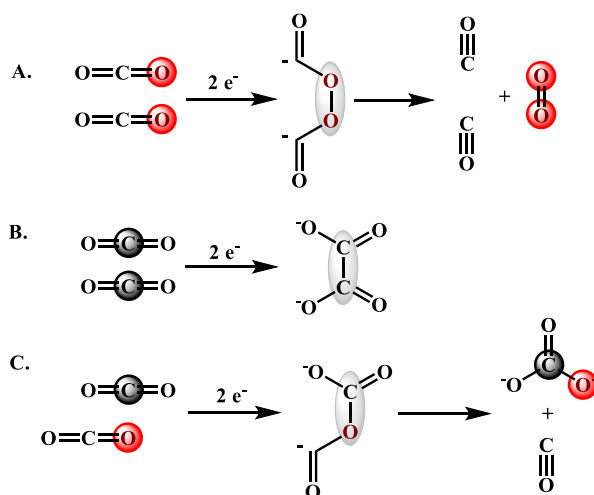


Figure 5.1. Reductive coupling modes of CO₂. A. Tail-to-tail (O,O) coupling. B. Head-to-head (C,C) coupling. C. Head-to-tail (C,O) coupling.

We have reported recently that the phosphine supported PDI chelate, $\text{Ph}_2\text{PPrPDI}^{16}$ allows for Mo catalyzed reactions, such as hydrosilylation of aldehydes to silyl ethers,¹⁷ hydroboration of CO_2 to methoxide,¹⁸ and reduction of H_2O to H_2 .¹⁹ However, in order to achieve reductive coupling of two CO_2 molecules, a metal complex with two open coordination sites in the *cis*-fashion is required.²¹ The addition of CO_2 to *cis*- $(\text{Me}_3\text{P})_4\text{Mo}(\text{N}_2)_2$, as reported by Chatt and co-workers,^{15a} allowed for the displacement of labile N_2 ligands to generate the corresponding bis(carbon dioxide) complex which undergoes head-to-tail reductive coupling to yield CO_3^{2-} bridged dimer upon disproportionation.^{15a,b} While Mo-mediated CO_2 coupling has exclusively observed in a head-to-tail mode to generate CO and CO_3^{2-} ,^{15a,b} we hypothesized that the rigid spatial orientation of tetra-coordinated α -diimine ligand, $\text{Ph}_2\text{PPrDI}^{22}$ supported Mo complex may provide the platform required to promote O-O coupling over C-O coupling when exposed to CO_2 atmosphere.

5.3. Results and Discussion

A six-coordinate Mo(II) diiodide complex, $(\text{Ph}_2\text{PPrDI})\text{MoI}_2$ (**13**, Fig. 5.2) was isolated when an equimolar mixture of $\text{Ph}_2\text{PPrDI}^{22}$ and $(\text{CH}_3\text{CN})_2(\text{CO})_3\text{MoI}_2^{23}$ was refluxed. Compound **13** showed broad paramagnetic resonances in the ^1H NMR spectrum over the range of 90 ppm to -50 ppm (Fig. 5.3) and exhibits a magnetic moment of $2.45 \mu_{\text{B}}$ suggesting two unpaired electrons on the metal center. This compound was further characterized by single crystal X-ray diffraction (Fig. 5.4, left) and was found to possess a distorted octahedral geometry about molybdenum. Significant elongation of C(2)-N(1) and C(3)-N(2) bond distances to 1.368 (4) and 1.350 (3) Å in the diimine fragment, and

contraction of C(2)-C(3) bond to 1.398 (3) Å suggest strong backdonation from Mo(II) to the π -accepting diimine chelate. Interestingly, unlike the PDI analogue, $[(^{\text{Ph}_2\text{PPr}}\text{PDI})\text{MoI}][\text{I}]$,¹⁸ compound **13** did not undergo ligand C-H activation upon reduction with K/Hg. However, a red diamagnetic bis(dinitrogen) complex, $(^{\text{Ph}_2\text{PPr}}\text{DI})\text{Mo}(\text{N}_2)_2$ (**14**, Fig. 5.2) with a singlet resonance in its ^{31}P NMR spectrum at 46.00 ppm (Fig. 5.6) was isolated. Symmetric chelate coordination about the metal was further confirmed by the presence of six methylene resonances in the ^1H NMR spectrum (Fig. 5.5).

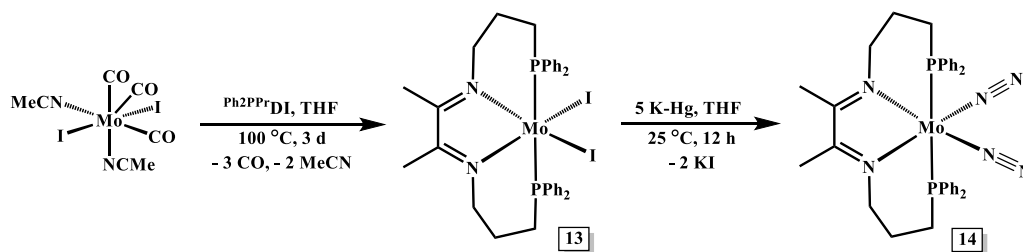


Figure 5.2. Synthesis of $(^{\text{Ph}_2\text{PPr}}\text{DI})\text{MoI}_2$ (**13**) and $(^{\text{Ph}_2\text{PPr}}\text{DI})\text{Mo}(\text{N}_2)_2$ (**14**).

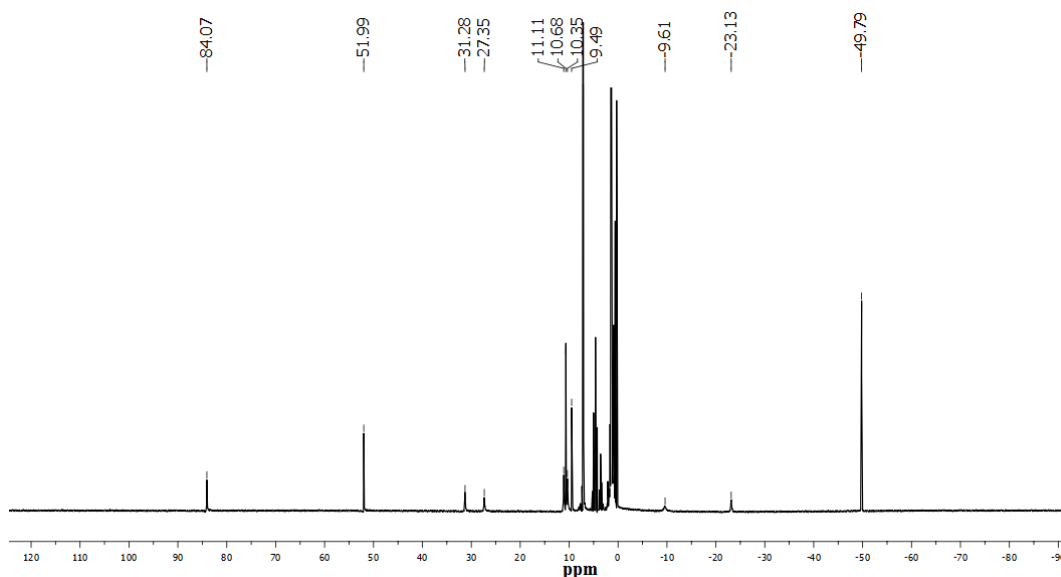


Figure 5.3. ^1H NMR of $(^{\text{Ph}_2\text{PPr}}\text{DI})\text{MoI}_2$ (**13**) in benzene- d_6 .

Moreover, two stretching frequencies at 1895 and 1980 cm^{-1} were identified in the infrared spectrum, corresponding to the symmetric and asymmetric $\text{N}\equiv\text{N}$ bond stretches for two *cis*-dinitrogen ligands and formation of $(^{\text{Ph}_2\text{PPrDI})\text{Mo}(\text{N}_2)_2$ (**14**) (Fig. 5.7). To confirm formation of the *cis*-isomer, the solid state structure of **14** was determined by single crystal X-ray diffraction (Fig. 5.4, middle). This compound was found to have two N_2 ligands and a near octahedral geometry around the metal with $\text{N}(1)\text{-Mo}(1)\text{-N}(2)$ and $\text{P}(1)\text{-Mo}(1)\text{-P}(2)$ angles of 73.24 (8) and 172.63 (2) $^\circ$, respectively. The elongation of $\text{C}(2)\text{-N}(1)$ and contraction of $\text{C}(2)\text{-C}(3)$ bond distances to 1.345 (5) and 1.405 (4) Å , respectively, are evidence for substantial π -back bonding between the expanded Mo d-orbitals to the low-lying LUMOs of DI chelate. Also, the slightly elongated $\text{N}(3)\text{-N}(4)$ and $\text{N}(5)\text{-N}(6)$ bond lengths to 1.147 (3) and 1.140 (3) Å suggest weak activation of the bound N_2 ligands.

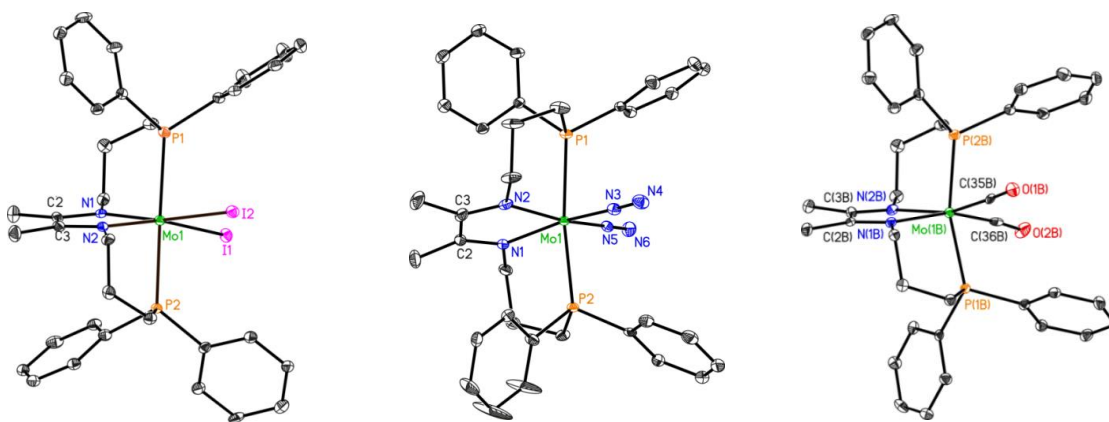


Figure 5.4. Single crystal structures of **13** (left), **14** (middle), and **15** (right).

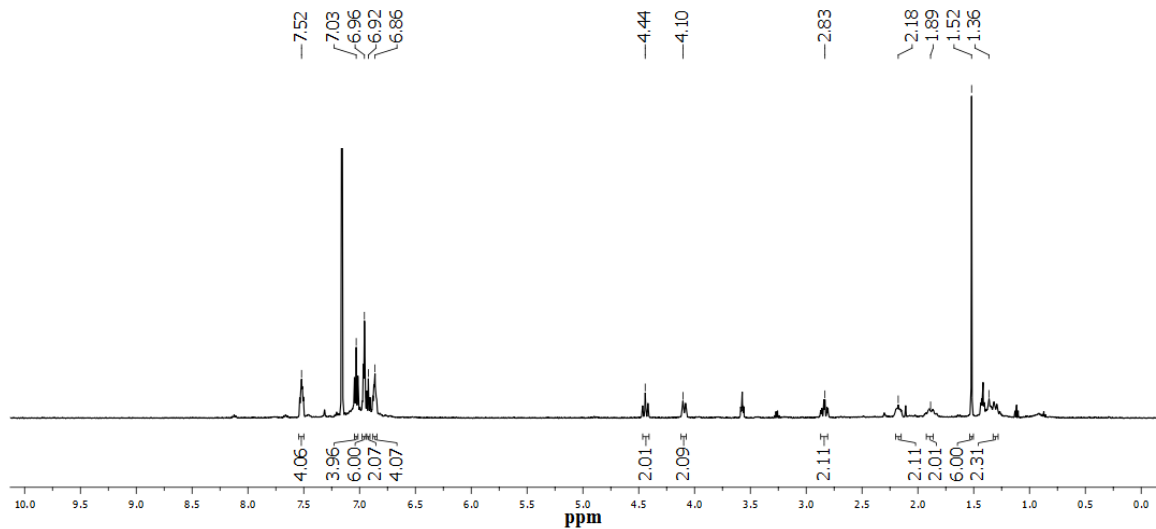


Figure 5.5. ^1H NMR of $(\text{Ph}_2\text{PPrDI})\text{Mo}(\text{N}_2)_2$ (**14**) in benzene- d_6 .

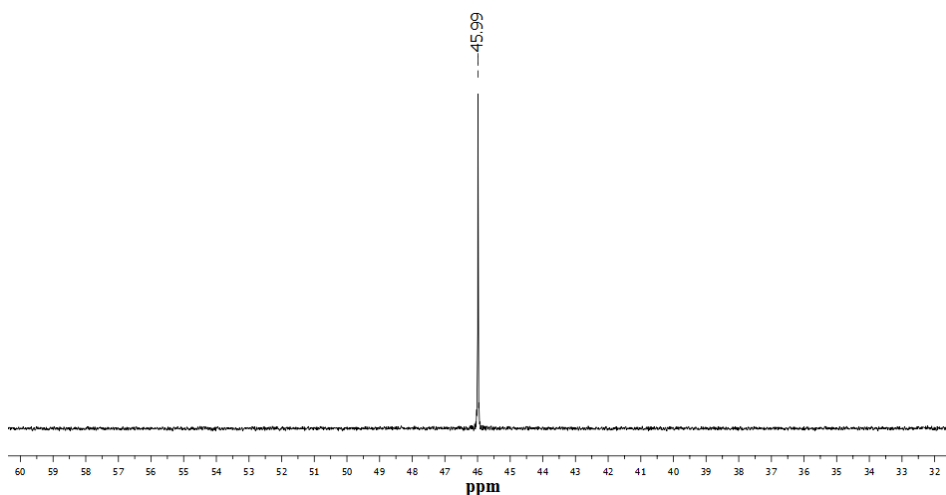


Figure 5.6. ^{31}P NMR of $(\text{Ph}_2\text{PPrDI})\text{Mo}(\text{N}_2)_2$ (**14**) in benzene- d_6 .

When a J. Young tube containing a frozen C_6D_6 solution of **14** was exposed to an atmosphere of CO_2 , complete conversion to a new diamagnetic compound with a color change from red to bluish-purple was observed by multinuclear NMR spectroscopy after 26 h at room temperature. The ^{31}P NMR spectrum showed a singlet at 57.94 ppm (Fig. 5.9) and the presence of six methylene resonances by ^1H NMR spectroscopy (Fig. 5.8) suggest

symmetric ligand coordination around Mo. Interestingly, infrared spectroscopy of the newly formed compound showed two stretching frequencies at 1845 and 1760 cm^{-1} (Fig. 5.10) consistent with the symmetric and asymmetric vibration modes of two *cis*-CO ligands, suggesting that the newly formed compound is the dicarbonyl complex, *cis*- $(\text{Ph}_2\text{PPrDI})\text{Mo}(\text{CO})_2$ (**15**, Fig. 5.7). Formation of this compound is also supported by the presence of a triplet at 246.1 ppm in the ^{13}C NMR spectrum suggesting the presence of CO ligands in the product. The identity of **15** was further confirmed by single crystal X-ray diffraction (Fig. 5.4, right). Notably, in case of **14** and **15**, due to competition between the π -accepting ligands, DI and N_2 , and DI and CO, respectively, the degree of backbonding towards DI in **14** and **15** is less than that observed in **13**, even though these compounds are zerovalent. Moreover, compound **15** can be prepared independently by refluxing $\text{Mo}(\text{CO})_6$ with Ph_2PPrDI at 110 $^\circ\text{C}$ (Fig. 5.7) while reaction of **15** with I_2 followed by heating to 100 $^\circ\text{C}$ affords **13**.

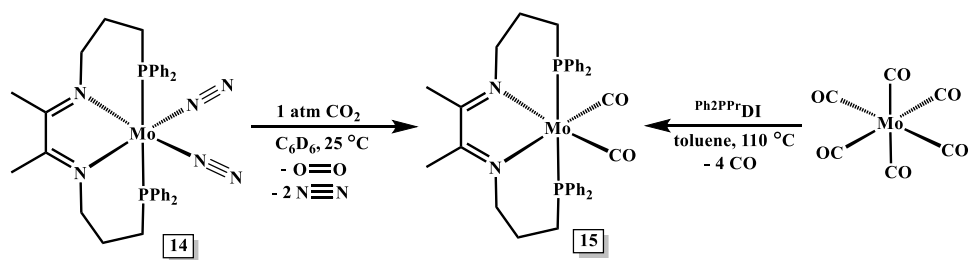


Figure 5.7. Formation of $(\text{Ph}_2\text{PPrDI})\text{Mo}(\text{CO})_2$ (**15**) from $(\text{Ph}_2\text{PPrDI})\text{Mo}(\text{N}_2)_2$ (**14**) and CO_2 (forward), and from $\text{Mo}(\text{CO})_6$ (reverse).

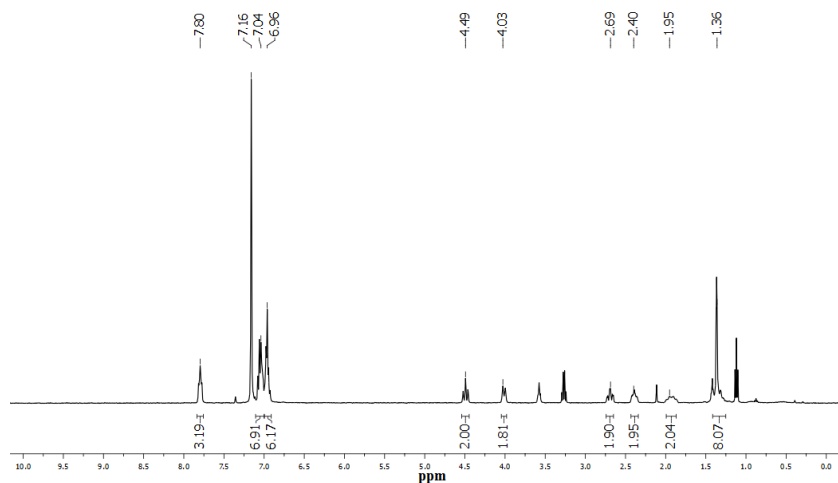


Figure 5.8. ^1H NMR of $(\text{Ph}_2\text{PPrDI})\text{Mo}(\text{CO})_2$ (**15**) in benzene- d_6 .

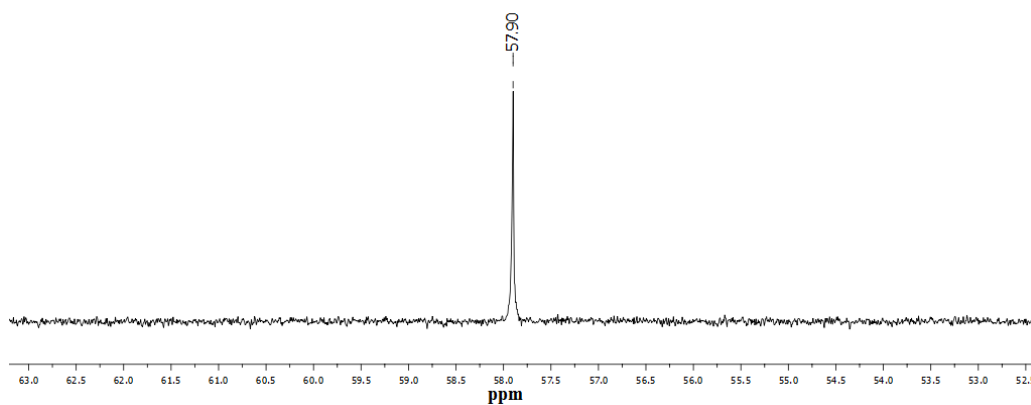


Figure 5.9. ^{31}P NMR of $(\text{Ph}_2\text{PPrDI})\text{Mo}(\text{CO})_2$ (**15**) in benzene- d_6 .

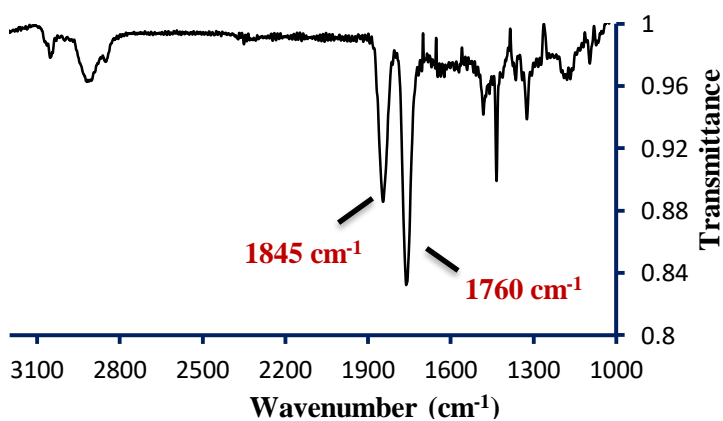


Figure 5.10. Infrared spectrum of $(\text{Ph}_2\text{PPrDI})\text{Mo}(\text{CO})_2$ (**15**) in KBr pellet.

Table 5.1. Notable bond lengths (Å) and angles (°) determined for **13**, **14**, and **15**.

| | 13 | 14 | 15 |
|-----------------|-----------|-----------|-----------|
| Mo(1)-N(1) | 2.064(5) | 2.102(2) | 2.164(3) |
| Mo(1)-N(2) | 2.068(5) | 2.101(2) | 2.153(3) |
| Mo(1)-N(3) | - | 2.002(2) | - |
| Mo(1)-N(5) | - | 2.003(2) | - |
| Mo(1)-P(1) | 2.551(18) | 2.465(6) | 2.451(11) |
| Mo(1)-P(2) | 2.533(18) | 2.467(6) | 2.443(11) |
| Mo(1)-I(1) | 2.821(7) | - | - |
| Mo(1)-I(2) | 2.841(7) | - | - |
| Mo(1)-C(35) | - | - | 1.965(4) |
| Mo(1)-C(36) | - | - | 1.946(4) |
| N(1)-C(2) | 1.369(8) | 1.341(3) | 1.325(5) |
| N(2)-C(3) | 1.351(8) | 1.347(3) | 1.327(5) |
| C(2)-C(3) | 1.397(9) | 1.405(4) | 1.438(6) |
| C(35)-O(1) | - | - | 1.175(5) |
| C(36)-O(2) | - | - | 1.181(5) |
| N(3)-N(4) | - | 1.134(3) | - |
| N(5)-N(6) | - | 1.128(3) | - |
| N(1)-Mo(1)-N(2) | 74.5(2) | 73.24(8) | 71.37(12) |
| N(3)-Mo(1)-N(5) | - | 97.29(8) | - |
| P(1)-Mo(1)-P(2) | 177.98(6) | 172.63(2) | 175.08(4) |
| I(1)-Mo(1)-I(2) | 91.79(2) | - | - |

To account for the two missing oxygen atoms, several experiments have been performed. The IR spectrum of the reaction mixture did not reveal Mo=O or CO₃²⁻ stretches and the ¹³C NMR spectrum also discarded the possibility of CO₃²⁻ formation. However, when the head-space of the completed reaction was analyzed by gas chromatography, formation of dioxygen (O₂) was observed. Thrilled by the formation of O₂ and CO from CO₂, the operating pathway was investigated. Using time-dependent ³¹P NMR spectroscopy, it was observed that the reaction goes through a left-right inequivalent intermediate, presumed to be (Ph²PP_rDI)Mo(CO₂)(N₂) (**16**), which exhibits two doublet resonances in the ³¹P NMR spectrum at 39.5 and 19.5 ppm (*J*_{PP} = 202 Hz) (Fig. 5. 11).

Insertion of the second CO₂ molecule into the Mo-O bond of **16** allows for O-O bond formation resulting from the tail-to-tail reductive coupling of CO₂ molecules to generate the energetically unfavorable diformyl peroxide metallacycle, (Ph²PP^rDI)Mo($\kappa_{C,C}$ -C₂O₄) (**17**, Fig. 5.12). At ambient temperature, the intermediate **17** spontaneously dissociates into O₂ and dicarbonyl complex, **15**. To further support our proposed mechanistic pathway, DFT calculations at B3LYP/LANL2DZ level are currently being performed.

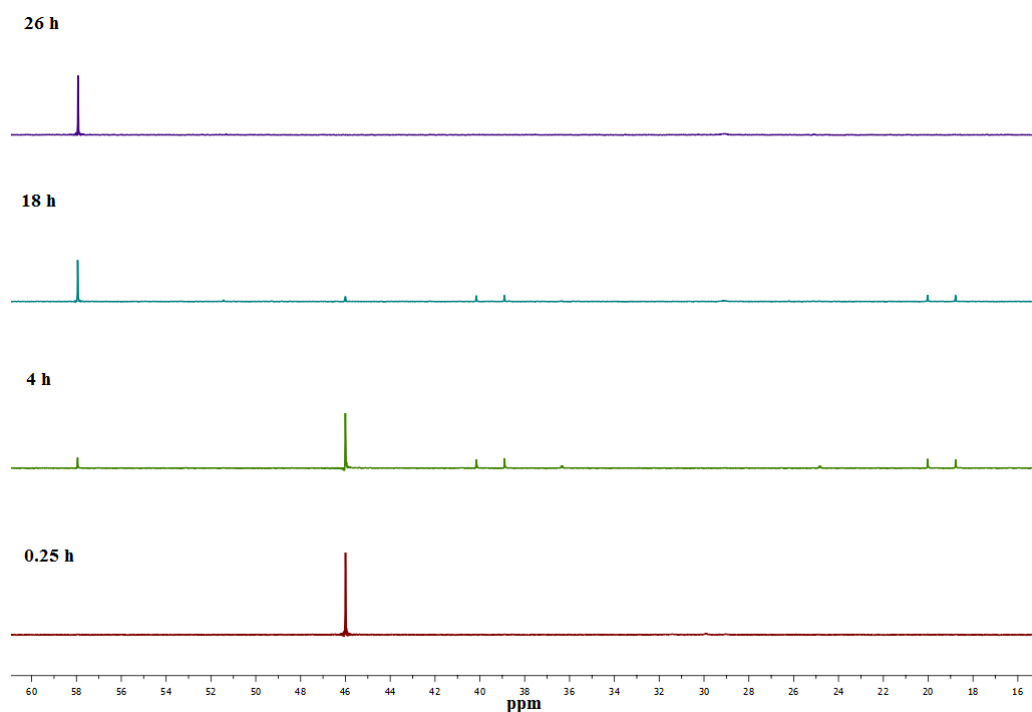


Figure 5.11. Time-dependent ³¹P NMR spectroscopy after addition of 1 atm CO₂ to **14**.

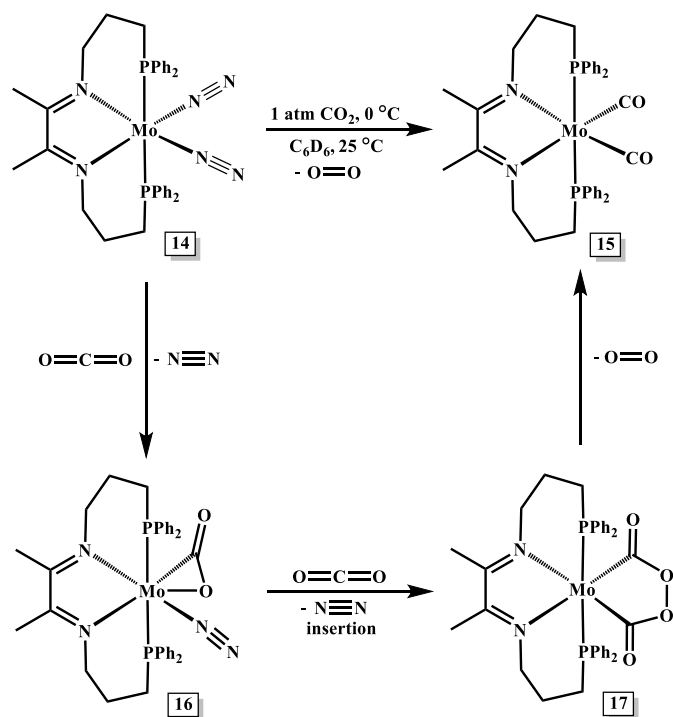


Figure 5.12. Proposed mechanistic pathway for the formation of $(\text{Ph}_2\text{PPrDI})\text{Mo}(\text{CO})_2$ (**15**) and O_2 from $(\text{Ph}_2\text{PPrDI})\text{Mo}(\text{N}_2)_2$ (**14**) and CO_2 .

5.4. Attempts Toward Catalytic O_2 Generation from CO_2

Realizing that reductant-free, direct conversion of CO_2 to O_2 and CO can be achieved at room temperature using **14**, several attempts have been made to make the reaction catalytic. However, due to the substantial backbonding from zero-valent Mo to CO ligands, neither heating the reaction mixture at as high as $130 \text{ }^\circ\text{C}$ nor exposing to UV radiation resulted in removal of the coordinated CO ligands, an essential step to turn over the reaction. In order to make the transformation catalytic, we hope to modify the electronic properties of the chelate to disfavor Mo-CO backbonding. It is anticipated that this modification will allow for thermolytic or photolytic dissociation of newly formed CO ligands to enable catalysis in presence of CO_2 . The extended π -backbone containing DI

chelates of acenaphthenequinone and phenanthrenequinone are better π -accepting ligands compared to the DI analogue. With this in mind, a series of novel Mo dicarbonyl complexes are currently being synthesized by refluxing $\text{Mo}(\text{CO})_6$ with the corresponding ligands (Fig. 5.13) and their catalytic activity will be investigated.

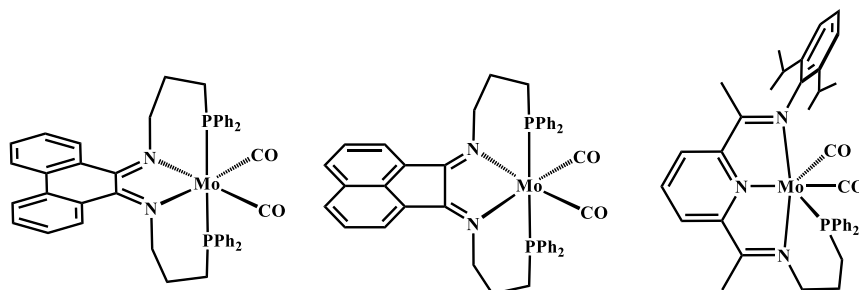


Figure 5.13. PDI and modified DI supported Mo dicarbonyl complexes.

Another approach to achieve a catalytic CO_2 to CO and O_2 transformation is to utilize the two-electron redox couple of $\text{Mo}^{0/\text{II}}$ to weaken Mo-CO backdonation. This can be done in two ways: i) oxidation of $\text{Mo}(0)$ to $\text{Mo}(\text{II})$ using a suitable oxidizing agent, such as $[\text{Cp}_2\text{Co}][\text{PF}_6]$ followed by thermal dissociation of the newly formed CO ligands with concomitant reduction of $\text{Mo}(\text{II})$ to $\text{Mo}(0)$ by *in situ* generated Cp_2Co , and ii) oxidative addition of a weak bond followed by CO liberation upon heating and reductive elimination to regenerate $\text{Mo}(0)$ to continue catalysis in presence of CO_2 .

5.5. Conclusion

The synthesis, characterization, and ability of a Mo bis(dinitrogen) complex to reduce CO_2 to CO and O_2 have been established. Our work demonstrates that well-defined monometallic molybdenum complex, **14** can couple CO_2 in a novel tail-to-tail fashion to form **17** upon O-O bond formation, which dissociates into O_2 and the corresponding di(carbonyl) complex **15**. A mild and reductant-free conversion of CO_2 to CO and O_2 is

exciting since CO can be converted to hydrocarbons using the Fischer-Tropsch process. Furthermore, direct conversion of CO₂ to O₂ is of great interest to scientists studying the colonization of Mars. This finding may provide suitable alternatives for designing a long-lived catalyst to the researchers who are planning on sending a rover to Mars in 2020 that will convert CO₂ (Martian atmosphere is 95% CO₂) into CO and O₂ using a solid oxide electrolysis at 800 °C, separate the O₂, and store it until 2030 for the astronauts arrive after 2030. Finally, the unprecedented transformation observed here will find applications in future O₂ generation systems, CO₂ utilization chemistry, and will shed light in designing non-aqueous artificial photosystems.

5.6. Experimental Details

5.6.1. General Considerations

Unless otherwise mentioned, all chemical manipulations were performed in an MBraun glovebox under an atmosphere of purified nitrogen. Diethyl ether, pentane, tetrahydrofuran, and toluene (Sigma Aldrich) were dried using a Pure Process Technology (PPT) solvent system, and stored in the glove box over activated 4Å molecular sieves and metallic potassium (Alfa Aesar) prior to use. Dichloromethane was purchased from Sigma Aldrich and dried over 4 Å molecular sieves before use. Acetonitrile was dried by distillation over calcium hydride and stored in the glove box over activated 3 Å molecular sieves. Acetonitrile-*d*₃, benzene-*d*₆ (Cambridge Isotope Laboratories) were dried over 3Å and 4Å molecular sieves, respectively, and metallic potassium (for benzene-*d*₆) prior to use. 2,3-Butadione (TCI America), Celite (Acros Organics), and Mo(CO)₆ (Strem) were used without further purification. ^{Ph2PPr}DI²² and (MeCN)₂(CO)₃MoI₂²³ were prepared according to literature procedures. Solution phase ¹H, ¹³C, and ³¹P nuclear magnetic

resonance (NMR) spectra were recorded at room temperature on either 400 MHz or 500 MHz Varian NMR spectrometer. All ^1H and ^{13}C NMR chemical shifts are reported relative to $\text{Si}(\text{CH}_3)_4$ using ^1H (residual) and ^{13}C chemical shifts of the solvent as secondary standards. ^{31}P NMR data are reported relative to H_3PO_4 . Elemental analyses were performed at Robertson Microlit Laboratories Inc. (Ledgewood, NJ).

5.6.2. X-ray Crystallography

Single crystals suitable for X-ray diffraction were coated with polyisobutylene oil in the glovebox and transferred to glass fiber with Apiezon N grease before mounting on the goniometer head of a Bruker APEX Diffractometer (Arizona State University) equipped with Mo K α radiation. A hemisphere routine was used for data collection and determination of the lattice constants. The space group was identified and the data was processed using the Bruker SAINT+ program and corrected for absorption using SADABS. The structures were solved using direct methods (SHELXS) completed by subsequent Fourier synthesis and refined by full-matrix, least-squares procedures on $[F^2]$ (SHELXL).

5.6.3. Synthesis of (Ph_2PPrDI) MoI_2 (13)

Method 1. A 100 mL thick-walled reaction vessel equipped with a magnetic stir bar was charged with 0.105 g (0.203 mmol) of $(\text{MeCN})_2(\text{CO})_3\text{MoI}_2$ and 0.110 g (0.203 mmol) of Ph_2PPrDI dissolved in 10 mL THF. The sealed bomb was frozen in liquid nitrogen and degassed on a Schlenk line before being refluxed at 120 °C in a preheated oil bath. After 24 h, the reaction mixture was cooled to room temperature and was once again degassed on the Schlenk line. Once the liberated CO gas was removed, the reaction was allowed to reflux for another 48 h at 120 °C to ensure reaction completion. After removing CO in the

same way, the bomb was brought inside the glove box and the solution was filtered through Celite. After removing the volatiles under vacuum, the product was washed with 5 mL acetonitrile and a dark green compound was extracted with dichloromethane and dried under vacuum to yield 0.155 g (0.175 mmol, 86%) of a green crystalline solid, identified as **13**. *Method 2.* A 100 mL thick-walled reaction vessel equipped with a magnetic stir bar was charged with 0.090 g (0.131 mmol) of **15** and 5 mL THF. To it, 0.035 g (0.137 mmol) iodine (I₂) dissolved in 5 mL THF was added slowly while stirring. An immediate color change from green to reddish-orange was observed, indicating oxidative addition of I₂. The sealed bomb was stirred at 25 °C for 2 h then frozen in liquid nitrogen and degassed on a Schlenk line before being refluxed at 100 °C in a preheated oil bath. After 1 h, the greenish reaction mixture was allowed to cool at room temperature and was once again degassed on the Schlenk line. Once the liberated CO gas was removed, the reaction was allowed to reflux for another 1 h at 100 °C to ensure reaction completion. After removing CO in the same way, the bomb was brought inside the glove box and the solution was filtered through Celite. After removing the volatiles under vacuum, the product was washed with 3 mL acetonitrile, extracted with dichloromethane, and dried under vacuum to yield 0.090 g (0.101 mmol, 78%) of a green crystalline solid identified as **13**. Single crystals suitable for X-ray diffraction were grown from a concentrated solution in THF at -35 °C. Anal. calcd. for C₃₄H₃₈N₂MoI₂P₂: Calcd. C, 46.07%; H, 4.32%; N, 3.16%. Found: C, 46.32%, H, 4.38%, N, 3.23%. ¹H NMR (benzene-*d*₆, 400 MHz): δ 84.0 (30.0 Hz), 52.0 (12.6 Hz), 31.3 (48.5 Hz), 27.3 (63 Hz), 1.1 (49.8 Hz), 10.6 (13.8 Hz), 10.3 (61.7 Hz), 9.5 (13.5 Hz), -9.6 (179.5 Hz), -23.1 (76.0 Hz), -49.8 (12.7 Hz). μ_{eff} = 2.45 μ_B.

5.6.4. Synthesis of (^{Ph}2PPrDI)Mo(N₂)₂ (**14**)

In a nitrogen-filled glove box, a 20 mL reaction vial was charged with 5.4 g of mercury and 5 mL of THF. To it, 0.021 g (0.536 mmol) of freshly cut metallic potassium was added and stirred for 30 min to form a clear potassium amalgam solution. To the solution, 0.095 g (0.107 mmol) of **13** in 10 mL of THF was slowly added and the mixture was allowed to stir at 25 °C for 15 h. The resulting red solution was filtered through Celite and the solvent was removed *in vacuo*. After washing with pentane and drying, 0.048 g (0.070 mmol, 65%) of a red solid identified as **14** was isolated. Single crystals suitable for X-ray diffraction were grown from a concentrated THF solution at -35 °C. ¹H NMR (benzene-*d*₆, 400 MHz): δ 7.52 (m, 4H, *Ph*), 7.03 (t, 8.0 Hz, 4H, *Ph*), 6.96 (m, 6H, *Ph*), 6.92 (t, 6.0 Hz, 2H, *Ph*), 6.86 (m, 4H, *Ph*), 4.44 (t, 9.6 Hz, 2H, NCH₂), 4.10 (d, 9.6 Hz, 2H, NCH₂), 2.83 (td, 11.2 Hz, 2H, CH₂), 2.18 (m, 2H, CH₂), 1.89 (m, 2H, CH₂), 1.52 (s, 6H, CH₃), 1.36 (m, 2H, CH₂). ¹³C NMR (benzene-*d*₆, 100.49 MHz): δ 150.0 (C=N), 136.8 (*Ph*), 133.8 (*Ph*), 133.4 (t, *J*_{CP} = 6.8 Hz, *Ph*), 131.9 (t, *J*_{CP} = 5.5 Hz, *Ph*), 128.98 (d, *J*_{CP} = 10.0 Hz, *Ph*), 128.4 (t, *J*_{CP} = 4.0 Hz, *Ph*), 127.9 (*Ph*), 52.2 (NCH₂), 28.4 (CH₂CH₂P), 24.3 (t, *J*_{CP} = 8.0 Hz, CH₂CH₂P), 14.2 (CH₃). ³¹P NMR (benzene-*d*₆, 161.78 MHz): 46.0 (PPh₂). IR (KBr): ν_{NN} = 1980 and 1895 cm⁻¹.

5.6.5. Synthesis of (^{Ph}2PPrDI)Mo(CO)₂ (**15**)

Method 1. In a nitrogen-filled glove box, a J. Young NMR tube was charged with 0.010 g (0.0145 mmol) of **14** dissolved in 0.7 mL of benzene-*d*₆. The tube was frozen at 0 °C, degassed, and 1 atm of CO₂ was added. After 26 h, complete formation of a new compound identified as **15** was observed by multinuclear NMR spectroscopy. Upon removal of excess

CO₂ and solvent, 0.0085 g (0.012 mmol, 85%) of a bluish-purple solid identified as **15** was isolated. *Method 2.* In a nitrogen-filled glove box, a 100 mL thick-walled reaction vessel equipped with a magnetic stir bar was charged with 0.040 g (0.151 mmol) of Mo(CO)₆ and 0.081 g (0.151 mmol) of ^{Ph}2PPrDI dissolved in 10 mL toluene. The sealed bomb was frozen in liquid nitrogen and degassed on a Schlenk line before being refluxed at 110 °C in a preheated oil bath. After 24 h, the bluish-purple reaction mixture was allowed to cool to room temperature and was once again degassed on the Schlenk line. Once the liberated CO gas was removed, the reaction was allowed to reflux for another 24 h at 110 °C to ensure reaction completion. After removing CO in the same way, the bomb was brought inside the glove box and the solution was filtered through Celite. After removing the volatiles under vacuum, the product was washed with 5 mL cold pentane and dried under vacuum to yield 0.101 g (0.147 mmol, 97%) of a bluish-purple solid identified as **15**. Single crystals suitable for X-ray diffraction were grown from a concentrated ether solution at -35 °C. Anal. calcd. for C₃₆H₃₈N₂MoO₂P₂: Calcd. C, 62.79%; H, 5.56%; N, 4.07%. Found: C, 62.52%, H, 5.54%, N, 3.89%. ¹H NMR (benzene-*d*₆, 400 MHz): δ 7.80 (m, 3H, *Ph*), 7.16 (overlap with C₆D₆, 4H, *Ph*), 7.04 (m, 7H, *Ph*), 6.96 (m, 6H, *Ph*), 4.49 (t, 12.4 Hz, 2H, NCH₂), 4.03 (d, 12.0 Hz, 2H, NCH₂), 2.69 (td, 15.2 Hz, 2H, CH₂), 1.95 (m, 2H, CH₂), 1.36 (m, 8H, CH₃, CH₂). ¹³C NMR (benzene-*d*₆, 100.49 MHz): δ 246.1 (CO), 151.8 (C=N), 135.1 (*Ph*), 133.4 (t, *J*_{CP} = 22.4 Hz, *Ph*), 132.3 (t, *J*_{CP} = 17.6 Hz, *Ph*), 128.9 (d, *J*_{CP} = 22.6 Hz, *Ph*), 128.3 (*Ph*), 128.0 (*Ph*), 127.7 (t, *J*_{CP} = 3.6 Hz, *Ph*), 56.7 (NCH₂), 29.4 (m, CH₂), 28.9 (m, CH₂), 14.3 (CH₃). ³¹P NMR (benzene-*d*₆, 161.78 MHz): 57.9 (PPh₂). IR (KBr): ν_{CO} = 1845 and 1760 cm⁻¹.

5.7. References

- (1) Falkowski, P.; Scholes, R. J.; Boyle, E.; Canadell, J.; Canfield, D.; Elser, J.; Gruber, N.; Hibbard, K.; Höglberg, P.; Mackenzie, F. T.; Moore, B.; Pedersen, T.; Rosenthal, Y.; Seitzinger, S.; Smetacek, V.; Steffen, W. *Science*, **290**, 291-296.
- (2) Appel, A. M.; Bercaw, J. E.; Bocarsly, A. B.; Dobbek, H.; DuBois, D. L.; Dupuis, M.; Ferry, J. G.; Fujita, E.; Hille, R.; Kenis, P. J. A.; Kerfeld, C. A.; Morris, R. H.; Peden, C. H. F.; Portis, A. R.; Ragsdale, S. W.; Rauchfuss, T. B.; Reek, J. N. H.; Seefeldt, L. C.; Thauer, R. K.; Waldrop, G. L. *Chem. Rev.* **2013**, *113*, 6621-6658.
- (3) Chen, Z.; Concepcion, J. J.; Brennaman, M. K.; Kang, P.; Norris, M. R.; Hoertz, P. G.; Meyer, T. J. *Proc. Natl. Acad. Sci. U. S. A.* **2012**, *109*, 15606-15611.
- (4) Aresta, M.; Dibenedetto, A.; Angelini, A. *Chem. Rev.* **2014**, *114*, 1709–1742.
- (5) Jin, W.; Zhang, C.; Chang, X.; Fan, Y.; Xing, W.; Xu, N. *Environ. Sci. Technol.* **2008**, *42*, 3064–3068.
- (6) Lu, Z.; Chang, C.; Yin, Q-Z.; Ng, C. Y.; Jackson, W. M. *Science*, **2014**, *346*, 61-64.
- (7) a) Kilpatrick, A. F. R.; Cloke, F. G. N. *Chem. Commun.* **2014**, *50*, 2769-2771. b) Noor, A.; Qayyum, S.; Bauer, T.; Schwarz, S.; Weber, B.; Kempe, R. *Chem. Commun.* **2014**, *50*, 13127-13130. c) Krogman, J. P.; Foxman, B. M.; Thomas, C. M. *J. Am. Chem. Soc.* **2011**, *133*, 14582-14585.
- (8) a) Kobayashi, K.; Tanaka, K. *Inorg. Chem.* **2015**, *54*, 5085-5095. b) Machan, C. W.; Chabolla, S. A.; Yin, J.; Gilson, M. K.; Tezcan, F. A.; Kubiak, C. P. *J. Am. Chem. Soc.* **2014**, *136*, 14598-14607. c) Fachinetti, G.; Floriani, C.; Chiesi-Villa, A.; Guastini, C. *J. Am. Chem. Soc.* **1979**, *101*, 1767-1775. d) Alvarez, R.; Carmona, E.; Poveda, M. L.; Sanchez-Delgado, R. *J. Am. Chem. Soc.* **1984**, *106*, 2731-2732. e) Lee, G. R.; Maher, J. M.; Cooper, N. J. *J. Am. Chem. Soc.* **1987**, *109*, 2956-2962.
- (9) a) DuBois, D. L.; Miedaner, A.; Haltiwanger, R. C. *J. Am. Chem. Soc.* **1991**, *113*, 8753-8764. b) Garg, K.; Matsubara, Y.; Ertem, M. Z.; Lewandowska-Andralojc, A.; Sato, S.; Szalda, D. J.; Muckerman, J. T.; Fujita, E. *Angew. Chem., Int. Ed.* **2015**, *54*, 14128-14132. c) Sato, S.; Morikawa, T.; Kajino, T.; Ishitani, O. *Angew. Chem., Int. Ed.* **2013**, *125*, 1022-1026. d) Feller, M.; Gellrish, U.; Anaby, A.; Diskin-Posner, Y.; Milstein, D. *J. Am. Chem. Soc.* **2016**, *138*, 6445-6454.
- (10) Aresta, M. In *Activation of Small Molecules*; Tolman, W. B., Ed.; Wiley-VCH, Weinheim, 2006; pp 1-42.

- (11) a) Herskovitz, T. *J. Am. Chem. Soc.* **1977**, *99*, 2391-2392. b) Calabrese, J. C.; Herskovitz, T.; Kinney, J. B. *J. Am. Chem. Soc.* **1983**, *105*, 5914-5915.
- (12) a) Aresta, M.; Nobile, C. F. *Dalton Trans.* **1977**, *7*, 708-711. b) Aresta, M.; Nobile, C. F. *Inorg. Chim. Acta* **1977**, *24*, L49-L50. c) Komiya, S.; Akita, M.; Kasuga, N. Hirano M.; Fukuoka, A. *Chem. Commun.* **1994**, *9*, 1115-1116. d) Sakamoto, M.; Shimizu, L.; Yamamoto, A. *Organometallics* **1994**, *13*, 407-409.
- (13) Castro-Rodriguez, I.; Nakai, H.; Zakharov, L.; Rheingold, A. L. Meyer, K. *Science* **2004**, *305*, 1757-1759.
- (14) a) Evans, W. J.; Seibel, C. A.; Ziller, J. W. *Inorg. Chem.* **1998**, *37*, 770-776. b) Paparo, A.; Silvia, J. S.; Kefalidis, C. E.; Spaniol, T. P.; Maron, L.; Okuda, J.; Cummins, C. C. *Angew. Chem. Int. Ed.* **2015**, *54*, 9115-9119. c) Angamuthu, R.; Byers, P.; Lutz, M.; Spek, A. L.; Bouwman, E. *Science* **2010**, *327*, 313-315. d) Farrugia, L. J., Lopinski, S., Lovatt, P. A. & Peacock, R. D. *Inorg. Chem.* **2001**, *40*, 558-559.
- (15) a) Chatt, J.; Kubota, M.; Leigh, G.-J.; March, F. C.; Mason, R.; Yarrow, D. J. *Chem. Commun.* **1974**, *24*, 1033-1034. b) Carmona, E.; Gonzalez, F.; Poveda, M. L.; Marin, J. M. *J. Am. Chem. Soc.* **1983**, *105*, 3365-3366. c) Langer, J.; Imhof, W.; Fabra, M. J.; García-Orduña, P.; Görls, H.; Lahoz, F. J.; Oro, L. A.; Westerhausen, M. *Organometallics* **2010**, *29*, 1642-1651. d) Herskovitz, T.; Guggenberger, L. J. *J. Am. Chem. Soc.* **1976**, *98*, 1615-1616. e) Dahlenburg, L.; Prengel, C. *J. Organomet. Chem.* **1986**, *308*, 63-71.
- (16) Ben-Daat, H.; Hall, G. B.; Groy, T. L.; Trovitch, R. J. *Eur. J. Inorg. Chem.* **2013**, 4430-4442.
- (17) Pal, R.; Groy, T. L.; Bowman, A. C.; Trovitch, R. J. *Inorg. Chem.* **2014**, *53*, 9357-9365.
- (18) Pal, R.; Groy, T. L.; Trovitch, R. J. *Inorg. Chem.* **2015**, *54*, 7506-7515.
- (19) Pal, R.; Cherry, B. R.; Flores, M.; Groy, T. L.; Trovitch, R. J. *Dalton Trans.* **2016**, *45*, 10024-10033.
- (20) Pal, R.; Laureanti, J. A.; Groy, T. L.; Jones, A. K.; Trovitch, R. J. *Chem. Commun.* **2016**, *52*, 11555-11558.
- (21) Carnahan, E. M.; Protasiewicz, J. D.; Lippard, S. J. *Acc. Chem. Res.* **1993**, *26*, 90-97.
- (22) Porter, T. M.; Hall, G. B.; Groy, T. L.; Trovitch, R. J. *Dalton Trans.* **2013**, *42*, 14689-14692.
- (23) Baker, P. K.; Fraser, S. G.; Keys, E. M. *J. Organomet. Chem.* **1986**, *309*, 319-321.

BIBLIOGRAPHY

Chapter 1

(1) (a) Pal, R.; Groy, T. L.; Bowman, A. C.; Trovitch, R. J. *Inorganic Chemistry* **2014**, *53*, 9357-9365. (b) Collman, J. P.; Hegedus, L. S.; Norton, J. R.; Finke, R. G. *Principles and Applications of Organotransition Metal Chemistry*; University Science Books: Sausalito, CA, 1987; pp 523-575.

(2) (a) Noyori, R. *Angew. Chem. Int. Ed.* **2002**, *41*, 2008-2022. (b) Carey, J. S.; Laffan, D.; Thomson, C.; Williams, M. T. *Org. Biomol. Chem.* **2006**, *4*, 2337-2347.

(3) Parshall, G. W.; Ittel, S. D. in *Homogeneous Catalysis: The Applications and Chemistry of Catalysis by Soluble Transition Metal Complexes*, 2nd Edition, John Wiley & Sons, Inc., New York, 1992, pp. 39-41.

(4) For examples of commonly used hydrosilylation catalysts see: (a) Speier, J. L.; Webster, J. A.; Barnes, G. H. *J. Am. Chem. Soc.* **1957**, *79*, 974-979. (b) Hitchcock, P. B.; Lappert, M. F.; Warhurst, N. J. W. *Angew. Chem. Int. Ed.* **1991**, *30*, 438-440.

(5) (a) Enthaler, S.; Junge, K.; Beller, M. *Angew. Chem. Int. Ed.* **2008**, *47*, 3317-3321. (b) Czaplík, W. M.; Mayer, M.; Cvengroš, J.; van Wangelin, A. J. *Chem. Sus. Chem.* **2009**, *2*, 396-417.

(6) (a) Gaillard, S.; Renaud, J.-L. *Chem. Sus. Chem.* **2008**, *1*, 505-509. (b) Troegel, D.; Stohrer, J. *Coord. Chem. Rev.* **2011**, *255*, 1440-1459.

(7) (a) Pratt, S. L.; Faltynek, R. A. *J. Organomet. Chem.* **1983**, *258*, C5-C8. (b) Hilal, H. S.; Abu-Eid, M.; Al-Subu, M.; Khalaf, S. *J. Mol. Catal.* **1987**, *39*, 1-11. (c) Mao, Z.; Gregg, B. T.; Cutler, A. R. *J. Am. Chem. Soc.* **1995**, *117*, 10139-10140. (d) Cavanaugh; M. D.; Gregg, B. T.; Cutler, A. R. *Organometallics* **1996**, *15*, 2764-2769. (e) Son, S. U.; Paik, S.-J.; Lee, I. S.; Lee, Y.-A.; Chung, Y. K.; Seok, W. K.; Lee, H. N. *Organometallics* **1999**, *18*, 4114-4118. (f) Son, S. U.; Paik, S.-J.; Chung, Y. K. *J. Mol. Catal. A: Chem.* **2000**, *151*, 87-90. (g) Chidara, V. K.; Du, G. *Organometallics* **2013**, *32*, 5034-5037. (h) Zheng, J.; Chevance, S.; Darcel, C.; Sortais, J.-B. *Chem. Commun.* **2013**, *49*, 10010-10012. (i) Mukhopadhyay, T. K.; Flores, M.; Groy, T. L.; Trovitch, R. J. *J. Am. Chem. Soc.* **2014**, *136*, 882-885.

(8) For representative Fe hydrosilylation catalysts see: (a) Brunner, H.; Fisch, K. *Angew. Chem. Int. Ed.* **1990**, *29*, 1131-1132. (b) Tondreau, A. M.; Lobkovsky, E.; Chirik, P. J. *Org. Lett.* **2008**, *10*, 2789-2792. (c) Langlotz, B. K.; Wadepohl, H.; Gade, L. H. *Angew. Chem. Int. Ed.* **2008**, *47*, 4670-4674. (d) Tondreau, A. M.; Darmon, J. M.; Wile, B. M.; Floyd, S. K.; Lobkovsky, E.; Chirik, P. J. *Organometallics* **2009**, *28*, 3928-3940. (e) Inagaki, T.; Ito, A.; Ito, J.; Nishiyama, H. *Angew. Chem. Int. Ed.* **2010**, *49*, 9384-9387. (f)

Kandepi, V. V. K. M.; Cardoso, J. M. S.; Peris, E.; Royo, B. *Organometallics* **2010**, *29*, 2777-2782. (g) Yang, J.; Tilley, T. D. *Angew. Chem. Int. Ed.* **2010**, *49*, 10186-10188. (h) Bhattacharya, P.; Krause, J. A.; Guan, H. *Organometallics* **2011**, *30*, 4720-4729. (i) Atienza, C. C. H.; Tondreau, A. M.; Weller, K. J.; Lewis, K. M.; Cruse, R. W.; Nye, S. A.; Boyer, J. L.; Delis, J. G. P.; Chirik, P. J. *ACS Catal.* **2012**, *2*, 2169-2172. (j) Tondreau, A. M.; Atienza, C. C. H.; Darmon, J. M.; Milsman, C.; Hoyt, H. M.; Weller, K. J.; Nye, S. A.; Lewis, K. M.; Boyer, J.; Delis, J. G. P.; Lobkovsky, E.; Chirik, P. J. *Organometallics* **2012**, *31*, 4886-4893. (k) Tondreau, A. M.; Atienza, C. C. H.; Weller, K. J.; Nye, S. A.; Lewis, K. M.; Delis, J. G. P.; Chirik, P. J. *Science* **2012**, *335*, 567-570. (l) Ruddy, A. J.; Kelly, C. M.; Crawford, S. M.; Wheaton, C. A.; Sydora, O. L.; Small, B. L.; Stradiotto, M.; Turculet, L. *Organometallics* **2013**, *32*, 5581-5588. (m) Peng, D.; Zhang, Y.; Du, X.; Zhang, L.; Leng, X.; Walter, M. D.; Huang, Z. *J. Am. Chem. Soc.* **2013**, *135*, 19154-19166.

(9) For representative Co hydrosilylation catalysts see: (a) Brunner, H.; Amberger, K. *J. Organomet. Chem.* **1991**, *417*, C63-C65. (b) Brookhart, M.; Grant, B. E. *J. Am. Chem. Soc.* **1993**, *115*, 2151-2156. (c) Tojo, S.; Isobe, M. *Tetrahedron Lett.* **2005**, *46*, 381-384. (d) Yong, L.; Kirleis, K.; Butenschön, H. *Adv. Synth. Catal.* **2006**, *348*, 833-836. (e) Konno, T.; Taku, K.; Yamada, S.; Moriyasu, K.; Ishihara, T. *Org. Biomol. Chem.* **2009**, *7*, 1167-1170. (f) Inagaki, T.; Phong, L. T.; Furuta, A.; Ito, J.; Nishiyama, H. *Chem. Eur. J.* **2010**, *16*, 3090-3096. (g) Yu, F.; Zhang, X.-C.; Wu, F.-F.; Zhou, J.-N.; Fang, W.; Wu, J.; Chan, A. S. C. *Org. Biomol. Chem.* **2011**, *9*, 5652. (h) Sauer, D. C.; Wadepohl, H.; Gade, L. H. *Inorg. Chem.* **2012**, *51*, 12948-12958. (i) Niu, Q.; Sun, H.; Li, X.; Klein, H.-F.; Flörke, U. *Organometallics* **2013**, *32*, 5235-5238.

(10) For representative Ni hydrosilylation catalysts see: (a) Tamao, K.; Miyake, N.; Kiso, Y.; Kumada, M. *J. Am. Chem. Soc.* **1975**, *97*, 5603-5605. (b) Tamao, K.; Kobayashi, K.; Ito, Y. *J. Am. Chem. Soc.* **1989**, *111*, 6478-6480. (c) Chakraborty, S.; Krause, J. A.; Guan, H. *Organometallics* **2009**, *28*, 582-586. (d) Tran, B. L.; Pink, M.; Mindiola, D. J. *Organometallics* **2009**, *28*, 2234-2243. (e) Porter, T. M.; Hall, G. B.; Groy, T. L.; Trovitch, R. J. *Dalton Trans.* **2013**, *42*, 14689-14692. (f) Miller, Z. D.; Li, W.; Belderrain, T. R.; Montgomery, J. *J. Am. Chem. Soc.* **2013**, *135*, 15282-15285.

(11) (a) Morris, R. H. *Chem. Soc. Rev.* **2009**, *38*, 2282-2291. (b) Bullock, R. M. *Catalysis without Precious Metals*; Wiley-VCH: Weinheim, Germany, 2010. (c) Junge, K.; Schroeder, K.; Beller, M. *Chem. Commun.* **2011**, *47*, 4849-4859.

(12) Molybdenum is the only second row metal that is widely utilized in biological systems. For a recent review see: Hille, R.; Hall, J.; Basu, P. *Chem. Rev.* **2014**, *114*, 3963-4038.

(13) Haynes, W. M. *CRC Handbook of Chemistry and Physics: A Ready-reference Book of Chemical and Physical Data*, 94th ed.; Taylor & Francis, Boca Raton, FL, 2013-2014.

(14) Fuchikami, T.; Ubukata, Y.; Tanaka, Y. *Tetrahedron Lett.* **1991**, *32*, 1199-1202.

- (15) Baricelli, P. J.; Melean, L. G.; Ricardes, S.; Guanipa, V.; Rodriguez, M.; Romero, C.; Pardey, A. J.; Moya, S.; Rosales, M. *J. Organomet. Chem.* **2009**, *694*, 3381-3385.
- (16) (a) Bullock, R. M.; Voges, M. H. *J. Am. Chem. Soc.* **2000**, *122*, 12594-12595. (b) Voges, M. H.; Bullock, R. M. *J. Chem. Soc., Dalton Trans.* **2002**, 759-770. (c) Kimmich, B. F. M.; Fagan, P. J.; Hauptman, E.; Bullock, R. M. *Chem. Commun.* **2004**, 1014-1015. (d) Kimmich, B. F. M.; Fagan, P. J.; Hauptman, E.; Marshall, W. J.; Bullock, R. M. *Organometallics* **2005**, *24*, 6220-6229.
- (17) Namorado, S.; Antunes, M. A.; Veiros, L. F.; Ascenso, J. R.; Duarte, M. T.; Martins, A. M. *Organometallics* **2008**, *27*, 4589-4599.
- (18) (a) Adams, K. P.; Joyce, J. A.; Nile, T. A.; Patel, A. I.; Reid, C. D.; Walters, J. M. *J. Mol. Catal.* **1985**, *29*, 201-208. (b) Keinan, E.; Perez, D. *J. Org. Chem.* **1987**, *52*, 2576-2580. (c) Abdelquader, W.; Ozkar, S.; Peynircioglu, N. B. *Z. Naturforsch. B: Chem. Sci.* **1993**, *48*, 539-540. (d) Schmidt, T. *Tetrahedron Lett.* **1994**, *35*, 3513-3516. (e) Kayran, C.; Rouzi, P. *Z. Naturforsch. B: Chem. Sci.* **2001**, *56*, 1138-1142. (f) Stosur, M.; Symańska-Buzar, T. *J. Mol. Catal. A: Chem.* **2008**, *286*, 98-105.
- (19) Dioumaev, V. K.; Bullock, R. M. *Nature* **2003**, *424*, 530-532.
- (20) (a) Fernandes, A. C.; Fernandes, R.; Romão, C. C.; Royo, B. *Chem. Commun.* **2005**, 213-214. (b) Reis, P. M.; Romão, C. C.; Royo, B. *Dalton Trans.* **2006**, 1842-1846. (c) Pontes da Costa, A.; Reis, P. M.; Gamelas, C.; Romão, C. C.; Royo, B. *Inorg. Chim. Acta* **2008**, *361*, 1915-1921.
- (21) Ziegler, J. E.; Du, G.; Fanwick, P. E.; Abu-Omar, M. M. *Inorg. Chem.* **2009**, *48*, 11290-11296.
- (22) (a) Khalimon, A. Y.; Simionescu, R.; Kuzmina, L. G.; Howard, J. A. K.; Nikonov, G. I. *Angew. Chem. Int. Ed.* **2008**, *47*, 7701-7704. (b) Oeterson, E.; Khalimon, A. Y.; Simionescu, R.; Kuzmina, L. G.; Howard, J. A. K.; Nikonov, G. I. *J. Am. Chem. Soc.* **2009**, *131*, 908-909. (c) Shirobokov, O. G.; Gorelsky, S. I.; Simionescu, R.; Kuzmina, L. G.; Nikonov, G. I. *Chem. Commun.* **2010**, *46*, 7831-7833. (d) Shirobokov, O. G.; Kuzmina, L. G.; Nikonov, G. I. *J. Am. Chem. Soc.* **2011**, *133*, 6487-6489. (e) Khalimon, A. Y.; Ignatov, S. K.; Simionescu, R.; Kuzmina, L. G.; Howard, J. A. K.; Nikonov, G. I. *Inorg. Chem.* **2012**, *51*, 754-756. (f) Khalimon, A. Y.; Shirobokov, O. G.; Peterson, E.; Simionescu, R.; Kuzmina, L. G.; Howard, J. A. K.; Nikonov, G. I. *Inorg. Chem.* **2012**, *51*, 4300-4313. (g) Khalimon, A. Y.; Ignatov, S. K.; Okhupkin, A. I.; Simionescu, R.; Kuzmina, L. G.; Howard, J. A. K.; Nikonov, G. I. *Chem. Eur. J.* **2013**, *19*, 8573-8590.
- (23) (a) Arias-Ugarte, R.; Sharma, H. K.; Morris, A. L. C.; Pannell, K. H. *J. Am. Chem. Soc.* **2012**, *134*, 848-851. (b) Sharma, H. K.; Arias-Ugarte, R.; Tomlinson, D.; Gappa, R.; Metta-Magaña, A. J.; Ito, H.; Pannell, K. H. *Organometallics* **2013**, *32*, 3788-3794.

- (24) Chakraborty, S.; Blacque, O.; Fox, T.; Berke, H. *ACS Catal.* **2013**, *3*, 2208-2217.
- (25) Trovitch, R. J. *Synlett* **2014**, *25*, 1638-1642.
- (26) Chiericato Jr., G.; Arana, C. R.; Casado, C.; Cusdrado, I.; Abruña, H. D. *Inorg. Chim. Acta* **2000**, *300-302*, 32-42.
- (27) Zeng, D.; Hampden-Smith, M. J. *Polyhedron* **1992**, *11*, 2585-2589.
- (28) Several complexes featuring κ^2 -*N,N*-PDI coordination have been identified. For crystallographically characterized examples, see: (a) Lu, S.; Selbin, J. *Inorg. Chim. Acta* **1987**, *134*, 229-232. (b) Heard, P. J.; Tocher, D. A. *J. Chem. Soc., Dalton Trans.* **1998**, 2169-2176. (c) Cosquer, N.; Le Gall, B.; Conan, F.; Kerbaol, J.-M.; Sala-Pala, J.; Kubicki, M. M.; Vigier, E. *Inorg. Chim. Acta* **2006**, *359*, 4311-4316.
- (29) Hiya, K.; Nakayama, Y.; Yasuda, H. *Macromolecules* **2003**, *36*, 7916-7922.
- (30) de Bruin, B.; Bill, E.; Bothe, E.; Weyhermüller, T.; Wieghardt, K. *Inorg. Chem.* **2000**, *39*, 2936-2947.
- (31) Knijnenberg, Q.; Gambarotta, S.; Budzelaar, P. H. M. *Dalton Trans.* **2006**, 5442-5448.
- (32) PDI redox-activity has proven to be important for enabling first-row metal catalyzed transformations. For a leading example see: Chirik, P. J.; Wieghardt, K. *Science* **2010**, *327*, 794-795.
- (33) Corn, I. R.; Astudillo-Sánchez, P. D.; Zdilla, M. J.; Fanwick, P. E.; Shaw, M. J.; Miller, J. T.; Evans, D. H.; Abu-Omar, M. M. *Inorg. Chem.* **2013**, *52*, 54657-54663.
- (34) Ben-Daat, H.; Hall, G. B.; Groy, T. L.; Trovitch, R. J. *Eur. J. Inorg. Chem.* **2013**, 4430-4442.
- (35) Complete delocalization would be expected if the electron(s) is(are) delocalized across the LUMO of the κ^3 -*N,N,N*-PDI chelate (see ref. 31). It is also possible that κ^2 -*N,N*-PDI chelates can behave as redox non-innocent ligands. For α -iminopyridine reduction see: Lu, C. C.; Weyhermüller, T.; Bill, E.; Wieghardt, K. *Inorg. Chem.* **2009**, *48*, 6055-6064.
- (36) If η^1 -substrate binding occurs, the steric hinderance of the carbonyl substituents would be further removed from the metal center.
- (37) Ojima, I.; Kogure, T. *Organometallics* **1982**, *1*, 1390-1399.

(38) Schneider, N.; Finger, M.; Haferkemper, C.; Bellemin-Laponnaz, S.; Hofmann, P.; Gade, L. H. *Chem. Eur. J.* **2009**, *15*, 11515-11529.

(39) Neese, F. *Orca, an Ab Initio, Density Functional and Semiempirical Electronic Structure Program Package*, version 2.9.1; Max Planck Institute for Bioinorganic Chemistry: Mülheim an der Ruhr, Germany, 2012.

(40) (a) Becke, A. D. *J. Chem. Phys.* **1993**, *98*, 5648-5652. (b) Lee, C. T.; Yang, W. T.; Parr, R. G. *Phys. Rev. B* **1988**, *37*, 785-789.

(41) (a) Klamt, A.; Schüürmann, G. *J. Chem. Soc., Perkin Trans. 2* **1993**, 799-805. (b) Sinnecker, S.; Rajendran, A.; Klamt, A.; Diedenhofen, M.; Neese, F. *J. Phys. Chem. A* **2006**, *110*, 2235-2245.

(42) Grimme, S. *J. Comput. Chem.* **2006**, *27*, 1787-1799.

(43) Pantazis, D. A.; Chen, X. Y.; Landis, C. R.; Neese, F. *J. Chem. Theory Comput.* **2008**, *4*, 908-919.

(44) *Molekel*, Advanced Interactive 3D-Graphics for Molecular Sciences, Swiss National Supercomputing Center. <http://www.cscs.ch/molekel>.

Chapter 2

(1) (a) Pal, R.; Groy, T. L.; Trovitch, R. J. *Inorganic Chemistry* **2015**, *54*, 7506-7515. (b) van Aardenne, J. A.; Dentener, F. J.; Oliver, J. G. J.; Goldewijk, M. K.; Lelieveld, J. *Global Biogeochem. Cy.* **2001**, *15*, 909-928. (c) Sims, R. E. H.; Schock, R. N.; Adegbululgbé, A.; Fenhann, J.; Konstantinaviciute, I.; Moomaw, W.; Nimir, H. B.; Schlamadinger, B.; Torres-Martínez, J.; Turner, C.; Uchiyama, Y.; Vuori, S. J. V.; Wamukonya, N.; Zhang, X. 2007: Energy supply. In *Climate Change 2007: Mitigation. Contribution of Working Group III to the Fourth Assessment Report of the Intergovernmental Panel on Climate Change*, Edited by Metz, B.; Davidson, O. R.; Bosch, P. R.; Dave, R.; Meyer, L. A., Cambridge University Press, Cambridge, United Kingdom and New York, NY, USA.

(2) (a) Keeling, C. D.; Whorf, T. P.; Wahlen, M.; van der Plicht, J. *Nature* **1995**, *375*, 666-670. (b) Forster, P.; Ramaswamy, V.; Artaxo, P.; Berntsen, T.; Betts, R.; Fahey, D. W.; Haywood, J.; Lean, J.; Lowe, D. C.; Myhre, G.; Nganga, J.; Prinn, R.; Raga, G.; Schulz, M.; Van Dorland, R. 2007: Changes in Atmospheric Constituents and in Radiative Forcing. In: *Climate Change 2007: The Physical Science Basis. Contribution of Working Group I to the Fourth Assessment Report of the Intergovernmental Panel on Climate Change*, Edited by Solomon, S.; Qin, D.; Manning, M.; Chen, Z.; Marquis, M.; Averyt, K. B.; Tignor, M.; Miller, H. L., Cambridge University Press, Cambridge, United Kingdom and New York, NY, USA.

(3) (a) Raupach, M. R.; Marland, G.; Ciais, P.; Le Quéré, C.; Canadell, J. G.; Klepper, G.; Field, C. B. *Proc. Natl. Acad. Sci. USA* **2007**, *104*, 10288-10293. (b) IPCC, 2007: Summary

for Policymakers. In: *Climate Change 2007: Mitigation. Contribution of Working Group III to the Fourth Assessment Report of the Intergovernmental Panel on Climate Change*, Edited by Metz, B.; Davidson, O. R.; Bosch, P. R.; Dave, R.; Meyer, L. A., Cambridge University Press, Cambridge, United Kingdom and New York, NY, USA.

(4) Meinshausen, M.; Meinshausen, N.; Hare, W.; Raper, S. C. B.; Frieler, K.; Knutti, R.; Frame, D. J.; Allen, M. R. *Nature* **2009**, *458*, 1158-1162.

(5) Solomon, S.; Plattner, G.-P.; Knutti, R.; Friedlingstein, P. *Proc. Natl. Acad. Sci. USA* **2009**, *106*, 1704-1709.

(6) (a) Caldeira, K.; Wickett, M. E. *Nature* **2003**, *425*, 365. (b) Bindoff, N. L.; Willebrand, J.; Artale, V.; Cazenave, A.; Gregory, J.; Gulev, S.; Hanawa, K.; Le Quéré, C.; Levitus, S.; Nojiri, Y.; Shum, C. K.; Talley L. D.; Unnikrishnan, A. 2007: Observations: Oceanic Climate Change and Sea Level. In: *Climate Change 2007: The Physical Science Basis. Contribution of Working Group I to the Fourth Assessment Report of the Intergovernmental Panel on Climate Change*, Edited by Solomon, S.; Qin, D.; Manning, M.; Chen, Z.; Marquis, M.; Averyt, K. B.; Tignor, M.; Miller, H. L., Cambridge University Press, Cambridge, United Kingdom and New York, NY, USA.

(7) Rogelj, J.; McCollum, D. L.; Reisinger, A.; Meinshausen, M.; Riahi, K. *Nature* **2013**, *493*, 79-83.

(8) For CO₂ capture and geologic storage see: (a) Markewitz, P.; Kuckshinrichs, W.; Leitner, W.; Linssen, J. Zapp, P.; Bongartz, R.; Schreiber, A.; Müller, T. E. *Energy Environ. Sci.* **2012**, *5*, 7281-7305. (b) Figueroa, J. D.; Fout, T.; Plasynski, S.; McIlvried, H.; Srivastava, R. D. *Int. J. Greenh. Gas Con.* **2008**, *2*, 9-20. (c) Davison, J. *Energy* **2007**, *32*, 1163-1176. (d) Steeneveldt, R.; Berger, B.; Torp, T. A. *Chem. Eng. Res. Des.* **2006**, *84*, 739-763.

(9) For general CO₂ fixation pathways see: (a) Martin, R.; Kleij, A. W. *ChemSusChem.* **2011**, *4*, 1259-1263. (b) Riduan, S. N.; Zhang, Y. *Dalton Trans.* **2010**, *39*, 3347-3357. (c) Yu, K. M. K.; Curcic, I.; Gabriel, J.; Tsang, S. C. E. *ChemSusChem* **2008**, *1*, 893-899. (d) Sakakura, T.; Choi, J.-C.; Yasuda, H. *Chem. Rev.* **2007**, *107*, 2365-2387.

(10) For examples of C-H carboxylation see: (a) Boogaerts, I. I. F.; Nolan, S. P. *Chem. Commun.* **2011**, *47*, 3021-3024. (b) Boogaerts, I. I. F.; Nolan, S. P. *J. Am. Chem. Soc.* **2010**, *132*, 8858-8859. (c) Boogaerts, I. I. F.; Fortman, G. C.; Furst, M. R. L.; Cazin, C. S. J.; Nolan, S. P. *Angew. Chem. Int. Ed.* **2010**, *49*, 8674-8677. (d) Zhang, L.; Cheng, J.; Ohishi, Z.; Hou, Z. *Angew. Chem. Int. Ed.* **2010**, *49*, 8670-8673. (e) Vechorkin, O.; Hirt, N.; Hu, X. *Org. Lett.* **2010**, *12*, 3567-3569.

(11) For polycarbonates from CO₂ see: (a) Kember, M. R.; Buchard, A.; Williams, C. K. *Chem. Commun.* **2011**, *47*, 141-163. (b) Sakakura, T.; Kohno, K. *Chem. Commun.* **2009**,

1312-1330. (c) Darensbourg, D. J.; *Chem. Rev.* **2007**, *107*, 2388-2410. (d) Coates, G. W.; Moore, D. R. *Angew. Chem. Int. Ed.* **2004**, *43*, 6618-6639.

(12) Mikkelsen, M.; Jørgensen, M.; Krebs, F. C. *Energy Environ. Sci.* **2010**, *3*, 43-81.

(13) Aresta, M. In *Activation of Small Molecules*, Edited by Tolman, W. B., Wiley-VCH, Weinheim, 2006, pp 1-42.

(14) For electrocatalytic CO₂ reduction see: (a) Windle, C. D.; Peruta, R. N. *Coord. Chem. Rev.* **2012**, *256*, 2562-2570, and references therein. (b) Benson, E. E.; Kubiak, C. P.; Sathrum, A. J.; Smieja, J. M. *Chem. Soc. Rev.* **2009**, *38*, 89-99. (c) Morris, A. J.; Meyer, G. J.; Fujita, E. *Acc. Chem. Res.* **2009**, *42*, 1983-1994.

(15) (a) Drake, J. L.; Manna, C. M.; Byers, J. A. *Organometallics* **2013**, *32*, 6891-6894. (b) Jeletic, M. S.; Mock, M. T.; Appel, A. M.; Linehan, J. C. *J. Am. Chem. Soc.* **2013**, *135*, 11533-11536. (c) Ono, T.; Planas, N.; Miró, P.; Ertem, M. Z.; Escudero-Adán, E. C.; Benet-Buchholtz, J.; Gagliardi, L.; Cramer, C. J.; Llobet, A. *ChemCatChem* **2013**, *5*, 3897-3903. (d) Jiang, Y.; Blacque, O.; Fox, T.; Berke, H. *J. Am. Chem. Soc.* **2013**, *135*, 7751-7760. (e) Ziebart, C.; Federsel, C.; Anbarasan, P.; Jackstell, R.; Baumann, W.; Spannenberg, A.; Beller, M. *J. Am. Chem. Soc.* **2012**, *134*, 20701-20704. (f) Langer, R.; Diskin-Posner, Y.; Leitus, G.; Shimon, L. J. W.; Ben-David, Y.; Milstein, D. *Angew. Chem. Int. Ed.* **2011**, *50*, 9948-9952. (g) Federsel, C.; Boddien, A.; Jackstell, R.; Jennerjahn, R.; Dyson, P. J.; Scopelliti, R.; Laurenczy, G.; Beller, M.; *Angew. Chem. Int. Ed.* **2010**, *49*, 977-9780. (h) Tanaka, R.; Yamashita, M.; Nozaki, K. *J. Am. Chem. Soc.* **2009**, *131*, 14168-14169. (i) Himeda, Y.; Onozawa-Komatsuzaki, N.; Sugihara, H.; Kasuga, K. *Organometallics* **2007**, *26*, 702-712. (j) Munshi, P.; Main, A. D.; Linehan, J. C.; Tai, C.-C.; Jessop, P. G. *J. Am. Chem. Soc.* **2002**, *124*, 7963-7971. (k) Jessop, P. G.; Ikariya, T.; Noyori, R. *Nature* **1994**, *368*, 231-233. (l) Gassner, F.; Leitner, W. *J. Chem. Soc., Chem. Commun.* **1993**, 1465-1466.

(16) (a) Bontemps, S.; Vendier, L.; Sabo-Etienne, S. *J. Am. Chem. Soc.* **2014**, *136*, 4419-4425. (b) LeBlanc, F. A.; Piers, W. E.; Parvez, M. *Angew. Chem. Int. Ed.* **2014**, *53*, 789-792. (c) Bontemps, S.; Sabo-Etienne, S. *Angew. Chem. Int. Ed.* **2013**, *52*, 10253-10255. (d) Berkefeld, A.; Piers, W. E.; Parvez, M.; Castro, L.; Maron, L.; Eisenstein, O. *Chem. Sci.* **2013**, *4*, 2152-2162. (e) Bontemps, S.; Vendier, L.; Sabo-Etienne, S. *Angew. Chem. Int. Ed.* **2012**, *51*, 1671-1674.

(17) (a) Tominaga, K.; Sasaki, Y.; Watanabe, T.; Saito, M. *Bull. Chem. Soc. Jpn.* **1995**, *68*, 2837-2842. (b) Tominaga, K.; Sasaki, Y.; Kawai, M.; Watanabe, T.; Saito, M. *J. Chem. Soc., Chem. Commun.* **1993**, 629-631.

(18) (a) Rezayee, N. M.; Huff, C. A.; Sanford, M. S. *J. Am. Chem. Soc.* **2015**, *137*, 1028-1031. (b) Wesselbaum, S. Moha, V.; Meuresch, M.; Broninski, S.; Thenert, K. M.; Kothe, J.; von Stein, T.; Englert, U.; Hölscher, M.; Klankermayer, J.; Leitner, W. *Chem. Sci.* **2015**,

6, 693-704. (c) Wesselbaum, S.; von Stein, T.; Klankermayer, J.; Leitner, W. *Angew. Chem. Int. Ed.* **2012**, *51*, 7499-7502. (d) Huff, C. A.; Sanford, M. S. *J. Am. Chem. Soc.* **2011**, *133*, 18122-18125.

(19) Eisenschmid, T. C.; Eisenberg, R. *Organometallics* **1989**, *8*, 1822-1824.

(20) Metsänen, T. T.; Oestreich, M. *Organometallics* **2015**, *34*, 543-546.

(21) Riduan, S. N.; Zhang, Y.; Ying, J. Y. *Angew. Chem.* **2009**, *121*, 3372-3375.

(22) (a) Courtemanche, M.-A.; Légaré, M.-A.; Maron, L.; Fontaine, F.-G. *J. Am. Chem. Soc.* **2013**, *135*, 9326-9329. (b) Wang, T.; Stephan, D. W. *Chem. Eur. J.* **2014**, *20*, 3036-3039. (c) Gomes, C. D. N.; Blondiaux, E.; Thuéry, P.; Cantat, T. *Chem. Eur. J.* **2014**, *20*, 7098-7106. (d) Wang, T.; Stephan, D. W. *Chem. Commun.*, **2014**, *50*, 7007-7010.

(23) Fujiwara, K.; Yasuda, S.; Mizuta, T. *Organometallics* **2014**, *33*, 6692-6695.

(24) Anker, M. D.; Arrowsmith, M.; Bellham, P.; Hill, M. S.; Kociok-Köhn, G.; Liptrot, D. J.; Mahon, M. F.; Weetman, C. *Chem. Sci.* **2014**, *5*, 2826-2830.

(25) (a) Chakraborty, S.; Zhang, J.; Krause, J. A.; Guan, H. *J. Am. Chem. Soc.* **2010**, *132*, 8872-8873. (b) Chakraborty, S.; Patel, Y. J.; Krause, J. A.; Guan, H. *Polyhedron* **2012**, *32*, 30-34. (c) Chakraborty, S.; Zhang, J.; Patel, Y. J.; Krause, J. A.; Guan, H. *Inorg. Chem.* **2013**, *52*, 37-47.

(26) Sgro, M. J.; Stephan, D. W. *Angew. Chem. Int. Ed.* **2012**, *51*, 11343-11345.

(27) (a) Wehmschulte, R. J.; Saleh, M.; Powell, D. R. *Organometallics* **2013**, *32*, 6812-6819. (b) Mitton, S. J.; Turculet, L. *Chem. Eur. J.* **2012**, *18*, 15258-15262. (c) Park, S.; Bézier, D.; Brookhart, M. *J. Am. Chem. Soc.* **2012**, *134*, 11404-11407. (d) Khandelwal, M.; Wehmschulte, R. J. *Angew. Chem. Int. Ed.* **2012**, *51*, 7323-7326. (e) Berkefeld, A.; Piers, W. E.; Parvez, M. *J. Am. Chem. Soc.* **2010**, *132*, 10660-10661. (f) Matsuo, T.; Kawaguchi, H. *J. Am. Chem. Soc.* **2006**, *128*, 12362-12363.

(28) Haynes, W. M. *CRC Handbook of Chemistry and Physics: A Ready-reference Book of Chemical and Physical Data*, 94th ed.; Taylor & Francis, Boca Raton, FL, 2013-2014.

(29) Pal, R.; Groy, T. L.; Bowman, A. C.; Trovitch, R. J. *Inorg. Chem.* **2014**, *53*, 9357-9365.

(30) Ben-Daat, H.; Hall, G. B.; Groy, T. L.; Trovitch, R. J. *Eur. J. Inorg. Chem.* **2013**, 4430-4442.

- (31) The oxidation addition of I₂ to **1** occurs in an ionic fashion, a pathway commonly observed for 18-electron precursors and electrophilic reagents. For a discussion see: Collman, J. P.; Hegedus, L. S.; Norton, J. R.; Finke, R. G. *Principles and Applications of Organotransition Metal Chemistry*; University Science Books: Sausalito, CA, 1987; pp 279-322.
- (32) Knijnenburg, Q.; Gambarotta, S.; Budzelaar, P. H. M. *Dalton Trans.* **2006**, 5442-5448.
- (33) Margulieux, G. W.; Turner, Z. R.; Chirik, P. J. *Angew. Chem. Int. Ed.* **2014**, *53*, 14211-14215.
- (34) Mukhopadhyay, T. K.; Flores, M.; Feller, R. K.; Scott, B. L.; Taylor, R. D.; Paz-Pasternak, M.; Henson, N. J.; Rein, F. N.; Smythe, N. C.; Trovitch, R. J.; Gordon, J. C. *Organometallics* **2014**, *33*, 7101-7112.
- (35) Mukhopadhyay, T. K.; Flores, M.; Groy, T. L. Trovitch, R. J. *J. Am. Chem. Soc.* **2014**, *136*, 882-885.
- (36) Trovitch, R. J. *Synlett* **2014**, *25*, 1638-1642.
- (37) This is strong evidence against the formation of a complex featuring a static or fluxional agnostic interaction, which are known to exhibit J_{CH} values between 80-100 Hz. Our inability to observe a second J_{CH} coupling constant is consistent with C-H bond oxidative addition. For more information, see: Brookhart, M.; Green, M. L. H. *J. Organomet. Chem.* **1983**, *250*, 395-408.
- (38) (a) Zhang, Y.; Hanna, B. S.; Dineen, A.; Williard, P. G.; Bernskoetter, W. H. *Organometallics* **2013**, *32*, 3969-3979. (b) Minato, M.; Zhou, D.-Y.; Sumiura, K.; Oshima, Y.; Mine, S.; Ito, T.; Kakeya, M.; Hoshino, K.; Asaeda, T.; Nakada, T.; Osakada, K. *Organometallics* **2012**, *31*, 4941-4949. (c) Ito, T.; Matsubara, T. *J. Chem. Soc., Dalton Trans.* **1988**, 2241-2242. (d) Ellis, R.; Henderson, R. A.; Hills, A.; Hughes, D. L. *J. Organomet. Chem.* **1987**, *333*, C6-C10. (e) Fong, L. K.; Fox, J. R.; Cooper, N. J. *Organometallics* **1987**, *6*, 223-231. (f) Lyons, D.; Wilkinson, G.; Thornton-Pett, M.; Hursthouse, M. B. *J. Chem. Soc., Dalton Trans.* **1984**, 695-700. (g) Darensbourg, D. J.; Rokicki, A.; Darensbourg, M. Y. *J. Am. Chem. Soc.* **1981**, *103*, 3223-3224.
- (39) Huang, F.; Zhang, C.; Jiang, J.; Wang, Z.-X.; Guan, H. *Inorg. Chem.* **2011**, *50*, 3816-3825.
- (40) (a) Miller, T. M.; Whitesides, G. M. *Organometallics* **1986**, *5*, 1473-1480. (b) Chappell, S. D.; Cole-Hamilton, D. J. *Polyhedron* **1982**, *1*, 739-777.

Chapter 3

- (1) (a) Pal, R.; Cherry, B. R.; Flores, M.; Groy, T. L.; Trovitch, R. J. *Dalton Transactions* **2016**, 45, 10024-10033 (b) Kubas, G. J. *J. Organomet. Chem.* **2001**, 635, 37-68.
- (2) Schrock, R. R. *Acc. Chem. Res.* **2005**, 38, 955-962.
- (3) Schrock, R. R. *Chem. Rev.* **2002**, 102, 145-179.
- (4) Kubas, G. J.; Ryan, R. R.; Swanson, B. I.; Vergamini, P. J.; Wasserman, H. J. *J. Am. Chem. Soc.* **1984**, 106, 451-452.
- (5) Chatt, J.; Dilworth, J. R.; Richards, R. L. *Chem. Rev.* **1978**, 78, 589-625.
- (6) (a) Arashiba, K.; Miyake, Y.; Nishibayashi, Y. *Nature Chem.* **2011**, 3, 120-125. (b) Kinoshita, E.; Arashiba, K.; Kuriyama, S.; Miyake, Y.; Shimazaki, R.; Nakanishi, H.; Nishibayashi, Y. *Organometallics* **2012**, 31, 8437-8443.
- (7) Laplaza, C.; Cummins, C. C. *Science* **1995**, 268, 861-863.
- (8) Yandulov, D. V.; Schrock, R. R. *Science* **2003**, 301, 76-78.
- (9) Schrock, R. R. Murdzek, J. S.; Bazan, G. C.; Robbins, J.; DiMare, M.; O'Regan, M. *J. Am. Chem. Soc.* **1990**, 112, 3875-3886.
- (10) For an early review of Mo(II) chemistry see: Sheldon, J. C. *Nature* **1959**, 184, 1210-1213.
- (11) For examples of Mo(III) complex reactivity see: (a) Laplaza, C.; Johnson, M. J. A.; Peters, J. C.; Odom, A. L.; Kim, E.; Cummins, C. C.; George, G. N.; Pickering, I. J. *J. Am. Chem. Soc.* **1996**, 118, 8623-8638. (b) Cummins, C. C. *Chem. Commun.* **1998**, 1777-1786.
- (12) Hille, R. *Chem. Rev.* **1996**, 96, 2757-2816.
- (13) Haynes, W. M. *CRC Handbook of Chemistry and Physics: A Ready-reference Book of Chemical and Physical Data*, 94th ed.; Taylor & Francis, Boca Raton, FL, 2013-2014. Like Mo(I), Mo(0) is omitted from this list since it does not occur naturally.
- (14) Wilson, F. C.; Shoemaker, D. P. *J. Chem. Phys.* **1957**, 27, 809.
- (15) (a) Wrighton, M. S.; Ginley, D. S. *J. Am. Chem. Soc.* **1975**, 97, 4246-4251. (b) Hughey, J. L.; Bock, C. B.; Meyer, T. J. *J. Am. Chem. Soc.* **1975**, 97, 4440-4441.
- (16) Xhuang, B.; Huang L.; Yang, Y.; Lu, J. *Inorg. Chim. Acta* **1986**, 116, L41-L43.

- (17) (a) Shiu, K.-B.; Curtis, M. D.; Huffman, J. C. *Organometallics* **1983**, *2*, 936-938. (b) Curtis, M. D.; Shiu, K.-B.; Butler, W. M.; Huffman, J. C. *J. Am. Chem. Soc.* **1986**, *108*, 3335-3343.
- (18) Bartlett, I. A.; Connelly, N. G.; Orpen, A. G.; Quayle, M. J.; Rankin, J. C. *Chem. Commun.* **1996**, 2583-2584.
- (19) McWhillie, S. L. W.; Jones, C. J.; McCleverty, J. A.; Collison, D.; Mabbs, F. E. *J. Chem. Soc., Chem. Commun.* **1990**, 940-942.
- (20) Connelly, N. G.; Geiger, W. E.; Lovelace, S. R.; Metz, B.; Paget, T. J.; Winter, R. *Organometallics* **1999**, *18*, 3201-3207.
- (21) Seidel, W. W.; Arias, M. D. I.; Schaffrath, M.; Jahnke, M. C.; Hepp, A.; Pape, T. *Inorg. Chem.* **2006**, *45*, 4791-4800.
- (22) Beissel, T.; Della Vedova, B. S. P. C.; Wieghardt, K.; Boese, R. *Inorg. Chem.* **1990**, *29*, 1736-1741.
- (23) Wang, M.; Weyhermüller, T.; Wieghardt, K. *Chem. Eur. J.* **2014**, *20*, 9037-9044.
- (24) Wang, M.; Weyhermüller, T.; Wieghardt, K. *Eur. J. Inorg. Chem.* **2015**, 3246-3254.
- (25) Roberts, K. A. E.; Brown, N. J.; Roberts, H. N.; McDouall, J. J. W.; Low, P. J.; Whitely, M. W. *Polyhedron* **2015**, *34*, 89-97.
- (26) Ben-Daat, H.; Hall, G. B.; Groy, T. L.; Trovitch, R. J. *Eur. J. Inorg. Chem.* **2013**, 4430-4442.
- (27) Pal, R.; Groy, T. L.; Bowman, A. C.; Trovitch, R. J. *Inorg. Chem.* **2014**, *53*, 9357-9365.
- (28) Pal, R.; Groy, T. L.; Trovitch, R. J. *Inorg. Chem.* **2015**, *54*, 7506-7515.
- (29) Baker, P. K.; Fraser, S. G.; Keys, E. M. *J. Organomet. Chem.* **1986**, *309*, 319-321.
- (30) DuBois, D. W.; Iwamoto, R. T.; Kleinberg, J. *Inorg. Chem.* **1970**, *9*, 968-970.
- (31) (a) Luca, O. R.; Crabtree, R. H. *Chem. Soc. Rev.* **2013**, *42*, 1440. (b) Lyaskovskyy, V.; de Bruin, B. *ACS Catal.* **2012**, *2*, 270-279. (c) Chirik, P. J.; Wieghardt, K. *Science* **2010**, *327*, 794-795. (d) Bouwkamp, M. W.; Bowman, A. C.; Lobkovsky, E.; Chirik, P. J. *J. Am. Chem. Soc.* **2006**, *128*, 13340-13341.
- (32) Knijnenburg, Q.; Gambarotta, S.; Budzelaar, P. H. M. *Dalton Trans.* **2006**, 5442-5448.
- (33) Crabtree, R. H. *Acc. Chem. Res.* **1990**, *23*, 95-101.

(34) Weil, J. A.; Bolton, J. R. *Electron paramagnetic resonance: Elementary theory and practical applications*; Wiley, Hoboken, NJ, 2007.

(35) Stoll, S.; Schweiger, A. *J. Magn. Reson.* **2006**, *178*, 42-55.

Chapter 4

(1) Bard, A. J.; Fox, M. A. *Acc. Chem. Res.* **1995**, *28*, 141–145.

(2) Gust, D.; Moore, T. A.; Moore, A. L. *Acc. Chem. Res.* **2009**, *42*, 1890–1898.

(3) Lewis, N. S.; Nocera, D. G. *Proc. Natl. Acad. Sci. U. S. A.* **2006**, *103*, 15729–15735.

(4) Walter, M. G.; Warren, E. L.; McKone, J. R.; Boettcher, S. W.; Mi, Q.; Santori, E. A.; Lewis, N. S. *Chem. Rev.* **2010**, *110*, 6446–6473.

(5) Thoi, V. S.; Sun, Y.; Long, J. R.; Chang, C. J. *Chem. Soc. Rev.* **2013**, *42*, 2388–2400.

(6) Esswein, A. J.; Nocera, D. G. *Chem. Rev.* **2007**, *107*, 4022–4047.

(7) Zee, D. Z.; Chantarojsiri, T.; Long, J. R.; Chang, C. J. *Acc. Chem. Res.* **2015**, *48*, 2027–2036.

(8) Karunadasa, H. I.; Chang, C. J.; Long, J. R. *Nature* **2010**, *464*, 1329–1333.

(9) Steele, B. C. H.; Heinzl, A. *Nature* **2001**, *414*, 345–352.

(10) Debe, M. K. *Nature* **2012**, *486*, 43–51.

(11) Ezaki, H.; Morinaga, M.; Watanabe, S. *Electrochim. Acta* **1993**, *38*, 557–564.

(12) Nocera, D. G. *Acc. Chem. Res.* **2012**, *45*, 767–776.

(13) Du, P.; Eisenberg, R. *Energy Environ. Sci.* **2012**, *5*, 6012.

(14) Dubois, D. L. *Inorg. Chem.* **2014**, *53*, 3935–3960.

(15) Gan, L.; Groy, T. L.; Tarakeshwar, P.; Mazinani, S. K. S.; Shearer, J.; Mujica, V.; Jones, A. K. *J. Am. Chem. Soc.* **2015**, *137*, 1109–1115.

(16) Baxley, G. T.; Avey, A. A.; Aukett, T. M.; Tyler, D. R. *Inorganica Chim. Acta* **2000**, *300-302*, 102–112.

(17) Blum, O.; Milstein, D. *J. Am. Chem. Soc.* **2002**, *124*, 11456–11467.

(18) Parkin, G.; Bercaw, J. E. *J. Am. Chem. Soc.* **1989**, *111*, 391–393.

- (19) Yoon, K.; Parkin, G.; Rheingold, A. L. *J. Am. Chem. Soc.* **1991**, *113*, 1437–1438.
- (20) Yoon, M.; Tyler, D. R. *Chem. Commun.* **1997**, 639–670.
- (21) Silavwe, N. D.; Bruce, M. R. M.; Philbin, C. E.; Tyler, D. R. *Inorg. Chem.* **1988**, *27*, 4669–4676.
- (22) Karunadasa, H. I.; Montalvo, E.; Sun, Y.; Majda, M.; Long, J. R.; Chang, C. J. *Science* **2012**, *335*, 698–702.
- (23) Thoi, V. S.; Karunadasa, H. I.; Surendranath, Y.; Long, J. R.; Chang, C. J. *Energy Environ. Sci.* **2012**, *5*, 7762.
- (24) Pal, R.; Groy, T. L.; Trovitch, R. J. *Inorg. Chem.* **2015**, *54*, 7506–7515.
- (25) Pal, R.; Groy, T. L.; Bowman, A. C.; Trovitch, R. J. *Inorg. Chem.* **2014**, *53*, 9357–9365.
- (26) Ben-Daat, H.; Hall, G. B.; Groy, T. L.; Trovitch, R. J. *Eur. J. Inorg. Chem.* **2013**, 4430–4442.
- (27) Baker, P. K.; Fraser, S. G.; Keys, E. M. *J. Organomet. Chem.* **1986**, *309*, 319–321.
- (28) Pal, R.; Cherry, B. R.; Flores, M.; Groy, T. L.; Trovitch, R. J. *Dalt. Trans.* **2016**.
- (29) Kilgore, U. J.; Roberts, J. A. S.; Pool, D. H.; Appel, A. M.; Stewart, M. P.; Dubois, M. R.; Dougherty, W. G.; Kassel, W. S.; Bullock, R. M.; Dubois, D. L. *J. Am. Chem. Soc.* **2011**, *133*, 5861–5872.
- (30) Baffert, C.; Artero, V.; Fontecave, M. *Inorg. Chem.* **2007**, *46*, 1817–1824.
- (31) Balaj, O. P.; Siu, C.-K.; Balteanu, I.; Fox-Beyer, B. S.; Beyer, M. K.; Bondybey, V. *E. J. Phys. Chem. A* **2004**, *108*, 7506–7512.

Chapter 5

- (1) Falkowski, P.; Scholes, R. J.; Boyle, E.; Canadell, J.; Canfield, D.; Elser, J.; Gruber, N.; Hibbard, K.; Höglberg, P.; Mackenzie, F. T.; Moore, B.; Pedersen, T.; Rosenthal, Y.; Seitzinger, S.; Smetacek, V.; Steffen, W. *Science*, **290**, 291–296.
- (2) Appel, A. M.; Bercaw, J. E.; Bocarsly, A. B.; Dobbek, H.; DuBois, D. L.; Dupuis, M.; Ferry, J. G.; Fujita, E.; Hille, R.; Kenis, P. J. A.; Kerfeld, C. A.; Morris, R. H.; Peden, C. H. F.; Portis, A. R.; Ragsdale, S. W.; Rauchfuss, T. B.; Reek, J. N. H.; Seefeldt, L. C.; Thauer, R. K.; Waldrop, G. L. *Chem. Rev.* **2013**, *113*, 6621–6658.

- (3) Chen, Z.; Concepcion, J. J.; Brennaman, M. K.; Kang, P.; Norris, M. R.; Hoertz, P. G.; Meyer, T. J. *Proc. Natl. Acad. Sci. U. S. A.* **2012**, *109*, 15606-15611.
- (4) Aresta, M.; Dibenedetto, A.; Angelini, A. *Chem. Rev.* **2014**, *114*, 1709–1742.
- (5) Jin, W.; Zhang, C.; Chang, X.; Fan, Y.; Xing, W.; Xu, N. *Environ. Sci. Technol.* **2008**, *42*, 3064–3068.
- (6) Lu, Z.; Chang, C.; Yin, Q-Z.; Ng, C. Y.; Jackson, W. M. *Science*, **2014**, *346*, 61-64.
- (7) a) Kilpatrick, A. F. R.; Cloke, F. G. N. *Chem. Commun.* **2014**, *50*, 2769-2771. b) Noor, A.; Qayyum, S.; Bauer, T.; Schwarz, S.; Weber, B.; Kempe, R. *Chem. Commun.* **2014**, *50*, 13127-13130. c) Krogman, J. P.; Foxman, B. M.; Thomas, C. M. *J. Am. Chem. Soc.* **2011**, *133*, 14582-14585.
- (8) a) Kobayashi, K.; Tanaka, K. *Inorg. Chem.* **2015**, *54*, 5085-5095. b) Machan, C. W.; Chabolla, S. A.; Yin, J.; Gilson, M. K.; Tezcan, F. A.; Kubiak, C. P. *J. Am. Chem. Soc.* **2014**, *136*, 14598-14607. c) Fachinetti, G.; Floriani, C.; Chiesi-Villa, A.; Guastini, C. *J. Am. Chem. Soc.* **1979**, *101*, 1767-1775. d) Alvarez, R.; Carmona, E.; Poveda, M. L.; Sanchez-Delgado, R. *J. Am. Chem. Soc.* **1984**, *106*, 2731-2732. e) Lee, G. R.; Maher, J. M.; Cooper, N. J. *J. Am. Chem. Soc.* **1987**, *109*, 2956-2962.
- (9) a) DuBois, D. L.; Miedaner, A.; Haltiwanger, R. C. *J. Am. Chem. Soc.* **1991**, *113*, 8753-8764. b) Garg, K.; Matsubara, Y.; Ertem, M. Z.; Lewandowska-Andralojc, A.; Sato, S.; Szalda, D. J.; Muckerman, J. T.; Fujita, E. *Angew. Chem., Int. Ed.* **2015**, *54*, 14128-14132. c) Sato, S.; Morikawa, T.; Kajino, T.; Ishitani, O. *Angew. Chem., Int. Ed.* **2013**, *125*, 1022-1026. d) Feller, M.; Gellrish, U.; Anaby, A.; Diskin-Posner, Y.; Milstein, D. *J. Am. Chem. Soc.* **2016**, *138*, 6445-6454.
- (10) Aresta, M. In *Activation of Small Molecules*; Tolman, W. B., Ed.; Wiley-VCH, Weinheim, 2006; pp 1-42.
- (11) a) Herskovitz, T. *J. Am. Chem. Soc.* **1977**, *99*, 2391-2392. b) Calabrese, J. C.; Herskovitz, T.; Kinney, J. B. *J. Am. Chem. Soc.* **1983**, *105*, 5914-5915.
- (12) a) Aresta, M.; Nobile, C. F. *Dalton Trans.* **1977**, *7*, 708-711. b) Aresta, M.; Nobile, C. F. *Inorg. Chim. Acta* **1977**, *24*, L49-L50. c) Komiyama, S.; Akita, M.; Kasuga, N.; Hirano, M.; Fukuoka, A. *Chem. Commun.* **1994**, *9*, 1115-1116. d) Sakamoto, M.; Shimizu, L.; Yamamoto, A. *Organometallics* **1994**, *13*, 407-409.
- (13) Castro-Rodriguez, I.; Nakai, H.; Zakharov, L.; Rheingold, A. L.; Meyer, K. *Science* **2004**, *305*, 1757-1759.
- (14) a) Evans, W. J.; Seibel, C. A.; Ziller, J. W. *Inorg. Chem.* **1998**, *37*, 770-776. b) Paparo, A.; Silvia, J. S.; Kefalidis, C. E.; Spaniol, T. P.; Maron, L.; Okuda, J.; Cummins, C. C. *Angew. Chem. Int. Ed.* **2015**, *54*, 9115-9119. c) Angamuthu, R.; Byers, P.; Lutz, M.; Spek,

A. L.; Bouwman, E. *Science* **2010**, 327, 313-315. d) Farrugia, L. J., Lopinski, S., Lovatt, P. A. & Peacock, R. D. *Inorg. Chem.* **2001**, 40, 558-559.

(15) a) Chatt, J.; Kubota, M.; Leigh, G.-J.; March, F. C.; Mason, R.; Yarrow, D. J. *Chem. Commun.* **1974**, 24, 1033-1034. b) Carmona, E.; Gonzalez, F.; Poveda, M. L.; Marin, J. M. *J. Am. Chem. Soc.* **1983**, 105, 3365-3366. c) Langer, J.; Imhof, W.; Fabra, M. J.; García-Orduña, P.; Görls, H.; Lahoz, F. J.; Oro, L. A.; Westerhausen, M. *Organometallics* **2010**, 29, 1642-1651. d) Herskovitz, T.; Guggenberger, L. J. *J. Am. Chem. Soc.* **1976**, 98, 1615-1616. e) Dahlenburg, L.; Prengel, C. *J. Organomet. Chem.* **1986**, 308, 63-71.

(16) Ben-Daat, H.; Hall, G. B.; Groy, T. L.; Trovitch, R. J. *Eur. J. Inorg. Chem.* **2013**, 4430-4442.

(17) Pal, R.; Groy, T. L.; Bowman, A. C.; Trovitch, R. J. *Inorg. Chem.* **2014**, 53, 9357-9365.

(18) Pal, R.; Groy, T. L.; Trovitch, R. J. *Inorg. Chem.* **2015**, 54, 7506-7515.

(19) Pal, R.; Cherry, B. R.; Flores, M.; Groy, T. L.; Trovitch, R. J. *Dalton Trans.* **2016**, 45, 10024-10033.

(20) Pal, R.; Laureanti, J. A.; Groy, T. L.; Jones, A. K.; Trovitch, R. J. *Chem. Commun.* **2016**, 52, 11555-11558.

(21) Carnahan, E. M.; Protasiewicz, J. D.; Lippard, S. J. *Acc. Chem. Res.* **1993**, 26, 90-97.

(22) Porter, T. M.; Hall, G. B.; Groy, T. L.; Trovitch, R. J. *Dalton Trans.* **2013**, 42, 14689-14692.

(23) Baker, P. K.; Fraser, S. G.; Keys, E. M. *J. Organomet. Chem.* **1986**, 309, 319-321.

APPENDIX A

UNPUBLISHED BIS(IMINO)PYRIDINE MOLYBDENUM CHEMISTRY

A.1. Preparation of $(^{\text{PyEt}}\text{PDI})\text{MoOCl}_2$

A 20 mL reaction vial was charged with 0.105 g (0.252 mmol) of $\text{Mo}(\text{THF})_3\text{Cl}_3^1$ and 5 mL of THF. To it, 0.095 g (0.256 mmol) of $^{\text{PyEt}}\text{PDI}^2$ and 0.040 g (0.333 mmol) of styrene oxide were added dropwise while stirring. Instantaneous color change from orange to blue was observed. After 24 h, the blue solution was filtered through Celite and dried under vacuum. After washing with pentane, 0.075 g (0.135 mmol) of a bluish-purple solid was isolated (54%). Recrystallized from benzene/pentane solution. ^1H NMR (benzene- d_6 , 400 MHz): δ 8.33 (d, 4.8 Hz, 2H, *Py*), 7.37 (d, 8.0 Hz, 2H, *Py*), 6.97 (t, 7.2 Hz, 2H, *Py*), 6.53 (d, 6.4 Hz, 2H, *Py*), 5.80 (t, 8 Hz, 1H, *Py*), 4.52 (d, 8.0 Hz, 2H, *Py*), 3.97 (t, 7.6 Hz, 4H, CH_2), 3.63 (t, 7.2 Hz, 4H, CH_2), 1.09 (s, 6H, CH_3).

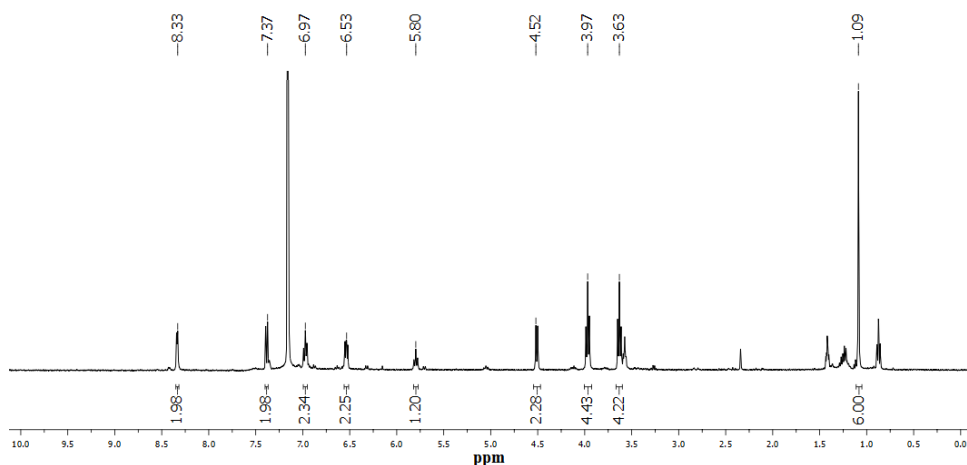


Figure A.1. ^1H NMR of $(^{\text{PyEt}}\text{PDI})\text{MoOCl}_2$ in benzene- d_6 .

A.2. Preparation of $[(\text{Ph}_2\text{PPrPDI})\text{MoCl}_2][\text{Cl}]$ using $\text{Mo}(\text{THF})_3\text{Cl}_3$

A 20 mL reaction vial was charged with 0.204 g (0.488 mmol) of $\text{Mo}(\text{THF})_3\text{Cl}_3$ ¹ and 5 mL of THF. To it, 0.295 g (0.481 mmol) of Ph_2PPrPDI ³ in 15 mL THF was added dropwise while stirring. Instantaneous color change from orange to amber was observed. After 24 h, the amber solid was isolated on top of a sintered frit and dried under vacuum. After washing with THF, 0.324 g (0.397 mmol) of amber solid was isolated (81%). Suitable crystals for X-ray diffraction were grown from CHCl_3 /toluene.

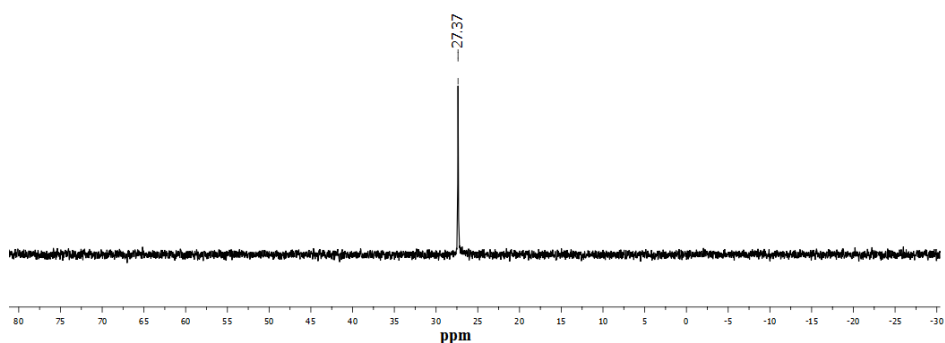


Figure A.2. ^{31}P NMR spectrum of $[(\text{Ph}_2\text{PPrPDI})\text{MoCl}_2][\text{Cl}]$ in chloroform-*d*.

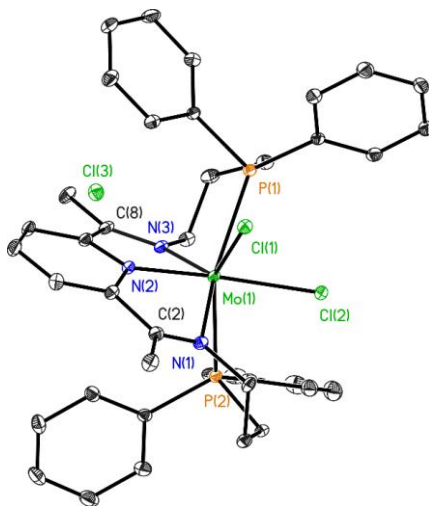


Figure A.3. Single crystal structure of $[(\text{Ph}_2\text{PPrPDI})\text{MoCl}_2][\text{Cl}]$.

A.3. Molecular Structure of (κ^6 -N,N,N,P,P,C-Ph²PPrPDI)MoCl

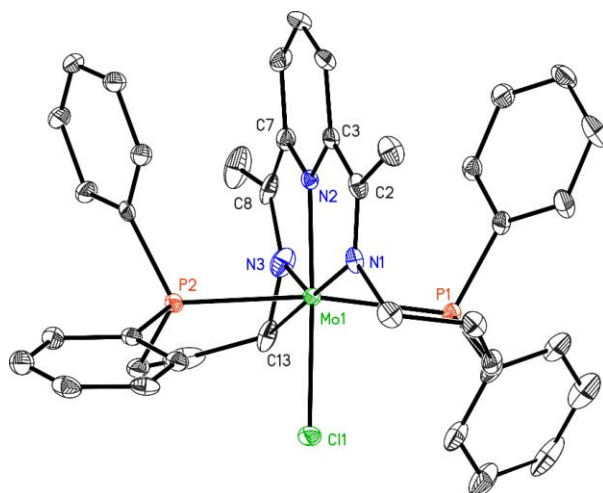


Figure A.4. Single crystal structure of (κ^6 -N,N,N,P,P,C-Ph²PPrPDI)MoCl.

A.4. Molecular Structure of [(Ph²PPrPDI)Mo(H₂O)][CO₃]

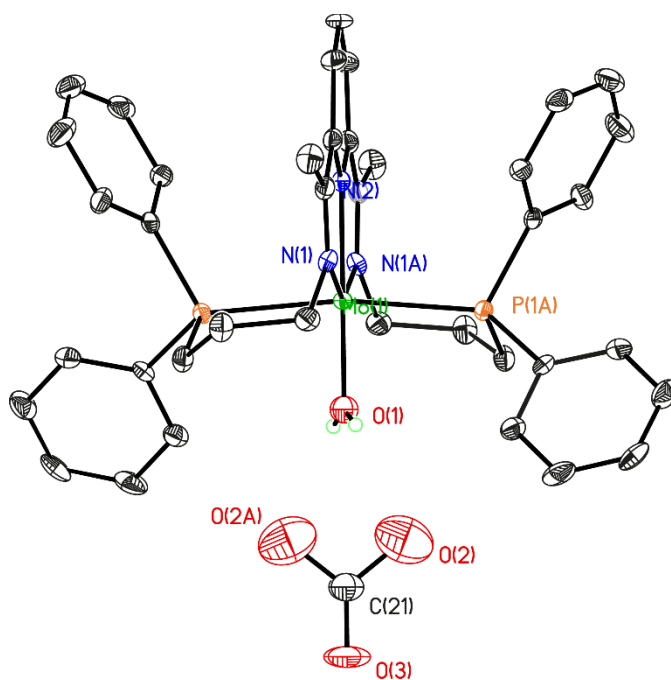


Figure A.5. Single crystal structure of [(Ph²PPrPDI)Mo(H₂O)][CO₃].

A.5. Preparation of (^{Ph}2PPrPDI)Mo(CH₂=CH₂)

Method A. In a nitrogen filled glove box, a 100 mL reaction bomb was charged with 4.2 g of mercury and 5 mL of THF. To it, 0.016 g (0.410 mmol) of freshly cut metallic potassium was added and stirred for 30 min to form a clear potassium amalgam solution. To the solution, 0.080 g (0.083 mmol) of **4**⁴ in 10 mL of THF was slowly added. The mixture was degassed on a Schlenk line at -196 °C before adding 1 atm of ethylene gas. The mixture was allowed to stir at 25 °C for 24 h. After removing excess ethylene, the resulting red solution was filtered through Celite and the solvent was removed *in vacuo* to yield a red solid. After washing with pentane and drying, 0.055 g (0.075 mmol, 90%) of (^{Ph}2PPrPDI)Mo(C₂H₄) was isolated. *Method B.* A J. Young NMR tube was charged with 0.010 g (0.0141 mmol) of **5**⁴ and 0.7 mL benzene-*d*₆. After degassing the tube in Schlenk line, 1 atm of ethylene gas was added at 0 °C. After heating the tube at 65 °C for 15 min, complete conversion to a red compound, identified as (^{Ph}2PPrPDI)Mo(C₂H₄) was observed by multinuclear NMR spectroscopy. Single crystals suitable for X-ray diffraction were grown from a concentrated THF solution at -35 °C. ¹H NMR (benzene-*d*₆, 400 MHz): δ 7.21 (m, 4H, *Ph*), 7.02 (t, 6.0 Hz, 7H, *Ph*), 6.93 (t, 6.0 Hz, 2H, *Ph*), 6.59 (t, 6.0 Hz, 2H, *Ph*), 6.49 (t, 6.0 Hz, 4H, *Ph*), 5.80 (t, 7.6 Hz, 2H, *Ph*), 5.71 (m, 4H, CH₂=CH₂), 5.14 (d, 8.8 Hz, 2H, *Ph*), 2.66 (s, 6H, CH₃), 2.55 (m, 4H, CH₂), 2.38 (m, 2H, CH₂), 2.11 (m, 2H, CH₂), 1.78 (m, 4H, CH₂). ³¹P NMR (benzene-*d*₆, 161.78 MHz): 24.65 (PPh₂).

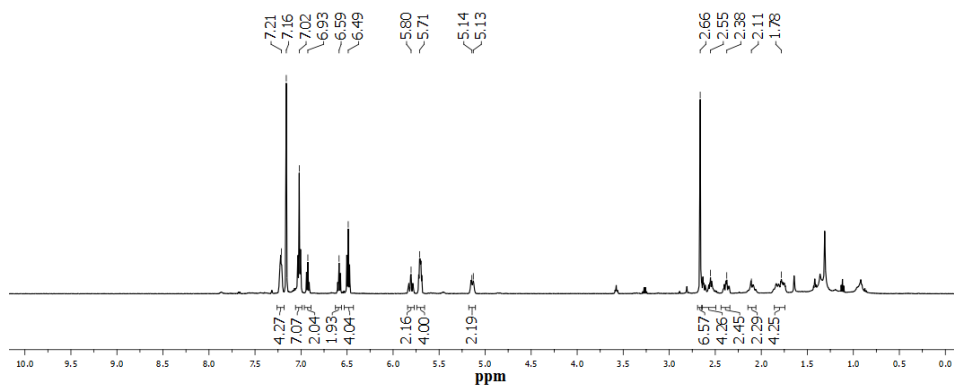


Figure A.6. ^1H NMR spectrum of $(\text{Ph}_2\text{PPrPDI})\text{Mo}(\text{CH}_2=\text{CH}_2)$ in benzene- d_6 .

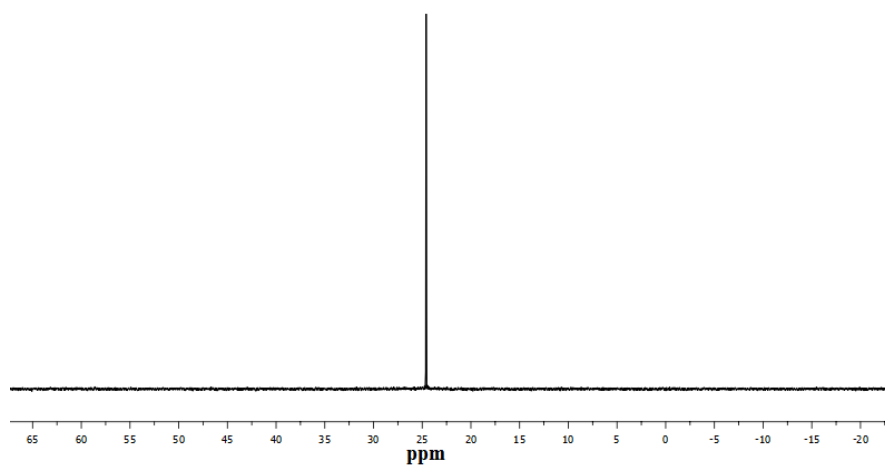


Figure A.7. ^{31}P NMR spectrum of $(\text{Ph}_2\text{PPrPDI})\text{Mo}(\text{CH}_2=\text{CH}_2)$ in benzene- d_6 .

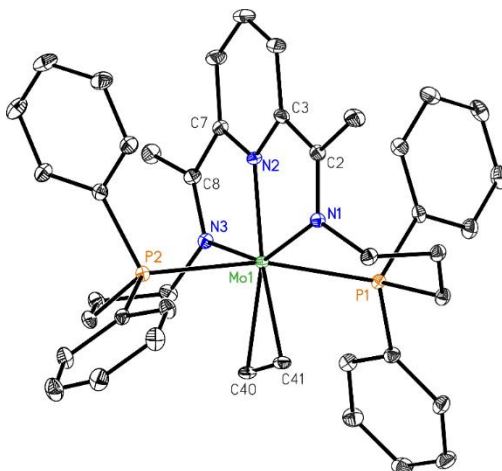


Figure A.8. Single crystal structure of $(\text{Ph}_2\text{PPrPDI})\text{Mo}(\text{CH}_2=\text{CH}_2)$.

A.6. Preparation of (^{Ph}2PEtPDI)MoCO

In a nitrogen filled glove box, a 100 mL thick-walled reaction vessel equipped with a magnetic stir bar was charged with 0.035 g (0.132 mmol) of Mo(CO)₆ and 0.077 g (0.132 mmol) of ^{Ph}2PEtPDI³ dissolved in 10 mL toluene. The sealed bomb was frozen in liquid nitrogen and degassed on a Schlenk line before being refluxed at 110 °C in a preheated oil bath. After 24 h, the green reaction mixture was cooled at room temperature and was once again degassed on the Schlenk line. Once the liberated CO gas was removed, the reaction was allowed to reflux for another 24 h at 110 °C to ensure reaction completion. After removing CO in the same way, the bomb was brought inside the glove box and the solution was filtered through Celite. After removing the volatiles under vacuum, the product was washed with 5 mL cold pentane and dried under vacuum to yield 0.090 g (0.126 mmol, 95%) of a green solid identified as (^{Ph}2PEtPDI)MoCO. Single crystals suitable for X-ray diffraction can be grown from a concentrated ether solution at -35 °C. ¹H NMR (benzene-*d*₆, 400 MHz): δ 7.67 (d, 8.0 Hz, 2H, *Py*), 7.08 (br, 4H, *Ph*), 6.97 (t, 6.0 Hz, 1H, *Py*), 6.80-6.72 (m, 16H, *Ph*), 4.76 (br, 2H, *CH*₂), 3.92 (br 2H, *CH*₂), 3.35 (br, 2H, *CH*₂), 2.89 (br, 2H, *CH*₂), 2.04 (s, 6H, *CH*₃). ³¹P NMR (benzene-*d*₆, 161.78 MHz): 74.84 (*PPh*₂).

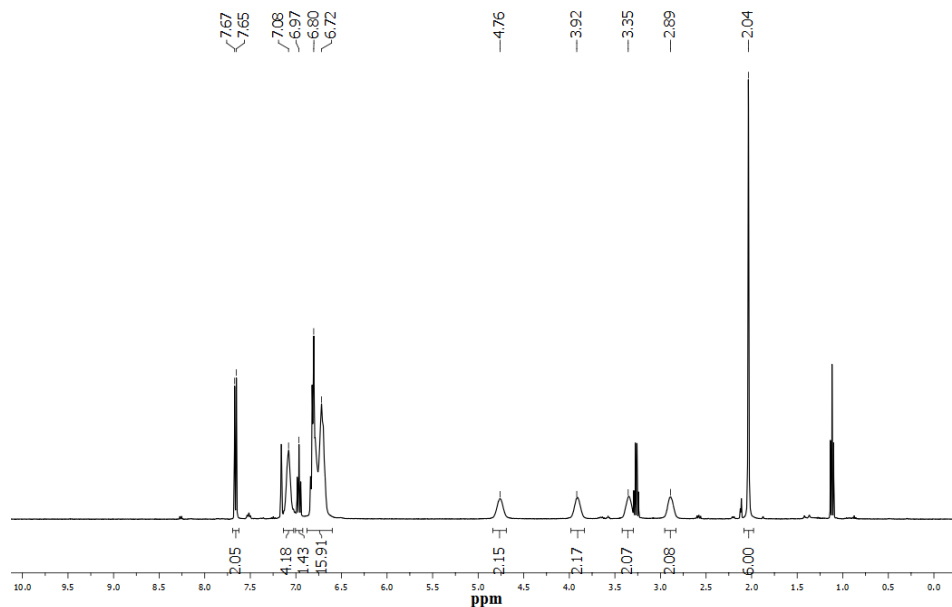


Figure A.9. ^1H NMR spectrum of $(\text{Ph}_2\text{PEtPDI})\text{Mo}(\text{CO})$ in benzene- d_6 .

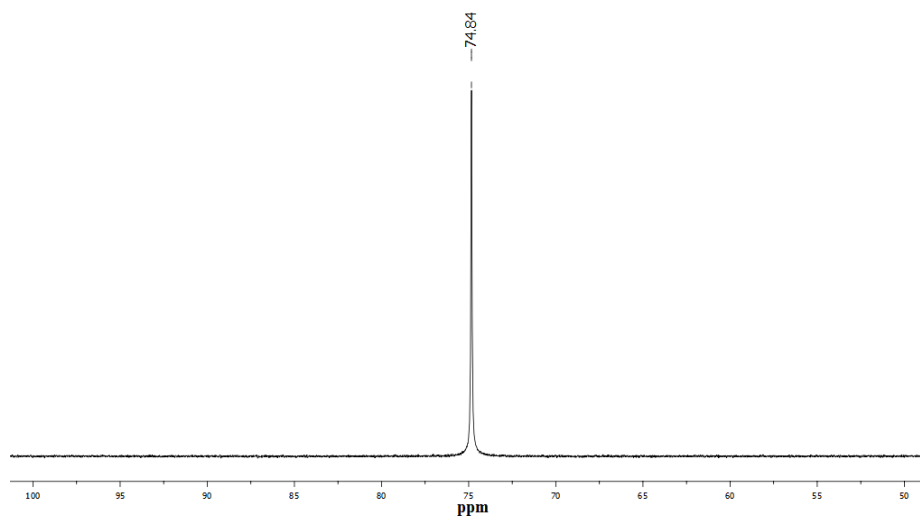


Figure A.10. ^{31}P NMR spectrum of $(\text{Ph}_2\text{PEtPDI})\text{Mo}(\text{CO})$ in benzene- d_6 .

A.7. Synthesis of $\text{iPrAr,Ph}_2\text{PPrPDI}$

A 100 mL reaction bomb was charged with 0.215 g of 2-(2,6-diisopropyl-1-imino)phenyl-6-acetylpyridine, 0.005 g of *p*-toluenesulfonic acid, 100 g of molecular sieves, and 5 mL

of toluene. After stirring the mixture for 5 min, a 10 mL toluene solution of 0.163 g of 3-aminopropyl diphenyl phosphine was added. The bomb was sealed under nitrogen and allowed to reflux at 110 °C for 3 d. The light yellow solution was cooled to room temperature and filtered through Celite and the filtrate was dried under vacuum. A light yellow solution was extracted with ether and dried to obtain 0.260 g of yellow solid (70%).

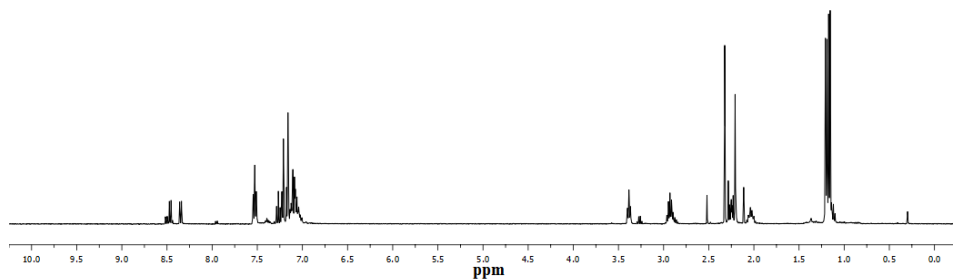


Figure A.11. ¹H NMR spectrum of *iprAr,Ph₂PPr*PDI in benzene-*d*₆.

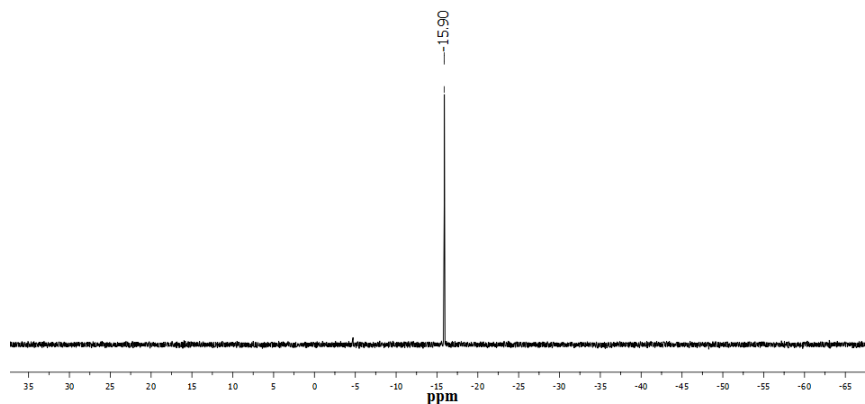


Figure A.12. ³¹P NMR spectrum of *iprAr,Ph₂PPr*PDI in benzene-*d*₆.

APPENDIX B

UNPUBLISHED BIS(IMINO)PYRIDINE COBALT CHEMISTRY

B.1. Preparation of $(^{\text{PyEt}}\text{PDI})\text{CoCl}_2$

A 20 mL reaction vial was charged with 0.15 g (1.155 mmol) CoCl_2 and 10 mL THF. To it, 0.43 g (1.155 mmol) of $^{\text{PyEt}}\text{PDI}^2$ in 5 mL THF was added while stirring. After 10 h, the olive-green solid was filtered on top of a sintered glass frit and washed with 5 mL of ether and dried under vacuum to obtain 0.55 g (1.098 mmol, 95%) of a light green solid identified as $(^{\text{PyEt}}\text{PDI})\text{CoCl}_2$.

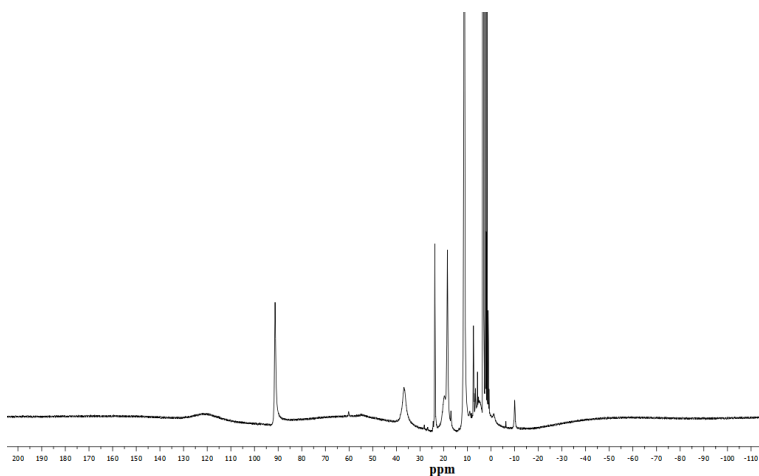


Figure B.1. ^1H NMR spectrum of $(^{\text{PyEt}}\text{PDI})\text{CoCl}_2$ in chloroform-*d*.

B.2. Preparation of $(^{\text{PyEt}}\text{PDIH})\text{Co}$

Method A. A 20 mL reaction vial was charged with 0.200 g (0.399 mmol) of $(^{\text{PyEt}}\text{PDI})\text{CoCl}_2$ and 10 mL toluene and the mixture was cooled to $-196\text{ }^\circ\text{C}$. To it, 0.800 mL of 1.0 M toluene solution of NaEt_3BH in 5 mL of toluene was slowly added while stirring. A color change to bluish-green was observed immediately. After 8 h, the reaction mixture was filtered through Celite and dried under vacuum to obtain 0.120 g (0.279 mmol, 69%) of bluish-green solid, identified as $(^{\text{PyEt}}\text{PDIH})\text{Co}$. *Method B.* A 20 mL

reaction vial was charged with 3.98 g of Hg, 0.023 g of Na, and 3 mL of THF. After stirring for 15 min, 0.100 g (0.199 mmol) of $(\text{PyEtPDI})\text{CoCl}_2$ was added and the mixture was allowed to stir for 15 h. The bluish-green solution was filtered through Celite and dried under vacuum to obtain 0.056 g (0.130 mmol, 65%) of bluish-green solid, identified as $(\text{PyEtPDIH})\text{Co}$. Single crystals suitable for X-ray diffraction were grown from a concentrated ether solution at $-35\text{ }^\circ\text{C}$. (Note: This complex is active for hydrosilylation and hydroboration of alkynes and carbonyls).

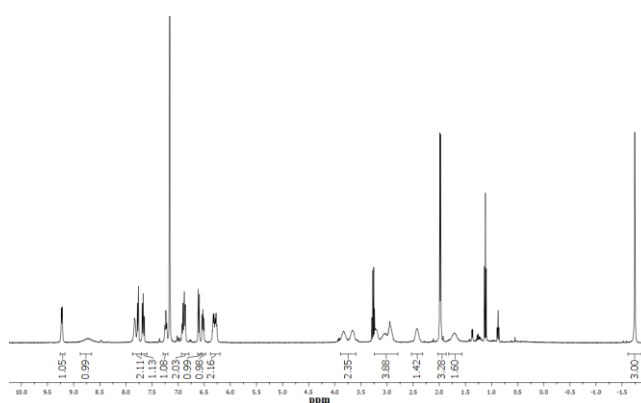


Figure B.2. ^1H NMR spectrum of $(\text{PyEtPDIH})\text{Co}$ in benzene- d_6 .

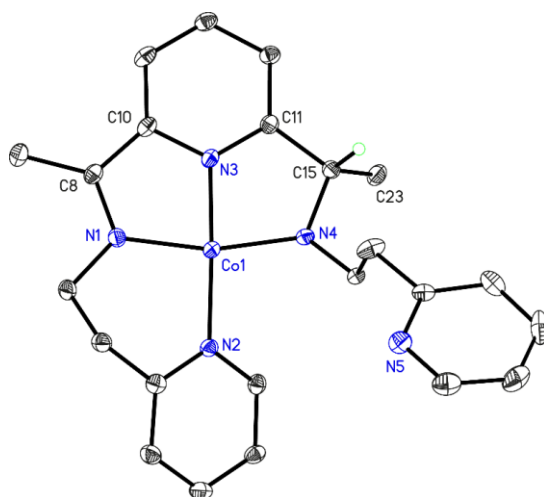


Figure B.3. Single crystal structure of $(\text{PyEtPDI-H})\text{Co}$.

APPENDIX C

UNPUBLISHED BIS(IMINO)PYRIDINE AND DIIMINE IRON CHEMISTRY

C.1. Preparation of $(^{\text{PyEt}}\text{PDI})\text{FeBr}_2$

A 20 mL reaction vial was charged with 0.200 g (0.950 mmol) of FeBr_2 and 10 mL THF. To it, 0.345 g (0.950 mmol) of $^{\text{PyEt}}\text{PDI}^2$ in 5 mL THF was added while stirring. After 10 h, the blue solid was filtered on top of a sintered glass frit and washed with 5 mL of THF and dried under vacuum to obtain 0.545 g (0.931 mmol, 98%) purple solid, identified as $(^{\text{PyEt}}\text{PDI})\text{FeBr}_2$.

C.2. Preparation of $(^{\text{PyEt}}\text{PDI})\text{Fe}$

A 20 mL reaction vial was charged with 3.92 g of Hg, 0.024 g of Na, and 3 mL of THF. After stirring for 15 min, 0.118 g (0.201 mmol) of $(^{\text{PyEt}}\text{PDI})\text{FeBr}_2$ was added and the mixture was allowed to stir for 7d. The bluish-green solution was filtered through Celite and dried under vacuum to obtain 0.057 g (0.133 mmol, 66%) of bluish-green solid, identified as $(^{\text{PyEt}}\text{PDI})\text{Fe}$. ^1H NMR (benzene- d_6 , 400 MHz): δ 9.05 (d, 7.6 Hz, 2H, *Py*), 7.58 (t, 7.6 Hz, 1H, *Py*), 7.54 (d, 5.6 Hz, 2H, *Py*), 6.53 (m, 4H, *Py*), 5.50 (t, 4.4 Hz, 2H, *Py*), 4.05 (td, 2H, CH_2), 3.58 (dd, 2H, CH_2), 3.34 (td, 2H, CH_2), 2.93 (d, 8.8 Hz, 2H, CH_2), 1.52 (s, 6H, CH_3). (Note: This complex is active for hydrosilylation and hydroboration of alkynes and carbonyls).

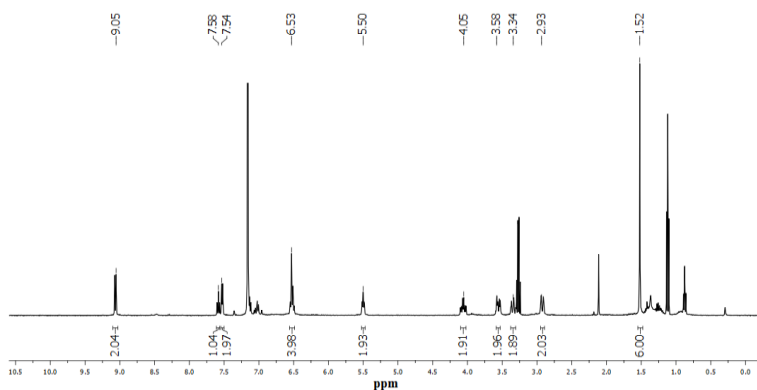


Figure C.1. ^1H NMR spectrum of $(\text{PyEtPDI})\text{Fe}$ in benzene- d_6 .

C.3. Preparation of PhPPr_2PDI

A 100 mL reaction bomb was charged with 0.303 g of 2,6-diacetylpyridine, 0.006 g of p-toluenesulfonic acid, 100 g of molecular sieves, and 5 mL of toluene. After stirring the mixture for 5 min, a 10 mL toluene solution of bis(3-aminopropyl)phenyl phosphine was added. The bomb was sealed under nitrogen and allowed to reflux at 110 °C for 3 d. The light yellow solution was cooled to room temperature and filtered through Celite and the filtrate was dried under vacuum. A light yellow solution was extracted with ether and dried to obtain 0.503 g of yellow foam (77%).

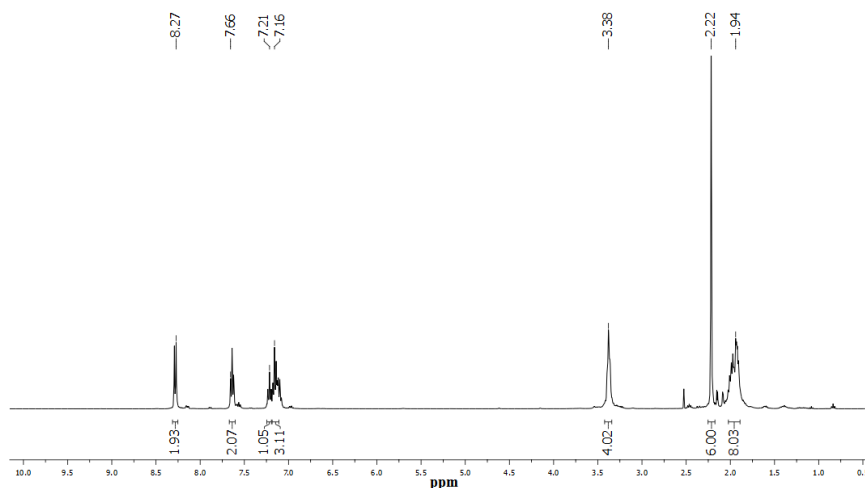


Figure C.2. ^1H NMR spectrum of PhPPr_2PDI in benzene- d_6 .

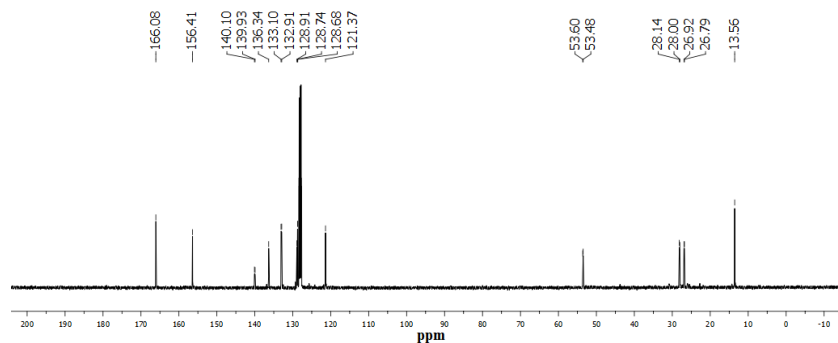


Figure C.3. ^{13}C NMR spectrum of PhPPr_2PDI in benzene- d_6 .

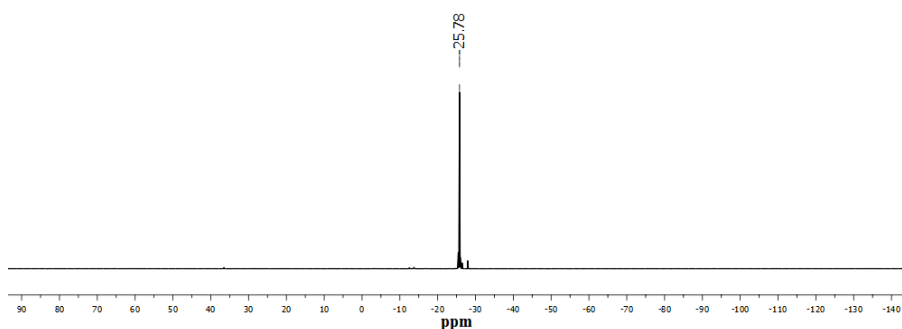


Figure C.4. ^{31}P NMR spectrum of PhPPr_2PDI in benzene- d_6 .

C.4. Preparation of $(\text{PhPPr}_2\text{PDI})\text{FeBr}_2$

A 20 mL reaction vial was charged with 0.207 g (0.960 mmol) of FeBr_2 and 10 mL THF. To it, 0.360 g (0.96 mmol) of PhPPr_2PDI in 5 mL THF was added while stirring. After 10 h, the purple solid was filtered on top of a sintered glass frit and washed with 5 mL of THF and dried under vacuum to obtain 0.470 g (0.83 mmol, 86%) purple solid, identified as $(\text{PhPPr}_2\text{PDI})\text{FeBr}_2$. (Insoluble in most NMR solvents).

C.5. Reduction of $(\text{PhPPr}_2\text{PDI})\text{FeBr}_2$

A 20 mL reaction vial was charged with 4.00 g of Hg, 0.020 g of Na, and 3 mL of THF. After stirring for 15 min, 0.005 mL of cyclooctatetraene was added and stirred for another 5 min followed by addition of 0.100 g (0.176 mmol) of $(\text{PhPPr}_2\text{PDI})\text{FeBr}_2$. The mixture

was allowed to stir for 24 h. The brownish-green solution was filtered through Celite and dried under vacuum to obtain 0.029 g (0.071 mmol, 40%) of brownish-green solid.

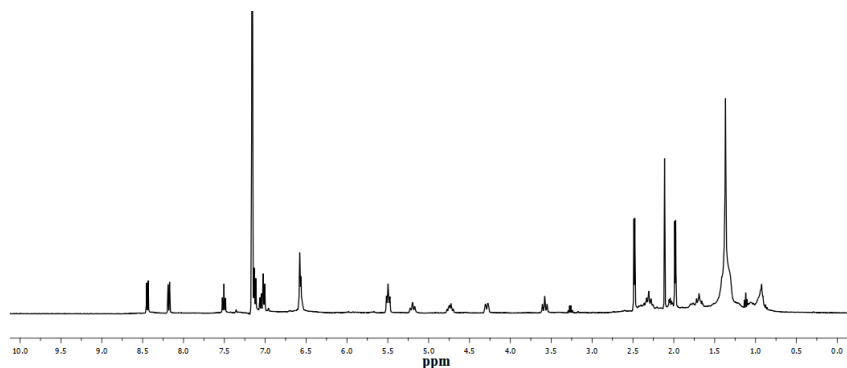


Figure C.5. ^1H NMR spectrum of PhPPr_2PDI in benzene- d_6 .

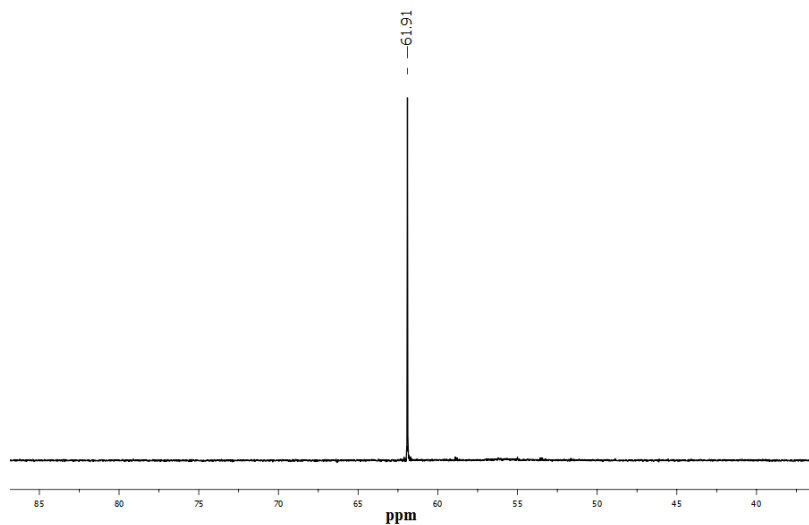


Figure C.6. ^{31}P NMR spectrum of PhPPr_2PDI in benzene- d_6 .

C.6. Preparation of $(\text{Ph}_2\text{PPrDI})\text{Fe}(\text{OTf})_2$

A 20 mL reaction vial was charged with 0.100 g (0.120 mmol) of $\text{Ph}_2\text{PPrDI}\text{FeBr}_2^5$ and 10 mL acetonitrile. After wrapping the vial with black-electric tape, 0.060 g (0.241 mmol) of AgOTf in 5 mL of acetonitrile was slowly added while stirring. The sealed vial was allowed

to heat at 60 °C. A color change to purple to reddish-orange was observed. After 4 h, the reaction mixture was cooled to room temperature and filtered through Celite and dried under vacuum to obtain 0.104 g (0.108 mmol, 90%) of red solid, identified as $(\text{Ph}_2\text{PPrDI})\text{Fe}(\text{OTf})_2$. (Note: This complex is an active water oxidation catalyst using pH=1 solution in trifluoroethanol with the onset at 0.6 V vs $\text{Fc}^{0/+}$).

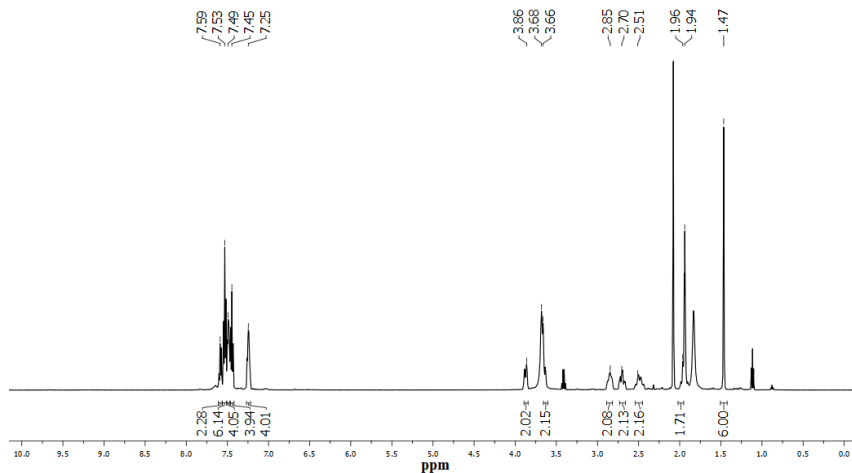


Figure C.7. ^1H NMR spectrum of $(\text{Ph}_2\text{PPrDI})\text{Fe}(\text{OTf})_2$ in acetonitrile- d_3 .

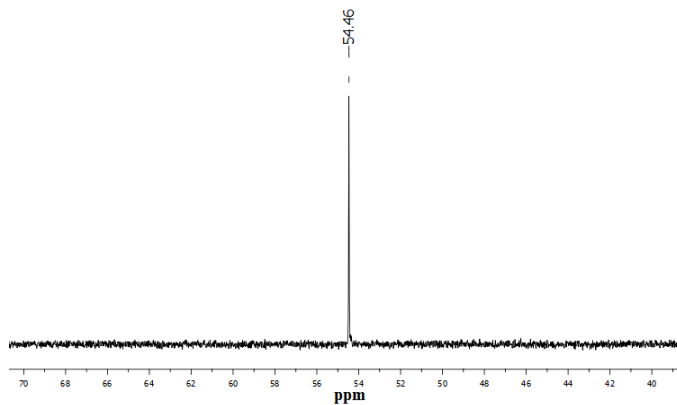


Figure C.8. ^{31}P NMR spectrum of $(\text{Ph}_2\text{PPrDI})\text{Fe}(\text{OTf})_2$ in acetonitrile- d_3 .

References

- (1) Stoffelbach, F.; Saurenz, D.; Poli, R. *Eur. J. Inorg. Chem.* **2001**, 2699-2270.
- (2) Pal, R.; Groy, T. L.; Bowman, A. C.; Trovitch, R. J. *Inorg. Chem.* **2014**, *53*, 9357-9365.
- (3) Ben-Daat, H.; Hall, G. B.; Groy, T. L.; Trovitch, R. J. *Eur. J. Inorg. Chem.* **2013**, 4430-4442.
- (4) Pal, R.; Groy, T. L.; Trovitch, R. J. *Inorg. Chem.* **2015**, *54*, 7506-7515.
- (5) Ghosh, C.; Groy, T. L.; Bowman, A. C.; Trovitch, R. J. *Chem. Commun.* **2016**, *52*, 4553-4556.



RightsLink®

[Home](#)[Create Account](#)[Help](#)ACS Publications
Most Trusted. Most Cited. Most Read.

Title: Preparation and Hydrosilylation Activity of a Molybdenum Carbonyl Complex That Features a Pentadentate Bis(imino)pyridine Ligand

Author: Raja Pal, Thomas L. Groy, Amanda C. Bowman, et al

Publication: Inorganic Chemistry

Publisher: American Chemical Society

Date: Sep 1, 2014

Copyright © 2014, American Chemical Society

LOGIN

If you're a [copyright.com](#) user, you can login to RightsLink using your [copyright.com](#) credentials. Already a [RightsLink](#) user or want to [learn more?](#)

PERMISSION/LICENSE IS GRANTED FOR YOUR ORDER AT NO CHARGE

This type of permission/license, instead of the standard Terms & Conditions, is sent to you because no fee is being charged for your order. Please note the following:

- Permission is granted for your request in both print and electronic formats, and translations.
- If figures and/or tables were requested, they may be adapted or used in part.
- Please print this page for your records and send a copy of it to your publisher/graduate school.
- Appropriate credit for the requested material should be given as follows: "Reprinted (adapted) with permission from (COMPLETE REFERENCE CITATION). Copyright (YEAR) American Chemical Society." Insert appropriate information in place of the capitalized words.
- One-time permission is granted only for the use specified in your request. No additional uses are granted (such as derivative works or other editions). For any other uses, please submit a new request.

[BACK](#)[CLOSE WINDOW](#)

Copyright © 2016 [Copyright Clearance Center, Inc.](#) All Rights Reserved. [Privacy statement](#). [Terms and Conditions](#).
Comments? We would like to hear from you. E-mail us at customercare@copyright.com



RightsLink®

[Home](#)[Create Account](#)[Help](#)ACS Publications
Most Trusted. Most Cited. Most Read.**Title:** Conversion of Carbon Dioxide to Methanol Using a C-H Activated Bis(imino)pyridine Molybdenum Hydroboration Catalyst**Author:** Raja Pal, Thomas L. Groy, Ryan J. Trovitch**Publication:** Inorganic Chemistry**Publisher:** American Chemical Society**Date:** Aug 1, 2015

Copyright © 2015, American Chemical Society

[LOGIN](#)

If you're a [copyright.com](#) user, you can login to RightsLink using your [copyright.com](#) credentials. Already a [RightsLink](#) user or want to [learn more?](#)

PERMISSION/LICENSE IS GRANTED FOR YOUR ORDER AT NO CHARGE

This type of permission/license, instead of the standard Terms & Conditions, is sent to you because no fee is being charged for your order. Please note the following:

- Permission is granted for your request in both print and electronic formats, and translations.
- If figures and/or tables were requested, they may be adapted or used in part.
- Please print this page for your records and send a copy of it to your publisher/graduate school.
- Appropriate credit for the requested material should be given as follows: "Reprinted (adapted) with permission from (COMPLETE REFERENCE CITATION). Copyright (YEAR) American Chemical Society." Insert appropriate information in place of the capitalized words.
- One-time permission is granted only for the use specified in your request. No additional uses are granted (such as derivative works or other editions). For any other uses, please submit a new request.

[BACK](#)[CLOSE WINDOW](#)

Copyright © 2016 [Copyright Clearance Center, Inc.](#) All Rights Reserved. [Privacy statement](#). [Terms and Conditions](#).
Comments? We would like to hear from you. E-mail us at customercare@copyright.com



RAJA PAL <rpal3@asu.edu>

Request for copyrights

3 messages

RAJA PAL <rpal3@asu.edu>
To: contracts-copyright@rsc.org

Mon, Oct 31, 2016 at 9:03 PM

Dear RSC Personnel:

This is Raja Pal, and I am writing this to request permission to reuse two of published articles in my Ph.D. thesis. Here are the two articles I have published with RSC as a first author and I am not sure how to ask for permission from RSC so that I can reuse my articles in my thesis.

Pal, R.; Cherry, B. R.; Flores, M.; Groy, T. L.; Trovitch, R. J. "Isolation of a Bis(imino)pyridine Molybdenum(I) Iodide Complex through Controlled Reduction and Interconversion of its Reaction Products." *Dalton Transactions* 2016, 45, 10024-10033.

and

Pal, R.; Laureanti, J. A.; Groy, T. L.; Jones, A. K.; Trovitch, R. J. "Hydrogen Production from Water using a Bis(imino)pyridine Molybdenum Electrocatalyst." *Chemical Communications* 2016, 52, 11555-11558.

I have carefully reviewed information described on RSC website for copyrights information, but if you can guide me how I can get permission for copyrights to use them as full documents in my thesis, it would be really helpful.

I appreciate your time and consideration.

Sincerely,
Raja Pal

CONTRACTS-COPYRIGHT (shared) <Contracts-Copyright@rsc.org>
To: RAJA PAL <rpal3@asu.edu>

Tue, Nov 1, 2016 at 9:00 AM

Dear Raja,

Thank you for your email.

The Royal Society of Chemistry (RSC) hereby grants permission for the use of your paper(s) specified below in the printed and microfilm version of your thesis. You may also make available the PDF version of your paper(s) that the RSC sent to the corresponding author(s) of your paper(s) upon publication of the paper(s) in the following ways: in your thesis via any website that your university may have for the deposition of theses, via your university's Intranet or via your own personal website. We are however unable to grant you permission to include the PDF version of the paper(s) on its own in your institutional repository. The Royal Society of Chemistry is a signatory to the STM Guidelines on Permissions (available on request).

Please note that if the material specified below or any part of it appears with credit or acknowledgement to a third party then you must also secure permission from that third party before reproducing that material.

Please ensure that the thesis states the following:

Reproduced by permission of the PCCP Owner Societies

11/2/2016

Arizona State University Mail - Request for copyrights

and include a link to the paper on the Royal Society of Chemistry's website.

Please ensure that your co-authors are aware that you are including the paper in your thesis.

Regards

Antonella

Antonella Tesoro

Customer Sales Support

Royal Society of Chemistry

Thomas Graham House,

Science Park, Milton Road,

Cambridge-CB4 0WF

Tel. +44 (0) 1223 432 675

tesoroa@rsc.org

Main Reception Tel. +44 (0) 1223 42 0066

www.rsc.org

Winner of The Queen's Awards for Enterprise, International Trade 2013



DISCLAIMER:

This communication (including any attachments) is intended for the use of the addressee only and may contain confidential, privileged or copyright material. It may not be relied upon or disclosed to any other person without the consent of the Royal Society of Chemistry. If you have received it in error, please contact us immediately. Any advice given by the Royal Society of Chemistry has been carefully formulated but is necessarily based on the information available, and the Royal Society of Chemistry cannot be held responsible for accuracy or completeness. In this respect, the Royal Society of Chemistry owes no duty of care and shall not be liable for any resulting damage or loss. The Royal Society of Chemistry acknowledges that a disclaimer cannot restrict liability at law for personal injury or death arising through a finding of negligence. The Royal Society of Chemistry does not warrant that its emails or attachments are Virus-free: Please rely on your own screening. The Royal Society of Chemistry is a charity, registered in England and Wales, number 207890 - Registered office: Thomas Graham House, Science Park, Milton Road, Cambridge CB4 0WF

<https://mail.google.com/mail/u/0/?ui=2&ik=bc108bad02&view=pt&search=Inbox&th=1581e0e471c8b4cd&siml=1581e0e471c8b4cd&siml=15820a18e1e6745a&s...> 2/3

BIOGRAPHICAL SKETCH

Raja Pal was born and brought up at Katwa, a small town in West Bengal, India. After graduating from Katwa Bharati Bhavan High School in 2006, he attended Katwa College with Chemistry Honors and earned a Bachelor of Sciences (B.Sc.) in 2009 with standing first in his class. Raja then moved to Indian Institute of Technology Bombay (IIT Bombay) where he spent two years and obtained a Masters of Sciences (M.Sc.) in Chemistry in 2011. While in IIT Bombay, he got the first exposure of doing research in chemistry when he started his master project under the supervision of Prof. G. K. Lahiri. During the year-long thesis, he had worked on synthesis and characterization of ruthenium complexes and studied their catalytic activity in water oxidation, epoxidation, and Wacker-type oxidation reactions. After completion of his M.Sc. degree, he moved to the USA to pursue his Ph.D. degree at Arizona State University in 2011 where he joined Prof. Ryan J. Trovitch's laboratory as one of his first graduate students. While setting up the laboratory, in Prof. Trovitch's lab, Raja worked on the exciting project of the development of homogeneous molybdenum catalysts, where he synthesized and characterized a series of molybdenum complexes spanning a range of oxidation states. The synthesized molybdenum complexes showed remarkable applications in activating various small molecules. While he was in graduate school, he had the opportunity to improve his teaching and mentoring skills and was also selected for the Outstanding Teaching Assistant award by the School of Molecular Sciences in 2016. During this doctoral research, he has acquired various skills and immense knowledge in the field of inorganic and organometallic chemistry and hopes to continue his interest in science in his future career.